University of Alberta

Influence of supports on gas-phase olefin polymerization over polymer-supported ($(n\text{-BuCp})_2\text{ZrCl}_2$/MAO) catalysts

by

Hassan Hammawa

©

A thesis submitted to the Faculty of Graduate Studies and Research
in partial fulfillment of the requirements for the degree of
Doctor of Philosophy in Chemical Engineering

Department of Chemical and Materials Engineering

Edmonton, Alberta

Fall 2004

Library and Archives Canada
Published Heritage Branch
395 Wellington Street
Ottawa ON K1A 0N4
Canada

Bibliothèque et Archives Canada
Direction du Patrimoine de l'édition
395, rue Wellington
Ottawa ON K1A 0N4
Canada

Your file Votre référence
ISBN: 0-612-95941-4
Our file Notre référence
ISBN: 0-612-95941-4

The author has granted a non-exclusive license allowing the Library and Archives Canada to reproduce, loan, distribute or sell copies of this thesis in microform, paper or electronic formats.

The author retains ownership of the copyright in this thesis. Neither the thesis nor substantial extracts from it may be printed or otherwise reproduced without the author's permission.

L'auteur a accordé une licence non exclusive permettant à la Bibliothèque et Archives Canada de reproduire, prêter, distribuer ou vendre des copies de cette thèse sous la forme de microfiche/film, de reproduction sur papier ou sur format électronique.

L'auteur conserve la propriété du droit d'auteur qui protège cette thèse. Ni la thèse ni des extraits substantiels de celle-ci ne doivent être imprimés ou aturement reproduits sans son autorisation.

In compliance with the Canadian Privacy Act some supporting forms may have been removed from this thesis.

While these forms may be included in the document page count, their removal does not represent any loss of content from the thesis.

Conformément à la loi canadienne sur la protection de la vie privée, quelques formulaires secondaires ont été enlevés de cette thèse.

Bien que ces formulaires aient inclus dans la pagination, il n'y aura aucun contenu manquant.

Canada

To my mom
&
my wife, Maisarah and our children, Khadija & Abdullah,
and to all my brothers and sisters

Acknowledgement

I am very grateful to my supervisors, Professor Sieghard E. Wanke, and Professor David T. Lynch, Dean of Engineering for relentlessly mentoring and supporting me through out the course of my research work. Learning from their experiences has been a great privilege to me.

I would like to express my gratitude to the technical staff of the department: Mr. Bob Smith, Mr. Bob Scott, and Mr. James Skwarok for reactor fabrication, Mrs. Naiyu Bu for molar mass measurements, Mrs. Andrée Koenig for setting up gas chromatograph, Mrs. Christina Barker for scanning electron microscopy, Mr. Walter Boddez and Mr. Richard Cooper for setting up the instrumentation/data acquisition hardware, and Mr. Jack Gibeau for his assistance on Opto22/LabView interfacing. I also thank Dr. Naihong Li for preparing the in-house supports and Dr. Long Wu for his constructive suggestions.

Finally, I wish to thank all my family members for their support and understanding during this work.

Table of Contents

1 Introduction 1

2 Literature Review 7

2.1 Homogeneous Metallocene/MAO catalyst systems 7

2.1.1 Roles of MAO 7

2.1.2 Roles of ligand substituents 9

2.2 Supported metallocene/MAO catalysts 9

2.2.1 Supporting methods 10

2.2.2 Polymer-supported metallocene/MAO catalysts 11

2.2.3 Effects of supporting metallocene/MAO on solid carriers 13

2.3 Ethylene/α-olefins polymerization with metallocene catalysts 17

2.3.1 Polymerization reactor systems 18

2.3.2 Reaction mechanism and polymerization kinetics of metallocene catalysts 19

2.3.3 Effects of polymerization conditions 25

2.4 Effects of support morphology on catalyst activity and product morphology 29

3 Experimental Methods 33

3.1 Materials 33

3.2 Preparation of supported metallocene/MAO catalysts 37

3.3 Gas-phase polymerization procedure 40

3.4 Characterization methods 42

3.4.1 Surface area and pore size distribution 43

3.4.2 Friability and swellability of the polymeric supports 45

3.4.3 Instrumental neutron activation analysis (INAA) 47

3.4.4 Scanning electron microscopy (SEM) and energy dispersive X-ray analysis (EDX) 49

3.4.5 Temperature rising elution fractionation (TREF) 50

3.4.6 Size exclusion chromatography (SEC) 52

4 Morphology of Supports and Supported Catalysts 54

4.1 Surface area and pore size distribution of supports and catalysts.................. 57

4.2 Effect of MAO loading on catalyst morphology 65

4.3 Al and Zr loading and distribution in supported catalysts 66

4.4 Catalyst composition 72

4.5 Effect of preparation methods on catalyst morphology 75

4.6 Friability and swellability 76

5 Exploratory Experiments I: Reactor Behavior 79

5.1 Description of the new polymerization reactor system 79

5.1.1 The reactor, feed purification, and data acquisition systems 81

5.1.2 The temperature control system.. 87

5.1.3 Gas-phase analysis system.. 89

5.2 Test runs with the new reactor... 92

5.2.1 Reactor tests and modifications 92

5.2.2 Effect of static mixers, stirring and NaCl seedbed.......................... 101

5.3 Reproducibility of the gas-phase polymerization.................................. 111

6 Exploratory Experiments II: Effect of Aluminum Alkyls 132

6.1 Sensitivity of catalysts to TIBA 132

6.2 Effect of aluminum alkyl type and concentration.................................. 136

6.3 Effect of inert gas and the contact mode of catalyst with TIBA 146

7 Rates of Ethylene/α-Olefin Polymerizations Over Polymer-supported (*n*-BuCp)$_2$ZrCl$_2$/MAO Catalysts in the Gas-phase 154

7.1 Influence of typical variation in zirconium loading and Al:Zr ratio.............. 155

7.2 Effects of chemical structure and morphology of support 164

7.3 Effects of polymerization temperature on rate profiles 175

7.4 Effects of monomer pressure on polymerization rate............................... 183

7.5 Influence of hydrogen on rate profile 187

8 Influence of Comonomer on Activity Profiles and Product Morphology for Gas-phase Polymerization Over Polymer-supported $(n\text{-BuCp})_2ZrCl_2$/MAO Catalysts 193

8.1 Influence of 1-hexene on polymerization rates and product morphology 193

8.1.1 Effect of 1-hexene on activity of Group-1 catalysts 194

8.1.2 Effect of 1-hexene on activity of Group-2 catalysts 202

8.1.3 Effect of 1-hexene on activity of Group-3 catalysts 208

8.2 Interaction between support fragility and comonomer in the development of product morphology during gas-phase polymerization 215

8.2.1 Catalyst fracture during ethylene homopolymerization 215

8.2.2 Catalyst fracture during ethylene/α-olefin copolymerization 222

9 Properties of the Polyolefin Products 237

9.1 Morphology and bulk density of polyolefin particles 237

9.2 Molar mass and polydispersity index 241

9.2.1 Influence of particle size and monomer pressure on molar mass 241

9.2.2 Effect of polymerization temperature on molar masses 246

9.2.3 Influence of hydrogen on molar mass and polydispersity 248

9.2.4 Influence of 1-hexene on molar mass and polydispersity 249

9.3 Comonomer incorporation 253

10 Conclusions and Recommendations for Future Work 262

10.1 Summary and conclusions 262

10.2 Recommendations for future work 266

References 270

Appendix A. Summary of catalysts preparation and composition 289

A-1 Description of catalysts preparation 290

A-2 Composition of supported catalysts 292

Appendix B. Summary of polymerization runs and polymer properties 293

B-1 Summary of polymerization conditions 294

B-2 Summary of polymer properties 303

List of Tables

Table 2.1 Key features of polymer-supported metallocene catalysts in the literature 12
Table 2.2 Typical test conditions and activities of supported metallocene catalysts in ethylene homopolymerization 15
Table 3.1 Description of polymeric supports used in catalyst synthesis 35
Table 3.2 Supports and pretreatment conditions for supported catalysts 39
Table 4.1 Mesopore characteristics of polymeric supports and supported catalysts 56
Table 4.2 Friability of selected supports 77
Table 5.1 Description of polymerization test runs in the new reactor 93
Table 5.2 Description of polymerization runs for temperature control 103
Table 5.3 Poor reproducibility observed in temperature controlled gas-phase olefin polymerization 112
Table 5.4 Reproducibility of gas-phase polymerization runs with temperature control 118
Table 6.1 Description of polymer-supported (n-BuCp)$_2$ZrCl$_2$/MAO catalysts 133
Table 6.2 Effect of Al alkyls on polymerization activity 133
Table 6.3 Effect of Al alkyls on polymerization activity at 80°C 1.4 MPa and 80g NaCl 136
Table 6.4 Description of ethylene homopolymerization runs to determine effect of inert gas and the contact order and concentration of TIBA 147
Table 7.1 Typical variations in catalyst compositions 155
Table 7.2 Influence of typical variations in the Zr loading and Al:Zr ratio on polymerization activity at 80°C and 1.4 MPa 157
Table 7.3 List of runs for the effects of support structure and morphology 165
Table 7.4 Summary of the influence of polymerization temperature on activity 176
Table 7.5 Parameters from the fit of Equation 7.1 182
Table 7.6 Summary of the influence of ethylene pressure on polymerization activity 184
Table 8.1 Influence of 1-hexene on the activity of Group-1 catalysts 194
Table 8.2 Effect of 1-hexene on the activity of Group-2 catalysts 202

Table 8.3 Influence of 1-hexene on the polymerization activity of Group-3 catalysts 208
Table 8.4 Classification of catalysts into Groups 1-3 according to polymerization activity (approximate run conditions: trace TIBA, 80°C, 1.4 MPa, and 15 mol/m^3 C_2H_4)........ 214
Table 8.5 Support friability and the morphology of supported catalysts 228
Table 8.6 Influence of comonomer on activity of catalysts 229
Table 9.1 Bulk densities of nascent polyolefin products........ 238
Table 9.2 Parameters of Equation 9.3 obtained from the data in Figure 9.5........ 246
Table 9.3 Influence of hydrogen on molar mass of ethylene homopolymers 248
Table 9.4 Molar masses of ethylene homopolymer and ethylene/1-hexene copolymers synthesized with supported catalysts at 80°C and 1.4 MPa........ 250
Table 9.5 Short chain branching distribution of ethylene/1-hexene copolymers........ 255

List of Figures

Figure 2.1 Cage structure of methylaluminoxane MAO 8

Figure 2.2 Bridged and unbridged metallocenes active in olefins polymerization in the presence of MAO (Kaminsky, 1996). Metallocene type (d) with $R_1 = n\text{-}C_4H_9$, and $R_2 = Cl$ was used in this thesis work 10

Figure 2.3 Ethylene polymerization mechanism at the active zirconocenium site 20

Figure 2.4 Possible chain termination reactions during C_2H_4 polymerization with metallocene/MAO catalyst. Route-A–*β*-hydride elimination, Route-B–chain transfer to ethylene, Route-C–chain transfer to hydrogen, and Route-D–chain transfer to MAO.. 21

Figure 2.5 Polymerization activity profiles for decay-type (curve a) and acceleration-decay-type (curve b) kinetics 22

Figure 2.6 Representation of active catalyst particle in MGM (Hutchinson *et al.*, 1992) 31

Figure 3.1 Schematic structures of cross-linked (a) poly(divinylbenzene) support (Glöckner, 1978) with no functional groups, and (b) poly(HEMA/divinylbenzene) support 36

Figure 3.2 Schematic structures of cross-linked (a) poly(divinylbenzene/acrylonitrile) support, and (b) poly(divinylbenzene/N-vinyl-2-pyrrolidinone) support 36

Figure 3.3 Schematic structures of cross-linked (a) poly(ethyleneglycol-dimethacrylate) support (Glöckner, 1978), and (b) poly(HEMA/PTMA) support 37

Figure 3.4 Profile of ethylene flowrate, reactor temperature, and pressure during a typical ethylene/1-hexene copolymerization run (HH20198) in which residual TIBA was not removed after the reactor scavenging 42

Figure 4.1 Influence of pretreatment condition on pore size distribution of alumina sample 55

Figure 4.2 Surface area and mesopore volume of supports and supported catalysts (see Table 3.1 for support identification) 56

Figure 4.3 Adsorption-desorption isotherms for HayeSep-R and Catalyst HH19 58

Figure 4.4 Adsorption-desorption isotherms for HayeSep-Q and Catalyst HH22...... 58

Figure 4.5 Pore size distributions of DVB based supports and supported catalysts having no functional groups (* – artifact peak) 60

Figure 4.6 Pore size distributions of DVB based supports with HEMA and supported catalysts (* – artifact peak).. 62

Figure 4.7 Pore size distribution of solid (n-BuCp)$_2$ZrCl$_2$/MAO complexes (* – artifact peak) 62

Figure 4.8 Pore size distribution of commercial supports having heteroatoms and the corresponding catalysts (* – artifact peak) 63

Figure 4.9 Pore size distribution of poly(EGDM) supports and catalysts (* – artifact peak) 64

Figure 4.10 Pore volume distribution of supports and catalysts.............................. 64

Figure 4.11 Effect of the amount of MAO (10 mass % solution) on (a) pore size and (b) pore volume distribution of in-house support and the corresponding catalyst 65

Figure 4.12 Effect of the amount of MAO (10 mass % solution) on (a) pore size and (b) pore volume distribution of commercial support and the corresponding catalyst.. 66

Figure 4.13 Morphologies of different supports (left column) synthesized in our laboratory and the corresponding supported catalysts (right column). Scale bar = 300μm 68

Figure 4.14 Morphologies of different commercial supports (left column) and the corresponding supported catalysts (right column). Scale bar = 150 μm..... 69

Figure 4.15 EDX line scans for aluminum distribution across (a) Catalyst HH18 and (b) Catalyst HH08 particles 70

Figure 4.16 EDX line scans for aluminum distribution across (a) Catalyst HH16 and (b) Catalyst HH22 particles 71

Figure 4.17 Variation of catalyst composition from estimates based on reactants used 73

Figure 4.18 Particle size distribution of fresh and milled supports (a) PE981124, and (b) HayeSep-Q 76

Figure 5.1 Comparison of the temperature control performance of the new 2-L reactor to the 1 L reactor 80
Figure 5.2 Reactor details: (a) – vertical cross-section; (b) – horizontal cross-section of reactor. (CA – catalyst injector; GC – gas chromatograph; MF – mass flowmeter; MS – Magnedrive stirrer; SP – syringe pump; SY – syringe injection port; T_i – thermocouple i mounted as in Figure 5.3; V – vent) 82
Figure 5.3 Schematic diagram of reactor system. (CA – catalyst injector; GC – gas chromatograph; GP – gas purifiers; F – filter 7μ; MF – mass flow meter; MP – metering pump; MS – Magnedrive stirrer; P – centrifugal pump; PG – pressure gauge; PR – pressure regulator; PT – pressure transducer; SP – syringe pump; SY – syringe injection port; T_i – thermocouple i; V – vent) 83
Figure 5.4 Side view and top view of the 11-inch top-flange........ 85
Figure 5.5 Impellers tested in the new 2-L gas-phase polymerization reactor (a) Teflon-tipped straight anchor (b) pitched Teflon paddle (c) steel paddle... 86
Figure 5.6 Photograph of the bottom side of the top flange showing pitched anchor impeller, blade stirrers and the GC sampling valve........ 88
Figure 5.7 Profiles of polymerization activity and gas-phase composition during ethylene/1-hexene copolymerization with continuous and batch 1-hexene addition........ 91
Figure 5.8 Activity profile of the first polymerization run in the new gas-phase reactor (JM29001)........ 92
Figure 5.9 Profiles of gas-phase ethylene/1-hexene copolymerization (JM38007) without NaCl seedbed........ 95
Figure 5.10 Effect of doubling the amount of TIBA on gas-phase ethylene/1-hexene copolymerization profile 96
Figure 5.11 Comparison of ethylene homopolymerization and ethylene/1-hexene copolymerization over catalyst JM38 98
Figure 5.12 Effect of polymerization temperature on gas-phase ethylene/1-hexene copolymerization over catalyst JM29 99

Figure 5.13 Effect of ethylene feed purification and temperature control variable selection on activity profile of ethylene/1-hexene copolymerization 100

Figure 5.14 Influence of NaCl seedbed and small variation in the amount of TEAL scavenger on ethylene/1-hexene copolymerization activity profile 102

Figure 5.15 Effect of temperature controller, blade stirrer speed, and NaCl seedbed on reactor temperature control 105

Figure 5.16 Effect of reactor size and configuration on temperature control 106

Figure 5.17 Influence of rate profile on temperature controller performance 109

Figure 5.18 Inadequacy of temperature control at high polymerization rate due to limitation of coolant temperature 110

Figure 5.19 Poor reproducibility observed in gas-phase ethylene homopolymerization in the presence of residual TIBA 113

Figure 5.20 Ethylene/1-hexene copolymerization with poor reproducibility in the absence of residual TIBA 115

Figure 5.21 Ethylene/1-hexene copolymerization Run HH21210 with 0.20 mmol residual TIBA and 4.5 mL 1-hexene 117

Figure 5.22 Reproducibility runs of ethylene/1-hexene copolymerization with Catalyst HH21 in the presence of ~0.3 mmol residual TIBA. Catalyst 47–49 mg; TIBA 0.28-0.30 mmol; 1-hexene 4.6 mL 119

Figure 5.23 Reproducibility of ethylene/1-hexene copolymerizations with Catalyst HH21 in the presence of ~0.6 mmol residual TIBA. Catalyst 52–60 mg; TIBA 0.57-0.65 mmol; 1-hexene 4.6 mL 120

Figure 5.24 Ethylene/1-hexene copolymerization with differently treated seedbed and catalyst transfer salt. Catalyst 40–42 mg; TIBA 0.59 mmol; 1-hexene 4.5–4.7 mL 122

Figure 5.25 Plugs of polyethylene formed on the catalyst injector (inside the reactor).. 123

Figure 5.26 Influence of stirrer start-up on activity profile and reproducibility of ethylene/1-hexene copolymerization over Catalyst HH17 with the residual TIBA vented. Catalyst 81–83 mg; 1-hexene 4.5 mL 124

Figure 5.27 Lumps of polymer formed in the reactor due to delay in stirrer start-up after catalyst injection 125
Figure 5.28 Reproducibility of ethylene homopolymerization using 100 mg of Catalyst HH07 and the TIBA venting mode 126
Figure 5.29 Reproducibility of ethylene/1-hexene copolymerization with Catalyst HH18 127
Figure 5.30 Reproducibility of ethylene homopolymerization with Catalyst HH09 128
Figure 5.31 Influence of the amount of catalyst charged to the reactor on reproducibility 129
Figure 6.1 Effect of TIBA on ethylene/1-hexene copolymerization activity for Catalyst HH05 (1-hexene = 3.0-3.2 mL) 134
Figure 6.2 Effect of TIBA on ethylene/1-hexene copolymerization activity for Catalyst HH06 (1-hexene = 3.0 mL) 135
Figure 6.3 Effect of residual TIBA on ethylene homopolymerization activity for Catalyst HH14 at 1.4 MPa 137
Figure 6.4 Effect of residual TIBA on the activity of Catalyst HH23 at 1.4 MPa C_2H_4 138
Figure 6.5 Effect of residual TIBA on ethylene homopolymerization activity for catalyst HH09 at 1.4 MPa 139
Figure 6.6 Effect of residual TIBA and TEA on copolymerization activity for Catalyst HH14 at 1.4 MPa (1-hexene = 5.3-5.5 mL) 140
Figure 6.7 Effect of the amount of TIBA and 1-hexene on copolymerization activity for Catalyst HH19 at 1.4 MPa 142
Figure 6.8 Effect of aluminum alkyl type on copolymerization activity of Catalyst HH19 at 1.4 MPa (1-hexene = 4.3 mL) 142
Figure 6.9 Effect of TIBA amount on copolymerization activity of Catalyst HH22 at 1.4 MPa (1-hexene = 4.6-4.9 mL) 144
Figure 6.10 Effect of higher TIBA and TNOA concentration on copolymerization activity of Catalyst HH22 at 1.4 MPa (1-hexene = 4.8 mL) 145
Figure 6.11 Effect of pre-exposure of Catalyst HH16 to (trace) TIBA and the presence of N_2 on ethylene homopolymerization activity 148

Figure 6.12 Effect of pre-exposure of Catalyst HH16 to (0.28 mmol) TIBA and the presence of N_2 on ethylene homopolymerization activity 149

Figure 6.13 Effect of pre-exposure of Catalyst HH09 to (0.59 mmol) TIBA and the presence of N_2 on ethylene homopolymerization activity 150

Figure 6.14 Effect of pre-exposure of Catalyst HH09 to (trace) TIBA and the presence of N_2 on ethylene homopolymerization activity 152

Figure 7.1 Ethylene polymerization activity with poly(DVB/N-V-2-P)-supported $(n\text{-BuCp})_2ZrCl_2$/MAO catalyst in presence of trace TIBA 156

Figure 7.2 Ethylene/1-hexene (4.48 ± 0.23 mL) copolymerization activity with poly(DVB/N-Vinyl-2-pyrrolidinone)-supported $(n\text{-BuCp})_2ZrCl_2$/MAO catalyst in presence of trace TIBA 158

Figure 7.3 Ethylene/1-hexene (4.4–4.5 mL) copolymerization activity with poly(DVB/N-Vinyl-2-pyrrolidinone)-supported $(n\text{-BuCp})_2ZrCl_2$/MAO catalyst in presence of 0.20 mmol TIBA 159

Figure 7.4 Polymerization activity of poly(DVB/N-Vinyl-2-pyrrolidinone)-supported $(n\text{-BuCp})_2ZrCl_2$/MAO catalyst in presence of trace TIBA (1-hexene comonomer) 160

Figure 7.5 Ethylene/1-hexene copolymerization activity with poly(DVB/N-Vinyl-2-pyrrolidinone)-supported $(n\text{-BuCp})_2ZrCl_2$/MAO catalyst in presence of trace TIBA (run details are in Table 7.3) 162

Figure 7.6 Ethylene homopolymerization activity over poly(HEMA/DVB)-supported $(n\text{-BuCp})_2ZrCl_2$/MAO catalyst 163

Figure 7.7 Ethylene/1-hexene copolymerization activity with poly(HEMA/DVB)-supported $(n\text{-BuCp})_2ZrCl_2$/MAO catalyst in presence of 0.20 mmol TIBA 164

Figure 7.8 Kinetic profiles of ethylene homopolymerization (trace TIBA) with poly(HEMA/DVB)-supported $(n\text{-BuCp})_2ZrCl_2$/MAO catalyst 166

Figure 7.9 Rate profiles of ethylene/1-hexene copolymerization (trace TIBA) with poly(HEMA/DVB)-supported $(n\text{-BuCp})_2ZrCl_2$/MAO catalyst 166

Figure 7.10 Activity profiles of ethylene homopolymerization (trace TIBA) with poly(DVB)-supported $(n\text{-BuCp})_2ZrCl_2$/MAO catalyst 168

Figure 7.11 Activity profiles of ethylene/1-hexene copolymerization (trace TIBA) with poly(DVB)-supported (n-BuCp)$_2$ZrCl$_2$/MAO catalyst 168

Figure 7.12 Morphology of polyethylene particles (left image, whole particles; right image, cut sections) produced with poly(STY/DVB)-supported (n-BuCp)$_2$ZrCl$_2$/MAO catalyst; (a, b) Run HH29294; (c, d) Run HH29296. Scale bar = 1.2 mm 169

Figure 7.13 Activity profiles of ethylene homopolymerization (trace TIBA) with different poly(DVB)-supported (n-BuCp)$_2$ZrCl$_2$/MAO 170

Figure 7.14 Kinetic profiles of ethylene/1-hexene copolymerization (trace TIBA) with (n-BuCp)$_2$ZrCl$_2$/MAO catalysts supported on different poly(DVB) 171

Figure 7.15 Kinetic profiles of ethylene/1-hexene copolymerization (in presence of TIBA) with (n-BuCp)$_2$ZrCl$_2$/MAO catalyst supported on different poly(DVB) 171

Figure 7.16 Ethylene homopolymerization activity with polymer-supported (n-BuCp)$_2$ZrCl$_2$/MAO catalyst (trace TIBA) 172

Figure 7.17 Ethylene polymerization activity with supported (n-BuCp)$_2$ZrCl$_2$/MAO catalyst in presence of trace TIBA 174

Figure 7.18 Ethylene polymerization activity with poly(DVB/N-Vinyl-2-pyrrolidinone)-supported (n-BuCp)$_2$ZrCl$_2$/MAO catalyst in presence of trace TIBA 174

Figure 7.19 Ethylene polymerization activity over poly(DVB/N-Vinyl-2-pyrrolidinone) supported (n-BuCp)$_2$ZrCl$_2$/MAO catalyst in presence of trace TIBA 175

Figure 7.20 Influence of polymerization temperature on ethylene polymerization activity of Catalyst HH09 177

Figure 7.21 Influence of polymerization temperature on the ethylene homopolymerization activity of Catalyst HH07 in the presence of trace TIBA 178

Figure 7.22 Temperature dependence of the average polymerization activity of (n-BuCp)$_2$ZrCl$_2$/MAO catalyst heterogenized on different supports 179

Figure 7.23 Effect of temperature on ethylene/1-hexene copolymerization over poly(DVB/PEI)-supported (n-BuCp)$_2$ZrCl$_2$/MAO catalyst 179

Figure 7.24 Fit of ethylene homopolymerization data of Catalyst HH09 to Equation 7.1 at different polymerization temperatures 182

Figure 7.25 Arrhenius plots of rate constants in Equation 7.1 183

Figure 7.26 Influence of ethylene pressure on the rate profile of Catalyst HH07....... 185

Figure 7.27 Influence of ethylene pressure on the rate profile of Catalyst HH09....... 186

Figure 7.28 Influence of ethylene pressure on the rate profile of Catalyst HH23....... 186

Figure 7.29 Influence of hydrogen on the rate profile of Catalyst HH15 187

Figure 7.30 Reversible effect of hydrogen during ethylene homopolymerization activity of Catalyst HH15 188

Figure 7.31 Depletion of hydrogen in the reactor (gas phase) during ethylene homopolymerization with Catalyst HH23 190

Figure 8.1 Influence of 1-hexene on the polymerization activity of Catalyst HH10 .. 195

Figure 8.2 Influence of 1-hexene on the polymerization activity of Catalyst HH22 .. 195

Figure 8.3 Influence of 1-hexene on the polymerization activity of Catalyst HH18 .. 196

Figure 8.4 Influence of the initial amount of 1-hexene in the polymerization reactor on average activity at 80°C and 1.4 MPa (the 4.0 mL data point of Catalyst HH11 was not included in the fit because of possible irreproducibility in the run).. 197

Figure 8.5 External surface (left) and cross-section (right) morphology of polymer particles produced with Catalyst HH22 in Runs (a and b) HH22148, ethylene homopolymer; (c and d) HH22147 ethylene/1-hexene copolymer. See Table 8.1 for run details............................... 198

Figure 8.6 SEM micrographs of whole (left) and cross-sections (right) of polymer particles produced by Catalyst HH10; (a and b) ethylene homopolymer Run HH10060, and ethylene/1-hexene copolymers with (c and d) 3.9 mL and (e and f) 4.9 mL 1-hexene... 199

Figure 8.7 External surface (left) and cross-section (right) morphology of polymer particles produced with Catalyst HH18 in Runs (a and b)

HH18104, (c and d) HH18103, (e and f) HH18105, and (g and h) HH18106. See Table 8.1 for run details 200

Figure 8.8 EDX line scans (Al) across polyethylene particles reveal unfragmented catalyst cores after polymerization with (a) Catalyst HH10 for 1 h to 23.5 g/g, and (b) Catalyst HH22 for 2.9 h to 136 g/g 201

Figure 8.9 Influence of 1-hexene on the polymerization activity of Catalyst HH07 .. 203

Figure 8.10 Influence of 1-hexene on the polymerization activity of Catalyst HH17 .. 204

Figure 8.11 Influence of 1-hexene on the polymerization activity of Catalyst HH21 .. 204

Figure 8.12 SEM micrographs of external surface (left) and cross-section (right) of polymer particles produced by Catalyst HH07 in Runs (a and b) HH07049, (c and d) HH07050, and (e and f) HH07048. See Table 8.2 for run details 205

Figure 8.13 SEM micrographs of external surface (left) and cross-section (right) of polymer particles produced by Catalyst HH17 in Runs (a and b) HH17101, (c and d) HH17100, and (e and f) HH17102. See Table 8.2 for run details 206

Figure 8.14 SEM micrographs of external surface (left) and cross-section (right) of polymer particles produced by Catalyst HH21 in Runs (a and b) HH21113, (c and d) HH21115, (e and f) HH21112, and (g and h) HH21208. See Table 8.2 for run details 207

Figure 8.15 Influence of 1-hexene on the polymerization activity of Catalyst HH06 .. 209

Figure 8.16 Influence of 1-hexene on the polymerization activity of Catalyst HH08 .. 209

Figure 8.17 Influence of 1-hexene on the polymerization activity of Catalyst HH09 .. 210

Figure 8.18 SEM micrographs of external surface (left) and cross-section (right) of polymer particles produced by Catalyst HH06 in Runs (a and b) HH06047, (c and d) HH06044, and (e and f) HH06046. See Table 8.3 for run details 211

Figure 8.19 SEM micrographs of external surface (left) and cross-section (right) of polymer particles produced by Catalyst HH08 in Runs (a and b) HH08054, (c and d) HH08052, and (e and f) HH08073. See Table 8.3 for run details 212

Figure 8.20 SEM micrographs of external surface (left) and cross-section (right) of polymer particles produced by Catalyst HH09 in Runs (a and b) HH09057, (c and d) HH09056, and (e and f) HH09072. See Table 8.3 for run details 213

Figure 8.21 Morphology of cross-sections of ethylene homopolymer particles produced with Catalyst HH07 in Runs (a and b) HH07283 at 60°C, (c and d) HH07237 at 80°C, and (e and f) HH07293 at 100°C gas-phase temperature 216

Figure 8.22 Morphology of cross-sections of ethylene/1-hexene copolymer particles produced with Catalyst HH18 in Runs (a and b) HH18288 at 70°C, (c and d) HH18291 at 80°C, and (e and f) HH18287 at 90°C gas-phase temperature 217

Figure 8.23 Morphology of ethylene homopolymer particles (cross-sections) produced with Catalyst HH07 in Runs (a and b) HH07253 at 1.4 MPa, (c and d) HH07251 at 2.1 MPa, and (e and f) HH07252 at 2.8 MPa ethylene, and 80°C gas-phase temperature 218

Figure 8.24 External surface morphology of ethylene homopolymer particles produced at 1.4 MPa and 80°C with Catalysts (top) HH18 100g/g, (center) HH17 230 g/g, and (bottom) HH21 210g/g 220

Figure 8.25 Morphology of the high friability (a and b) support –PE9023, and (c and d) the corresponding catalyst HH06 222

Figure 8.26 Morphology of Catalyst HH10 particles after 1 min copolymerization (Run HH10120). Arrow shows the section of micrograph (a) magnified in (b) 224

Figure 8.27 Morphology of Catalyst HH10 particles after 10 min copolymerization (Run HH10119). Arrow shows the section of micrograph (a) magnified in (b) 225

Figure 8.28 Morphology of Catalyst HH10 particle after 1.75 h copolymerization (Run HH10121). Arrow shows the section of micrograph (a) magnified in (b) 226

Figure 8.29 Morphology of ethylene/1-hexene copolymers of (a) Group-1 and (b) Group-2 catalysts, and the homo- and copolymer of Group-3 catalysts (c and d respectively) showing the globular structure 227

Figure 8.30 Effect of comonomer on the polymerization activity of Catalyst HH21 (total pressure ≈1.4 MPa) 230

Figure 8.31 Effects of propylene on ethylene/propylene copolymerization activity of Catalyst HH15 (total pressure ≈1.4 MPa)................................. 231

Figure 8.32 Influence of propylene on polymer particle morphology (a and b) Run HH15095, no comonomer; (c and d) Run HH15192, 5 mol % C_3H_6; (e and f) Run HH15193, 16 mol % C_3H_6 232

Figure 8.33 Morphology of ethylene/propylene copolymer particles produced with Catalyst HH26 in Run HH26194 (a) external surface, and (b) cross-section 233

Figure 8.34 Influence of 1-hexene and 1-decene on the activity of Catalyst HH15 at 80°C and 1.4 MPa 234

Figure 8.35 Influence of comonomer on particle morphology (a) Run HH15093, 3.2 mol% 1-hexene, (b and c) Run HH15162, 3.7 mol% 1-decene. Scale bar = 1.2 mm 235

Figure 8.36 Proposed fracture mechanism of low and high friability polymer-supported metallocene/MAO catalyst particles during gas-phase olefins polymerization.. 236

Figure 9.1 External surface (left) and cross-section (right) morphologies of ethylene/1-hexene copolymer particles produced in (a and b) Run HH19123, (c and d) Run HH19125, and (e and f) Run HH01015. Scale bar = 1.2 mm 240

Figure 9.2 Optical images of the three size-groups of ethylene homopolymer particles produced with Catalyst HH09 at 80°C gas-phase temperature and (a-c) 0.7 MPa, (d-f) 1.4 MPa, (g-i) 2.1 MPa, and (j-l) 2.8 MPa ethylene. Scale bar = 1.0 mm 241

Figure 9.3 Influence of particle size and ethylene pressure on molar masses of polyethylenes produced with Catalyst HH09 (80°C, trace TIBA) 242

Figure 9.4 Comparison of particle size distribution of Support PE971124 to polyethylene produced at different yields and ethylene pressures (for support ordinate is cumulative volume fraction) 244

Figure 9.5 Influence of ethylene concentration on number average chain length 245

Figure 9.6 Dependence of polymer molar mass on the polymerization temperature (● = M_w and ○ = M_n) 247

Figure 9.7 Influence of hydrogen on the molar masses of ethylene homopolymers produced with Catalyst HH23 at 80°C and 2.76 MPa (400 psi) reactor pressure 249

Figure 9.8 Effect of 1-hexene on the distribution of molar masses of ethylene/1-hexene copolymers (Catalyst HH29, swellable STY/1%-DVB support) at 80°C and 1.4 MPa 251

Figure 9.9 Influence of 1-hexene on the molar masses of ethylene/1-hexene copolymers produced by Catalyst HH29 (swellable STY/1%-DVB support) at 80°C and 1.4 MPa (○ = M_0/M_w; ● = M_0/M_n) 252

Figure 9.10 TREF profiles of ethylene homopolymer and ethylene/1-hexene copolymers produced with Catalyst HH18 at 80°C and 1.4 MPa (Repeat analyses shown for each sample) 254

Figure 9.11 Dependence of C_N on the total polymer yield for (n-BuCp)$_2$ZrCl$_2$/MAO catalysts supported on different low friability commercial supports (solid symbols) and high friability in-house support (open symbols) 256

Figure 9.12 TREF profiles of different parts of a polymer particle produced with Catalyst HH14 (Run HH14131: 80°C, 4.6 mL 1-hexene, 1.4 MPa) 257

Figure 9.13 TREF profiles of ethylene/1-hexene copolymers showing the homopolymer peak (profiles were off set for clarity) 258

Figure 9.14 TREF profiles of ethylene/propylene and ethylene/1-decene copolymers produced with Catalyst HH15 259

Figure 9.15 Enhancement of 1-hexene incorporation at low polymerization temperature 260

List of Nomenclature and Abbreviations

Nomenclature

$[M]$	monomer concentration
C^*	concentration of active site
C_d	concentration of deactivated sites
C_m	monomer concentration
C_N	average concentration of short chain branches
K	equilibrium constant
k_c	rate constant for transition from site type I to site type II
k_d	deactivation rate constant
k_i	initiation rate constant
k_{obsd}	observed polymerization rate constant
k_p	propagation rate constant
k_{tm}	rate constant for chain transfer to monomer
M_0	molar mass of monomer
M_n	number average molar mass
M_w	mass average molar mass
P	pressure
r_n	chain length (M_n/M_0)
R_{pmax}	maximum polymerization activity
t_{Rmax}	time taken to attain maximum polymerization activity
θ	parameter (product) of initial number of active sites, propagation and equilibrium rate constants

Abbreviations

AIBN	2,2'-azobisisobutyronitrile
AN	acrylonitrile
CCD	chemical composition distribution
DC	direct current
DEAC	diethylaluminum chloride
DVB	divinylbenzene
EA	ethylacrylate
EDX	energy dispersive X-ray analysis
EGDM	ethyleneglycoldimethacrylate
GC	gas chromatograph
GPC	gel permeation chromatograph
HDPE	high-density polyethylene
HEMA	2-hydroxyethylmethacrylate
INAA	instrumental neutron activation analysis
IPRA	isoprenyl aluminum
LDPE	low density polyethylene
LLDPE	linear low-density polyethylene
MAO	methylaluminoxane
MGM	multigrain model
MMAO-4	modified methylaluminoxane type-4
NAA	neutron activation analysis
NMR	nuclear magnetic resonance (analysis)
N-V-2-P	N-vinyl-2-pyrrolidinone
NVP	N-vinylpyrridine
PE	polyethylene
PEI	polyethyleneimine
PP	polypropylene
PS4VPy	poly(styrene-co-4-vinylpyridine)
PSAm	poly(styrene-co-acrylamide)

PTMA	pentaerythritoltrimethacrylate
PTMG	polytetramethylene (ether) glycol
SEC	size exclusion chromatography
SEM	scanning electron microscopy
SLOWPOKE	Safe LOW POwer Kritical Experiment
STY	styrene
TEA	triethylaluminum
TIBA	triisobutylaluminum
TMA	trimethlaluminum
TNOA	tri-*n*-octylaluminum
TREF	temperature rising elution fractionation
4-V-Py	4-vinyl-pyridine

1. Introduction

The global demand for commodity polyolefins (polyethylenes, PE, and polypropylenes, PP) is over 80 million tons annually and PE accounts for over 60% of this demand (Robinson, 2001). Technological advances in catalysts and process developments have continued to expand the versatility of these commodity plastics, making it possible to replace traditional materials that are more difficult to manufacture or less environmentally friendly (Kaminsky and Laban, 2001; Böhm, 2003). As a result, the markets for polyethylenes and polypropylenes have increased nearly 6% and 10% annually in the past two decades (Trautz, 2002).

Polyethylenes are broadly classified into high-density polyethylene, HDPE, linear low-density polyethylene, LLDPE, and low-density polyethylene, LDPE, according to the microstructure of the polymer molecules; the microstructure is closely related to the polymer density. HDPE are linear ethylene homopolymers with few or no short-chain branches. LLDPE are linear polyethylenes with many short-chain ranches introduced by incorporation of α-olefin comonomers. LDPE molecules are characterized by statistical distribution of short and long chain branches formed by inter- and intramolecular radical transfer reactions (Klimesch *et al.*, 2001).

High-pressure free radical processes at 120 to 300 MPa and 130 to 350°C are used to produce LDPE, while the HDPE and LLDPE are commercially produced using transition metal catalysts in solution, slurry, or gas-phase processes at milder conditions. Low-pressure gas-phase processes (3.0–3.5 MPa, 80–100°C) using Ziegler-Natta catalysts are mainly used to produce the LLDPE, HDPE, and PP (Xie *et al.*, 1994). Polyethylene properties are determined by molar mass, molar mass distribution, and the nature, amount and distribution of chain branching (chemical composition distribution, CCD). These parameters define the end use application of the polymer, and they are adjusted by catalyst design and polymerization conditions.

High activity metallocene/methylaluminoxane (MAO) catalyst systems for olefin polymerization were serendipitously discovered in Kaminsky's laboratory in the late 1970s. This discovery sparked tremendous research activity that resulted in the synthesis and test of many new metallocenes, for example the research group of Helmult G. Alt alone synthesized and tested more than 600 different metallocenes in one decade (Alt, 1999). The new single-site (metallocene/MAO) catalyst systems are more active and offer better control of polymer microstructure than the conventional Ziegler-Natta catalysts.

Metallocene/MAO systems proved to be super active [up to $3 \cdot 10^5$ kg PE/(g Zr·h); Alt, 1999] only in the homogeneous phase and in the presence of very high MAO (cocatalyst) concentrations, typically aluminum to metallocene molar ratios of about 10^4. This large MAO requirement impacts negatively on both the process economics and product properties. In addition, homogeneous systems are characterized with reactor fouling/instability, costly solvent removal step and poor product morphology control; therefore, the homogeneous metallocene/MAO systems are unsuitable for industrial processes. Commercial gas-phase or slurry polyolefin processes require the use of solid catalysts.

For stable reactor operation and ease of post-reactor product handling it is essential to control the morphology of the nascent polyethylene particles to obtain spherical polymer granules with the desired size, high pourability, high bulk density, and narrow particle size distribution. Controlling the nascent polymer morphology eliminates the need for a pelletization step in the manufacture of polyolefins (Covezzi, 1995). The pelletization step is one of the most energy intensive steps in polymer plants (Muñoz-Escalona, 1984); this step accounted for more than half of the total power required to produce 1 ton of granulated polyethylene homopolymer in a fluid bed reactor process (Mills, 1993).

Considerable research efforts have been directed towards supporting metallocenes on catalyst carriers in order to reduce the MAO requirement, adapt the catalyst to the existing gas-phase and slurry processes, and to improve the product morphology. Silica, alumina, and magnesium compounds are commonly reported inorganic supports; the use of these supports obviously stems from their success in Ziegler-Natta and Phillips-type chromium catalysts. Organic materials, natural and synthetic polymers have been investigated to a lesser extent even though these present environments that are much closer to the homogeneous systems than the inorganic oxides.

Prior work by other investigators on polymer supported metallocene and Ziegler-Natta catalysts focused on chemically binding the metallocene to support surfaces, in most cases involving in situ synthesis of the metallocene on the support. In addition, all the catalysts were tested in slurry polymerizations often with a large amount of additional MAO added to the slurry process prior to polymerization. Most researchers only report average polymerization activity, which gives very limited information on the polymerization kinetics. There is an obvious dearth of information on metallocene/MAO catalysts supported on porous polymer beads and their use in gas-phase ethylene/α-olefins polymerization.

Preliminary investigations on supporting metallocene/MAO catalyst on porous polymeric supports in our laboratory revealed a great potential for this class of supports in immobilizing metallocene/MAO catalysts especially for gas phase polymerization; high polymerization activity and excellent morphology replication from the catalyst to polymer particles were achieved (Zhou *et al.*, 2003). However, the preliminary investigations only considered poly(2-hydroxyethylmethacrylate) cross linked with divinylbenzene (DVB) as support particles. The effects of chemical structure and morphology of support were not investigated although these could affect the catalyst performance. In addition, the gas-phase polymerizations in the preliminary work were conducted in a one-liter steel reactor immersed in a constant temperature bath for reactor temperature control. The high polymerization activities obtained made reactor temperature control inadequate; hence, large temperature excursions were observed rendering the obtained polymerization rate data unsuitable for kinetic studies.

The objective of this thesis work was, therefore, to design, fabricate, and test a new gas-phase polymerization reactor with improved temperature control capability, and to investigate the effects of chemical and morphological properties of polymeric supports (such as functional group types, cross link types, porosity, and fragility) on the performance of supported (*n*-BuCp)$ZrCl_2$/MAO catalysts in gas-phase polymerization. The performance criteria included the polymerization activity of the supported catalysts, as well as the particle morphology, and the microstructure of the resulting ethylene homopolymers and ethylene/α-olefin copolymers.

Details of the chemical composition of the polymeric supports, the catalyst preparation procedure, and the polymerization procedure are presented in Chapter 3. The characterization and analyses procedures for the polymeric supports, supported catalysts, and polyolefin products employed in this work are also presented in the chapter.

Chapter 4 discusses the morphological properties of the polymeric supports and the supported catalysts. The effect of MAO loading on the surface area, and pore size/pore size distributions is also discussed. The loading and radial distribution of aluminum and zirconium in some selected catalysts is presented, and the discrepancy between expected and measured catalyst compositions are discussed. Finally, the friability (fragility) and swellability of some selected in-house and commercial polymeric supports are presented.

In Chapter 5, the newly fabricated polymerization reactor and the associated systems for temperature control, gas-purification, catalysts injection, and the online gas sampling/analysis are described in detail. The following are also discussed in this chapter: the first part of the exploratory polymerization runs performed in the new reactor, the influences of static mixers, stirring, and sodium chloride seedbed on the new reactor performance. Finally, results of an extensive investigation of reproducibility of gas-phase polymerization in the new reactor are presented.

Aluminum alkyls are used as cocatalyst and impurity scavengers in Ziegler-Natta or metallocene/MAO catalyzed olefin polymerizations. However, the presence of excess amounts of aluminum alkyls could poison the active sites and alter the polymerization kinetics. The second part of the exploratory polymerizations focuses on the effects of aluminum alkyl types and concentration on polymerization rates and product properties. The effect of contact mode of catalyst, aluminum alkyl, and monomer in the polymerization milieu is also presented in the chapter. The experiments presented in

Chapters 5 and 6 were used to establish suitable operating conditions for subsequent polymerization studies.

The influence of physicochemical properties of the supports on the polymerization activity of the supported catalysts is presented in Chapter 7. As a prelude to the interpretation of the above influence, the effect of typical variations of aluminum and zirconium loadings are discussed first. The effects of polymerization temperature, monomer pressure, and hydrogen on polymerization rates are also discussed in Chapter 7. Ethylene homopolymerization rate profiles for some selected catalysts are fitted to a semi empirical kinetic model.

α-Olefin comonomers have profound effects on both polymerization activity and product morphology in the gas-phase polymerization of ethylene over the supported catalysts. The influence of comonomer type and concentration on these parameters is presented in Chapter 8. Based on SEM observations of the nascent polymer particles morphology, the above comonomer influences are related to the support fragility.

The effects of support and polymerization conditions on the nascent morphology and the microstructure of the produced polyolefins are discussed in Chapter 9. These include the effects of ethylene pressure, 1-hexene concentrations, polymerization temperature, and the amount of hydrogen on polymer molar masses and polydispersity indices. The effect of catalyst particle size on molar mass of ethylene homopolymer, and the results of comonomer incorporation as determined by temperature rising elution fractionation were also investigated. Finally, a summary of the findings of this work and the recommendations for future work are presented in Chapter 10.

2. Literature Review

Metallocenes in combination with aluminum alkyls such as TMA, and DEAC, were known to catalyze olefins polymerization since the 1950s (Alt, 1999). However, it was the discovery of MAO that led to the realization that metallocene/MAO systems are highly valuable for both scientific research and industrial application. The high potential value of metallocenes in commercial polyolefins production resulted in tremendous research efforts that generated a large volume of scientific data in this field. No attempt was made in the current study to review all the aspects of olefin polymerization catalysis by metallocenes.

The literature review in this chapter is mainly centered on heterogeneous (i.e., supported) metallocene/MAO catalysts with special attention to polymeric supports, gas-phase polymerization, and to relevant aspects of Ziegler-Natta catalysts. In addition, the laboratory scale reactors and the experimental procedures used in gas-phase and slurry polymerizations were also reviewed since this thesis work involved the design and fabrication of a new gas-phase polymerization reactor. However, a brief overview of homogeneous systems is pertinent.

2.1 Homogeneous metallocene/MAO catalyst systems

The current interest in metallocene catalysts originated from the super high activity of metallocenes in ethylene and α-olefins polymerization when combined with MAO as cocatalyst in the homogeneous phase.

2.1.1 Roles of MAO

Despite the importance of MAO, its structure is not fully understood; however, several investigations reveal that MAO is an oligomeric compound consisting of aluminum, oxygen, and methyl groups. The aluminum and oxygen atoms are alternately bonded while the methyl groups saturate the free valences (Kaminsky, 1998). Sinn (1995) suggested a basic building unit of [$Al_4O_3Me_6$] which join together through the unsaturated aluminum atoms to form clusters and cages (see Figure 2.1) of molar mass 1200–1600 Da. MAO is also believed to consist of different $(AlOMe)_n$ oligomers in multiple equilibria, some of these oligomers are inactive as cocatalysts towards metallocenes. Zurek and Ziegler (2003) suggested seven active forms of MAO oligomers all of which contain strained Lewis acidic bonds.

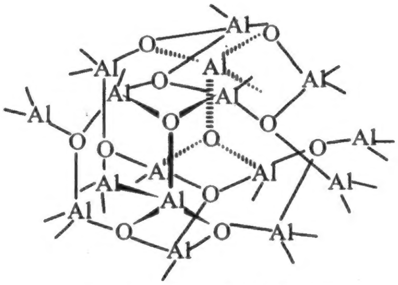

Figure 2.1 Cage structure of methylaluminoxane MAO

Several investigators have concluded that in olefin polymerization catalysis by metallocene/MAO, the MAO first methylates the metallocene by a fast ligand exchange followed by abstraction of a halide (X^-) or CH_3^- ion to form the active metallocenium cation having a vacant coordination site as shown below (Kaminsky, 1996).

$$Cp_2ZrCl_2 + MAO \rightarrow Cp_2Zr(Me)Cl \rightarrow Cp_2Zr^+(Me) + [MAO{\cdot}Cl]^-$$

$$Cp_2Zr(Me)_2 + MAO \rightarrow Cp_2Zr^+(Me) + [MAO{\cdot}Me]^-$$

Other reagents can also be used to generate the active species (see Britovsek *et al.*, 1999). The ligand exchange is believed to take place with the free TMA that is always present in MAO (Barron, 2000). In addition, MAO serves to stabilize the metallocenium cation and scavenge impurities e.g. O_2, and moisture according to the following reactions:

$$\mathrm{MAO(TMA)} + \mathrm{H_2O} \rightarrow 1/n[\mathrm{(Me)Al(O)}]_n + 2\mathrm{CH_4}$$

$$\mathrm{MAO(TMA)} + \mathrm{O_2} \rightarrow 1/n[\mathrm{Me_2Al(OMe)}]_n$$

$$\mathrm{MAO(TMA)} + \mathrm{HCl} \rightarrow \tfrac{1}{2}[\mathrm{Me_2Al(\mu\text{–}Cl)}]_2 + \mathrm{CH_4}$$

Trialkyl aluminums, being strong Lewis acids, also interact with metallocenes to form complexes that are inactive in olefin polymerization for example (Barron, 2000):

$$\mathrm{Cp_2ZrX_2} + \mathrm{Al(^{\it i}Bu)_3} \rightarrow \mathrm{Cp_2Zr(X)[\,\mu\text{–}X\ Al(^{\it i}Bu)_3]}; \quad X = \mathrm{Cl^-}, \mathrm{Me^-}$$

Therefore, it is essential to have an optimum amount of TMA in MAO for good catalytic activity and sufficient capacity to scavenge impurities.

2.1.2 Roles of ligand substituents

The versatility of metallocenes in ethylene/α-olefins polymerization lies in the possibilities of varying the ligands sandwiching the metal center. Figure 2.2 shows structures of several metallocene compounds that are active in ethylene/α-olefin polymerization. The ligand substituents influence the catalytic activity, polymer molar mass, comonomer incorporation, and stereoregularity (for polymerization involving prochiral monomers) of metallocenes through a balance of electronic and steric effects on the metal center. The effects of ligand substituents have been studied in detail (Karol and Kao, 1994; Karol *et al.*, 1997; Piccolrovazzi *et al.*, 1990; Lee *et al.*, 1992; Spaleck *et al.*, 1994).

2.2 Supported Metallocene/MAO Catalysts

Metallocene/MAO catalysts are immobilized on solid carriers to minimize the problems of homogeneous systems (see Chapter 1). Inorganic supports such as silica, alumina, and $MgCl_2$ are the predominant supports used for metallocene/MAO systems because they are the common supports for Ziegler-Natta and Phillips (chromium) catalysts; however, polymeric supports have also been investigated lately (see below).

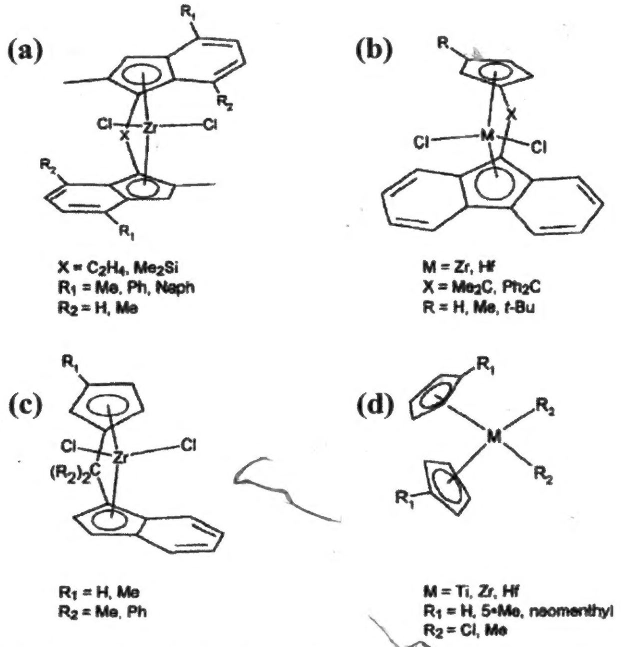
(a)
R1
R2
Cl
X
Zr
Cl
R2
R1
X = C2H4, Me2Si
R1 = Me, Ph, Naph
R2 = H, Me
(b)
R
X
Cl
M
Cl
M = Zr, Hf
X = Me2C, Ph2C
R = H, Me, t-Bu
(c)
R1
Cl
Zr
Cl
(R2)2C
R1 = H, Me
R2 = Me, Ph
(d)
R1
R2
M
R2
R1
M = Ti, Zr, Hf
R1 = H, 5-Me, neomenthyl
R2 = Cl, Me

Figure 2.2 Bridged and unbridged metallocenes active in olefins polymerization in the presence of MAO (Kaminsky, 1996). Metallocene type (d) with R_1 = *n*-C_4H_9, and R_2 = Cl was used in this thesis work.

Although only polymeric supports were used in this work, the relevant aspects of both organic and inorganic supports are reviewed due to the similarity in the employed heterogenization procedure.

2.2.1. Supporting methods

Most of the methods used to support metallocenes especially on inorganic carriers can be categorized into the following three groups (Ribeiro *et al.*, 1997):

1. Direct immobilization by contacting the support with the precursor solution (e.g., see Rahiala *et al.*, 1999; Costa Vaya *et al.*, 2001). The metallocene may react with functional groups on the supports (e.g. –OH groups on silica) to form anchored

metallocene species that are inactive in olefin polymerization (Collins *et al.,* 1992). Therefore, the support is often passivated by reaction with organometallic compounds e.g. Al alkyls prior to metallocene adsorption (Moroz *et al.*, 1998). Metallocenes immobilized on the support using this method are activated by MAO treatment.

2. The support is first impregnated with MAO or aluminum alkyls followed by the reaction with metallocene. The MAO is adsorbed from a solution (Ribeiro *et al.*, 1997) or made in situ by reacting aluminum alkyls with adsorbed water on the support (Meshkova *et al.*, 2000). In this method the metallocenes generally do not interact with the support due to the organoaluminum layer separating the two. The immobilized metallocene just 'floats' on the MAO; hence, these catalysts resemble the homogeneous ones (e.g., see Collins *et al.*, 1992 and Kaminsky and Renner, 1993). High reactivity of the organoaluminum compounds limits the effect of heterogenization conditions, such as contact time and temperature, on the performance of supported catalysts prepared using this procedures, e.g., see Meng *et al.* (1999).
3. The third method involves tethering aryl ligands of the metallocene to the support followed by reaction with a transition metal salt to form a chemically bound metallocene to the support surface (Bortolussi *et al.*, 2002; Hlatky, 2000). This method involves cumbersome synthetic steps that generate significant amounts of impurity in the support matrix that could be difficult to extract (Roscoe *et al.*, 2000).

2.2.2. Polymer-supported metallocene/MAO catalyst

Most of the polymer-supported metallocene/MAO catalyst investigations focused on the third method above because the method can be finely controlled on polymeric supports. The nature and distribution of the anchoring groups on polymeric supports are more amenable to control than the sites on inorganic supports. Table 2.1 summarizes the key features of polymer-supported metallocene catalysts.

Table 2.1 Key features of polymer-supported metallocene catalysts in the literature

Support*	Catalyst	Key features and reference
Poly(STY/2%-DVB)	$(Ind)_2ZrCl_2$; 0.02-0.20 mass% Zr	Very low activity due to support influence, Nishida *et al.* (1995).
Poly(STY/2%-DVB)	Cp_2TiCl_2;	Tethering the titanocene with 17-atom long spacer produced catalyst resembling homogeneous one; Barrett and de Miguel (1998).
Amine-functionalized poly(STY/1%-DVB)	$(C_5HMe_4)_2HfMe_2/[B(C_6F_5)_4^-]$; 2.5-13.7 mass % Hf	Catalyst immobilized by coordination interaction between N on support and the Hf. Choice of diluent and polymerization condition critical in preventing catalyst leaching; Roscoe *et al.* (1998).
Poly(4-vinylpyridine/ 2%-DVB)	$Cp_2ZrMe_2/[B(C_6F_5)_4^-]$; 0.76 mass % Zr	Use of functional monomer and higher crosslink density support improved catalyst immobilization over the work of Roscoe et al. above; Musikabhumma *et al.* (2000).
Poly(STY/acrylamide/ 5%-DVB)	Cp_2ZrCl_2/MAO	Some reactive functional groups of the support were inaccessible to MAO; Liu *et al.* (1999).
Crosslinked polystyrene	Cp_2ZrCl_2/MAO	Metallocene-attached soluble polymer was crosslinked by Diels-Alder reaction to form supported catalyst; Stork *et al.* (1999).
Cross-linked poly(styrene-co-4-vinylpyridine),	Cp_2ZrCl_2	Crosslink density and 4-vinylpyridine content of support increased activity per mole Zr; only the 4-vinylpyridine content increased the Al and Zr loading on catalyst; Meng *et al.* (1999).
Reversibly cross-linked polystyrene	$Me_2Si(2\text{-}MeBenzInd)_2ZrCl_2$/ MAO	Reversibly (not DVB) crosslinked support improved catalyst fragmentation. Koch *et al.* 2000; 2001.
Polyethylene	$[C_{13}H_8C(Me)(C_4H_7)C_5H_3{}^tBu]ZrCl_2$	Metallocene catalysts with olefin/alkyne function were copolymerized with ethylene to form supported catalyst. Alt, 1999.
Poly(HEMA/ DVB)	$(n\text{-}BuCp)_2ZrCl_2$/-MAO	Porous support beads impregnated with MAO then metallocene; Zhou *et al.* 2003.
MAO-diol adduct	Cp_2ZrCl_2/MAO	Metallocene supported on porous MAO-1,6-hexanediol and MAO-1,6-decanediol adducts; Janiak *et al.* (1993).
Poly(DVB/STY/ EA/AA)	Cp_2ZrCl_2/MAO	Porous support beads impregnated with MAO then metallocene; Qin *et al.* (2003).

* STY = styrene; EA = ethylacrylate; AA = acrylic acid; HEMA = 2-hydroxyethylmethacrylate

Polymeric supports have also been used as carriers for Ziegler-Natta catalysts to exploit the excellent support morphology but these have not gained industrial acceptance. This could be due to low activity (Ran, 1993), low bulk density (Mix *et al.*, 1990) or lengthy preparation steps often involving support functionalization. Sun *et al.* (1994a) prepared high activity poly(ethylene-co-acrylic acid)-supported $TiCl_4/n\text{-}Bu_2Mg$ catalyst; the support powder was obtained after continuously ball milling the polymer in anhydrous heptane for 5 days. The activity profiles are mostly non-decay type in 1-2 h polymerization runs (Sun *et al.*, 1994b; Mteza *et al.*, 1996).

2.2.3. Effects of supporting metallocene/MAO on solid carriers

Supporting metallocene/MAO catalysts on solid carriers influence, to varying degrees, the polymerization activity of the catalysts, the product morphology and the microstructure of the resulting polyolefins. This influence is contributed to by the chemical structure and pore size of the support, and by the heterogenization procedure.

2.2.3.1. Effect of heterogenization on activity

Immobilizing metallocene/MAO systems on solid carriers is normally accompanied by a decrease in catalytic activity. The cause of this activity drop is not well understood (Rahiala *et al.*, 1999) but various explanations have been given, the classic ones relate to reduced access of monomer to the active sites due to geometric restrictions (van Looveren *et al.*, 1998; Michelotti *et al.*, 1998) and deactivation of some metal centers during the immobilization (Braca *et al.*, 1996), i.e. low ratio of active to total Zr centers (Chien, 1999). Woo *et al.* (1995) proposed that low probability of entrapment of both zirconocene and MAO in the same supercage of NaY zeolite is a possible cause of low activity while Harrison *et al.* (1998) attributed the lower activity of supported metallocene/MAO catalyst to a decrease in propagation rate.

Supported metallocene/MAO catalysts usually exhibit lower activities than the homogeneous ones; however, the former often exhibit more stable kinetic profiles that could lead to higher average activities (Braca *et al.*, 1996). The stability of supported catalysts is partly due to the same geometric restriction that lowers the polymerization activity. The small and regular pores of MCM-41/MAO/Et(Ind)$_2$ZrCl$_2$ catalyst suppressed the formation of the inactive homodinuclear (Zr–Zr) and heterodinuclear (Zr–Al) complexes resulting in non-decay type kinetic profiles for propylene polymerization (Ko *et al.*, 1996).

Table 2.2 gives a spectrum of polymerization conditions and activities of some supported metallocene catalysts. It is difficult to make meaningful comparison of the performance of different catalysts from different research groups due to the strong influence of catalyst preparation, and polymerization conditions on the polymerization activity. For example, normalizing the activities of two catalysts (tested at different monomer pressures) with respect to monomer concentration may not be a sufficient basis for ranking the catalysts. Monomer concentration may affect the activities of the catalysts differently due to other factors such as catalyst fragmentation. Nonlinear (Xu *et al.*, 2001; Pasquet and Spitz, 1993) and even slightly negative (Chung *et al.*, 2002) dependences of activity on monomer pressure have been reported. There are relatively few studies involving gas-phase polymerization. In addition to Table 2.2, the research groups of Ray, and Westerterp are also involved in gas-phase studies with supported metallocene/MAO catalysts, e.g., see Chakravarti and Ray (2001) and Roos *et al.* (1997), respectively.

Table 2.2 Typical test conditions and activities of supported metallocene catalysts in ethylene homopolymerization.

Support	Catalyst/Cocatalyst	[Mt]^a	Al:Zr	Test Conditions	R_p^{b}	Reference
None	$Et(Ind)_2ZrCl_2/MAO$	23	610	Gas-phase, 50°C, P_{Pr}=5 bar, 2 h	2200	Tsutsui and Kashiwa, 1991
SiO_2	Cp_2ZrCl_2/MAO	NA	NA	Toluene, 40°C, 1 h	1550	Soga *et al.* 1993
$MgCl_2$	Cp_2TiCl_2/MAO	NA	500	Xylene, 40°C, 1 h	141	Sarma *et al.*, 1994
SiO_2	$(n\text{-}BuCp)_2ZrCl_2/MAO$	10	870	n-C_6, TEAL, 70°C, P_{Et}=4 bar, 1 h	5700	Kamfjord *et al.*, 1998
HY Zeolite	$Et(Ind)_2ZrCl_2/MAO$	NA	2000	Toluene, 20°C, 1 h, P_{Et}=5 bar, 1-C_6	1390	Michelotti *et al.*, 1998
Polystyrene	$(C_5HMe_4)_2HfMe_2/PFB^c$	240	-	n-C_6, 40°C, P_{Et}=5 bar, 1-$C_6^=$	3210	Roscoe *et al.*, 1998
Sol-gel Al_2O_3	$Et(Ind)_2ZrCl_2/MAO$	0.6	640	n-C_6, 75°C, 1 h, P_{Et}=5 bar, 1-C_6	144000	Harrison *et al.*, 1998
SiO_2	$Cp_2ZrCl_2/MAO/B(C_6F_5)_3$	480	50	Toluene, 70°C, 1 h, P_{Et}=5 bar, ½ h	10600	Tian *et al.*, 1999
SiO_2	$(n\text{-}BuCp)_2ZrCl_2/MAO$	40	3000	Toluene, 70°C, P_{Et}=1 bar, ½ h	410	dos Santos *et al.*, 1999a
PS4VPy^d	Cp_2ZrCl_2/MAO	47	400	Toluene, 50°C, P_{Et}=1.4 bar	1230	Meng *et al.*, 1999
Polystyrene	Cp_2ZrCl_2/MAO	100	1500	i-Bu, 70°C, P_{Et}=40 bar	5300	Stork *et al.*, 1999
PSAm^e	Cp_2ZrCl_2/MAO	45	2500	Toluene, 50°C, P_{Et}=1.4 bar, 1 h	2810	Liu *et al.*, 1999
PS4VPy^d	Cp_2ZrMe_2/PFB	83	40	n-C_6, 60°C, P_{Et}=5 bar, 1-$C_6^=$	1081	Musikabhumma *et al.*, 2000
Polystyrene	MSBI/MAO^f	44	840	n-C_6, 50°C, P_{Pr}=4 bar, ½ h	33100	Koch *et al.*, 2000
SiO_2	$(n\text{-}BuCp)_2ZrCl_2/MAO$	93	2500	Toluene, 60°C, P_{Et}=1.6 bar, ½ h	2000	Galland *et al.*, 1999
SiO_2	$(n\text{-}BuCp)_2ZrCl_2/MAO$	22	330	Toluene, 20°C, TIBA, P_{Et}=2 bar, 5/6 h	1700	Goretzki *et al.*, 1999
SiO_2	$(n\text{-}BuCp)_2ZrCl_2/MAO$	20	200	Gas-phase, 80°C, P_{Et}=4.5 bar, 1 h	1000	Kallio *et al.*, 2001
Polystyrene	$Me_2Si[Ind]_2ZrCl_2/MAO$	19	10000	Gas-phase, 80°C, P_{Et}=4 bar	15220	Chung and Hsu, 2002
Poly(HEMA/DVB)	$(n\text{-}BuCp)_2ZrCl_2/MAO$	34	185	Gas-phase, 80°C, P_{Et}=14 bar	1765	Zhou *et al.*, 2003

a – Metal loading, μmol/g-cat (μmol/g-SiO_2 for Galland e al.); b – Activity, kg PE/(mol Metal·h); c – PFB=$[B(C_6F_5)_4^-]$; d – Poly(styrene-*co*-4-vinylpyridine); e – Poly(styrene-*co*-acrylamide) f – MSBI = $Me_2Si(2\text{-}MeBenzInd)_2ZrCl_2$; NA – Not available

2.2.3.2. Effect of heterogenization on product morphology

Generally, for low to moderate activity systems, the polyolefin product particles replicate the catalyst to produce granular and free-flowing product in both slurry and gas-phase polymerizations (e.g., see, Nishida *et al.*, 1995; Ko *et al.*, 1996; Roscoe *et al.*, 1998; Koch *et al.*, 2000; Liu *et al.*, 2001). However, even under these conditions, catalyst leaching in slurry polymerizations (Tait *et al.*, 2000), or the use of unsuitable template (e.g., needle-like) morphology hinders the replication process (Ko *et al.*, 1996). With proper support and polymerization conditions, good morphology could be obtained even at relatively high polymerization activity (Zhou *et al.*, 2003).

Poor morphologies have been reported for gas-phase and slurry polymerizations in which high activities were attained rapidly (Harrison *et al.*, 1998); these polymerizations were also associated with poor temperature control. In such instances, the increased reactor temperature causes the softening or partial dissolution of the polymer product. The rapid initial activity could also cause early disintegration of catalyst particles resulting in ill-defined product particles smaller than the initial catalyst (Roscoe *et al.*, 2000; Muñoz-Escalona *et al.*, 1984).

2.2.3.3. Effect of heterogenization on polyolefin properties

Like the polymerization activity and product morphology, heterogenization affects the polyolefin properties such as molar mass and crystallinity (comonomer incorporation) relative to homogenous product. These effects originate either from the change in the electronic/steric environment at the active center or the geometry of the confining walls of the support. Steric hindrance was thought to decrease the chain transfer rate in ethylene polymerization over NaY-zeolite-supported Cp_2ZrCl_2/MAO catalyst, thereby producing higher molar mass HDPE (Woo *et al.*, 1995). Decrease in support pore size resulted in higher molar mass and higher stereoregularity polypropylenes due to limited propylene concentration at the active site, and its unidirectional approach to the sites (Ko *et al.*, 1996; Ko and Woo, 2003). In another study in the gas-phase, Kumkaew *et al.* (2003a) observed a systematic increase in 1-hexene incorporation with increasing support pore size.

Low activity ethylene polymerization by MAO/Cp_2TiCl_2 supported inside 2.7 nm pores of mesoporous silica fiber (MSF) produced ultrahigh molar mass polyethylene (M_V = 6,200,000) with unusually high crystallinity (Kageyama *et al.*, 1999). The pore size (nine times smaller than polyethylene lamellar thickness, Anwander 2001), suppressed chain folding, thereby forcing the formed polyethylene chains to extrude out of the mesopores in what was termed "extrusion polymerization".

Supported metallocene/MAO catalysts usually produce polyolefins with higher molar masses compared to homogeneous metallocenes (Kaminsky and Renner, 1993; Janiak and Rieger, 1994; Sacchi *et al.*, 1995; Ferreira and Damiani, 2001; Musikabhumma *et al.*, 2000). However, supported catalysts with high mobility of the anchored metallocene due to a tethering segment or a MAO layer shielding the support produce polyolefins of similar molar mass as the homogeneous systems (Barrett and de Miguel, 1998; Koch *et al.*, 2000).

2.3 Ethylene/α-olefin polymerization with metallocene catalysts

Metallocene/MAO catalysts are highly sensitive to impurities such as moisture, oxygen and sulfur compounds, and to operating conditions such as monomer/comonomer types and concentration, temperature, and aluminum alkyls. The precise control of these parameters, and hence the role of the reactor system in laboratory scale polymerization is important in polyolefin catalysis research.

Catalyst handling and reactor operating procedure in the gas-phase and slurry olefin polymerization over supported metallocene catalysts is quite similar to the practice with heterogeneous Ziegler-Natta systems. Both are considered in the review below of laboratory practices in polymerization with supported catalysts.

2.3.1. Polymerization reactor systems

The greatest challenges posed by the sensitivity of metallocene/MAO catalysts are the proper and reproducible handling of the catalyst prior to its injection into the reactor, and the reactor temperature control after injection of high activity catalyst. The metallocene/MAO catalysts are best handled under inert atmosphere (dry glove box). Wide variations in glove-box purity levels have been reported, for example Jejelowo *et al.* (1991) reported oxygen and moisture contents of about 2 ppm and 3 ppm respectively while Samson *et al.* (1998, 1999) reported less than 0.1 ppm for both.

Dry catalyst injection is the most suitable for gas-phase polymerization; however, dry injection of small amounts of catalyst is prone to irreproducibility (Kumkeaw *et al.*, 2003b). Small quantities of catalyst (1-4 mg) can be introduced in the reactor reliably as a suspension (Weickert *et al.*, 1995) but the associated solvent removal by evacuation (Chung and Hsu, 2002) or purging (Samson *et al.*, 1996, 1999) can affect the quality of the initial polymerization data and the catalyst activity. Solvent removal may also be accompanied by loss of volatile Al alkyls (Samson *et al.*, 1999).

The temperature of lab-scale reactors is generally controlled by coolant circulation in the reactor jacket (Samson *et al.*, 1998) or cooling coils (Hutchinson and

Ray, 1991; Chung and Hsu, 2002). Han-Adebekun *et al.* (1997a) combined external electrical heating and water-cooling to control the reactor temperature; the copper-cooling coil was soldered to the reactor wall for good thermal contact. Tian *et al.* (1999) used external spiral jacket welded to the reactor body. Polymerization reactor temperature control had been improved by adjusting the amount of catalyst Busico *et al.* (2002).

In gas-phase (semi-batch) ethylene/α-olefin copolymerizations, the comonomer composition in the reactor changes continuously during the polymerization because the comonomer is usually fed in a batch mode while ethylene feed is continuous. The change in reactor composition has resulted in product with heterogeneous microstructure (Roscoe *et al.*, 2000). This can be avoided by terminating the reaction after a short period (Sun *et al.*, 1994a) or by operating the reactor in a "purge mode" (Han-Adebekun *et al.*, 1997a; Chakravarti and Ray, 2001). Gas chromatography (flame ionization detector for ethylene/α-olefins and thermal conductivity detector for H_2/olefins) or FTIR are used to analyze the headspace gas composition in polymerization reactors. Blom and Dahl (1999) recorded one chromatogram every 10 min with their on-line GC analysis system. The high sensitivity of hydrogen used with metallocene and hence low mole fraction in reactor makes GC analysis difficult (Blom and Dahl, 1999; Kaminsky and Luker, 1984).

2.3.2. Reaction mechanism and polymerization kinetics of metallocene catalysts

The coordinatively unsaturated metallocenium cation (see Section 2.1.1) is believed to be the active species in metallocene-catalyzed olefin polymerizations. The basic mechanism of olefin polymerization at the active sites of Ziegler-Natta catalysts is generally applied to metallocene/MAO systems (for example, see Huang and Rempel, 1995). The basic steps are shown in Figure 2.3 (Kaminsky, 1998). These involve the coordination of the olefins to the vacant site (Step A) followed by its insertion and alkyl migration (Step B). The energy released upon the transformation of the Zr←(C=C) π bond into Zr–C σ bond drives the insertion step while the migration of the (alkyl) growing chain facilitates further monomer coordination at the resulting vacant site (Lauher and Hoffmann, 1976).

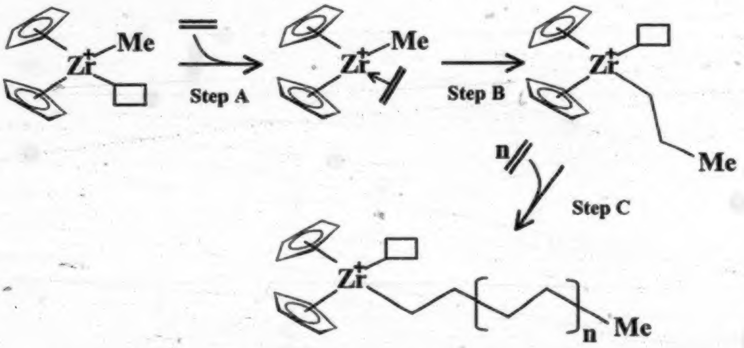

Figure 2.3 Ethylene polymerization mechanism at the active zirconocenium site.

The monomer coordination-insertion process (Step C) above is eventually terminated by a chain transfer reaction (see Figure 2.4). The chain transfer reactions are as follows (Rappé *et al.*, 2000):

- β-Hydride elimination where the transition metal center abstracts one H from the β-carbon of the growing chain to form a transition metal–H complex and a vinyl-ended polymer chain (Route A in Figure 2.4). β-Methyl elimination also occurs in C_3H_6 polymerization (Resconi *et al.*, 1992).
- Chain transfer to monomer where a β-hydrogen is transferred to an incoming monomer generating a metal-alkyl complex and a vinyl-terminated polymer chain (Route B).

- Chain transfer to counteranion e.g. MAO generating metal-alkyl complex and a polymer molecule "capped" by an organometallic functional group (Route D).
- Chain transfer to chain-transfer agents such as hydrogen or aluminum alkyls generating a metal-H complex and saturated polymer or a metal-alkyl complex and a polymer "capped" with organo-Al complex (Route C).

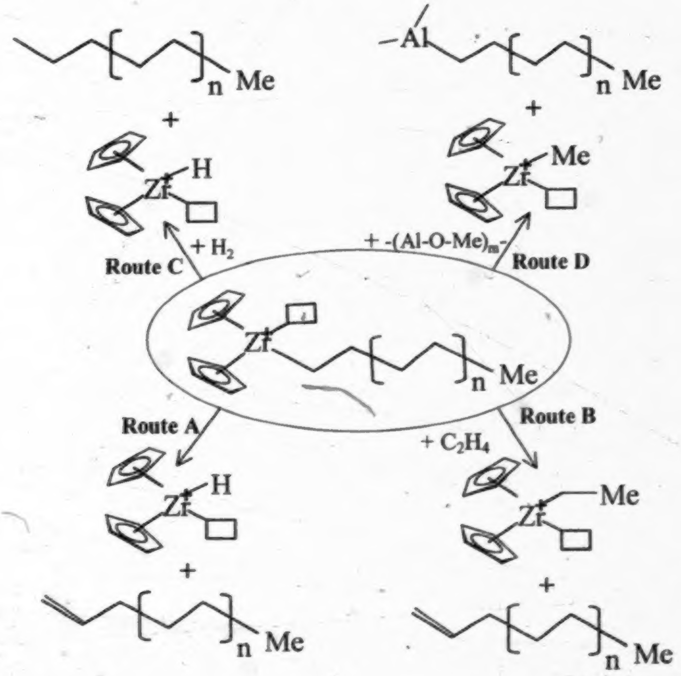

Figure 2.4 Possible chain termination reactions during C_2H_4 polymerization with metallocene/MAO catalyst. Route-A–β-hydride elimination, Route-B–chain transfer to ethylene, Route-C–chain transfer to hydrogen, and Route-D–chain transfer to MAO

The polymerization process continues through reinitiation of the chain growth cycle at the metal-H and metal-alkyl complexes generated in the above chain transfer reactions until the active sites undergo an irreversible deactivation (by reaction with impurities or spontaneously). MAO (Kaminsky, 2001) or H_2 (Rappé *et al.*, 2000) may reactivate some of the reversibly deactivated (dormant) centers.

Regardless of the true monomer coordination and insertion mechanism, the formation and stability of the active species in the metallocene/MAO systems impact the overall kinetics and polymerization activity of the catalysts significantly. For catalyst systems in which the metallocene and MAO have been precontacted it would be expected that the number of active sites is maximum at the beginning of polymerization resulting in the decay-type activity profile (curve *a* in Figure 2.5); this has been observed in some cases (see Chien and Wang, 1990; Fischer and Mülhaupt, 1991; Chung and Hsu, 2002). However, some of the reported decay-type kinetics could be due to loss of the initial polymerization data arising from the start-up procedure (e.g. see Roos *et al.*, 1997; Andersen *et al.*, 2001).

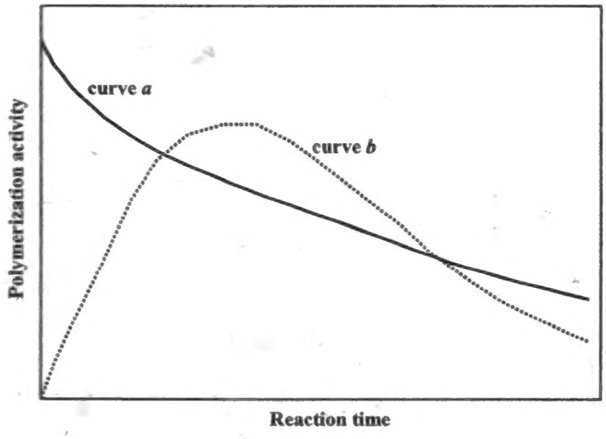

Figure 2.5 Polymerization activity profiles for decay-type (curve *a*) and acceleration-decay-type (curve *b*) kinetics.

Most metallocene/MAO-catalyzed polymerizations exhibit the acceleration-decay activity profiles (curve *b*) with widely varying acceleration periods. Since the active sites in metallocene/MAO catalysts are nearly identical (single site), it is difficult to explain the different activity profiles with the multisite phenomenon in which different site types respond differently to the reaction conditions as in Ziegler-Natta catalyst (Kissin *et al.*, 1999). Therefore, the differences in activity profiles in metallocene/MAO systems indicate difference in the change in active center concentration with time. Increase in the active center concentration during the acceleration period could be due to a shift in equilibrium between dormant and active sites, or enhanced monomer access to active sites due to physical fragmentation of polymerizing catalyst particles.

The exact nature of the dormant sites is not well understood but several postulates have been made based on both theoretical and experimental evidences. α-Hydrogen transfer reaction between the active center and MAO results in a dormant dinuclear Zr–CH_2–Al or Zr–CH_2–Zr species and methane evolution. The dinuclear species can be reactivated by further reaction with MAO (Kaminsky, 1996; Kaminsky and Strübel, 1998). Active sites generation in metallocene/MAO system is favored by high MAO concentration (high Al:Zr ratio) and temperature (Han *et al.*, 1996; Chien and Sugimoto, 1991; Chien and He, 1991b).

The kinetics of olefin polymerization by Ziegler-Natta and metallocene/MAO are generally modeled with the pseudo first order approximation with respect to monomer and active site concentration. The main difference between models is in the distribution of the active site concentration with time. Chien and Wang (1990) postulated at least two types of sites to explain the change in propagation rate constant, k_p, with zirconium concentration in the homogeneous Cp_2ZrCl_2/MAO system since radio labeling measurements revealed nearly all the Zr centers were active. The difference between the two site types could be due to difference in the number of MAO molecules associated with each. With first order deactivation, the productivity was modeled as follows:

$$P(t)=[M]\sum_i k_{p,i}[C^*_{i,0}](1-e^{-k_{d,i}t}) \tag{2.1}$$

where $[M]$ is the monomer concentration, $k_{p,i}$ and $k_{d,i}$ are the propagation and deactivation rate constants respectively for site i, and $[C^*_{i,0}]$ is the initial concentration of site i.

Vela Estrada and Hamielec (1994) observed higher deactivation rates of homogeneous Cp_2ZrCl_2/MAO catalysts at 50°C than at 71°C. The catalyst also produced polyethylene with distinctly bimodal molar mass distribution at 50°C compared to unimodal one produced at 71°C. Therefore, they proposed a two-site model that involves instantaneous formation of Site-I that produces the lower molar mass polymer at 50°C, transition of Site-I to Site-II that produces the higher molar mass polymer at 50°C, and first order deactivation of Site-II. First order propagation with respect to monomer and active sites, and β-hydride transfer were also assumed. Their polymerization rate data was well correlated with the following semi empirical model.

$$Rate=\left[\theta_1 e^{-k_c t}+\frac{k_c\theta_2}{k_c-k_{d2}}\left(e^{-k_{d2}t}-e^{-k_c t}\right)\right]P_{C_2H_4} \tag{2.2}$$

where k_c and k_{d2} are the rate constants for transition from Site-I to Site-II and deactivation of Site-II respectively, the parameters θ_1 and θ_2 are related to the propagation rate constants and the initial number of active sites.

For homogeneous Cp_2TiR_2/MAO system, Ewen (1984) considered reversible reactions for active site generation (equilibrium constant K_{MAO}) and monomer (C_3H_6) coordination to the active site (equilibrium constant K_m), and proposed the following polymerization rate equation:

$$Rate=k_{obsd}[C_3H_6][MAO][Ti] \tag{2.3}$$

with the observed rate constant k_{obsd} given by:

$$k_{obsd} = k_p K_{MAO} K_m / (1 + K_m [C_3H_6] + K_{MAO}[MAO]) \tag{2.4}$$

where k_p is the propagation rate constant, and $K_m[C_3H_6] + K_{MAO}[MAO] << 1$.

Huang and Rempel (1997) assumed a single site and a dynamic equilibrium between the active sites and two types of inactive Zr species, and inverse dependence of the irreversible site deactivation to MAO concentration. Their model predicted active site concentration $[C^*]$ as follows:

$$[C^*] = \left[-(K_2[MAO]-1) + \sqrt{(K_2[MAO]-1)^2 + 8K_1([Zr]-[C_d])} \right] \Big/ (4K_1)$$

where K_1 and K_2 are equilibrium constants, and the concentration of the irreversibly deactivated sites $[C_d]$ is given by $[C_d] = \int (k_d [C^*]/[MAO]) dt$.

2.3.3. Effects of polymerization conditions

In addition to the primary role of metallocene type, polymerization conditions such as temperature, monomer, comonomer, and aluminum alkyl concentrations significantly affect the polymerization activity and properties of the final product.

2.3.3.1. Effects of polymerization temperature

The overwhelming majority of researchers report increases in polymerization rate and decreases in activation periods (faster attainment of maximum activity) with increase in polymerization temperature (Xu *et al.*, 2001a; Chakravarti and Ray, 2001; Wu *et al.*, 1999; Korber *et al.*, 2001; Eskelinen and Seppälä, 1996; Mortara, 2001; Pietikäinen and Seppälä, 1994). Higher polymerization temperature also increases catalyst deactivation rates; therefore, higher polymerization temperatures may lower average activities.

The molar masses of polyolefins decrease monotonically with increasing polymerization temperature due to higher activation energy for chain termination than chain propagation reactions. Meng *et al.* (1999) reported increase in polyethylene molar mass with polymerization temperature up to 50°C for a poly(styrene-co-4-vinyl pyridine)-supported Cp_2ZrCl_2/MAO catalyst; this is followed by decrease in molar mass at higher temperatures. It signifies that the support had significant influence on the polymer microstructure. The molar masses of polyethylenes produced with the same catalyst in homogeneous phase decreased monotonically for the same temperature range.

2.3.3.2. α-Olefin comonomer effects

α-Olefin comonomers e.g. C_3H_6, 1-C_4H_8, 1-C_6H_{12}, and 1-C_8H_{16} have widely been reported to enhance ethylene polymerization activity for both Ziegler-Natta and metallocene/MAO catalysts (Chien and Nozaki, 1993; Camurati *et al.*, 2001). The comonomer enhancement has been attributed to one or more of the physical and chemical effects below; more of the investigations involved Ziegler-Natta catalysts.

- Enhanced fracturing of catalyst particle to expose new active sites (Tait *et al.*, 1988; Muñoz-Escalona *et al.*, 1987; Wester and Ystenes, 1997)
- Enhanced diffusion of monomer molecules through the semi crystalline ethylene/α-olefin copolymer encapsulating the catalyst particles (Koivumäki and Seppälä, 1993)
- Formation of new catalyst sites and/or activation of dormant sites exclusively by α-olefins (Pasquet and Spitz, 1993; Calabro and Lo, 1988)
- Increase in propagation rate constant k_p by α-olefins (Han *et al.*, 1996; Kashiwa and Yoshitake, 1988)

The ethylene/α-olefin synergism seems to occur only in non-homogeneous polymerization systems, i.e., polymerization over supported catalysts (Han-Adebekun *et al.*, 1997) or initially homogeneous systems in which the polymer formed is insoluble in the solvent and precipitates out of the solution (Chien and Nozaki, 1993; Atiqullah *et al.*, 1998). When polymer precipitates from an initially homogeneous system, the active center becomes encapsulated in the precipitated polymer. Eskelinen and Seppälä (1996), observed a sharp increase in ethylene homopolymerization activity (*n*-heptane diluent) in the 70°C–90°C range due to the change from polymer-encapsulated-catalyst to solution polymerization system. In truly homogeneous systems where both the catalyst and the polymer product remain in solution, there is no comonomer enhancement; often, negative comonomer effects are observed (Koivumäki and Seppälä, 1993; Chien and Nozaki, 1993). The comonomer enhancement effect is less prominent with propylene/higher-α-olefin polymerization with homogeneous or supported metallocene catalysts. Arnold *et al.* (1996) reported enhancement in propylene polymerization by 1-butene and 1-hexene but not 1-octene, 1-hexadecene or 1-dodecene while Xu *et al.* (2001b) observed a reduction in propylene polymerization activity by 1-hexene, 1-octene, 1-decene, and 1-dodecene. Koivumaki *et al.* (1994) also observed a monotonic reduction in propylene polymerization activity with increasing 1-octadecene/propylene ratio.

2.3.3.3. Effects of hydrogen

Hydrogen is used to control the molar mass of polyolefins produced by conventional Ziegler-Natta catalysts (Hsieh, 1984). Hydrogen is also a very effective chain transfer agent in metallocene/MAO-catalyzed polymerizations; hydrogen/ethylene mole ratio of 0.01 reduced the polyethylene molar mass to less than one third the value without hydrogen (Kaminsky and Luker, 1984). In addition to the chain transfer, hydrogen reduces the activity of both Ziegler-Natta (Kissin, 1999), and the metallocene/MAO catalysts (Chien and Wang, 1990; Kaminsky, 1996; Blom and Dahl, 1999; 2001), but this effect is reversible. Different metallocene catalysts have different sensitivities to hydrogen. Hydrogen is seldom used with metallocene/MAO catalysts because the polyolefin molar masses are usually in the desired range without hydrogen. This contrasts Ziegler-Natta catalysts that frequently produce ultra high molar mass polyethylenes in the absence of hydrogen.

2.3.3.4. Effects of aluminum alkyls

Aluminum alkyls are often used as impurity scavengers and seldom as cocatalyst in gas-phase or slurry polymerization with supported metallocene catalysts (Ribeiro *et al.*, 1997; Soga *et al.*, 1993; Soga and Kaminaka, 1993; Panin *et al.*, 2001; Liu et al., 1997; Chu *et al.*, 2000a). In addition to scavenging impurities, aluminum alkyls affect both the polymerization activity and polymer properties. The net effect of aluminum alkyls depends on the catalyst and the polymerization system.

The formation of Lewis acid-base complex $Cp_2Zr(X)[\mu\text{-}XAl(^tBu)_3]$ between $Al(^tBu)_3$ and Cp_2ZrX_2 (where X = CH_3^- or Cl^-) (Harlan *et al.*, 1995) can render the metallocene inactive in olefin polymerization at sufficiently high aluminum alkyl concentration (Barron, 2000). Therefore, an optimum amount of aluminum alkyl is desired in the polymerization reactor, i.e. an amount that is sufficient to scavenge impurities but not excessive to substantially inhibit the catalytic activity. Partial replacement of MAO resulted in the change of kinetic profile from the maximum initial activity to the induction type at TMA:MAO ratio of about 100 (Chien and Wang, 1988).

This could be due to the reversible complexation reactions between metallocene, MAO, and the aluminum alkyl (Bochman and Lancaster, 1994).

Satyanarayana and Sivaram (1993) reported a steady increase in polyethylene molar mass with increasing Al_{TIBA}:Ti ratio for $MgCl_2$ supported Cp_2TiCl_2 catalyst. Increasing TIBA concentration was reported to increase (Panin *et al.*, 2001) as well as decrease (Petoff *et al.*, 1999) the molar masses of polypropylenes produced with metallocene catalysts.

The undesirable aluminum alkyl-metallocene interaction is often avoided in laboratory gas-phase polymerization by venting off and/or evacuating the excess aluminum alkyl after the impurities scavenging (Chakravarti and Ray, 2001). This procedure is not possible with the continuous industrial processes.

2.4 Effect of support morphology on catalyst activity and product morphology

Early studies on supported chromium catalysts indicated that the support morphology influences both the polymerization activity and the morphology of the product polyolefins. The initial acceleration in polymerization activity was attributed to the increase in number of active sites due to fragmentation of the catalyst particles during polymerization (Whittaker and Wills, 1969). Radiotracer studies proved that the rate profile of ethylene polymerization over silica and alumina supported chromium oxide catalyst is due to the change in the number of active sites with time (Zakharov and Ermakov, 1971).

Later studies by McDaniel (1981) showed that the activity of silica supported chromium catalysts, and silica supported Ziegler-Natta catalysts increased with the support porosity. McDaniel (1981) also noted that the porosity of the support recovered from polymer particles differed from the initial morphology only for pore sizes greater that 60 nm, an indication that the catalyst particles fractured along the macropores only. Floyd *et al.* (1987) noted preference for silica supports with 10-60 nm pores in industrial application. In another study on the effect of support on catalyst performance, Muñoz-Escalona *et al.* (1984) reported different ethylene polymerization behavior of silica-supported Ziegler-Natta catalysts prepared identically on supports with different morphologies.

Several models have been developed to explain the polymerization behavior of supported catalysts; see Wu (1999) for a review of both the kinetic and the mass transfer aspects of these models. The multigrain model (MGM) is the most notable of the transport resistance models applied to olefin polymerization over supported catalysts (see Laurence and Chiovetta, 1983; Floyd *et al.*, 1987; Ferrero and Chivetta, 1987a; Ferrero and Chiovetta, 1987b; Hutchinson *et al.*, 1992) and it is based on experimental observation of catalyst fragmentation during polymerization (Kakugo *et al.*, 1989a; 1989b). In the MGM, the polymerizing catalyst particle (macroparticle) is believed to consist of assemblage of microparticles. At the beginning of polymerization, the macroparticles are assumed to fragment instantaneously to the microparticles (Figure 2.6) on which the polymerization takes place. The polymer produced holds the fragmented microparticles together.

The MGM attributes monomer transport in the macro- and micropores by diffusion only, and the particle radius as the characteristic path length. For high activity catalysts, this would suggest high diffusion limitation or necessitate the use of unrealistically high values for the monomer diffusion coefficient. Experimental evidence obtained through monomer supply interruptions (Doi *et al.*, 1982; Chien *et al.*, 1985) and comparison of homopolymerization kinetics of propylene to that of 1-decene (Choi and Ray, 1985) suggest that diffusion limitation is not important in high activity $MgCl_2$-supported $TiCl_4$ catalysts.

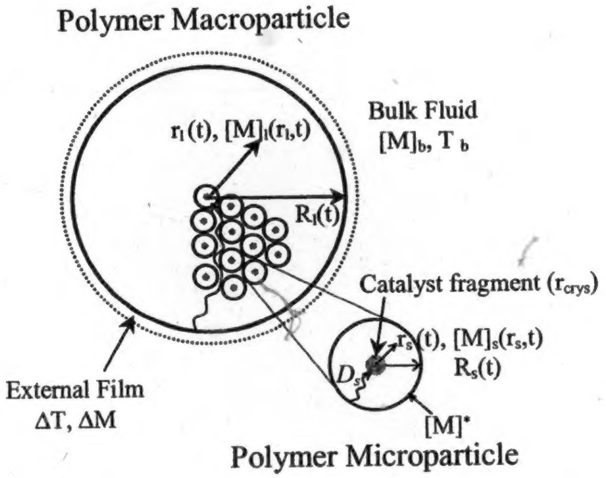
Polymer Macroparticle
$r_l(t)$, $[M]_l(r_l,t)$
Bulk Fluid
$[M]_b$, T_b
$R_l(t)$
Catalyst fragment (r_{crys})
$r_s(t)$, $[M]_s(r_s,t)$
$R_s(t)$
D_s
External Film
ΔT, ΔM
$[M]^*$
Polymer Microparticle

Figure 2.6 Representation of active catalyst particle in MGM (Hutchinson *et al.*, 1992)

Morphological evidence from nascent polyolefin particles suggest that the characteristic macro particle diffusion path length could be less than the particle radius due to the development of macro cracks and voids in the particles (McKenna and Mattioli, 2001; Kittilsen *et al.*, 2001a; Zhou *et al.*, 2003). The monomer concentration in these voids is the same as in the bulk fluid. The development of the macro cracks and channels would depend on the support morphology, catalyst activity, and polymerization conditions. Kittilsen *et al.* (2001a) linked mass transfer resistance and the evolution of polyolefin particle morphology to obtain a model that predicts higher monomer transport rates, and which better agrees with the experimental results. The activities of typical industrial gas-phase Ziegler-Natta catalysts range from about 10 to over 100 kg PE/(g

Ti·h) (McKenna and Soares, 2001). At such activities, the rapid monomer consumption inside the catalyst particle would develop finite pressure drop that would result in convective monomer influx; this has been theoretically investigated (Kittilsen *et al.*, 2001b; Veera *et al.*, 2002).

In summary, the observed polymerization activity of supported olefin polymerization catalysts is a combined effect of the intrinsic kinetics, and mass transfer resistance of the monomer. The latter is strongly influenced by the mechanical strength and pore structure of the support. A good understanding of the above influence is essential in the design of optimum support for immobilizing metallocene/MAO. Porous polymeric supports are ideal for this investigation because both the mechanical, and the pore characteristics can be varied systematically. However, other extraneous factors such as impurities and residual aluminum alkyls can also significantly affect activity profiles of catalysts and make reproducibility very difficult.

3. Experimental Methods

The first part of this work involved the design, fabrication, and testing of a gas-phase polymerization reactor system. Therefore, details of the new reactor system and results of polymerization test runs with the new reactor are presented in Chapter 5. The reactor design and fabrication was jointly done with another graduate student (Tariq M. Mannan).

The remaining experimental aspects of this work consisted of the following: Preparation of heterogeneous metallocene/MAO catalysts with polymeric supports; evaluating the supported catalysts in gas-phase ethylene/α-olefin polymerization; and characterizing the resulting polyolefin products. The description and the sources of all the materials used in this work are given in Section 3.1. This is followed by the catalyst preparation, and the gas-phase polymerization procedures in Sections 3.2 and 3.3 respectively. Finally, the procedures used for characterization of supports, catalysts, and polyolefin products are described in Section 3.4.

3.1 Materials

MAO (10 wt % in toluene) from Sigma-Aldrich, and Modified MAO type-4, MMAO-4 (in toluene, 6.92 wt % Al) from Akzo Nobel (Deer Park, TX) were used as received. MMAO-4 contains ~12% isobutyl and ~88% methyl groups; it is only moderately soluble in aliphatic hydrocarbons. Neat TEA, neat TIBA, and neat TNOA from Texas Alkyls were stored in a glove box and used without further purification. Metallocene $(n\text{-BuCp})_2ZrCl_2$ and 1-hexene were both donated by NOVA Chemicals, Calgary, Alberta and used as received.

Anhydrous toluene was purchased from Sigma-Aldrich and used as received. Ultra-High-Purity (UHP) nitrogen (grade 5.0) and polymerization grade (3.0) ethylene were purchased from Prax Air or Matheson Gas in Edmonton, Alberta. Ethylene was further purified in Alltech (Deerfield, IL) columns before entering the reactor.

The porous polymeric supports used in this work were either purchased from commercial sources or synthesized in our laboratory. Table 3.1 summarizes the sources and morphological properties of the supports. Details of the synthesis procedure for the locally made supports have been given elsewhere (Zhou *et al.*, 2003). The HayeSep products were purchased from HayeSep Separations Inc., (Bandera, TX); Porapak type T was purchased from Chromatographic Specialties Ltd (Brockville, ON). Support Number 4 in Table 3.1 is a swellable 1%-crosslinked poly(styrene-co-divinylbenzene) purchased from Sigma-Aldrich.

The supports presented in Table 3.1 can be divided into the following four broad categories based on their functional groups:

- Supports 1–4 have no functional groups; their skeletal structure consist of C_6 aromatic rings cross linked with short C_2–C_4 aliphatic segments (see Figure 3.1a).
- Supports 5–10 contain 2-hydroxyethylmethacrylate (HEMA) monomer that has –OH, >CO, and –O– functional groups (and styrene in supports 5-7); these are cross-linked with the aromatic based divinylbenzene as shown in Figure 3.1b.
- Supports 11–15 contain monomers that have at least one functional group (N and/or O based); these are also cross-linked with divinylbenzene (Figure 3.2).
- Supports 16–18 also possess functional groups (N and/or O), but these supports have no aromatic component; they consist of only linear segments (see Figure 3.3).

Table 3.1 Description of polymeric supports used in catalyst synthesis

Support description	Source	Composition[a] (mass %)	d_P[b] µm	S_A[c] m^2/g	V_P[d] cm^3/g	r_P[e] nm
1 PE981124	In-house	DVB	30-170	353	0.45	2.6
2 HayeSep-Q	Commercial	DVB	150-180	592	0.69	2.3
3 PE991119	In-house	STY/DVB (50/50)	40-160	7	0.09	27.1
4 Poly(STY/DVB)	Commercial	STY/DVB (99/1)	150-210	ND	ND	ND
5 PE001018A	In-house	HEMA/STY/DVB[f]	74-200	39.3	0.12	6.0
6 PE001018B	In-house	HEMA/STY/DVB[f]	200-400	25.5	0.13	10.3
7 PE9023	In-house	HEMA/STY/DVB[g]	50-300	224	0.27	2.4
8 PE971124	In-house	HEMA/DVB (50/50)	60-300	375	0.45	2.4
9 PE971204	In-house	HEMA/DVB (50/50)	60-300	620	0.79	2.5
10 PE990212	In-house	HEMA/DVB (80/20)	25-125	<0.01	0.03	$\approx \infty$
11 HayeSep-A	Commercial	DVB/EGDM	125-150	526	0.77	2.9
12 HayeSep-B	Commercial	DVB/PEI	125-150	575	0.57	2.0
13 HayeSep-C	Commercial	DVB/Acrylonitrile	125-150	442	0.75	3.4
14 HayeSep-R	Commercial	DVB/N-V-2-P[h]	125-150	640	0.98	3.0
15 HayeSep-S	Commercial	DVB/4-Vinylpyridine	125-150	583	0.58	2.0
16 HayeSep-T	Commercial	EGDM	125-150	250	0.46	3.7
17 Porapak-T	Commercial	EGDM	106-125	313	0.56	3.6
18 PE990908	In-house	HEMA/PTMA (80/20)	–	–	–	2.0

a: mass % monomer in reaction mixture; technical grade DVB in the synthesis

b: particle size range obtained from source or estimated from SEM of pictures

c: surface area obtained by BET method

d: mesopore volume

e: pore radius (nm) obtained as $2000V_p/S_A$; most probable value for PE990908

f: composition HEMA=10%, Styrene=70%, DVB=20%

g: composition HEMA=15%, Styrene=40%, DVB=45%

h: N-V-2-P = N-vinyl-2-pyrrolidinone

ND= not determined

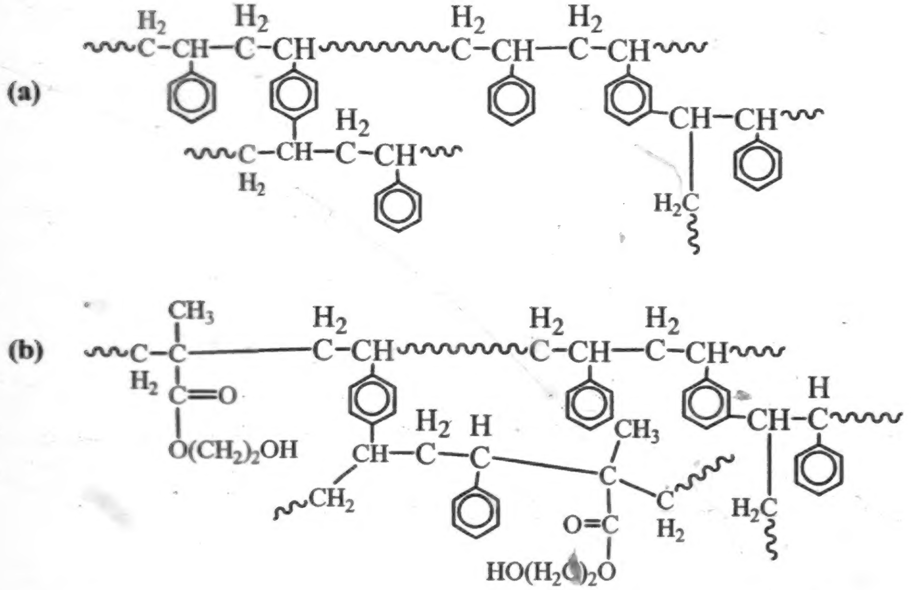

Figure 3.1. Schematic structures of cross-linked (a) poly(divinylbenzene) support (Glöckner, 1978) with no functional groups, and (b) poly(HEMA/divinylbenzene) support.

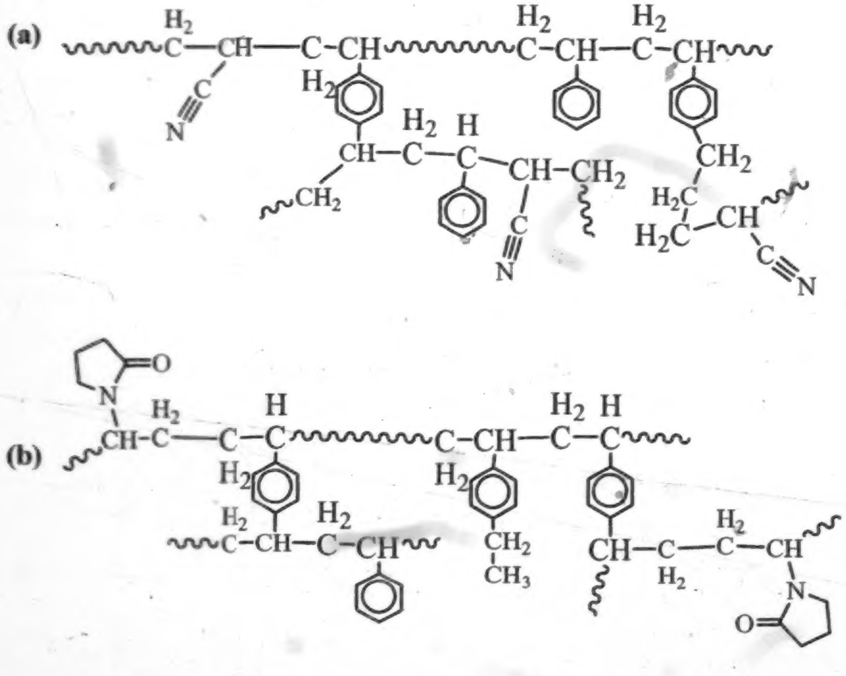

Figure 3.2. Schematic structures of cross-linked (a) poly(divinylbenzene/acrylonitrile) support, and (b) poly(divinylbenzene/N-vinyl-2-pyrrolidinone) support.

The microstructure of the supports shown in Figures 3.1 to 3.3 and the morphological properties in Table 3.1 show that there is wide variation in the physicochemical properties of the supports, even those in the same class. The effects of these differences will be elaborated in the subsequent sections of this work.

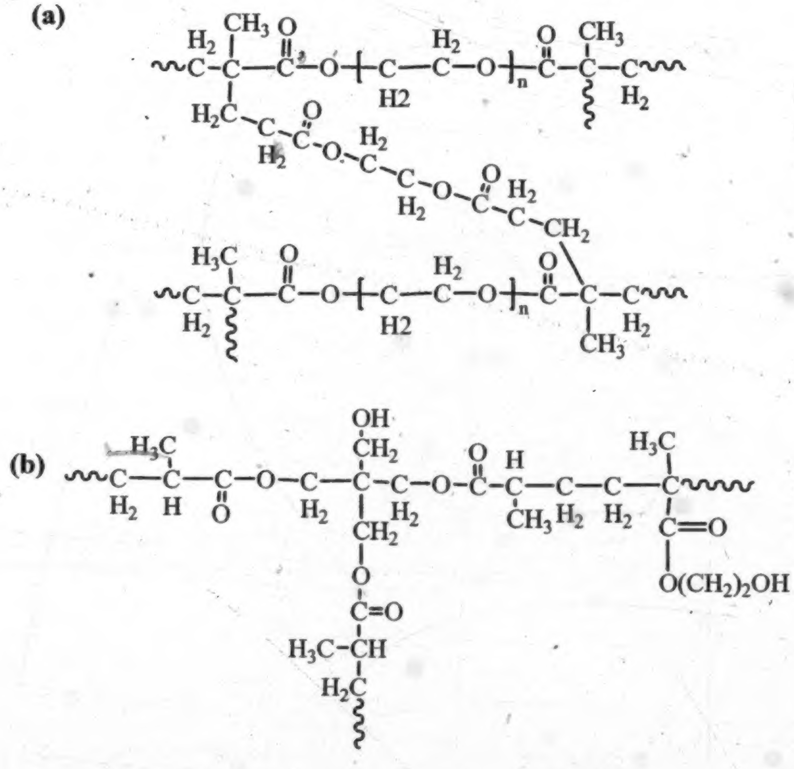

Figure 3.3. Schematic structures of cross-linked (a) poly(ethyleneglycoldimethacrylate) support (Glöckner, 1978), and (b) poly(HEMA/PTMA) support.

3.2 Preparation of supported metallocene/MAO catalysts

Catalysts were typically prepared by weighing the desired amount of organic support in a 3-neck flask and heating (at ~75-90°C) while evacuating for about 16 hours. The evacuated support was suspended in anhydrous toluene 5–10 mL followed by the addition of predetermined amount of the MAO solution. The support/MAO suspension was left on a shaker (Maxi-Mix III™ Thermolyne; Dubuque, Iowa) at 200 rpm and room temperature for 2–3 h followed by the addition of the metallocene solution that was prepared by dissolving the desired amount of (n-BuCp)$_2$ZrCl$_2$ in about 5 mL anhydrous toluene. This was allowed to react for 1–3 h on the shaker then dried by solvent evacuation at room temperature; the scheme below summarizes the preparation method.

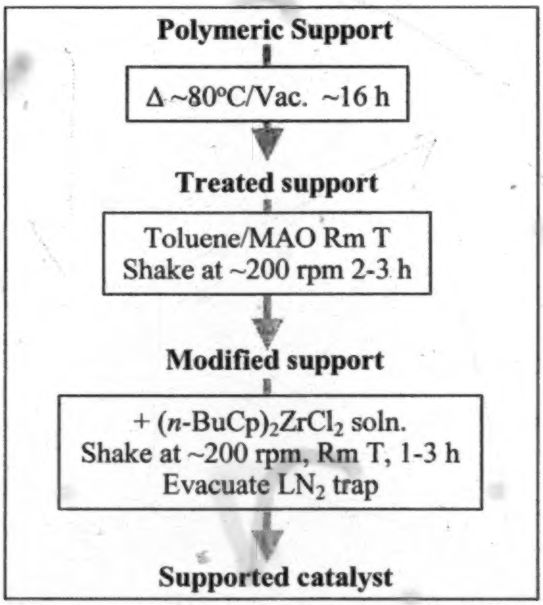
Polymeric Support
Δ ~80°C/Vac. ~16 h
Treated support
Toluene/MAO Rm T
Shake at ~200 rpm 2-3 h
Modified support
+ (n-BuCp)$_2$ZrCl$_2$ soln.
Shake at ~200 rpm, Rm T, 1-3 h
Evacuate LN$_2$ trap
Supported catalyst

Catalysts HH01, HH23 and HH24 were prepared differently as follows: In preparing catalyst HH01, the support/MAO suspension was first dried by solvent evacuation at room temperature for ~3½ h, followed by the addition of the metallocene solution (containing TIBA, $Al_{TIBA}/Zr = 8$). The new suspension was left on a shaker for 14 h, then dried by solvent evacuation at room temperature for 1⅓ h until it looked liquid free. The catalyst flask was place in oil bath at 55°C and further evacuated for ~5½ h. No support was used in the preparation of catalysts HH23 and HH24. The same metallocene/MAO solution was split into two equal parts and dried slightly differently to obtain the two catalysts. The first part was evacuated at room temperature for 1⅔ h to obtain catalyst HH23. For catalyst HH24, the second solution was evacuated at room temperature for ½ h, and further evacuated for 5 h in a bath at 45°C.

Table 3.2 Supports and pretreatment conditions for the supported catalysts

Catalyst	Support		Comments on preparation method
	Name	Pretreatment	
HH01	PE971124	80 °C, 18 h	Support/MAO dried prior to metallocene addition
HH02	PE971204	86 °C, 16 h	
HH03	PE990908	70 °C, 5 h	MMAO-4 used
HH04	PE001018	50 °C, 21 h	Support/MMAO-4 evacuated then metallocene added
HH05	PE001018	78 °C, 16.5 h	Support and MMAO-4 contacted for about 70 h
HH06	PE9023	70 °C, 20 h	
HH07	Porapak-T	80 °C, 16 h	Treated support cooled in salt/ice bath
HH08	PE981124	85 °C, 18.7 h	
HH09	PE971124	75 °C, 16.5 h	
HH10	PE971204	80 °C, 17 h	
HH11	PE990212	70 °C, 16 h	
HH12	PE991119	82 °C, 18 h	
HH13	PE971124	85 °C, 18.7 h	
HH14	PE971124	75 °C, 16 h	
HH15	PE971124	87 °C, 18 h	
HH16	HayeSep-T	85 °C, 18.3 h	
HH17	HayeSep-A	80 °C, 16 h	
HH18	HayeSep-S	75 °C, 17.5 h	
HH19	HayeSep-R	65 °C, 16 h	
HH20	HayeSep-C	70 °C, 17 h	
HH21	HayeSep-B	75 °C, 15.7 h	
HH22	HayeSep-Q	75 °C, 17 h	
HH23	None	–	MAO/metallocene dried at room T
HH24	None	–	MAO/metallocene dried at room T and 45°C
HH25	HayeSep-R	75 °C, 16 h	
HH26	HayeSep-R	75 °C, 16.5 h	
HH27	HayeSep-R	75 °C, 20 h	
HH28	HayeSep-R	82 °C, 20 h	Support first treated with TMA in excess of (N+O)
HH29	Sty/Dvb 1%	90 °C, 20 h	

The different catalysts were prepared by varying the support material, the cocatalyst, the precursor loading, and the Al/Zr ratio. Detailed information of the catalyst preparation conditions for all the catalysts are summarized in Appendix A, Table A-1.

3.3 Gas-phase polymerization procedure

Details of the new polymerization reactor system are given in Chapter 5. There have been some variations in the polymerization procedure since the first test-run with the new reactor. These variations evolved with the understanding of the reactor behavior and the effects of other operating conditions such as the type and the amount of scavenger used. This section describes details of the commonly used polymerization procedure and the variations from it.

The reactor preparation commences at least a day before the date of polymerization. A typical ethylene homopolymerization run involves the following steps:

1. The reactor was cleaned, loaded with the desired amount of NaCl (typically 80 g), and assembled.
2. The reactor was subjected to heating ~90°C and evacuation <10 mtorr overnight (~16 h); the catalyst holder and the syringe for the scavenger were also evacuated overnight in the glove box antechamber.
3. On the day of the polymerization experiment, the desired amount of supported catalyst was loaded into the catalyst holder and the desired amount of aluminum alkyl scavenger was placed in a 500-μL gas-tight Hamilton syringe inside the glove box.

4. The pre-purified reactor was filled with ultra pure nitrogen to ~25 psi and the catalyst holder was connected to the reactor under nitrogen flow.
5. The reactor was evacuated (~10 mtorr) and fed with ethylene to about 15 psi followed by injection of the aluminum alkyl. Data acquisition normally commences at the end of this evacuation step (see Figure 3.4).
6. The reactor was fed with ethylene to about 0.7 MPa (100 psi). The reactor was cooled to the polymerization temperature, usually 80°C in about 20-30 min while stirring at 450 rpm. The aluminum alkyl scavenged impurities in the reactor during this time.
7. Catalyst was injected using 1.4 MPa ethylene and the reactor pressure was maintained at this value by continuous ethylene feed to replenish the amount consumed in the reactor. The stirrer was briefly stopped during catalyst injection.
8. At the end of the polymerization, the reactor was quickly vented and cooled to room temperature.
9. The polymer/salt mixture from the reactor was thoroughly washed with warm tap water and dried in oven at 60°C overnight. The weight of the recovered polyolefin product was measured and used in calculating the average activity.

During ethylene/1-hexene copolymerization runs, an ISCO Model 500D syringe pump (Isco Inc., Superior Lincoln, Nebraska) was used to dose the desired amount of 1-hexene into the reactor (in step five above) after scavenger injection. The residual aluminum alkyl was vented and/or evacuated (after the scavenging period) in some polymerization runs; in such runs, nitrogen was used instead of ethylene in Steps 5 and 6. The amount of scavenger used in such runs was denoted as *trace* in the tables summarizing the polymerization conditions as well as in the discussion of results. These runs would have < 0.1 μmol TIBA left in the reactor assuming that complete evaporation of the injected TIBA took place.

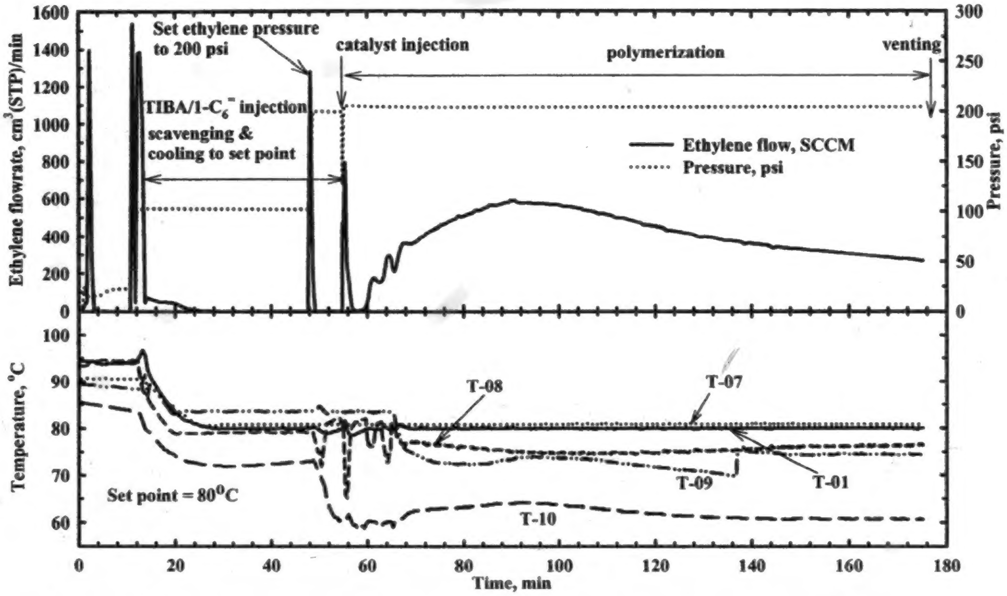

Figure 3.4 Profiles of ethylene flowrate, reactor temperature, and pressure during a typical ethylene/1-hexene copolymerization run (HH20198) in which residual TIBA was not removed after the reactor scavenging.

Some polymerization runs involved contacting the supported catalyst with the aluminum alkyl in the reactor prior to introducing ethylene. In such runs, the catalysts were injected using 50-psia nitrogen, which remained in the reactor for the duration of the run. Further details on polymerization procedures that differ from the usual ones above are discussed with the polymerization results of the individual runs.

3.4 Characterization methods

Several analytical methods were used in the characterization of the supports, catalysts, and polyolefin products. No details will be given on the theories of these analytical techniques. However, brief overview of the most important steps and relevant references for the underlying theories are given.

3.4.1 Surface area and pore size distribution

Nitrogen sorption measurements at 77 K were used to characterize the surface area and pore size distribution of all the supports and catalysts. Leofanti *et al.* (1998) reviewed the principles and limitations of this technique. An Omnisorp 360 sorptometer (Miami Lakes, FL) was used in the continuous flow mode as follows:

1. The samples were out gassed in vacuo for at least 3 h at 125°C for supports or for at least 1 h at 50°C for supported catalysts. The catalysts were treated at a milder condition in order to keep it in a state close to the state it enters the polymerization reactor. The out gassing temperature of the supports is higher than the pretreatment temperature (75–90°C) used in catalyst preparation, but it is heated for a much shorter time (1–4 h) compared to the 16–20 h in the latter. The above outgassing temperatures are generally lower than the 300–350°C (6–10 h) used for inorganic oxides and activated carbons.
2. Helium calibration measurement was done on each sample at 77 K to determine the dead volume (volume of manifold, holder, and the sample).
3. A mass flow controller was used to deliver a constant rate (0.5 or 1.0 mL/min) of the adsorptive gas (N_2) continuously to the sample at 77 K and the raw data, nitrogen pressure in sample holder and saturation nitrogen pressure as a function of time were recorded.
4. The volume of N_2 adsorbed by the sample at each relative pressure (P/P_o) was calculated by subtracting the dead volume from the volume of N_2 dosed to the

sample. The adsorption isotherm was constructed from the volume of N_2 adsorbed vs. relative pressure data.

5. The desorption isotherm data was obtained by removing the adsorbed gas at constant flow rate (0.5 or 1.0 mL/min), and calculating the incremental desorbed volume at decreasing relative pressures.

For each sample complete adsorption isotherm (i.e. to $P/P_o \approx 1$) was measured. Surface areas were calculated using uptakes for $0.05 \leq P/P_o \leq 0.25$. The monolayer volumes were calculated according to the Brunauer, Emmett and Teller (BET) Equation 3.1 (Brunauer *et al.*, 1938), and the specific surface area S_{BET} calculated according to Equation 3.2.

$$\frac{P}{V(P_0 - P)} = \frac{1}{V_m c} + \frac{c-1}{V_m c}\frac{P}{P_0} \qquad 3.1$$

where V is the volume adsorbed, V_m the monolayer volume, P the sample pressure, P_o the saturation vapor pressure (measured at every pressure point), and c the BET constant related to the enthalpy of adsorption.

$$S_{BET} = \frac{1}{m}\left(\frac{V_m}{V_L}\right)N_A A_m \qquad 3.2$$

where m is the sample mass, V_L the molar volume of nitrogen at STP (22.414 L), N_A Avogadro's number (6.02×10^{23}), and A_m the cross-sectional area of a nitrogen molecule ($0.162\ nm^2$)

The micropore volumes were obtained from t-plot calculations (Lippens and DeBoer, 1965). The Barrett, Joyner and Holender (BJH) method (Barrett *et al.*, 1953) was used on the desorption isotherm to obtain the mesopore size distribution for most samples. Only a few samples (with relatively low surface area) had unrealistic desorption isotherms, in such cases, the adsorption isotherm data were used to calculate the mesopore size distribution. The Omnisorp 360 performs all the measurements automatically and logs the data to a PC. Data analysis was done using Omnisorp 360 version 4.0 software.

3.4.2 Friability and swellability of the polymeric supports

3.4.2.1 Friability

The friability of catalyst particles plays a vital role in the particle replication process from catalyst to polymer. For the supporting methods used in this work (Section 3.3) the friability of the supported catalyst are mainly dependent on that of the support particles. Friability of solids is widely tested in the fields of mining, construction, food science, pharmaceutical science, and catalysis. In all these areas, friability is usually an undesirable effect that degrades the quality of the final product. For example, dust formation in pelletized catalysts, or medicinal tablets.

The commonly used friability test methods: impact, vibration, shear, and tumbler tests are designed for coarser and denser particles than the porous polymeric supports. There is no standard for testing the friability of fine materials (Ortega-Rivas, 2001). Therefore, a wide range of techniques is used to suit the individual test objectives (see for example Grizotto and De Menezes, 2002). Oulahna *et al.* (2003) determined the friability index of granulated powder as percentage of broken particles after 200 revolutions in a special cell. Great Lakes Co. (Indiana, USA) tests the friability of their polymer additives by shaking the pellets with glass balls; friability index is reported as percentage of particles less than 180 μm. McDaniel (1981) sonicated slurries of silica particles (~0.07

g/mL) in an ultrasonic cell disruptor and used the resulting particle size distribution to characterize the relative fragility of the different silica.

A method similar to that of Great Lakes Co. above was used in this work. The size of the support particles, and their hardness makes the use of glass balls ineffective. The following procedure was used for testing the friability of supports:

1. Twenty-six stainless steel balls (10×¼″ diameter and 16×3/16″ diameter) with a total mass of 17.8 g were loaded in a 20 mL glass vial
2. 0.12–0.15 g of support was added to the vial and the vial was capped
3. The capped vial was mounted on a Maxi-Mix III™ Thermolyne (Dubuque, Iowa) shaker (with a ~20 cm Fisher clamp) and milled for 1 min at 800 rpm
4. Acetone was used to quantitatively recover pulverized support in a sample bottle
5. The above suspension was dried at room temperature
6. The dry powder was re-suspended in 1–2 mL ethanol and charged into MALVERN dispersion unit maintained at 3000 rpm (water was the dispersion medium)
7. Particle size distribution was acquired (at 10–15 % obscuration) twice and averaged
8. Friability was computed as volume % of pulverized particles lying outside the size range of the support (see Section 4.2)

3.4.2.2 Swellability

The support swellability was determined from the bulk-expanded volume of the polymer beads due to toluene absorption. The bed volume of the dry polymer (V_0) and that of the swollen polymer (V) were measured. The bed swelling of the sample is determined as $(V-V_0)/V_0$. For uniform cylinders, such as the NMR tubes used for the swellability measurements, this reduces to $(h-h_0)/h_0$; h_0 is the height of dry polymer bed, and h the height of expanded bed. Note that when accurate values of swellability are desired, this method cannot be used directly (Biffis, *et al.*, 1996); more sophisticated techniques are also available (Selic and Borchard, 2001). NMR sample tubes 4.20 ± 0.05 mm internal diameter, 178 mm long (Norell Inc, Landisville, NJ) were used. The closed ends of the NMR tubes were cut-off (with a diamond knife) and covered with a 7μ Nylon Mesh monofilament cloth (Small Parts Inc., Miami Lakes, FL) for solvent permeation. About 0.5–0.6 g of polymeric support was weighed in each tube, and the tubes were gently tapped on a lab bench to a constant bed height (until no change in the bed height was observed between two successive sets of 100 taps). The loaded tubes were immersed in toluene at room temperature; heights of the expanded beds were recorded.

3.4.3 Instrumental neutron activation analysis (INAA)

INAA was used to analyze the aluminum and zirconium content of the catalysts; hence, there was no sample treatment involved in the analysis. The nuclear reactions involved in the analysis were the following:

$$ {}^{27}_{13}Al + n \rightarrow {}^{28}_{13}Al + \gamma \text{ (1779 keV)} \tag{3.3} $$

$$ {}^{96}_{40}Zr + n \rightarrow {}^{97}_{40}Zr + \gamma \text{ (743 keV)} \tag{3.4} $$

This analytical technique has the advantage of insignificant interference by the support matrix in the catalysts; in addition to the Al and the Zr, the catalyst samples only contained H, C, O, N, and Cl. These do not interfere in the delayed gamma-NAA employed in the analyses. In NAA the sample is irradiated in a beam of neutrons. Stable atoms under assay capture the neutrons to form radioactive daughter nuclides that emit gamma rays of specific energies. The emitted gamma rays are detected and analyzed.

Campbell and Bewick (1978) reviewed the neutron activation analysis technique. The SLOWPOKE nuclear reactor facility at the University of Alberta was used to irradiate the samples. Chatt and Katz (1980) described the SLOWPOKE reactor. The analytical procedure consisted of the following steps:

1. Catalyst samples (50–150 mg) were weighed in microtube polyethylene vials and sealed inside the glove box. The vials were filled to approximately the same volume; therefore, larger masses of the higher bulk density samples were used. It was essential to have approximately the same sample volume in the vials to maintain similar sample-detector geometry during counting.
2. The samples and standards were first irradiated in the SLOWPOKE reactor for 60 s under a flux of 1×10^{11} neutrons cm^{-2} s^{-1}, allowed to decay for 120 s, and counted (γ) for 60 s to determine the aluminum content. The low $t_{½}$ (2.3 min) of the $^{27}Al(n,\gamma)^{28}Al$ reaction and the high cross-section of Al necessitated this procedure.
3. For zirconium analysis, the samples and standards were irradiated at higher flux (5×10^{11} neutrons cm^{-2} s^{-1}) for a longer period (1 h), allowed to decay for about 24 h, and counted for about 1 h. This irradiation-decay-count scheme was chosen because of the low concentration of Zr in the samples and the relatively longer half-life (compared to ^{28}Al) of the daughter nuclide ($t_{½}$ = 16.91 h for ^{97}Zr). There was sufficient sensitivity to use this nuclide.
4. The detected radiations were analyzed to produce energy spectra (counts vs. γ-rays energy) for each sample. These energy spectra were converted to mass percents of Al and Zr in the samples using the calibration made from the spectra of coal fly ash

standard (NIST 1633a) for Al and standard solution (997μg Zr/mL, SCP Science Lot No. SC3050827) for Zr respectively.

3.4.4 Scanning electron microscopy (SEM) and Energy dispersive X-ray analysis (EDX)

3.4.4.1 Scanning electron microscopy

Scanning electron micrographs of supports, catalysts, and polymer particles were obtained using Hitachi S-2700 scanning electron microscope interfaced with PGT image acquisition system. Catalyst samples were first deactivated by allowing air to slowly diffuse though partially sealed sample vials over periods of 3–5 days. Slight discoloration was observed for some catalyst samples but this is not expected to change the catalyst morphology. Knoke *et al.* (2003) gradually replaced the Ar atmosphere of their supported metallocene catalysts with air in preparation for SEM. No fuming was observed when small amounts of the catalysts in this work were exposed to air even in an uncontrolled manner. However, the catalyst preparation flask for the higher MAO catalysts fumed upon exposure to the atmosphere (after catalyst removal in the glove box). This was probably due to MAO residue that formed on the walls of the flask during solvent evaporation.

The sectioned polyolefin particles were hand cut (No. 10 surgical blade, Fisher scientific) and mounted on the SEM sample stubs using precision tweezers at room temperature. Some large polyethylene particles were cooled to 77 K (below T_g) and fractured quickly to avoid the smearing effect observed in hand cut samples.

Specimens were mounted on stubs using conducting carbon tape and coated with a thin carbon layer by high temperature evaporation in vacuum. Coating with a thin layer of gold followed this carbon coating. Coated specimens were examined under 10 kV accelerating voltage. Adding a droplet of conducting glue at the point of contact with the carbon tape enhanced conduction with the bigger polymer particles. Using 10 kV accelerating voltage minimizes sample (non-conducting) charging during SEM examinations. Scanning electron micrographs of some samples were obtained during EDX measurements. Such samples were only carbon coated and the SEM pictures were obtained at 20 kV accelerating voltage.

3.4.4.2 Energy dispersive X-ray analysis

Deactivated catalyst particles were embedded in the ultra low viscosity LR White™ (acrylic) Resin mixed with 90% ethanol and cured at 60°C for 8 h. The samples were sectioned with a diamond knife in a Reichert ultra microtome unit at room temperature. Point and line scans for aluminum and zirconium were recorded at 20 kV accelerating voltage. The polyolefin particles used in EDX analysis were hand cut as described in section 3.5.4.1 above.

3.4.5 Temperature rising elution fractionation (TREF)

TREF fractionates polyolefin molecules according to their crystallizability. The analysis involves sample dissolution, crystallization, and elution steps. First, the polyolefin samples were dissolved completely at high temperature. The dissolved polymer molecules were crystallized on non-porous glass beads according to their branching during a slow cooling cycle; molecules with least branching crystallize out first, i.e. at higher temperature. Finally, the crystallized molecules were gradually heated in a column under eluent flow. The dissolved molecules were washed out of the column and detected with an IR detector tuned at 2860 cm^{-1} (the stretching frequency of C–H bond in polyethylene).

The crystallizability data (elution temperature vs. mass fraction of polymer eluted) obtained in the above were then used to infer comonomer incorporation in the polymer chains, i.e. short chain branching. An in-house built TREF system was used in this work; detailed description of the system was given elsewhere (Lacombe, 1995; Zhang, 1999).

The following steps were used in the analytical TREF measurements:

1. About 1.5 g of glass beads (80–100 mesh) was added into a 20 mL glass vial, and 5–10 mg of the polymer sample was added
2. *o*-xylene (with 0.25 g/L 2,6-tert-butyl-4-methylphenol, anti-oxidant) was added to achieve a concentration of ~1 mg PE/mL o-xylene
3. A disposable (12 mm × 3 mm) magnetic stirrer bar was placed in the vial and crimp-sealed with Tegrabond disc 90/10 MIL (Chromatographic Specialties Inc.) with the Teflon face exposed to solvent.
4. The sealed bottle was heated gradually (with vigorous stirring) in a silicon bath to 125°C and maintained at this temperature for 2 h to ensure complete sample dissolution.
5. Sample was quickly transferred to ethylene glycol (heat) bath/circulator (Endcal RTE 220; interfaced with a PC for programmed temperature control) and held at 125°C for a further 2 h without stirring
6. Dissolved sample was cooled to –8°C at the rate of 1.5°C/h; cooling rates slower than 2°C/h prevents the undesirable co-crystallization and recrystallization (Wild, 1991). During this process, the polymer molecules crystallize on the glass-beads in the order of decreasing crystallinity.

7. The polymer-coated glass beads were sandwiched between two layers of the fresh glass beads in a TREF column and mounted in the TREF system. The TREF column consisted of a stainless steel tube 9.5 mm internal diameter, and 63.5 mm long fitted with 5-µm and 10-µm filter frits (Swagelok) at the solvent inlet and outlet respectively.
8. Sample was eluted with o-dichlorobenzene (containing 0.25 g/L 2,6-tert-butyl-4-methylphenol, anti-oxidant) pumped at 1.0 cm^3/min while the column temperature was ramped from 0°C–125°C at 1°C/min

3.4.6 Size exclusion chromatography (SEC)

An Alliance GPCV2000 equipped with a differential refractometer and three HT6E columns (Waters Corp., Milford, MA) was used to measure the molar masses of the polyolefin products. The columns and the detector were both maintained at 145°C. The eluent, HPLC-grade 1,2,4-trichlorobenzene (Fisher scientific) containing 0.3 g/L 2,6-tert-butyl-4-methylphenol (anti-oxidant), was pumped at the rate of 1.0 cm^3/min. The following standard samples were used to calibrate the molar masses of the polyolefin products: Linear alkanes C_{20}, C_{40}, and C_{60}; Standard reference polyethylene 1475, 1482, 1483, and 1484 (NIST NBS, Gaithersburg, MD); and a series of TSK Standards polystyrene of molar mass 870 to 8,420,000 (TOSOH Corp, Tokyo Japan). The retention time and molar masses of the standards were fitted by cubic equation –calibration curve. Before constructing the calibration curves, the molar masses of polystyrene standards were first converted to the polyethylene equivalents using the Mark-Houwink equation:

$$KM^{\alpha} = K'M'^{\alpha'} \qquad (3.1)$$

where M is the molar mass of polystyrene standard, M′ molar mass of polyethylene equivalent; K and α are the Mark-Houwink parameters for polystyrene; K′, and α′ are the corresponding values for polyethylene. O'Donohue and Meehan (1999) have given values of the Mark-Houwink parameters for polyethylene and polystyrene in TCB at different temperatures.

Each polymer sample was prepared in two concentrations (0.04–0.07 mass % in 1,2,4-trichlorobenzene), and each of these two solutions was injected twice; the reported molar masses are the average of these four measurements unless stated otherwise. Molar mass of a standard reference polyethylene is measured along with the samples; this provided a quick and reliable check on the performance of the GPC system.

4. Morphology of Supports and Supported Catalysts

The importance of catalyst morphology to gas-phase polymerization of ethylene and α-olefins was discussed in Section 2.4. The morphological properties of interest are the catalyst surface area, pore-size distribution, and pore volume. The surface area is important in dispersing the catalytic sites; however, the right pore size is necessary for this to occur. During polymerization monomer molecules must traverse the tortuous pore network in the catalyst particle to reach an active site. The rate or mechanism of diffusion in the pore network depends on the pore size – convection and bulk diffusion in macropores, and Knudsen diffusion in mesopores and micro pores (Leofanti *et al.*, 1998).

Results of the morphological investigation of the polymeric supports and those of the supported catalysts are presented in this chapter. The effects of support morphology, metallocene/MAO loading, and preparation methods on the catalyst precursors distribution are also discussed. Finally, the swellability and friability of some selected supports are discussed. The polymerization behavior of these catalysts is presented in subsequent chapters of this work.

4.1 Surface area and pore size distribution of supports and catalysts

Nitrogen sorption measurements as described in Section 3.4.1 were used to determine the surface area and pore size distribution of supports and catalysts. The sample outgassing temperatures were 50°C and 125°C for the catalysts and supports respectively. To check the significance of different outgassing temperatures on the measured surface area and pore size distribution, a National Bureau of Standards (reference material #8571) alumina sample was treated at similar conditions and analyzed. The result in Figure 4.1 shows that the pore size distribution at the two outgassing temperatures is essentially the same (within 4%). Similarly, the different sample pretreatment temperatures used in the BET measurements should not have significant effect on the measured properties. The catalysts were outgassed at 50°C to avoid significant change in the porosity compared to the catalysts injected into the polymerization reactor. Presumably for the same reason, Rahiala *et al.* (1999) pretreated MCM-41 support at 150°C and the supported metallocene/MAO catalyst at 70°C for BET measurements.

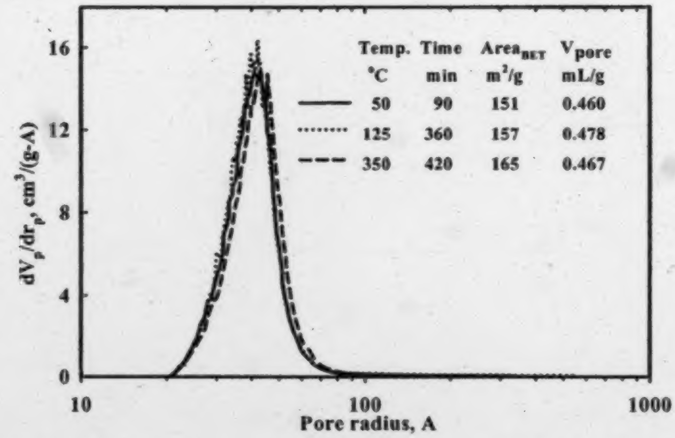

Figure 4.1. Influence of pretreatment condition on pore size distribution of alumina sample

Figure 4.2 presents the BET surface areas, and the mesopore (pores diameter 2-50 nm) volumes for several supports and their corresponding catalysts plotted in the order of increasing support surface area. Both the BET area and the pore volumes of the catalysts follow the trends of the corresponding supports. Some of the fluctuations observed in Figure 4.2 are partly due to the difference in MAO loading on the supports as indicated by the mass % Al in Table 4.1. dos Santos *et al.* (1997) reported no change in support surface area with typical metallocene loadings of up to 1 wt %.

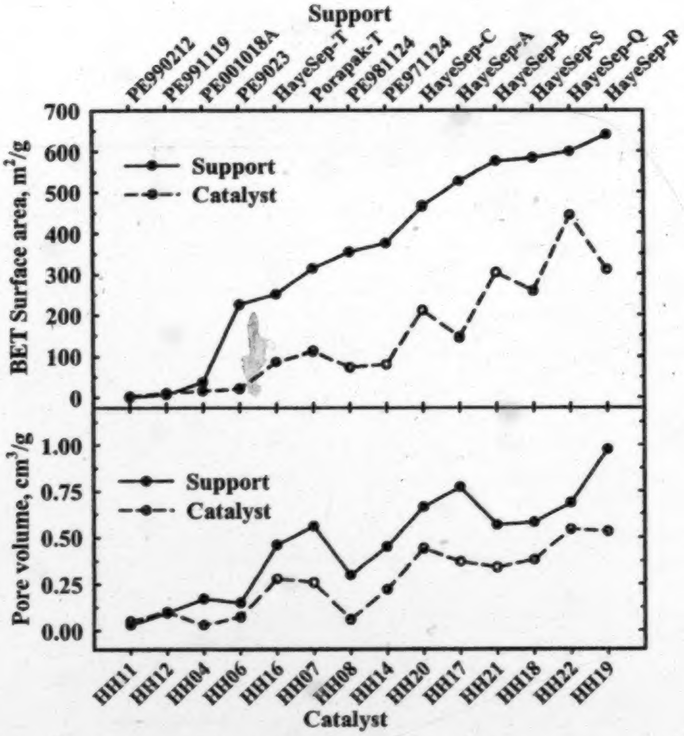

Figure 4.2. Surface area and mesopore volume of supports and supported catalysts (see Table 3.1 for supports identification).

As previously described (Section 3.5.1), the Omnisorb system uses the Kelvin equation on desorption isotherm data to determine the sample pore size distribution. Before discussing the pore size distributions of the supports and the catalysts, it is important to note the limitations of the Kelvin equation. The adsorption/desorption isotherms for two support/catalyst pairs are shown in Figure 4.3 (HayeSep-R/HH19) and in Figure 4.4 (HayeSep-Q/HH22). The desorption isotherms of most supports and catalysts show an accelerated drop in *volume adsorbed* around a *relative pressure* (P/P_0) value of 0.4 (more prominent in Figure 4.4 than in 4.3). This manifests in the pore size distribution curve as a strong and uniform artifact peak near the 2 nm pore size (Figure 4.5). The position of this peak is adsorbate dependent, and it is due to the tensile strength effect of the adsorbate film; Gregg and Sing (1982) discussed this extensively. A meniscus separating capillary-condensed liquid from its vapor can only stand pressure difference equal to the surface tension of the liquid. When this value is exceeded, the meniscus falls apart and the Kelvin equation becomes invalid.

Table 4.1 Mesopore characteristics of polymeric supports and supported catalysts

Catalyst	t-plot area, m^2/g		Mesopore volume cm^3/g		Mean pore radius nm		Precursor loading mass%	
	Support	Catalyst	Support	Catalyst	Support	Catalyst	Zr	Al
HH04	39.3	16.24	0.114	0.027	5.82	3.28	0.159±0.004	15.8 ± 0.4
HH06	89.21	16.19	0.213	0.074	4.78	9.12	0.152±0.003	11.7 ± 0.3
HH07	274.41	113.25	0.527	0.244	3.84	4.31	0.128±0.003	16.5 ± 0.4
HH08	179.40	33.48	0.365	0.050	4.07	2.96	0.209±0.008	16.4 ± 0.4
HH12	12.61	10.59	0.112	0.037	17.81	7.07	0.119±0.003	7.7 ± 0.2
HH14	182.83	44.33	0.354	0.117	3.87	5.28	0.235±0.004	14.9 ± 0.4
HH16	210.52	74.05	0.419	0.256	3.98	6.93	0.131±0.003	11.1 ± 0.3
HH17	301.08	116.51	0.702	0.359	4.66	6.16	0.102±0.003	11.4 ± 0.3
HH18	213.39	104.41	0.523	0.373	4.90	7.15	0.162±0.003	10.1 ± 0.2
HH19	437.40	177.03	0.975	0.531	4.46	5.99	0.164±0.004	11.2 ± 0.3
HH20	345.89	81.08	0.710	0.382	4.10	9.42	0.181±0.004	11.8 ± 0.3
HH22	358.88	285.13	0.607	0.488	3.38	3.43	0.112±0.003	3.7 ± 0.1
HH29	–	–	–	~0.013	–	–	0.128±0.002	7.1 ± 0.2

The continuum-principles basis of the Kelvin equation is generally not valid for pores that are few molecular diameters wide; both the molar liquid volume and the surface tension deviate considerably from the bulk liquid values. The artifact peak that results from the above limitation frequently appears in the pore size distributions of macroporous gels. It is sometimes left unnoticed in the presence of stronger peaks as in Zhang *et al.* (2003) or wholly attributed to the pore structure of the gels (Rosenburg and Flodin, 1986, 1987a, 1987b).

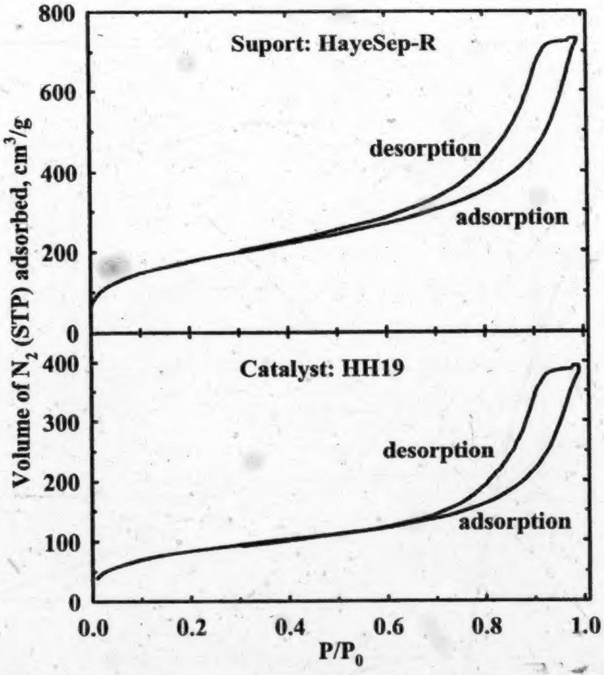

Figure 4.3 Adsorption-desorption isotherms for HayeSep-R and Catalyst HH19

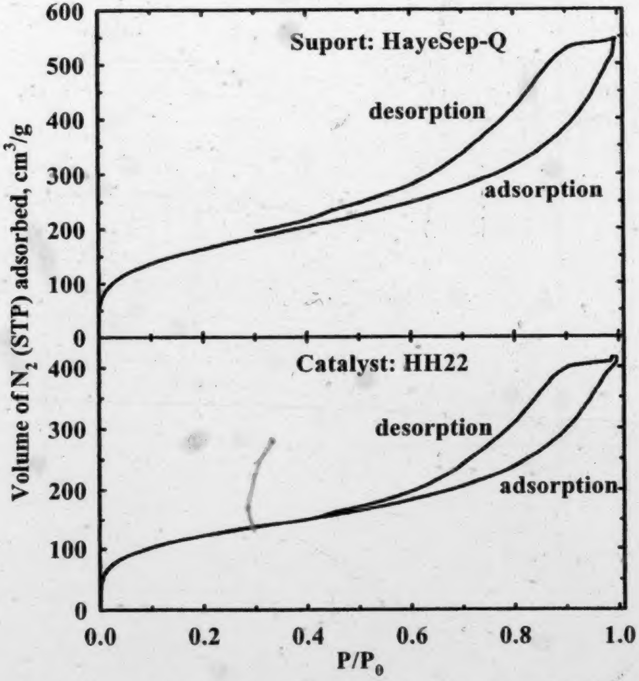

Figure 4.4 Adsorption-desorption isotherms for HayeSep-Q and Catalyst HH22

Due to the above limitations of the Kelvin equation, the sharp pore size distribution peaks in the 1 to 2 nm pore radius range were considered artifacts and neglected in pore size analysis. Broeckhoff and Beek (1979), and Carrado and Xu (1999) have similarly ignored these artifact peaks. The Omnisorb manual also alerts users to the presence of the "artifact peak" in the pore size distribution at pore radius of 1 to 2 nm.

The pore size distributions in Figure 4.5 are representative of the first group of supports in Table 3.1 and the corresponding catalysts. There is a wide variation in the pore size distribution of the supports, but the pore size distribution for each pair of support and catalyst are similar. This similarity signifies that the metallocene and MAO largely diffused into and coated the pore walls of the support, thereby reducing the pore radii. The decrease in pore size of catalyst relative to the corresponding support was more pronounced with the smaller pores. This can result in an increase in the mean pore size from support to catalyst (Table 4.1). The mean pore radii ($\bar{r}_P$, nm) were calculated according to Equation 4.1 below. Note that the most probable pore sizes of the catalysts, as observed from BET plots, are similar to those of the corresponding supports.

$$\bar{r}_P = \frac{2000V_P}{A_P} \tag{4.1}$$

where V_P is the pore volume in cm^3/g and A_P the surface area in m^2/g

Uniform coating of the pore walls would ideally result in a shift in the pore size distribution towards smaller pores as observed with silica impregnated with ~1–7 wt % metallocene (Quijada *et al.*, 1998). The procedure of Quijada *et al.* (1998) also involved washing off the excess metallocene from the impregnated silica using toluene. The form of coating that results from impregnating a support with metallocene/MAO at 18–57 mass % (without washing) as used in this work would be far from ideal; hence, the shift in pore size distribution was only observed in a few cases.

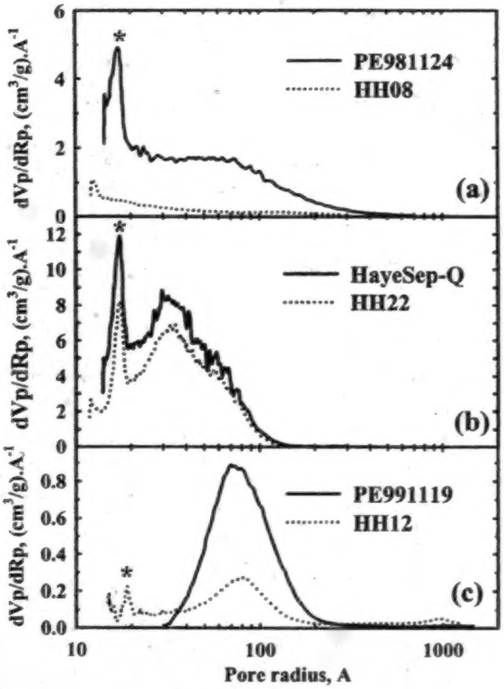

Figure 4.5 Pore size distributions of DVB based supports and supported catalysts having no functional groups (* – artifact peak).

Supports PE981124 and HayeSep-Q in Figure 4.5 were both synthesized from divinylbenzene monomer; however, the in-house support PE981124 had lower surface area of 353 m^2/g mainly contributed by pores of radius 2–10 nm, and relatively small but significant surface area contribution from pores >10 nm radius. On the other hand, HayeSep-Q has a normal unimodal pore size distribution with mean pore radius of ~30 Å (solid lines in Fig 4.5 a and b). The pore volume of Catalyst HH08 is only ~30% of the support pore volume while the pore volume of Catalyst HH22 is 80% of the support pore volume due to lower Al loading (Table 4.1). Support PE991119 did not exhibit the artifact peak near 2 nm because it had no pores <3 nm in radius; hence, there was a cut off in the pore size distribution at relative pressure higher than 0.4.

Representative pore-size distributions of the second group of supports are shown in Figure 4.6. PE971124 is almost identical to PE981124 (see Figure 4.5a); PE9023 also has similar pore size distribution but with only 60 % the pore volume of the former two supports. Expectedly, the catalysts also showed similar pore size distributions. Note that PE990212 is virtually non-porous, it appears as clear glass beads under optical microscope with too low surface area for nitrogen sorption measurements; Figure 4.6d is shown for the completeness of discussion only. Due to low porosity of Support PE990212 (0.03 cm^3/g, Table 3.1), most of the metallocene and MAO used in the preparation of Catalyst HH11 was left on the particle exterior surface as irregular chunks similar to Catalysts HH23 and HH24, the solid $(n\text{-BuCp})_2ZrCl_2$/MAO complex. The pore size distribution of HH11 (Figure 4.6d; dotted line) is the sum of the pore size distributions of the support (solid line), and the solid $(n\text{-BuCp})_2ZrCl_2$/MAO complexes. The pore size distributions of Catalysts HH23 and HH24 are shown in Figure 4.7.

The pore size distributions of four commercial supports possessing heteroatoms (third group in Table 3.1) are presented in Figures 4.8. Except for HayeSep-R, the pore size distributions appears to be rather flat in the 20–100 Å pore radius range similar to Figures 4.5(a) and 4.6(a and b). However, the pore size distribution of catalysts HH17–HH20 (Figure 4.8) differed from those of HH08, HH06, and HH14 (Figures 4.5 and 4.6). In Figure 4.8, the extent of pore fill-up progressively decreases with increasing pore size; a more uniform pore fill-up was observed with the in-house supports (Figures 4.5a, 4.6a and b).

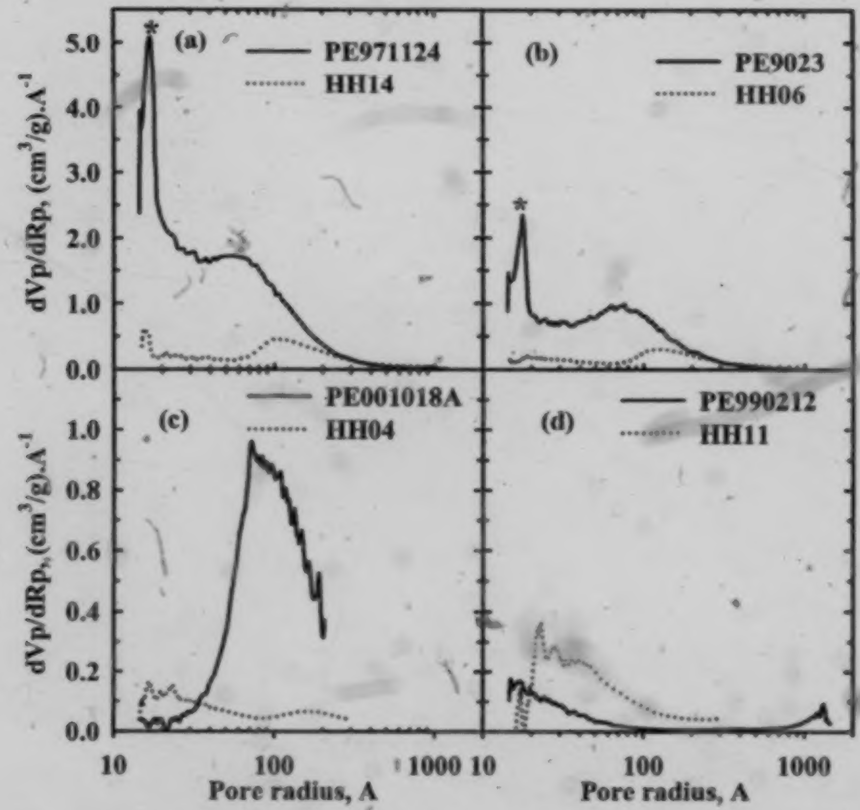

Figure 4.6 Pore size distributions of DVB based supports with HEMA and supported catalysts (* – artifact peak).

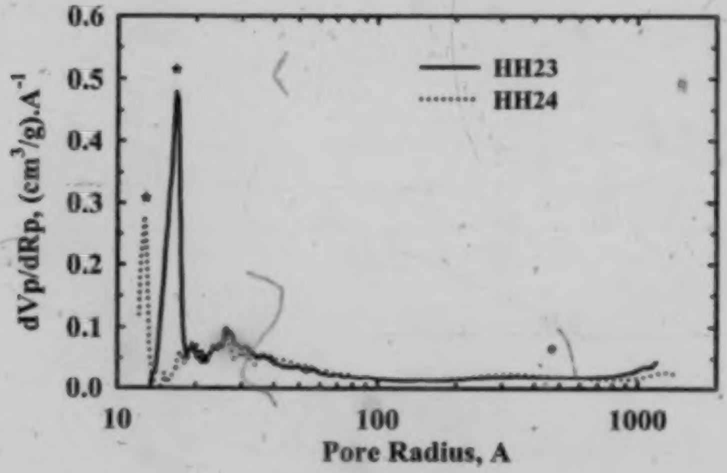

Figure 4.7 Pore size distribution of solid $(n\text{-BuCp})_2ZrCl_2$/MAO complexes (* – artifact peak).

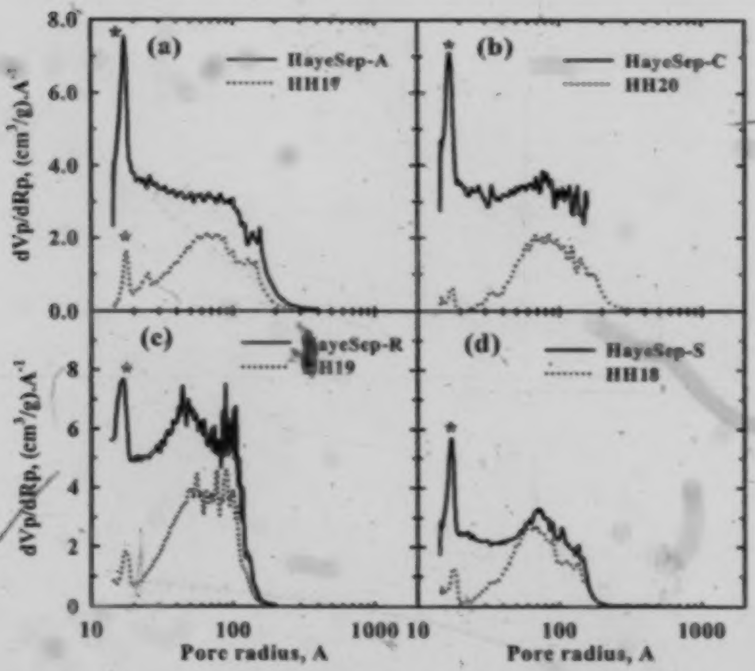

Figure 4.8 Pore size distributions of commercial supports having heteroatoms and the corresponding catalysts (* – artifact peak).

The commercial supports HayeSep-T and Porapak-T are cross-linked with (poly)ethyleneglycol dimethacrylate segments; the pore size distribution of these supports are shown in Figures 4.9. In both supports, impregnation with metallocene/MAO had greater effect on the smaller mesopores. This effect was less severe than the previous supports (Figure 4.8), even though approximately the same amount of metallocene/MAO (per unit mass of support) was used in preparing Catalyst HH16 and Catalysts HH17–HH20. Catalyst HH07 had even greater amount of metallocene/MAO than HH17–HH20.

Figure 4.10 shows representative variation of cumulative pore volumes for the pore radii range: 1-2 nm, 2-3 nm, 3-4 nm, 4-5 nm, 5-10 nm, 10-20 nm, 20-30 nm, and >30 nm. The median value of each range was used as the abscissa in the figure (1 nm = 10 Å). Each of the support/catalyst pair in Figure 4.10 belongs to a different category of supports (in Section 3.1). The pore volume distributions for the catalysts closely follow those of the corresponding supports, again confirming the coating of pore walls by the metallocene and MAO.

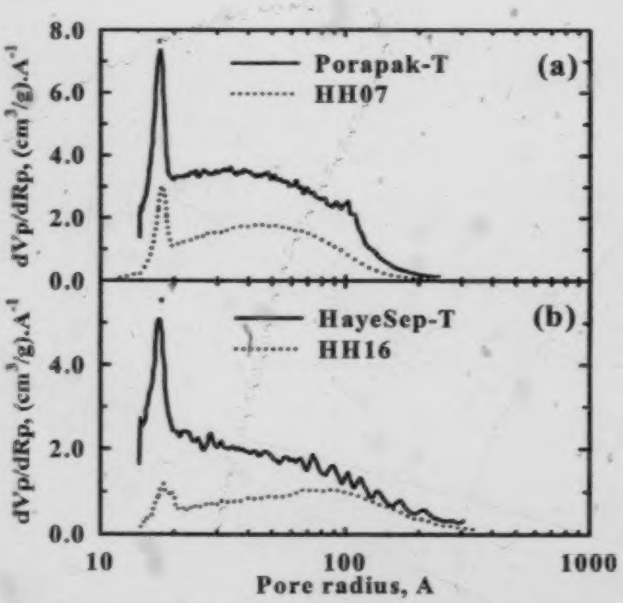

Figure 4.9 Pore size distribution of poly(EGDM) supports and catalysts(* – artifact peak).

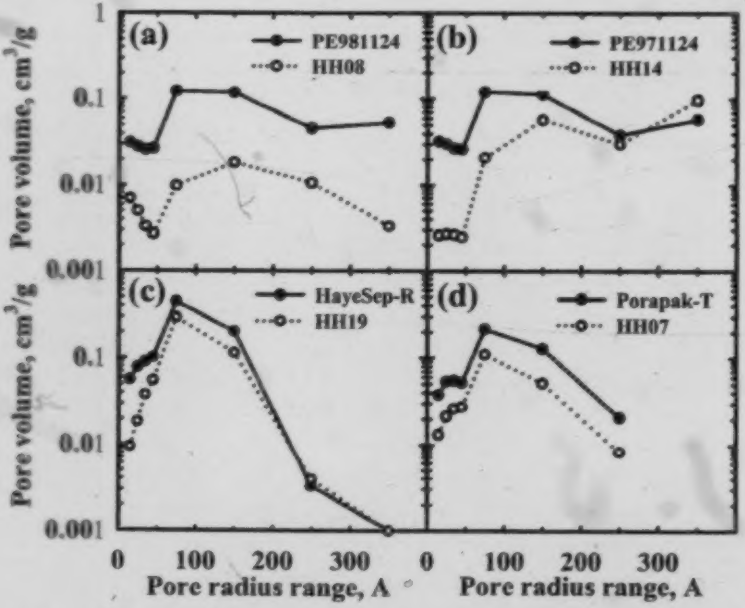

Figure 4.10 Pore volume distribution of supports and catalysts.

4.2 Effect of MAO loading on catalyst morphology

Increases in the metallocene and MAO loadings progressively reduced the pore size and pore volume of the catalysts relative to the support (see Figure 4.11 for in-house and Figure 4.12 for commercial support). This indicates loading of the metallocene and MAO into the pores. The similarity in pore size and pore volume distributions of catalysts with similar metallocene/MAO loadings shows the reproducibility of the heterogenization process.

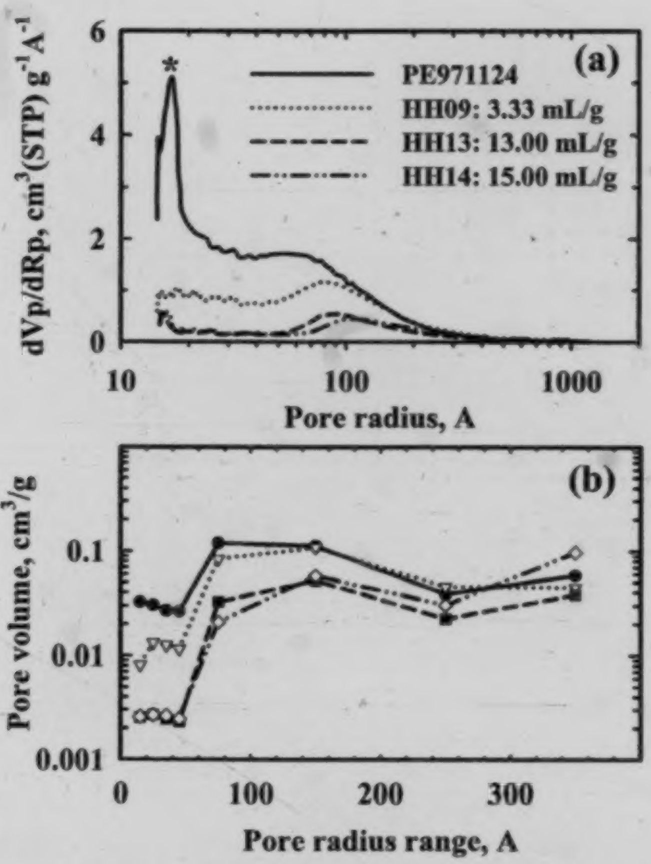

Figure 4.11 Effect of the amount of MAO (10 mass % solution) on (a) pore size and (b) pore volume distribution of in-house support and the corresponding catalyst.

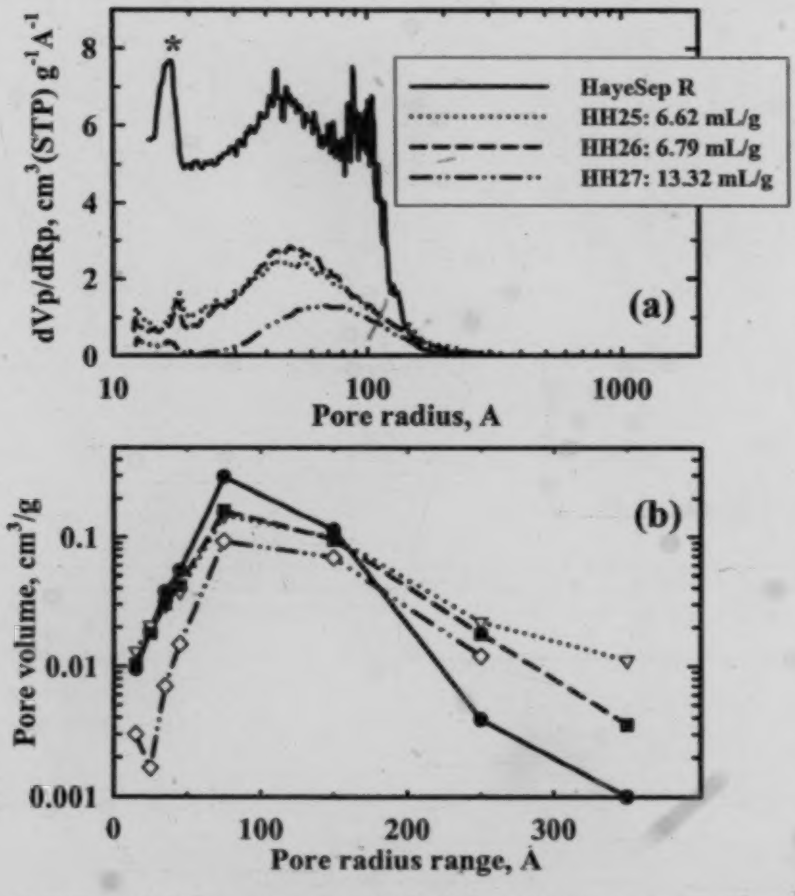

Figure 4.12 Effect of the amount of MAO (10 mass % solution) on (a) pore size and (b) pore volume distribution of commercial support and the corresponding catalyst.

4.3 Al and Zr loading and distribution in supported catalysts

The support pore size largely determines the loading and the distribution of metallocene/MAO impregnated in the support. In the catalyst preparation procedure employed in this work (Section 3.3), the MAO and metallocene adsorbed on the support are probably in equilibrium with the bulk solution prior to the commencement of solvent evacuation. When the solvent evacuation starts, the solution becomes more concentrated, but it is unlikely to maintain the above equilibrium due to the low diffusivity of (macromolecular) MAO and the gelling of the concentrated solution. The excess metallocene/MAO remain on the surface of the catalyst particles and on the walls of the flask. Representative morphologies of supports and the corresponding catalysts are shown in Figures 4.13 for supports synthesized in our laboratory and in Figure 4.14 for commercial supports.

It is clear from the SEM micrographs that the catalysts retain the morphology of the supports except for the excess MAO/metallocene coated on the outer surface of some of the catalyst beads (e.g. Catalyst HH16, Figure 4.14b). The same amount of MAO (per gram of support) was used in making the catalysts in Figures 4.13 and 4.14; in both figures, the coating on supports with smaller pore-volume are more prominent (Figure 4.13h and 4.14b). However, there may be other factors influencing the total amount adsorbed; the pore volume of HayeSep-T was greater than that of PE9023 but HH06 is less coated than HH16.

The qualitative distribution of aluminum inside some catalyst particles, as determined by EDX is shown in Figures 4.15 and 4.16. These catalysts were selected based on the difference in their activity behavior (see Chapter 7). Most of the catalyst particles have uniform distribution of aluminum. The shape of the linescan in Figure 4.15b is due to uneven particle surface not the Al distribution. The EDX method used was not sensitive enough for zirconium. However, zirconium distribution is expected to follow that of aluminum because the smaller size metallocene molecules can diffuse through the support pores more easily and form the active complex with MAO. Metallocene loading on polymeric supports was reported to increase with the amount of immobilized MAO (Liu *et al.*, 1999; Meng *et al.*, 1999), and for the catalyst preparation

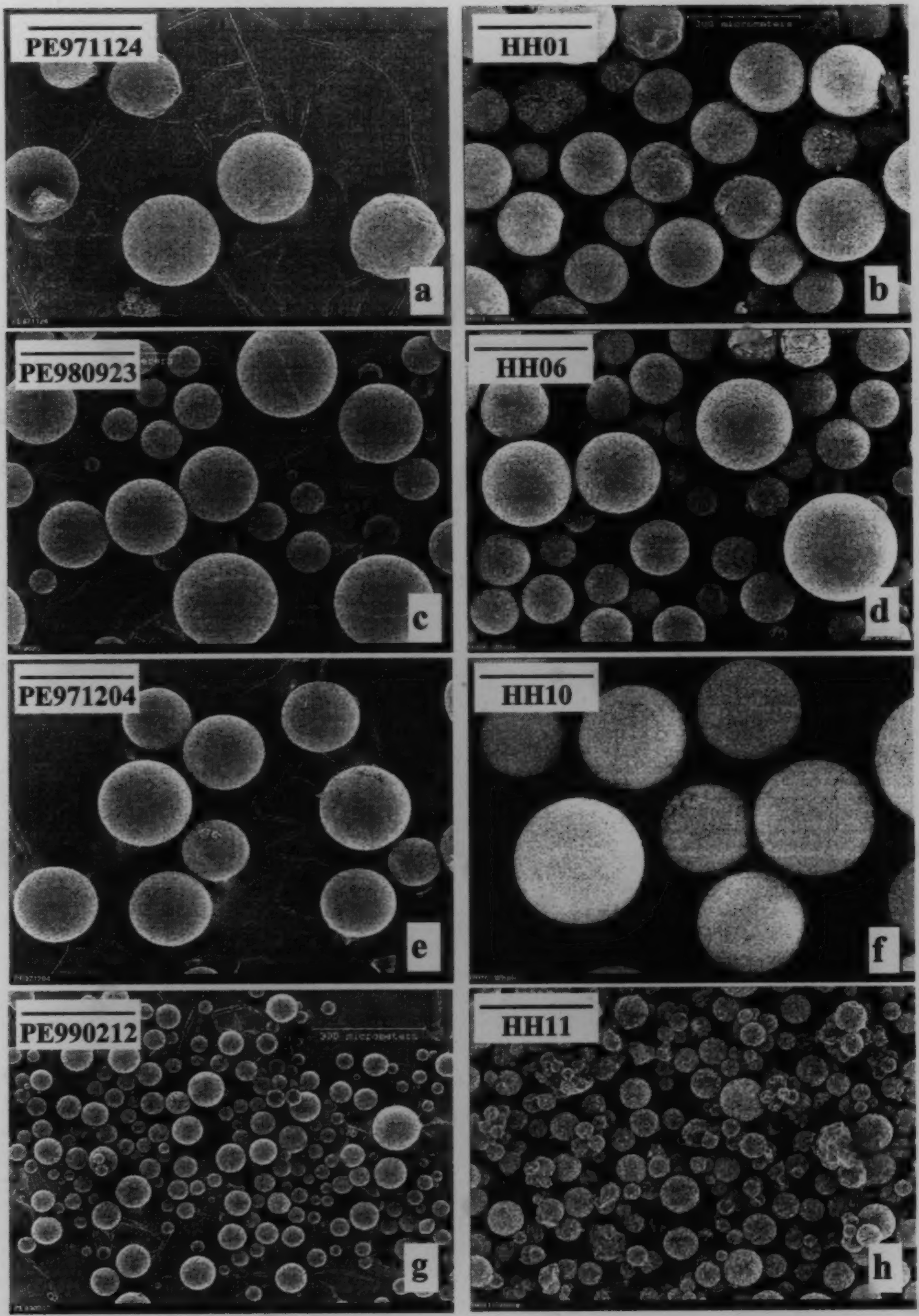
PE971124
HH01
300 micrometers
a
b
PE980923
HH06
c
d
PE971204
HH10
e
f
PE990212
300 micrometers
HH11
g
h

Figure 4.13 Morphologies of different supports (left column) synthesized in our laboratory and the corresponding supported catalysts (right column). Scale bar = 300μm.

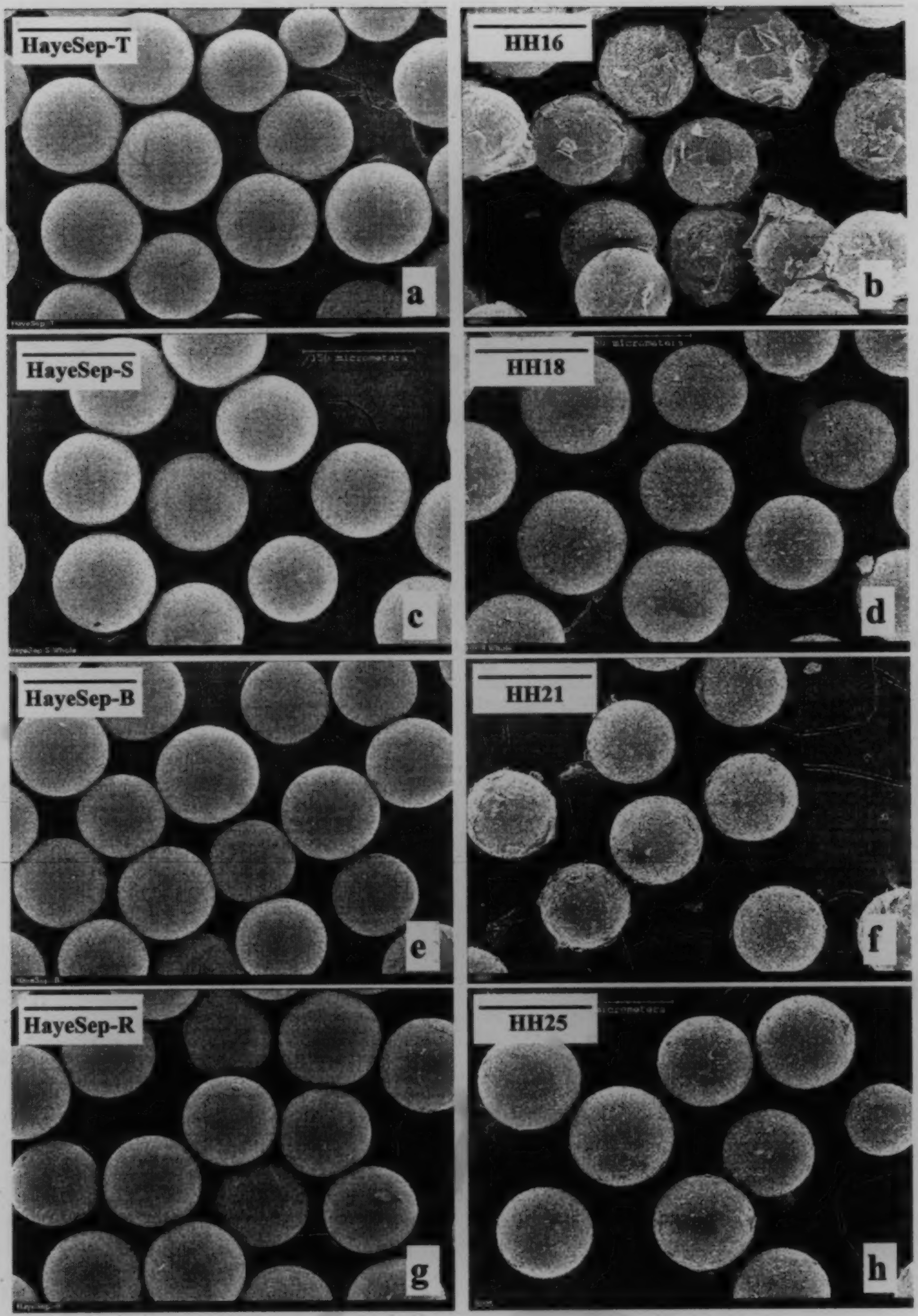
HayeSep-T
HH16
a
b
HayeSep-S
HH18
c
d
HayeSep-B
HH21
e
f
HayeSep-R
HH25
g
h

Figure 4.14 Morphologies of different commercial supports (left column) and the corresponding supported catalysts (right column). Scale bar = 150 μm.

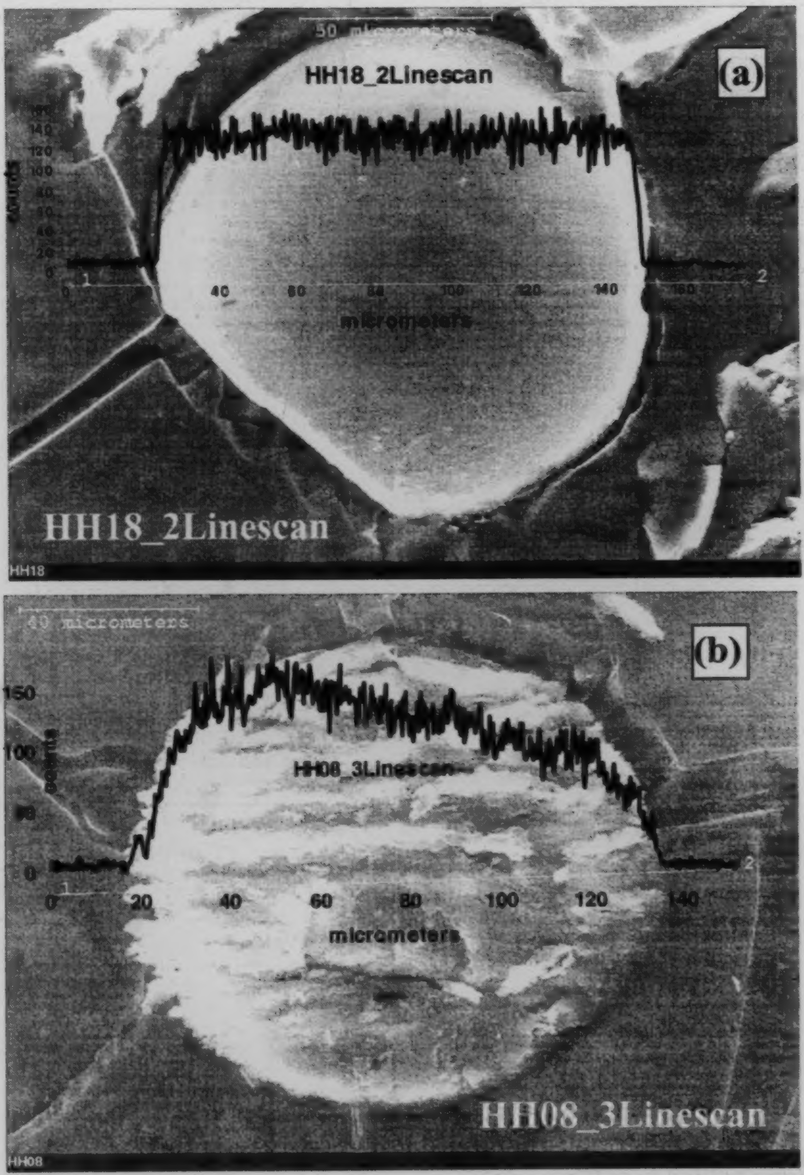

Figure 4.15 EDX line scans for aluminum distribution across (a) Catalyst HH18 and (b) Catalyst HH08 particles.

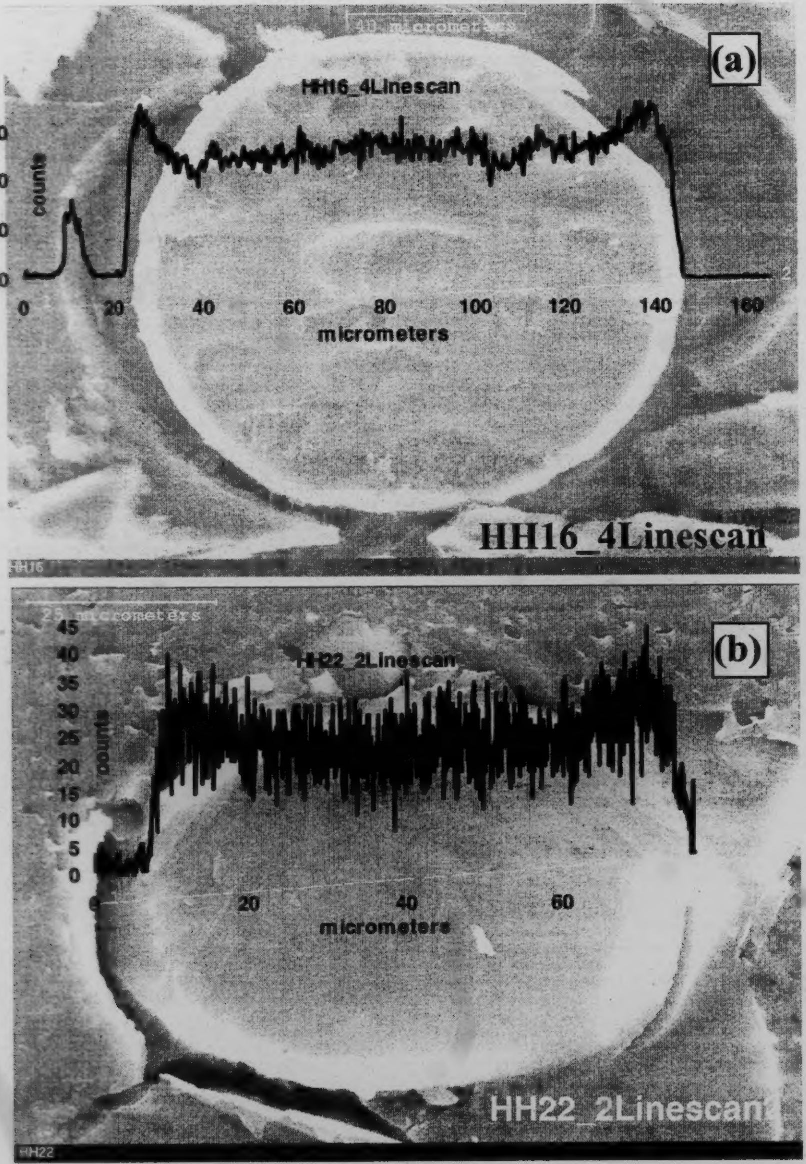

Figure 4.16 EDX line scans for aluminum distribution across (a) Catalyst HH16 and (b) Catalyst HH22 particles.

method employed, the aluminoxane-metallocene chemistry, rather than the support material dominates the interaction between the MAO modified surface and the metallocene (Harrison *et al.*, 1998).

Uneven cocatalyst (Al) distribution was reported for supported (industrial) metallocene catalyst; this was largely responsible for non-uniform polymerization start-up of individual catalyst particles inside the reactor (Knoke *et al.*, 2003; Rytter and Ott, 2001). The polymerization start-up of individual catalyst particles was shown to correspond to the activity growth in ethylene polymerization catalyzed by supported metallocene/MAO catalysts (Zoellner and Reichert, 2001; Zöllner and Reichert, 2002). In spite of the potential for producing catalyst particles with uneven precursor loading, the current "indirect" heterogenization method was employed because it is industrially the most promising method (Kaminsky and Laban, 2001).

4.4 Catalyst composition

The measured aluminum contents (by INAA) of all the supported catalysts were lower than the estimated values based on the total amount of reagents as shown in Figure 4.17a (see Appendix A, Table A-2 for a complete listing of catalyst composition). This could be due to one or more of the following factors:

- The unadsorbed metallocene/MAO dries up on the walls of the catalyst preparation flask, sometimes agglomerating the catalyst particles. The composition for such fraction recovered from preparation of Catalyst HH15 had 20 mass% aluminum compared to <12 mass% Al in the free flowing catalyst.
- No mass loss of the supports was assumed in the composition calculations although there could be loss of residual solvents during the heating/evacuation stage of the

catalyst preparation. Liquid condensation was occasionally observed on the colder parts of the flask during heating/evacuation. This was not observed with any of the commercial supports; the latter were preconditioned by the manufacturer at 165-200°C under N_2 flow. Gas evolution during reaction of support with MAO would also tend to lower the mass of the supported MAO, but this effect is not significant.

- The mass of MAO used in catalyst preparation was based on the manufacturer's value. However, it is well known that MAO gels with age; this was also observed in our laboratory. The aluminum composition of the clear MAO solution used in the catalyst preparations is likely lower than the original (average) value stated by the MAO supplier since MAO concentration is higher in the gel than the clear solution.

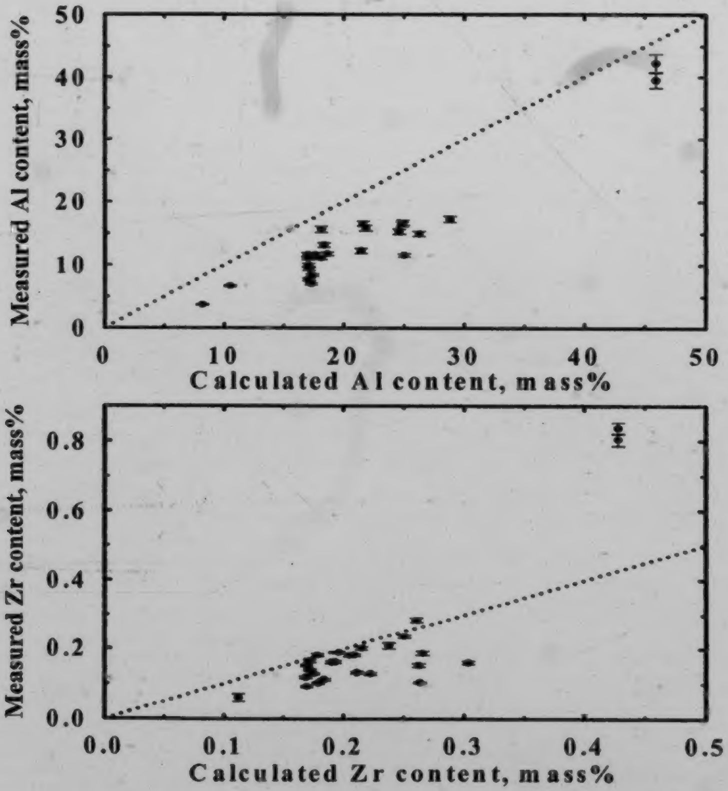

Figure 4.17 Variation of catalyst composition from estimates based on reactants used

The last point is further clarified by comparing the calculated and measured compositions of Catalysts HH23 and HH24 [unsupported, solid $(n\text{-BuCp})_2ZrCl_2$/MAO complexes]. In particular, the measured aluminum content of HH24 (that was heated/evacuated longer) was quite close to the value calculated using Equation 4.2 (42.2 mass % and 45.9 mass % respectively). Note that MAO gelling should not have significant effect on the calculated mass % Al value because gelling has the same effect on $mass_{Al}$ and $mass_{MAO}$ in Equation 4.2, and the 25 mg of metallocene used in the catalyst preparation was insignificant. The aluminum content of solid MAO (46.5 mass %, based on –Al–Me–O– unit) is independent of gelling.

$$mass\,\%\,Al = \frac{mass_{Al}}{mass_{(n-BuCp)_2ZrCl_2} + mass_{MAO}} \times 100 \tag{4.2}$$

However, gelling of the MAO solution used in the catalyst preparation should affect the zirconium composition of the catalyst. MAO gelling would result in lower than anticipated mass of solid MAO in Equation 4.3 (from a given volume of MAO solution). This will tend to exaggerate the zirconium content; the measured value was higher than the calculated (0.84 mass % and 0.43 mass % respectively), Figure 4.17 b.

$$mass\,\%\,Zr = \frac{mass_{Zr}}{mass_{(n-BuCp)_2ZrCl_2} + mass_{MAO}} \times 100 \tag{4.3}$$

Figure 4.17a shows that the measured Al content remained relatively flat for values of calculated Al content higher than 20 mass % probably due to pore saturation. The excess metallocene/MAO from these catalyst preparations would typically be left as a coating on the flask walls. From the above discussion, it is clear that the measured aluminum and zirconium contents of the catalysts are more reliable than the estimated values based on the amount of reagents used in the catalyst preparation. Therefore, subsequent discussions in this work are based on the measured aluminum and zirconium contents of the catalysts.

4.5 Effect of preparation methods on catalyst morphology

The heterogenization procedure of metallocene catalyst has underlining importance on its performance in polymerization (Knoke *et al.*, 2003). By varying the heterogenization procedure, it is possible to prepare supported metallocene/MAO catalysts with the MAO (and hence, the metallocene) uniformly distributed inside the catalyst particles (Rytter and Ott, 2001; Fink, 1999) or simply deposited on the surface (Goretzki *et al.*, 1999). One supporting procedure was generally used in this work (Chapter 3) except for small variations in Catalyst HH01 and HH28.

In Catalyst HH01, the support/MAO suspension in toluene was evacuated to dryness prior to addition of metallocene solution. The added metallocene solution also contained 0.12 mL neat TIBA. SEM micrographs of catalyst HH01 shows that its morphology is quite similar to the morphology of Catalyst HH09 and HH13-HH15 (made from the same support). However, their porosities are quite different; Catalyst HH01 with macropores only, had lower surface area and pore volume.

The support used in preparing Catalyst HH28 was first treated with TMA solution (35 vol % in heptane) containing $(Al)_{TMA}/(N+O)_{Support}$ ratio = 1 overnight and vacuum dried before preparing the catalyst in the normal procedure described in Chapter 3. The TMA treated support had 5.59 ± 0.12 mass % aluminum. Thus, Catalyst HH28 has higher aluminum content than Catalysts HH25 and HH26 prepared with the same support and with similar amounts of MAO (see details in Appendix A, Tables A-1 and A-2).

4.6 Friability and swellability

The friability of polymeric supports was determined after 1 min grinding as described in Section 3.4.2.1. The friability was quantified as the volume % of the ground support that had sizes smaller than the original support. This is shown as the shaded areas in Figure 4.18. Both polymeric supports PE981124 and HayeSep-Q in Figure 4.18 are poly(divinylbenzene), but the in-house support PE981124 was more friable. The friability of other supports is summarized in Table 4.2.

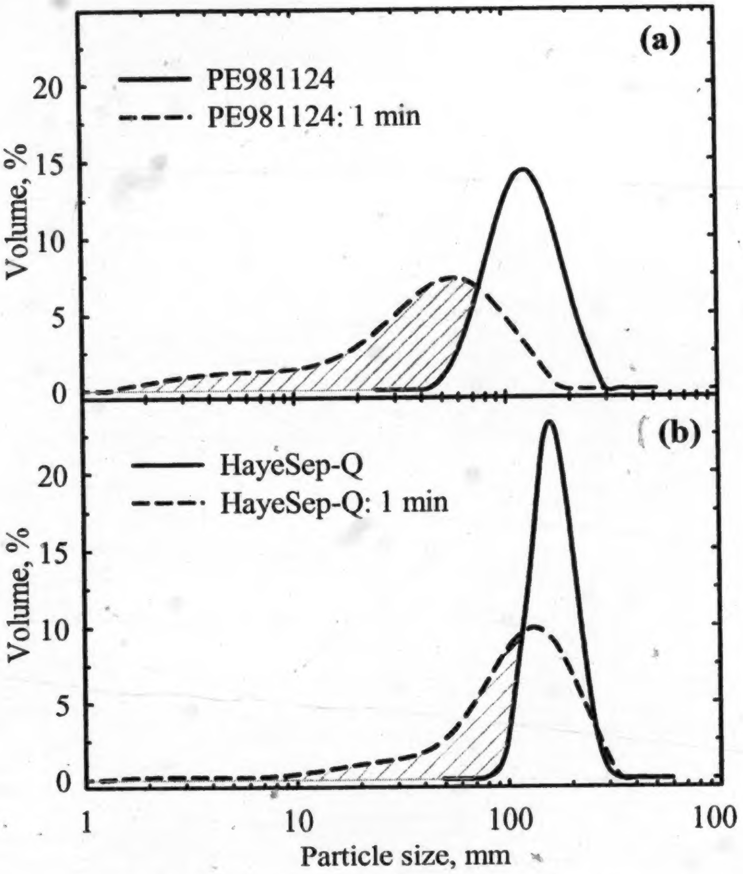

Figure 4.18 Particle size distribution of fresh and milled supports (a) PE981124, and (b) HayeSep-Q

Table 4.2 Friability of selected supports

Support designation	Monomer*	Friability, vol %
HayeSep-A	DVB/EGDM	27.3
HayeSep-B	DVB/PEI	22.1
HayeSep-C	DVB/Acrylonitrile	15.3
HayeSep-R	DVB/N-Vinyl-2-pyrrolidinone	18.1
HayeSep-S	DVB/4-Vinylpyridine	19.4
HayeSep-Q	DVB	23.7
Porapak-T	EGDM	16.0
PE981124	DVB	49.7
PE991119A	STY/DVB	43.0
PE9023	HEMA/STY/DVB	43.8
PE971124	HEMA/DVB	66.0

* Acronyms are defined in *List of Abbreviations and Nomenclature*

The fraction of the divinylbenzene crosslink agent used in synthesizing the in-house supports (Table 3.1) is high enough to guarantee non-swelling beads even in good solvent (Sherrington, 1998). On the other hand, only the components of the commercial supports are known. Therefore, some selected commercial supports were tested for swellability in toluene because toluene was the solvent used in the catalyst preparation. Among the five supports tested [HayeSep-A, HayeSep-Q, HayeSep-S, HayeSep-T, and poly(STY/1%-DVB)], only the poly(STY/1%-DVB) swelled by 78 %. The swelling of the remaining four was between 0.0-2.4 %, well within experimental error of the method.

The poly(STY/1%-DVB) is a gel-type swellable beads. The significant swelling of this support probably explains why Catalyst HH29 has the lowest MAO loading (7 mass % Al) of the catalysts prepared with comparable amounts of MAO/g-support (Appendix A, Tables A-2). During catalyst drying, the swollen gel beads shrink, thereby "squirting out" the swelling solution (containing metallocene and MAO). On the contrary, the non-swelling beads have permanent pores from which only the solvent evaporates during the catalyst drying.

Summary of the morphology of supports and catalysts

Impregnation of the support particles by MAO reduced the pore size of the support. The metallocene and MAO diffused into the support particles to form supported catalysts with fairly uniform aluminum distributions. The measured Al and Zr content of the supported catalysts were lower than expected (based on the amount of reactants used) due to MAO aging and the incomplete absorption of the metallocene/MAO solution. Incomplete absorption of the metallocene/MAO solution resulted in the formation of flaky $(n\text{-BuCp})_2ZrCl_2$/MAO complex on the catalyst particles. The presence of this complex is more prominent with the low pore volume supports.

A relatively simple method was devised that allows measuring the friability of less than 1 g of support. Using this method, support friability was found to be in the range of 15-66%, with the commercial supports having lower friability (15 to 30%) while the friability of the in-house supports tested is between 43 to 66%. The catalysts made with the in-house supports retained the pore size distribution of the latter. For the commercial supports, the pore size distribution is altered because the smaller pores are affected more strongly. The effects of the support/catalyst morphologies and the catalyst compositions (discussed in this chapter) on polymerization activity and polymer properties are presented in Chapters 7-9.

5. Exploratory Experiments I: Reactor Behavior[*]

The first part of this thesis work involved the design and fabrication of a gas-phase polymerization reactor. Details of the following major features of the new reactor system are presented in Section 5.1: Feed purification, data acquisition, temperature control, and gas-phase analysis. On setting up the reactor system, several polymerization runs were conducted to study the reactor behavior, i.e. to understand the impact of procedural steps involved in running gas-phase polymerizations with the new reactor system. The second objective of this set of runs was to detect any malfunctions in the system and rectify them accordingly. Section 5.2 presents the results of these test-runs. Equipment modifications and operational changes during the test-runs and subsequently in the course of the author's research using the reactor are also discussed. Results of the investigation of the effects of stirrer type, stirring rate, sodium chloride seedbed, and the static mixers on reactor temperature control are also presented in Section 5.2. Finally, the importance of reproducibility in gas-phase polymerization over supported metallocene/ MAO catalysts necessitated the dedication of Section 5.3 to this subject.

5.1 Description of the new polymerization reactor system

The configurations used in controlling the temperature in lab-scale polymerization reactors (Section 2.3.1) have their limitations: Circulating coolant in external jackets with single liquid inlet and outlet is characterized by poor coolant flow distribution; limpet coils are used to improve flow distribution (Hewitt *et al.*, 1994). Cooling jackets normally have lower heat transfer coefficient than cooling coils (*ibid* p. 939). Winding the cooling coil on the external surface of the reactor results in poor thermal contact between the coils and the reactor walls. To overcome this, Han-Adebekun *et al.* (1997) soldered copper (cooling) coils to the outside of their reactor. Placing cooling coils inside the reactor provides much better heat transfer, but interferes with the agitator configuration and makes reactor cleaning very difficult. Operating the reactor in supercondensed mode can improve heat transfer considerably (Jiang *et al.*, 1997), but could be too expensive to apply in lab-scale reactors. The new reactor was, therefore, designed with the objective to improve temperature control and head gas analysis, while avoiding the above shortcomings.

---

[*] Parts of this chapter are in press in The Canadian Journal of Chemical Engineering

The temperature control performance of the new reactor is demonstrated in Figure 5.1 by comparing its performance to the performance of a 1 L reactor under similar initial polymerization conditions (1.4 MPa, 80°C, ~14 mol/m^3 1-hexene). Further discussion on the temperature control performance of the reactor is presented in Section 5.1.2.

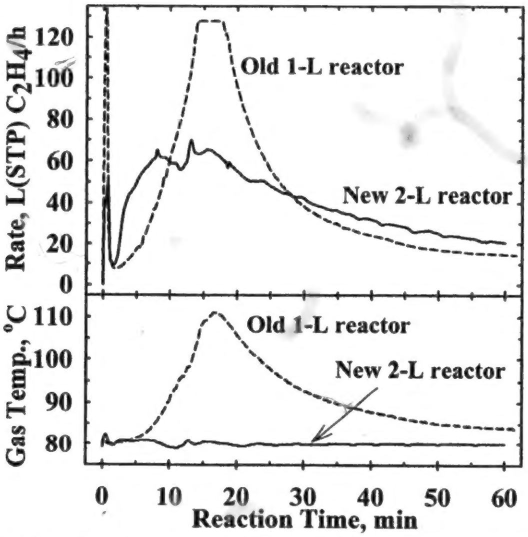

Figure 5.1 Comparison of the temperature control performance of the new 2 L reactor to the 1 L reactor.

5.1.1 The reactor, feed purification, and data acquisition systems

The new 2-L reactor (Figure 5.2a) was fabricated from a single piece of solid stainless steel (316) cylinder. The reactor has a torispherical bottom that provides smooth (tangential) connection between the sidewall and the bottom surface of the reactor; sharp corners serve as dead space for fine particles. Twenty cylindrical channels (6.35 mm internal diameter, 181 mm long) were drilled on the reactor wall as shown in Figure 5.2 to enhance heat exchange between the reactor and the coolant. The channels were placed symmetrically with sufficient gaps for side thermocouples (Figure 5.2 b).

The relatively high total flow cross-section of the above 20 channels (6.33 cm^2) makes the coolant flow highly laminar; Reynolds number was generally less than 100 even at high coolant circulation rate. Therefore, 20 Kenics-type static mixers (6.35 mm diameter, 187 mm long, 17.5 mm element length) as described by Šír and Lecjaks (1982), were custom-built (from rectangular strips of stainless steel) and inserted into the channels. The mixing elements in each of the mixers were welded together for ease of insertion and retrieval.

The coolant exits the channels into a ⅜″ × ⅜″ gutter around the reactor (Figure 5.2a). The gutter is covered by an o-ring sealed aluminum ring header from which the coolant flows back to the heat bath through six equally spaced outlets. This multi-outlet design ensures better flow distribution (and hence heat transfer) as compared to single inlet-outlet designs commonly used in jacketed lab-scale reactors. Eight thermocouples (Type-J; 3 mm stainless steel sheathed) were used to measure the temperature at various axial and radial locations in the reactor as shown in Figures 5.2 and 5.3.

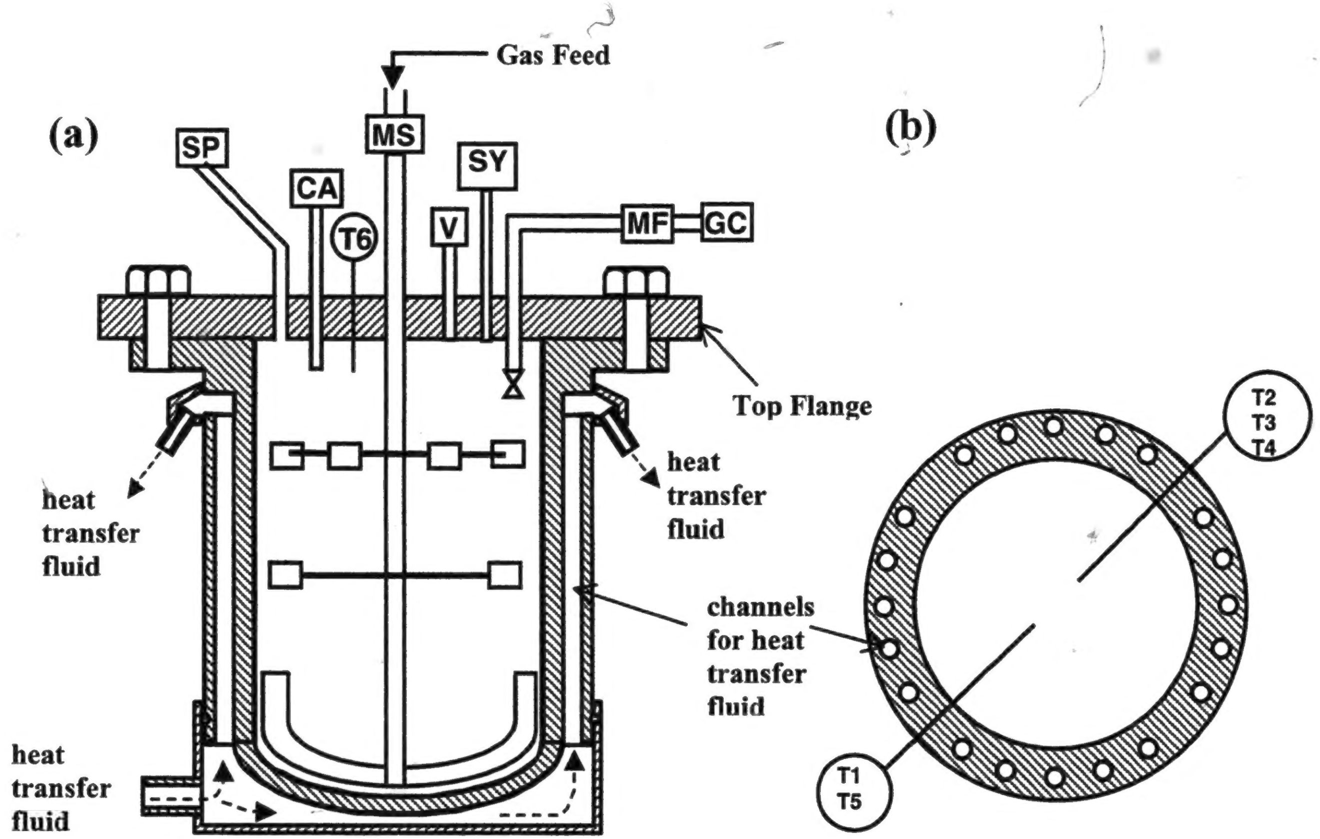
(a)
Gas Feed
SP
MS
CA
T6
SY
V
MF
GC
Top Flange
heat transfer fluid
heat transfer fluid
heat transfer fluid
channels for heat transfer fluid
(b)
T2
T3
T4
T1
T5

Figure 5.2. Reactor details: (a) – vertical cross-section; (b) – horizontal cross-section of reactor. (CA – catalyst injector; GC – gas chromatograph; MF – mass flowmeter; MS – Magnedrive stirrer; SP – syringe pump; SY – syringe injection port; T_i – thermocouple *i* mounted as in Figure 5.3; V – vent)

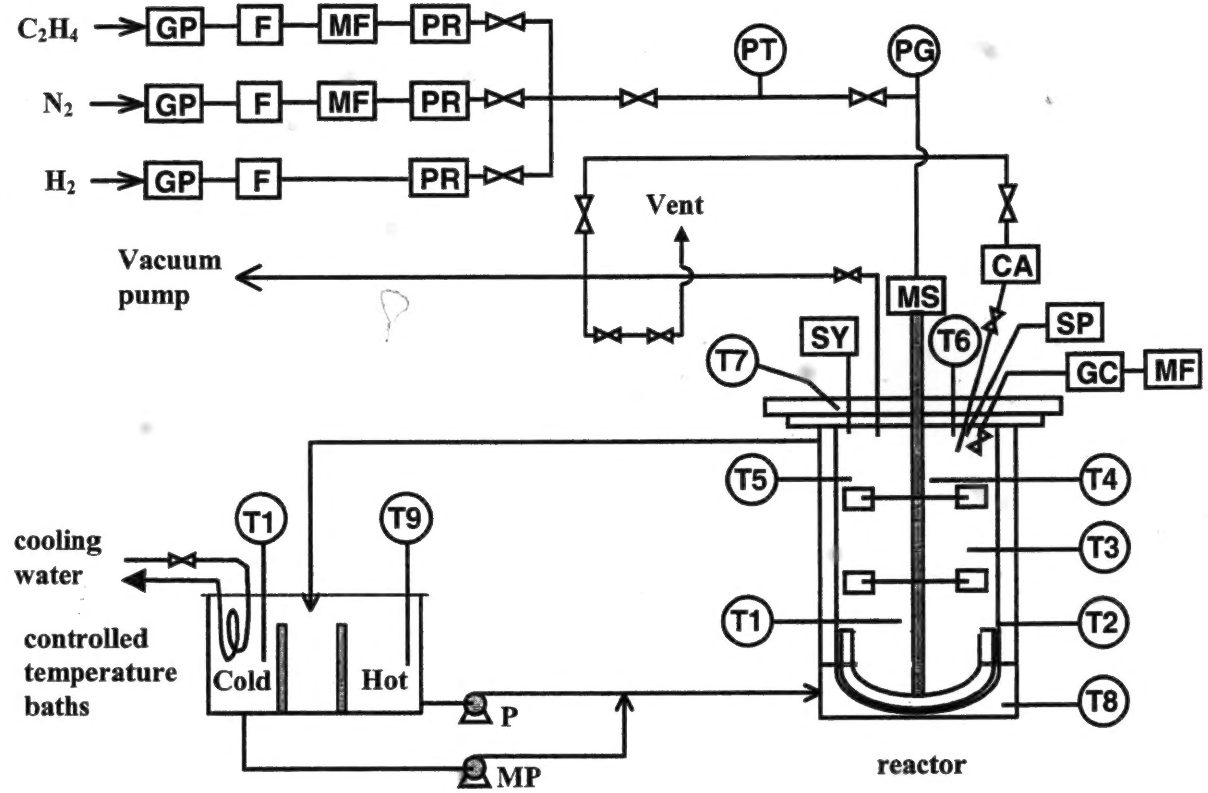
C_2H_4
N_2
H_2
GP
F
MF
PR
PT
PG
Vent
Vacuum pump
CA
MS
SY
SP
GC
MF
T1
T2
T3
T4
T5
T6
T7
T8
T9
cooling water
controlled temperature baths
Cold
Hot
P
MP
reactor

Figure 5.3. Schematic diagram of reactor system. (CA – catalyst injector; GC – gas chromatograph; GP – gas purifiers; F – filter 7m; MF – mass flow meter; MP – metering pump; MS – Magnedrive stirrer; P – centrifugal pump; PG – pressure gauge; PR – pressure regulator; PT – pressure transducer; SP – syringe pump; SY – syringe injection port; T_i – thermocouple *i*; V – vent)

The reactor attaches to a circular stainless steel flange 279.4 mm in diameter and 17.46 mm thick (11"×11/16"). The flange (Figure 5.4) is permanently mounted on a stand and it contains the following ports: dry catalyst injection, comonomer feed, scavenger injection, GC-sampling valve (two ports), vent/vacuum line, thermocouple, and one additional port for future use. The portholes were drilled at an angle of 5° from the vertical in a direction towards the center of the flange, in top view, to increase the clearance between the port connections and the stirrer drive. Gaseous monomer enters the reactor through the stirrer shaft housing during polymerization; this reduces the build-up of polymer particles in the shaft assembly.

Eight cartridge heaters (6.35 mm diameter by 88.9 mm long; Omega Engineering, Inc., Stamford, CT) were symmetrically embedded in the top flange through equally spaced holes drilled on the side of the flange. The number of cartridge heaters was chosen to provide even temperature distribution in the flange during heating. The power rating of the heaters (200 W at 240 V) was reduced by connecting them to 120 V supply. An Omron digital controller E5CK (Omron Corp., Tokyo, Japan) was used to control the flange temperature at the desired set point independently of the reactor temperature.

A magnetically driven stirrer (Autoclave Engineers, Erie, PA) was mounted on the top flange and used for mixing the reactor contents. A Plexiglass replica of the reactor was used to visualize the gas/solids mixing in the reactor using four different impeller types: Teflon-tipped straight anchor, pitched Teflon paddle, steel paddle (Figure 5.5 a-c), and pitched anchor steel impeller as shown in Figure 5.6. These impellers were also used in actual polymerization test runs in the steel reactor; results for these test runs are discussed in Section 5.2 below.

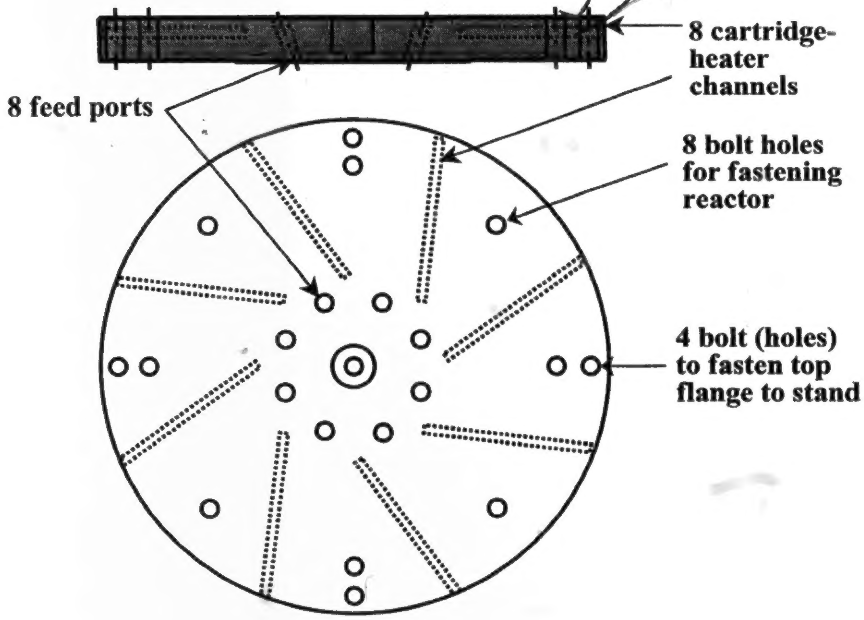
8 cartridge-heater channels
8 feed ports
8 bolt holes for fastening reactor
4 bolt (holes) to fasten top flange to stand

Figure 5.4 Side view and top view of the 11-inch top-flange

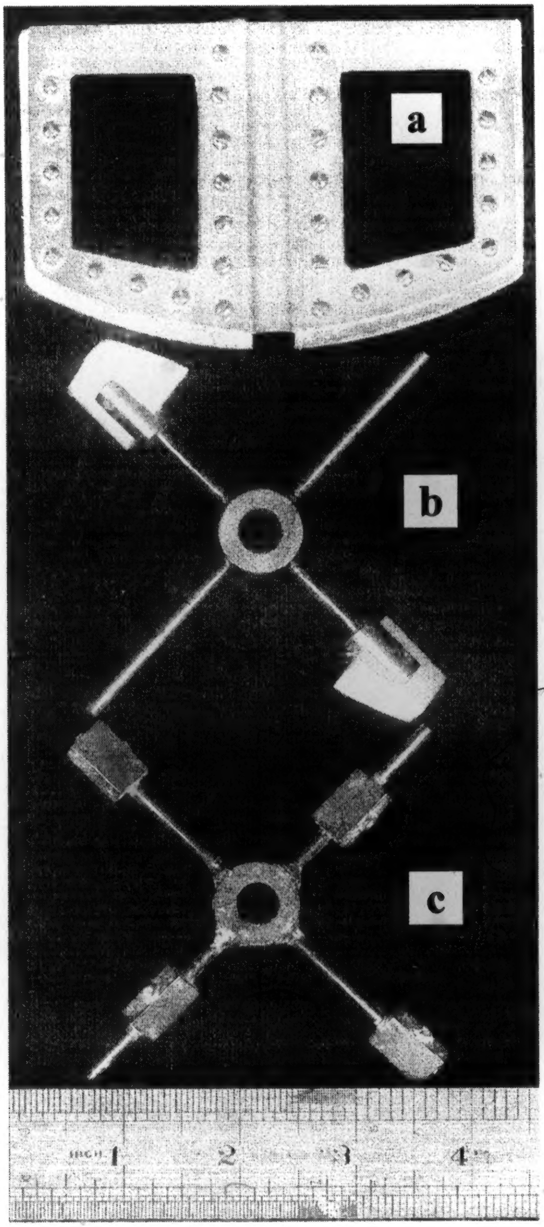

Figure 5.5 Impellers tested in the new 2-L gas-phase polymerization reactor (a) Teflon-tipped straight anchor, (b) pitched Teflon paddle, (c) steel paddle.

The optimum stirrer configuration adapted was the pitched-blade anchor-type impeller mounted at the shaft end; see Figure 5.6. Two sets of paddle-type impellers were mounted at the middle and the upper parts of the stirrer shaft. The upper paddles were orientated to minimize the amount of fine particles reaching the top flange, thereby keeping it clean during polymerization runs. The latter was also enhanced by the depth to diameter (H:D = 2) ratio of the reactor. After a series of trial runs (Sections 5.2 and 5.3), an impeller speed of 450 rpm was adapted as the standard used in the polymerization runs to minimize transport resistance (heat and mass) between the polymerizing particles and the gas-phase without excessive particle grinding.

High pressure Oxy-Trap and Gas-Drier columns (Alltech, Deerfield, IL) were used to purify the gaseous monomer feed and the N_2 used in the reactor. The purified gases pass through 7-micron in-line filters (Swagelok, F-Series); mass flow meter (Matheson, model 8141, 2SLPM); and a 500-psi diaphragm sensed pressure-reducing regulator (Tescom Corp., Elk River, MN) before entering the reactor. A 500-psi pressure transducer (Wika Instruments Corp., Lawrenceville, GA) was installed on the ethylene feed line downstream of the Tescom regulator.

5.1.2 The temperature control system

A closed-loop circulation of silicone oil (Dow Corning 200 fluid, 50 centistokes) as shown in Figure 5.3 using a modified Neslab high temperature bath EX-251HT (Neslab Instruments, Inc., Newington, NH) was used to control the reactor temperature. The heat bath was partitioned into three (hot, cold, and return-line) compartments. The hot compartment temperature (set at 5–10°C above the polymerization temperature) was maintained by the original heater/controller of the Neslab bath. A cooling coil (using tap

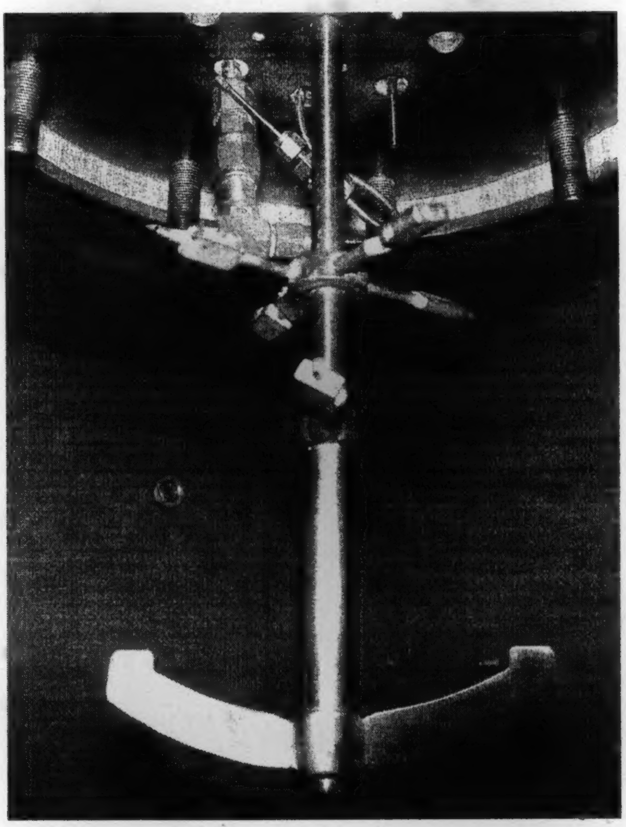

Figure 5.6 Photograph of the bottom side of the top flange showing pitched anchor impeller, blade stirrers and the GC sampling valve.

water) immersed in the cold compartment continuously cooled the heat transfer fluid in the cold compartment. The cold compartment also contained a 1.1 kW Lauda immersion heater-controller (Type MS #G08019) installed to prevent overcooling; overcooling in the cold compartment can result in reactor temperature oscillation. The circulation pump (centrifugal) of the Neslab heat bath maintained a constant flow of the hot fluid during polymerization runs while a variable speed Magnedrive gear pump (Micropump Inc., Model GD-M35 PVSE) was used to control the cold fluid flow. The pump was directly coupled to a ½-horsepower, DC TEFC motor with speed control (4-20 mA signal). A virtual PID controller, written in LabView, uses the temperature from thermocouple T1 as input signal to control the pump speed (cold oil flow), and hence the temperature T8 of coolant entering the reactor channels (see Figure 5.3 for location of these thermocouples). The reactor data acquisition system was based on Opto-22 interfaced with LabView. All process and control parameters were displayed in the LabView front panel and logged in a PC in real time. The data log rate and parameter settings could be changed from the LabView front panel in real time during polymerization.

5.1.3 Gas-phase analysis system

Gas chromatography (GC) was used to analyze the gas phase during some polymerization runs. The gas chromatograph (HP 5890 Series II) was equipped with a six-port gas sampling valve, a thermal conductivity detector, and a hydrogen flame ionization detector. The thermal conductivity detector was used to analyze ethylene/hydrogen mixtures during homopolymerization runs with H_2 as chain transfer agent. The flame ionization detector was used in monitoring the 1-hexene/ethylene mole ratio. The GC column (6.35 mm diameter by 0.91 m long) was packed with 80–100 mesh cross-linked divinylbenzene polymer, HayeSep-Q. The column was operated isothermally at 35°C for hydrogen/ethylene analysis and at 185°C for 1-hexene/ethylene analysis. Both analyses used argon carrier at 30 cm^3 (STP)/min. The retention times were 0.15 min and 1.22 min for hydrogen and ethylene respectively at 35°C. During ethylene/1-hexene analysis at 185 °C, their retention times were 0.20 min and 2.0 min respectively.

A unique gas-sampling valve was made by modifying a Nupro S-series metering valve SS-SS2 as follows: The inlet half of the valve body up to the valve seat was cut off to completely eliminate the dead volume on the high pressure side of the valve. The bonnet was turned down to ¼" outside diameter and connected to a straight-union compression fitting (Swagelok); the other end of this fitting was connected to a ¼" tube that extends outside of the reactor through one of the top-flange ports. A straight piece of stainless steel (~2 mm diameter) was welded to the valve stem to extend it outside the reactor through the above ¼" tube; a valve handle was attached to the extended stem. The modified valve was mounted inside the reactor; its outlet end was connected to a stainless steel tube (⅛" diameter by 8" long) that extends outside the reactor through another port on the top flange. A Swagelok shut-off valve was installed at the end of the steel tube. Teflon tubing (½ mm inside diameter, 0.9 m long) connected the downstream side of the shut-off valve to the GC. The gas sampling line was maintained at 80°C by a heat tape connected to a Variac. The use of heated Teflon tube for gas sampling prevents adsorption and re-condensation of 1-hexene inside the tube; this was earlier observed with unheated steel tubing.

Gas was withdrawn from the reactor at a constant rate between 5 to 10 cm^3 (STP)/min for GC analysis. A 20 cm^3 (STP)/min Matheson mass flow meter (Model LF-20) measured the flow rate of this gas-stream. Under this condition, the depletion of 1-hexene or hydrogen in the reactor due to gas sampling was less than 2% in a typical 1 h polymerization run. The use of a valve with zero dead volume (on the high pressure side), and the use of small diameter tubing reduces delay time for gas sampling to less than 1 min in a typical run (1.4 MPa and 80°C).

The fast gas sampling and analysis system of the new reactor allowed the use of 1-hexene analysis result as feedback for continuous (manual) addition of the comonomer to keep reactor composition fairly constant as in industrial reactors (see Figure 5.7). The system can also be modified for automated and continuous 1-hexene injection during polymerization. One-time addition of comonomer in semi batch reactors results in continuous change in reactor composition during copolymerization runs and this affects the activity profile. Although this alters the reaction kinetics, it is still the common practice with lab reactors. The change in reactor composition due to comonomer depletion is avoided in lab investigations by using short run times to limit the total comonomer consumption (Sun *et al.*, 1994) or by operating the reactor in a "purge mode", i.e. continuously feeding and venting the (excess) monomer/comonomer mixture during the polymerization (Han-Adebekun *et al.*, 1997; Chakravarti and Ray, 2001). More GC analyses results for hydrogen, ethylene, propylene, and 1-hexene analyses during gas-phase polymerization in the new reactor are discussed in Chapters 7 and 8.

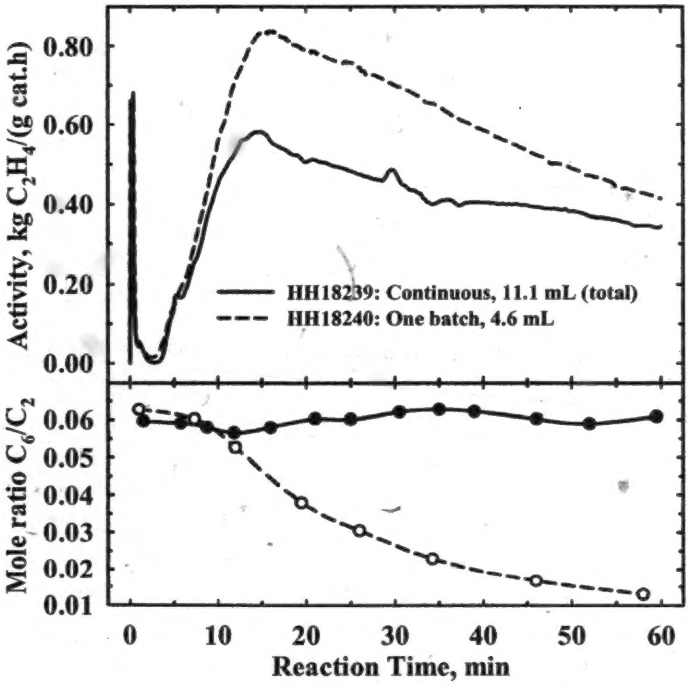

Figure 5.7 Profiles of polymerization activity and gas-phase composition during ethylene/1-hexene copolymerization with continuous and batch 1-hexene addition.

5.2 Test runs with the new reactor

5.2.1 Reactor tests and modifications

The reactor preparation and the polymerization conditions for the test-runs are summarized in Table 5.1 (first four characters of run number represent catalyst number). First, Catalysts JM29, known to be active in the old 1-L reactor in our lab was used. Figure 5.8 shows the activity, temperature, and pressure profiles of the first polymerization run made in the new reactor using 132 g NaCl as seedbed. The run produced ethylene homopolymer at lower activity than the corresponding run in the 1 L reactor. Reactor pressure, temperature, and polymerization activity all showed oscillatory behavior. The reactor pressure unexpectedly dropped by ~7 psi during the run despite the presence of a constant pressure regulator on the ethylene feed line. The in-line pressure regulator was supposed to supply ethylene at the rate it is consumed in the reactor to maintain the pre-set reactor pressure, i.e. semi-batch operation mode.

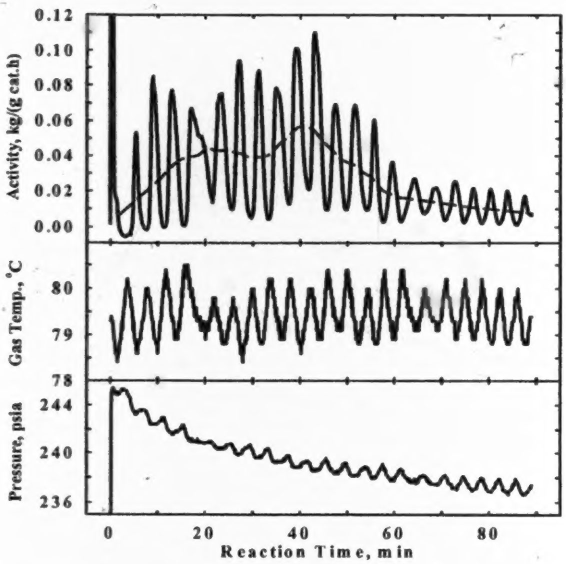

Figure 5.8 Activity profile of the first polymerization run in the new gas-phase reactor (JM29001).

Table 5.1. Description of polymerization test runs in the new reactor*

Run Number[a]	T_{evac}[b] °C	Al Alkyl Used	Amount charged to reactor				t_{scav}[c] min	P_{Total} MPa	Gas[d] Temp. °C	Activity, g PE/(g cat·h)		t_{Rmax}[e] h	t_p[f] h
			NaCl g	Cat. mg	Al-alkyl mmol	1-C_6H_{12} mL				Avg.	Max		
JM29001[g]	90	TIBA	132	151	0.59	–	30	1.65	79	38.8	110	0.72	1.4
JM38007	90	TIBA	–	103	0.59	2.31	20	1.39	80	134.3	187	4.15	9.5
JM29009	110	TIBA	80	101	0.59	2.0	20	1.39	80	18.1	53	0.32	2.2
JM38010	110	TIBA	80	109	1.18	2.63	20	1.36	83	755.4	2520	0.20	1.8
JM38011	110	TIBA	80	101	1.18	–	20	1.35	80	22.9	31	NA	3.7
JM29012	110	TIBA	80	109	1.18	2.27	20	1.38	84	583.4	2690	3.88	5.5
[illegible]M29013	110	TIBA	80	50	1.18	2.50	15	1.38	80	144.5	276	NA	8.0
[illegible]M29014	110	TIBA	80	51	1.18	2.48	15	1.37	90	86.2	196	NA	6.8
HH01001	114	TIBA	80	109	1.14	2.73	25	1.40	80	45.2	117	NA	3.5
HH01002	110	TIBA	80	110	1.18	2.74	33	1.40	80	87.1	164	NA	2.4
HH01003[h]	110	TIBA	80	108	1.18	3.01	23	1.41	82	34.7	64	NA	2.0
HH01004	90	TEA	–	113	1.28	2.8	30	1.41	86	480	1330	2.29	3.0
HH01005	90	TEA	80	82	1.46	3.31	31	1.41	80	69.7	174	NA	2.6
HH01006	90	TEA	80	106	1.60	2.95	26	1.40	81	124.2	360	NA	3.0

* See notes at end of table, next page

Table 5.1. Description of polymerization test runs in new reactor (continued)

Run Number[a]	T_{evac}[b] °C	Al Alkyl Used	Amount charged to reactor				t_{scav}[c] min	P_{Total} MPa	Gas[d] Temp. °C	Activity, g PE/(g cat·h)		t_{Rmax}[e] h	t_p[f] h
			NaCl g	Cat. mg	Al-alkyl mmol	1-C_6H_{12} mL				Avg.	Max		
JM54007	90	TEA	80	96	1.10	2.62	40	1.40	82	143.2	261	1.16	3.5
JM54008	90	TIBA	80	96	1.18	2.64	25	1.40	83	206.6	331	0.99	1.3
JM54009[i]	93	TIBA	80	96	1.54	2.95	28	1.42	81	355.8	686	1.80	3.3
JM54010[i]	92	TIBA	80	98	1.58	2.62	24	1.45	80	275.5	715	1.50	1.5
HH01014[j]	90	TEA	80	92	1.17	3.00	22	1.40	80	162.0	323	2.94	3.6
HH01015[j, k]	91	TEA	80	93	1.02	3.09	24	1.40	81	284.0	569	3.04	3.7
HH01016	91	TIBA	80	93	1.30	2.93	36	1.40	80	92.2	174	NA	3.5

a–the first 4 characters represent catalyst number; catalyst composition mass % (Al, Zr): JM29 = (11.3, 0.283), JM38 = (13.4, 0.265), JM54 = (22.5, 0.206), HH01 – not analyzed; b–reactor temperature during overnight evacuation; c–scavenging time; d–temperature from Thermocouple 1 (T1); average T calculated as $N^{-1}\sum T_i$ where N is the number of equally spaced measurements (usually 600 for a 1 h run); e–time to attain maximum activity (NA = max. activity not attained)

f–total duration of run; g–reactor contained 25 psi N_2; h–reactor wall temperature, T2 used as control variable;

i–simple catalyst injector made from ¼″ tube and 2 valves; j–paddle impeller used; k–TEA applied to NaCl layer above the catalyst placed in the simple catalyst holder described in *i* above.

In Run JM38007 (Figure 5.9), Catalyst JM38 was used in ethylene/1-hexene copolymerization. No NaCl seedbed was used in this run (cf. 132 g NaCl used in JM29001). Changing the controller settings eliminated the oscillations observed in Run JM29001 (Figure 5.8); however, the higher frequency oscillations still occurred. This was later found to originate from the in-line pressure regulator. The small pressure differential required to open the regulator valve results to more discernible changes in flow rates due to the size of the reactor (2.27 L). The results in Figure 5.9 also show a prolonged activity increase for a period of ~4 h.

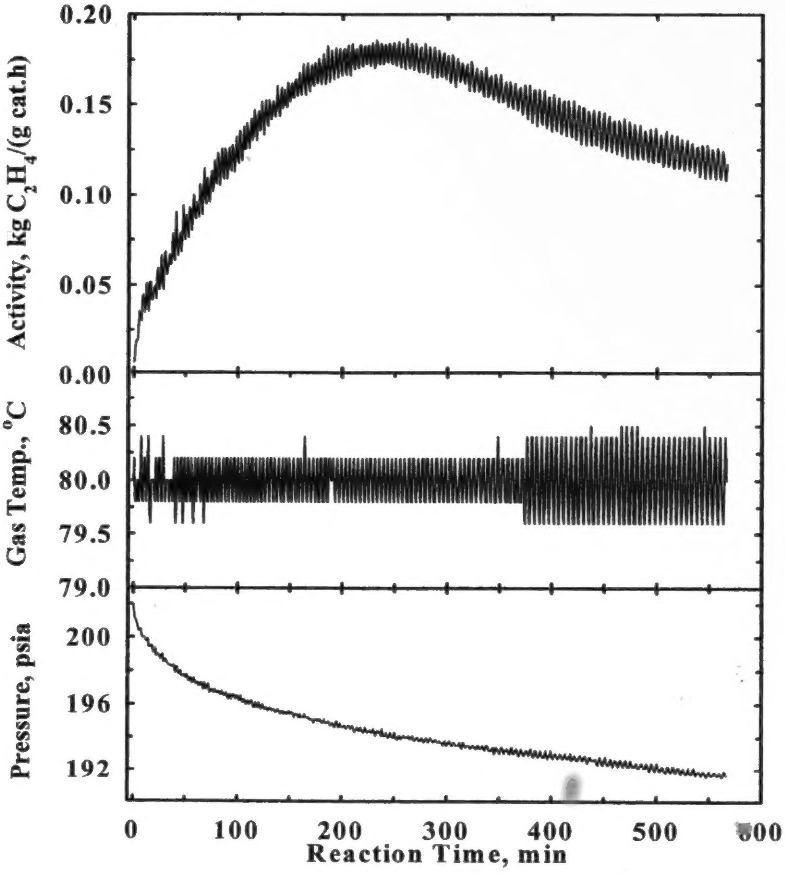

Figure 5.9 Profiles of gas-phase ethylene/1-hexene copolymerization (JM38007) without NaCl seedbed.

Figure 5.10 shows the activity, temperature, and pressure profiles for two copolymerization runs (JM29009 and JM29012). In both runs 80 g NaCl seedbed were used, and the amount of 1-hexene added to the reactor was about the same in each case (Table 5.1). Doubling the amount of TIBA from 0.15 mL to 0.30 mL increased the average activity 32 fold. This suggests either the 0.15 mL TIBA was not sufficient for scavenging or some impurities were introduced to the reactor following scavenging that requires higher amounts of residual TIBA to maintain high polymerization activity in the reactor. The occurrence of maximum activity was also considerably delayed to ~ 3.8 h in the presence of higher TIBA amount.

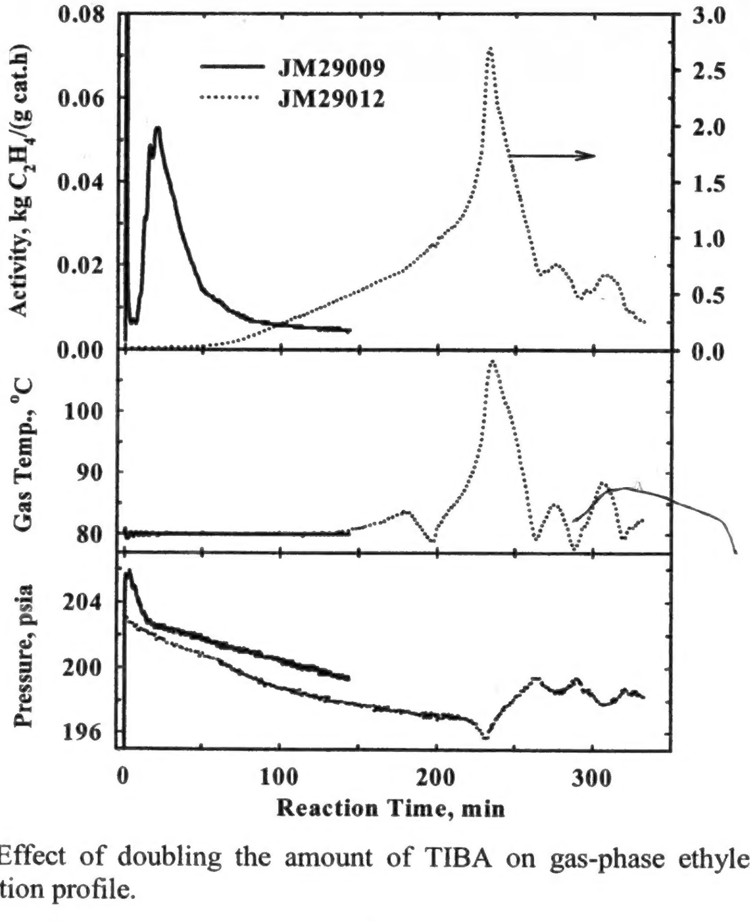

Figure 5.10 Effect of doubling the amount of TIBA on gas-phase ethylene/1-hexene copolymerization profile.

Homo- and co-polymerization profiles of Catalyst JM38 are compared in Figure 5.11 (with 0.30 mL TIBA and 80 g NaCl seedbed in both runs). The average copolymerization activity was 33 times higher than the homopolymerization one. For copolymerization, the maximum activity was attained rapidly (10 min) but the catalyst also deactivated quickly, probably due to overheating of the polymerizing particles; temperature of the catalyst particles can be considerably higher than the gas temperature in gas-phase polymerizations (Webb *et al.*, 1991). This sharply contrasts the homopolymerization run in which the maximum activity was not attained. The homopolymerization activity gradually increased through the 3.7 h run. Runs JM29012 (Figure 5.10) and JM38010 (Figure 5.11) show that at high polymerization activities the temperature control was not effective; gas-phase temperatures were 19°C and 28°C higher than the set-points, respectively. The maximum activities of runs JM29012 and JM38010 correspond to ethylene consumption rates of 3.65 L (STP)/min and 3.92 L (STP)/min respectively.

The copolymerization profiles shown in Figure 5.12 (JM29013 and JM29014) were run at 80°C and 90°C respectively. The amount of catalyst was reduced to 50 mg, about half that used in the previous runs, the scavenging time was also further reduced to 15 min but TIBA amount was kept unchanged at 0.30 mL. Considerable delay in the attainment of maximum activity was observed in both runs; activity continuously increased for the entire 8.0 h and 6.8 h duration of the runs respectively. This was likely due to higher amount of residual TIBA per mg catalyst in the reactor. Reduction of catalytic activity due to decrease in the amount of catalyst would also suggest that part of the catalyst was deactivated (probably during the catalyst injection or reactor preparation step). If the amount of catalyst that undergoes this deactivation is the same, the effect will be more pronounced in runs with small amount of catalyst.

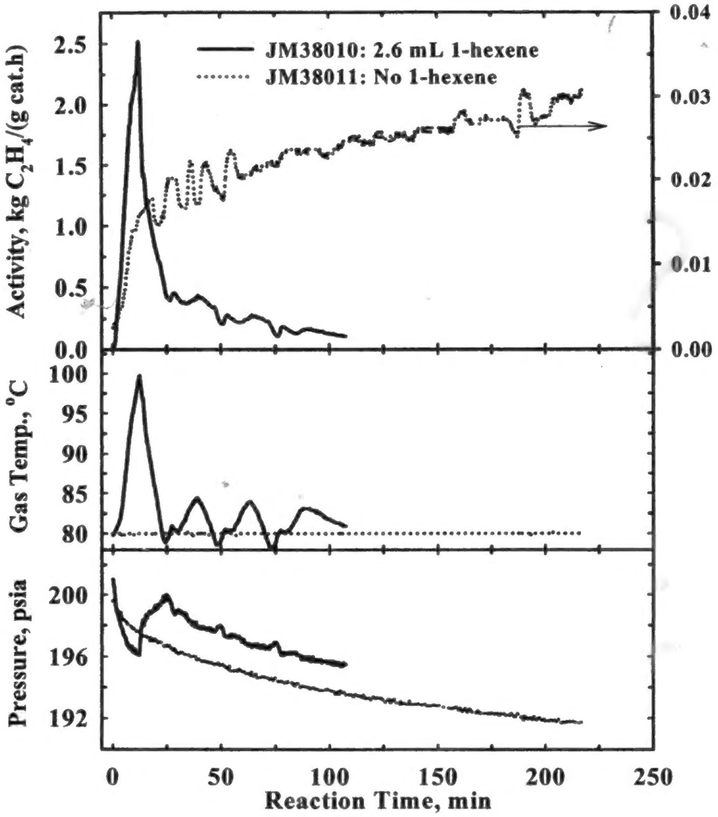

Figure 5.11 Comparison of ethylene homopolymerization and ethylene/1-hexene copolymerization over catalyst JM38.

Alternatively, the observed decrease in activity with the amount of catalyst could have been due to incomplete catalyst injection. This problem might originate from the electrostatic charging of the catalyst during handling and injection. As a result of low bulk density of the catalyst and electrostatic charging, some catalyst remained on the inner walls of the catalyst injector after the dry injection. The amount of catalyst left in the injector largely depends on the morphology and the electrostatic nature of the catalyst, and less on the initial amount in the catalyst holder. Therefore, higher fraction of catalyst will be 'wasted' in a run utilizing lower catalyst amount than the one with larger amount of the same catalyst. Unfortunately the amount of catalyst left in the injector could not be measured reliably.

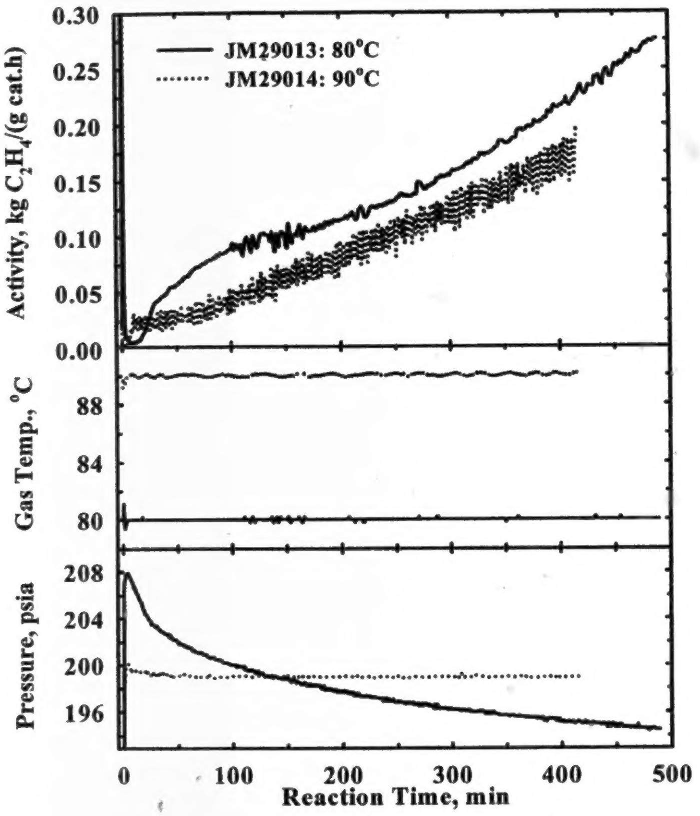

Figure 5.12 Effect of polymerization temperature on gas-phase ethylene/1-hexene copolymerization over catalyst JM29.

All the runs shown in Figures 5.8 to 5.12 show a drop in total reactor pressure with time. This problem was eliminated when the single stage pressure regulator on the ethylene cylinder was replaced with a dual stage one. Run JM29014 in Figure 5.12 and subsequent runs show more constant reactor pressure profiles.

A new catalyst, HH01 was tested for ethylene/1-hexene copolymerization using 80 g NaCl seedbed and 0.30 mL TIBA scavenger (see Table 5.1 and Figure 5.13). This new catalyst also shows a low but steadily rising activity profile (Run HH01001); maximum activity was not attained in the 3.45 h of the run. In the remaining two runs of Figure 5.13, ethylene supply from the old 1-L reactor line was used. In Run HH01002, the polymerization grade ethylene (from the cylinder) was used without further purification while in HH01003 it was purified in the 1-L reactor purifiers before use. This was done as a comparative check to the ethylene supply and purifiers (both new) on the new reactor. Polymerization with the as-received ethylene surprisingly resulted in higher activity than with the purified ethylene (cf. Run HH01002 to HH01001 and HH01003).

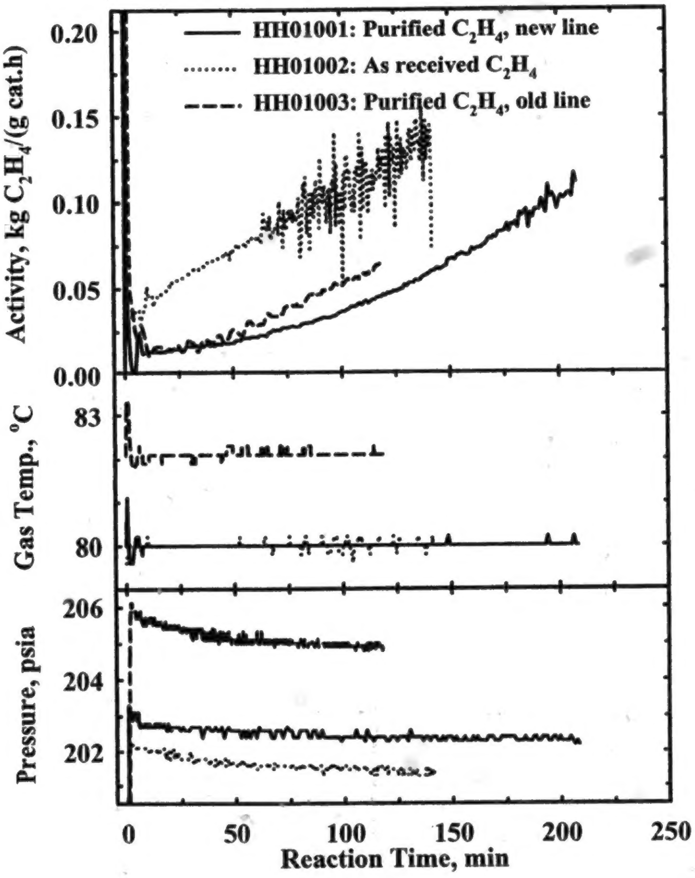

Figure 5.13 Effect of ethylene feed purification and temperature control variable selection on activity profile of ethylene/1-hexene copolymerization.

This was later found to be due to the effect of the residual Al-alkyls on the metallocene catalyst. Higher amount of impurities entering the reactor with the unpurified ethylene reacts with the excess residual TIBA thereby preventing the TIBA from forming dormant complex with the active zirconocenium center (see Chapter 6). In Run HH01003 the reactor wall temperature (T2 in Figure 5.2) was set at 80°C and used as the control variable. This mimics the 1-L reactor in our lab that is immersed in constant temperature bath for reactor temperature control. The gas-phase temperature was controlled at 82°C; polymerization activity was about 25% higher than the corresponding 80°C run (within the same time range). The reactor flange temperature was also set to 85°C, but this was found to have no effect on catalyst left in the injector. The fluctuations in activity in Run HH01002 was due to partial blockage of the ethylene feed inlet in the stirrer shaft housing by fine polymer material. This problem did not follow any specific pattern. However, flushing the ethylene feed line with nitrogen (2.1 – 2.8 MPa) occasionally during reactor cleanup eliminated the problem.

Figure 5.14 shows activity profiles of three copolymerization runs with catalyst HH01 using slightly varying TEAL scavenger amounts. Run HH01004 had no NaCl seedbed and it had the highest catalytic activity (that resulted in the highest rise in gas temperature) among the three runs; hence, the amount of NaCl seedbed may influence the polymerization activity of the catalyst. This is further discussed in the next section.

5.2.2 Effect of static mixers, stirring and NaCl seedbed

Several experiments were done to determine how the stirrer type, stirring speed, and the amount of NaCl seedbed affected reactor temperature control at high polymerization rates. Table 5.2 summarizes these experiments. The PID temperature control mode (Column 7 in Table 5.2) indicates whether the controller was turned ON or OFF. Temperature control ON means the PID controller was switched ON and worked normally (as explained in Section 5.1.2 above) to control the reactor temperature. Temperature control OFF means the PID controller was not used; the coolant fluid entered the channels in the reactor wall at a constant temperature of 80°C.

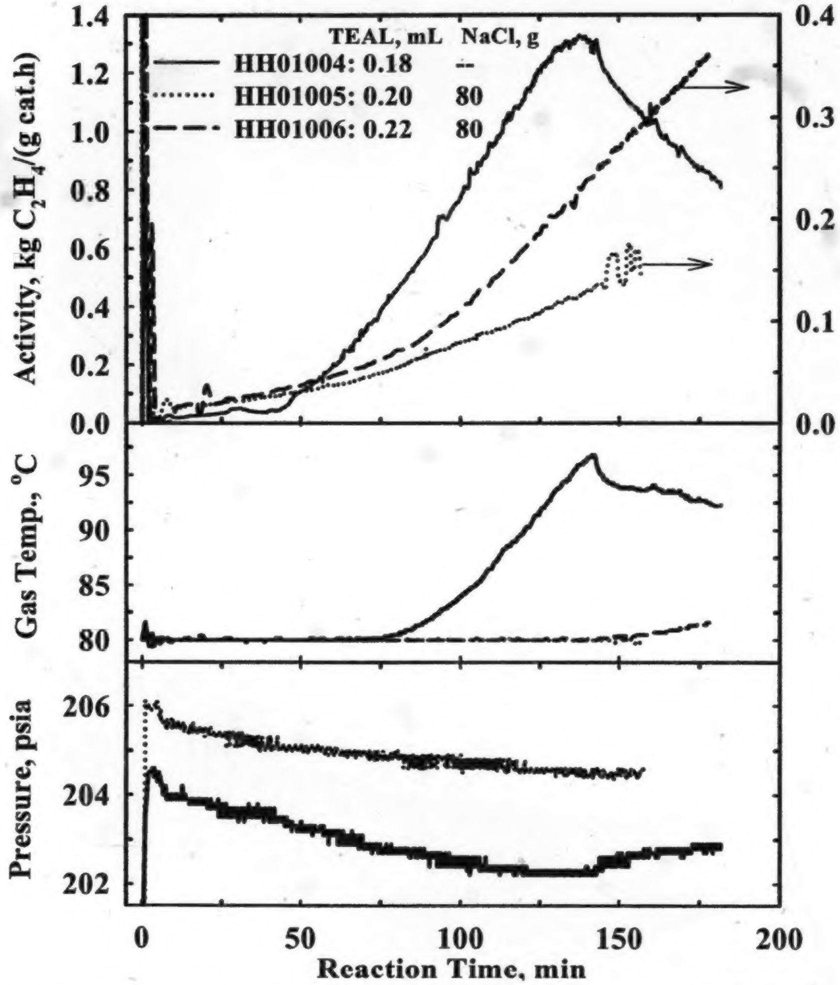

Figure 5.14 Influence of NaCl seedbed and small variation in the amount of TEAL scavenger on ethylene/1-hexene copolymerization activity profile.

Table 5.2. Description of polymerization runs for temperature control

Run Number	Amount in reactor		Stirrer		Static Mixer Used	PID Temp. Control	Temperature[a]		Total Rates[b]		Average Activity g PE/(g cat·h)
	Cat. mg	1-C_6H_{12} mL	Type	Speed RPM			Max °C	Avg. °C	Max. mol/h	Avg. mol/h	
HH13078	41.3	4.28	blade	600	No	OFF	97.1	87.1	4.1	2.5	1,702
HH13075	40.8	4.31	blade	300	No	ON	95.0	83.0	4.0	2.4	1,676
HH13077	40.7	4.31	blade	300	No	ON	80.9	80.0	1.9	1.4	992
HH13074	40.6	4.31	blade	600	No	ON	80.5	80.1	2.3	1.4	970
HH13079	41.9	4.37	anchor	300	No	ON	81.9	80.1	3.7	1.8	1,224
HH15088[c]	42.5	2.10[c]	blade	300	No	–	110.9	90.8	>6	2.2	1,429
HH15090	42.7	4.32	anchor	600	No	OFF	92.7	86.0	3.7	2.2	1,470
HH15089	42.6	4.32	anchor	600	No	ON	80.9	80.0	3.1	2.0	1,324
HH15091	42.5	4.34	anchor	600	No	ON	81.8	80.0	3.5	2.1	1,400
HH15092	42.8	4.38	anchor	600	Yes	OFF	87.6	84.6	2.8	1.9	1,222
HH14128	60.0	–	anchor	450	Yes	ON	80.5[d]	80.4	3.4	1.0	234
HH21217	60.0	4.51	anchor	450	Yes	ON	80.7[d]	80.0	3.6	2.6	1,457

a–From Thermocouple 1 (T1); averaged as $\sum T1_i/N$ where N is the number of equally spaced measurements (usually 600 for 1 h run); weighted average for unequally spaced measurements

b–Maximum rates calculated from ethylene flow reading; Average determined gravimetrically from polymer yield

c–Run made in 1-L reactor (1-hexene vapor pressure approximately same as 4.3 mL in the 2-L reactor)

d–Initial 2 – 4 min temperature spike ignored

The total pressure for all the runs in Table 5.2 was 1.36 (±0.05) MPa except Run HH15092 (1.24 MPa) and the set point temperature was 80°C. All the runs were ethylene/1-hexene copolymerizations except HH14128 which is an ethylene homo-polymerization run. A seedbed consisting of 80 g NaCl was used in all the runs except HH13077 for which the salt amount was doubled to 160 g. In all the runs in Table 5.2, the residual TIBA was evacuated after scavenging the reactor with about 0.1 mL of neat TIBA. The total polymerization rates, which directly determine the heat generation rates in the reactor is the most important factor in evaluating the effectiveness of temperature control. Therefore, variation of the catalyst, the catalyst amount, and the amount of 1-hexene charged into the reactor (see Table 5.2) would not alter the conclusions drawn from this section.

Figure 5.15 shows the effect of the PID controller, blade stirrer speed, and the amount of NaCl seedbed on the reactor temperature control. The total polymerization rates were assumed to be the rate of ethylene addition to the reactor because the comonomer fractions in the polyethylene products were small. The top panel in Figure 5.15 shows the variation of total polymerization rate with reaction time; the initial spike in ethylene flow was due to reactor fill-up to the set pressure following catalyst injection. Temperature profiles of Thermocouple 1 are shown in the lower panel of Figure 5.15; this thermocouple always showed the highest temperature of all the thermocouples in the reactor. The initial temperature spike was due to the essentially adiabatic compression caused by the rapid addition of ethylene during dry catalyst injection and the subsequent reactor fill-up. This temperature spike was typically 2 to 4°C in magnitude, but it was of short duration; it accurately indicated the beginning of polymerization run. The shortlived temperature spike had negligible effect on polymerization behavior, and is ignored in the subsequent discussions.

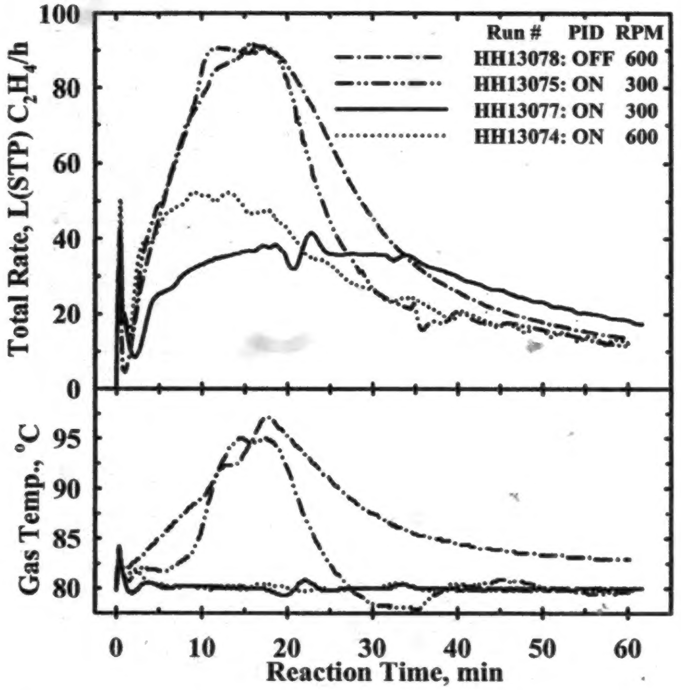

Figure 5.15 Effect of temperature controller, blade stirrer speed, and NaCl seedbed on reactor temperature control

Comparison of Runs HH13078 and HH13074 in Figure 5.15 shows the effect of the temperature controller when the reactor was stirred with the pitch blade impeller at 600 rpm. Runs HH15090 and HH15089 in Figure 5.16 show a similar effect for the anchor impeller. For both the blade and the anchor impellers, switching the controller OFF results in poor reactor temperature control even at high stirring rate, but the anchor impeller performed slightly better. This type of operation is similar to the operation with a jacketed reactor and a constant temperature fluid flowing through the jacket, or for operation in which the reactor is immersed in a constant temperature bath. Turning the stirrer ON and reducing the stirring rate from 600 to 300 rpm also resulted in poor temperature control for the blade impeller (Run HH13075, Figure 5.15), but the anchor impeller showed considerable improvement over the run with the controller switched OFF (cf. Runs HH15090 and HH13079, Figure 5.16). The anchor impeller performed reasonably well at 300 rpm, gas temperature was controlled to ±0.5°C of the set point, except for the approximately 2°C rise in the gas-phase temperature about 19 min after the start of polymerization. During the 3 min period of this temperature rise, the polymerization rate almost doubled; this increase cannot be due to the 2°C temperature rise. It is likely that the temperature of the growing particles rose more than the 2°C. The stirrer speed affects both the heat transfer from reactor to the circulating coolant and the heat transfer between the polymerizing particles and the gas. Therefore, stirring rates above 300 rpm are required to reduce the temperature difference between the gas phase and the polymer particles.

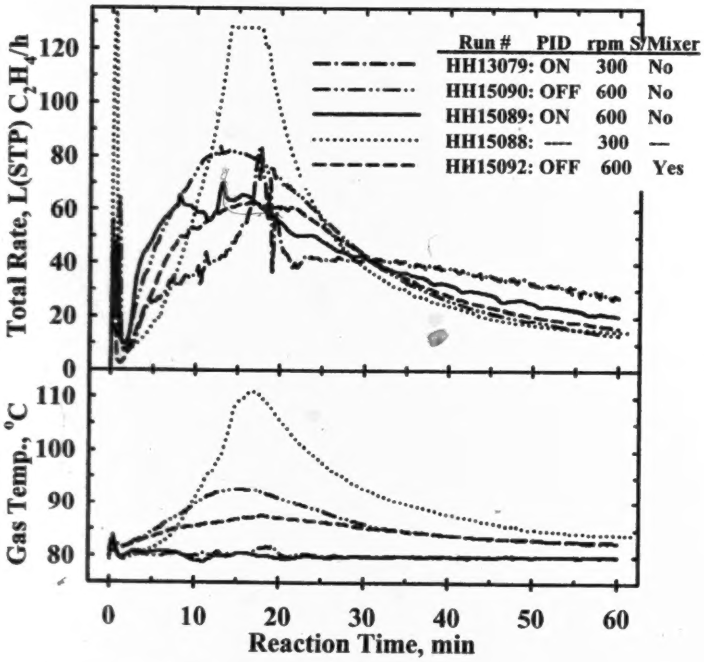

Figure 5.16 Effect of reactor size and configuration on temperature control

Runs HH13075 and HH13077 (Figure 5.15) show the effect of the NaCl seedbed on temperature control. Doubling the salt amount from 80 to 160 g resulted in improved temperature control for the blade impeller at 300 rpm. However, the presence of large amounts of NaCl in the reactor has the undesirable effect of grinding the polymer particles. The impurity associated with the NaCl also increases the scavenging requirement of the reactor (see Section 5.2.1 above); this could partly be responsible for the lower polymerization rate observed in run HH13077 since approximately the same amount of TIBA was used for scavenging in both runs.

The four operational modes of the 2-L reactor (with the anchor impeller) shown in Figure 5.16 had better temperature control than a similar polymerization done in the old 1-L reactor of Lynch and Wanke (1991), that uses blade impellers. The 1-L reactor was immersed in oil bath for temperature control. The initial conditions (including the partial pressure of 1-hexene) for all the five runs in Figure 5.16 were essentially the same. However, the gas-phase temperature rose by over 30^oC and the polymerization rate exceeded 132 L (STP) C_2H_4/h, the maximum range of the mass flow meter; thus the flat part of the rate profile for run HH15088. In Figures 5.15 and 5.16, poor temperature control was associated with higher polymerization rates due to the autocatalytic nature of the exothermic reaction. Poor temperature control also result in more rapid deactivation rates. Hence, good temperature control is required for the investigation of activation-deactivation behavior of catalysts during gas-phase polymerization.

Runs HH15090 and HH15092 (Figure 5.16) demonstrate the influence of the static mixers. The presence of these mixers reduced the maximum temperature rise (above set point) from ~13^oC to ~8^oC. The Kenics-type static mixers installed in the reactor channels can improve the heat transfer coefficient from tube surface to the fluid inside by up to three times the value for empty tubes, Cybulski and Werner (1986), and the heat transfer improvement by static mixers is greatest in laminar flow (Josji *et al.* 1995); this is the case for our polymerization reactor. Therefore, the installed static mixers were left permanently in the channels for all subsequent runs.

The above investigations revealed that high stirrer rate, anchor type impeller, and high amount of NaCl seedbed enhanced temperature control. Unfortunately, all these factors aggravated particle grinding in the reactor. The choice of pitch-anchor impeller operating at 450 rpm with 80 g NaCl seedbed represented a reasonable compromise; this was used in all subsequent polymerization runs, except where specifically stated.

The above configuration controls the reactor temperature quite well as shown in numerous polymerization runs in the latter chapters of this work. However, there are still cases where the temperature control would fail for various reasons: One example of such failures is for runs with high polymerization rates in which the maximum rates are attained very rapidly such as Run HH14128 in Figure 5.17. The rate increased to about 80 L (STP) C_2H_4/h in 2 min, and the gas temperature rose by 6°C above the set point. Under such rapid increase in polymerization rates it is difficult to control the temperature. Comparatively, Run HH21217 had a more gradual increase in polymerization rate; the temperature control was much better (maximum ΔT was ±1°C from set point) even though the polymerization rate was higher than in Run HH14128. Note that the ordinate of Figure 5.17 is the absolute rate of monomer consumption; this is not normalized with the amount of catalyst in the reactor, and it is directly proportional to the rate of heat generation in the reactor due to polymerization.

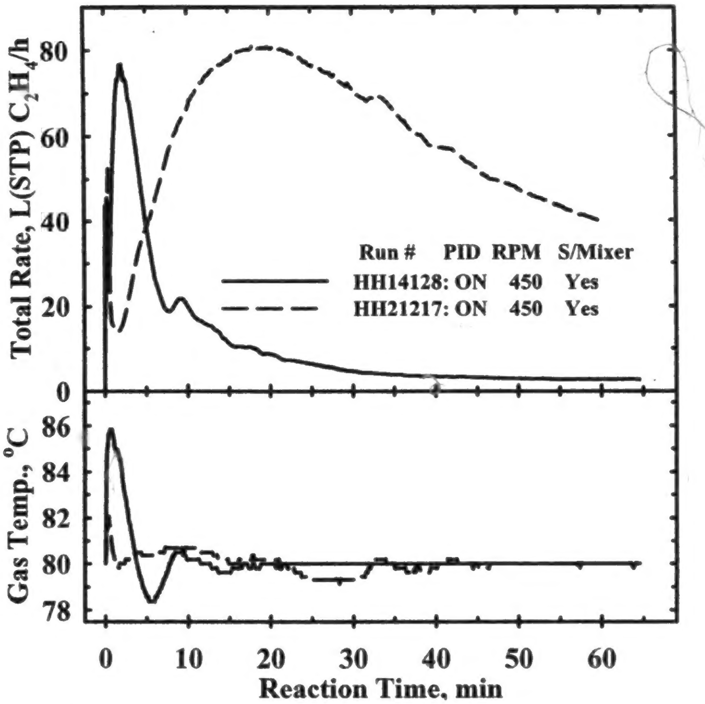

Figure 5.17 Influence of rate profile on temperature controller performance

High and sustained polymerization rates results in high and sustained cold oil circulation rates due to controller action. This results in the increase of the cold compartment oil temperature as shown in Figure 5.18 and consequently poor cold compartment temperature control because the cooling coil in that compartment cannot adequately maintain the set point temperature. Eventually the hot and cold compartment temperatures (T9 and T10 respectively, Figure 5.2) equalize. This fixes T8, the temperature of oil entering the reactor channels to a constant value independent of the reactor temperature. The relatively low polymerization temperature setpoint of 60°C in Run HH15135 (Figure 5.18) also worsened the controller performance. Low polymerization temperature requires even lower set point temperature in the cold oil compartment. This reduces the temperature (driving force) difference between the oil in the cold

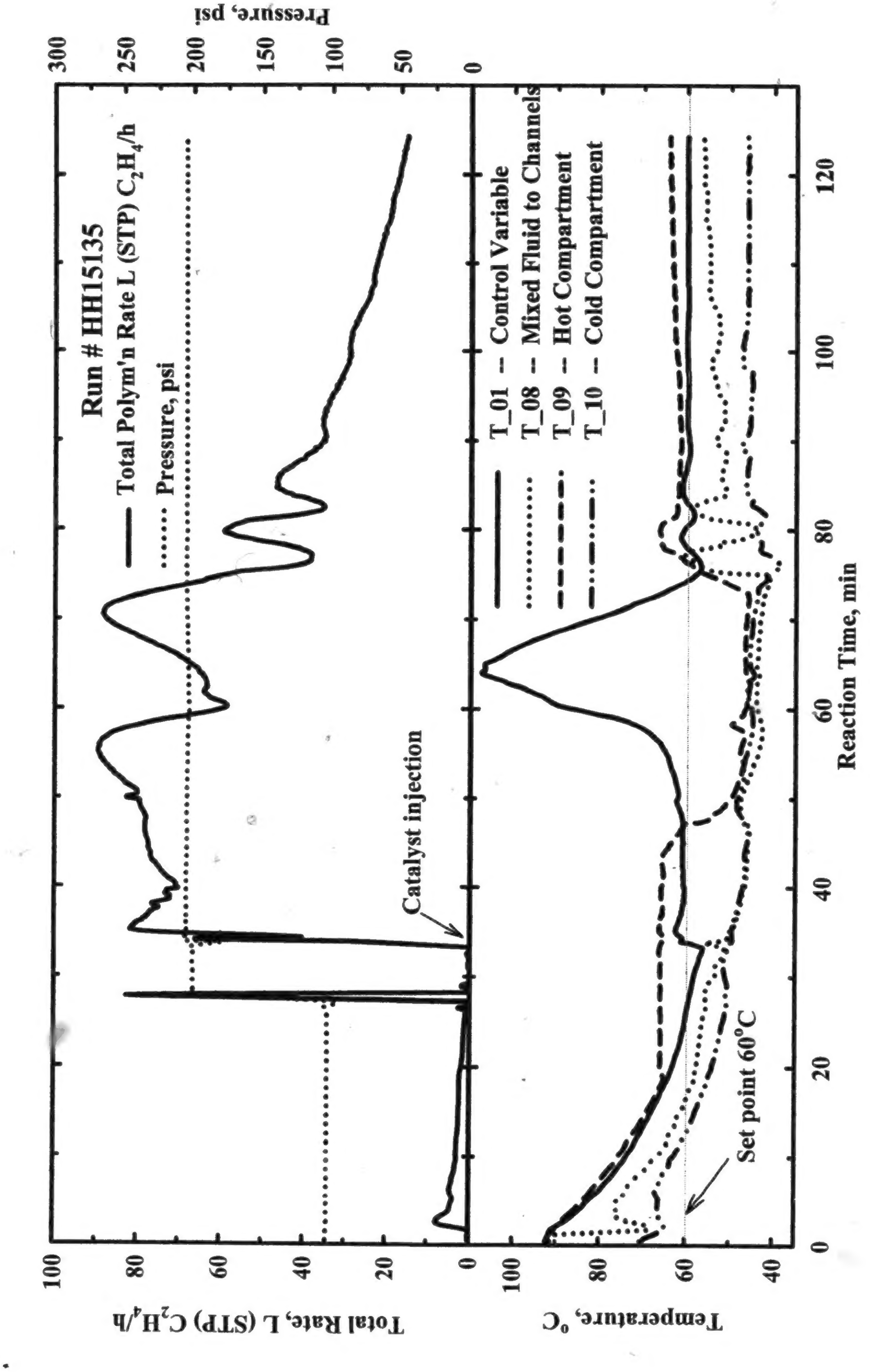

Figure 5.18 Inadequacy of temperature control at high polymerization rate due to limitation of coolant temperature

compartment and the cooling water. Better temperature control would result if polymerization runs with similar rates to Run HH15135 in Figure 5.18 were conducted at 80°C. Increasing the cooling capacity of the cold compartment would also enhance the reactor temperature control.

5.3 Reproducibility of the gas-phase polymerization

Metallocene/MAO catalysts, like the heterogeneous Ziegler-Natta ones are extremely sensitive to impurities. This sensitivity combined with the milligram-amounts of catalyst used in polymerization runs make experimental reproducibility a challenging task. Keii was reported to have commented that reproducing some experimental findings in Ziegler-Natta catalysis is as important as the findings (Kissin, 1985). As observed from the previous section, several extraneous factors seem to affect the gas-phase polymerization. These and other potential causes of irreproducibility in the gas-phase polymerization reactor (using dry catalyst injection) were formally identified and investigated as follows:

- Residual impurities in the reactor/seedbed and possible leaks into the reactor when it is under sub atmospheric pressure
- The type and amount of aluminum alkyl used in the reactor
- Electrostatic interference of dry catalyst injection and stirrer start-up
- Reactor temperature control system

The amount of residual impurities (moisture and oxygen) in the reactor can vary with evacuation temperature and time, vacuum pump performance, integrity of seals, or even the atmospheric conditions. Table 5.3 summarizes the runs used to demonstrate reproducibility problems in gas-phase polymerization. Figure 5.19 compares ethylene

Table 5.3. Poor reproducibility observed in temperature controlled gas-phase olefin polymerizations

Run		Amount in reactor			Temperature[a], °C		t_{Rmax}, h	Total Rates[b], g PE/h		Average Activity g PE/(g cat·h)
Number	Date	Catalyst, mg	1-C_6H_{12}, mL	TIBA, mmol Al	Max	Avg.		Max.	Avg.	
HH14128	12/24/01	60.0	–	trace	85.8	80.1	0.03	96.1	14.1	235.5
HH14130	01/14/02	60.2	–	0.20	80.7	80.1	0.43	59.6	23.1	384.4
HH14156	04/04/02	61.2	–	0.20	82.4	80.1	0.12	104.2	28.5	465.7
HH14159	04/20/02	61.4	–	0.20	80.7	80.0	0.32	63.8	23.9	388.7
HH14163	04/29/02	60.3	–	0.24	84.6	80.3	0.05	94.2	20.3	336.5
HH14164	05/03/02	61.8	–	0.20	84.9	80.0	0.12	71.5	15.9	257.0
HH14165	05/04/02	60.7	–	0.20	82.1	80.1	0.17	96.7	81.2	1337.7
HH21208	09/08/02	78.0	6.53	trace	80.2	80.0	0.17	23.2	20.7	264.9
HH21209	09/09/02	77.8	6.31	trace	80.2	80.0	0.13	11.7	7.3	94.0
HH21210	09/13/02	77.8	4.48	0.28	102.5	82.1	0.84	113.0	95.8	1,231

a–From Thermocouple 1 (T1); averaged as $\sum T1_i/N$ where N is the number of equally spaced measurements (usually 600 for 1 h run); weighted average for unequally spaced measurements; initial 2 – 4 min temperature spike ignored

b–Maximum rates calculated from ethylene flow reading; Average determined gravimetrically from polymer yield

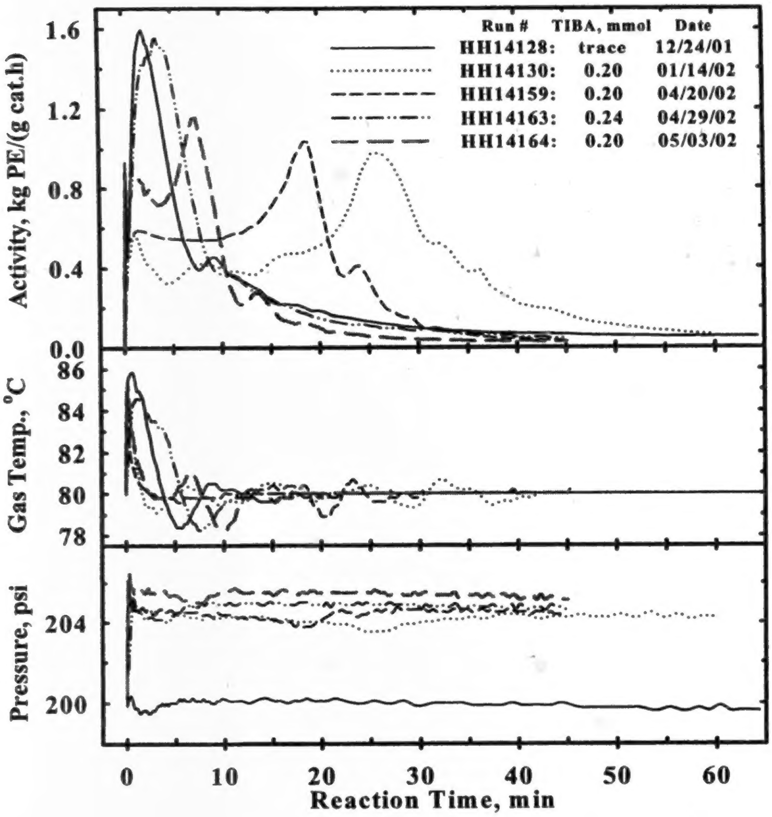

Figure 5.19 Poor reproducibility observed in gas-phase ethylene homopolymerization in the presence of residual TIBA.

homopolymerization runs made under the same conditions. Run HH14128 was done differently from the rest, it is included for comparison only. In Run HH14128 the reactor was vented and evacuated to 45 mtorr (after scavenging) to remove the residual TIBA (see Chapter 3). The presence of residual TIBA in the reactor delayed the occurrence of the maximum activity in all the runs when compared to Run HH14128. Polymerization with different catalysts revealed that the extent of this delay varies with the catalyst used, but it normally increases with the amount of residual TIBA in the reactor. Detailed study of the effect of aluminum alkyls is presented in Chapter 6. The irreproducibility of the activity profiles in Figure 5.19 is evidenced by the wide variation in the time required to attain the maximum activity, t_{Rmax} (3 – 26 min) as well as the maximum activity values. Neither the occurrence of the maximum activities nor the maximum activity values followed any chronological pattern; Run HH14163 was done between HH14159 and HH14164. Also, slightly more TIBA was used in HH14163 but it had the shortest (instead of the longest) t_{Rmax} of all the runs with residual TIBA. This irreproducibility could be related to impurities in the reactor. If higher level of impurities were initially present in the reactor in Run HH14163, then almost complete consumption of the TIBA scavenger could have taken place resulting in an activity profile resembling the trace-TIBA one. Such differences in activities for similar runs were noticeable when comparing the reactor performance over long periods. Lahelin *et al.* (2003) reported same-day consistency in polymerization activity of metallocene catalysts, but up to 10 times difference after one month; the runs in Figure 5.19 span about five months.

The molar masses of ethylene homopolymers in Table 5.3 varied significantly (67-114 kDa, see Appendix B, Table B-2), but the polydispersities are close to the most probable value of 2.0. It is not clear whether the molar mass differences was due to irreproducibility of polymerization or the individual polymer particles used in the molar mass measurements. It is shown in Chapter 9 that the molar masses of ethylene homopolymers produced with Catalyst HH09 (same support as Catalyst HH14 in Table 5.3) varied with particle size; particle size dependence of molar mass was not measured for the polymers listed in Table 5.3.

Figure 5.20 shows two ethylene/1-hexene copolymerizations (Catalyst HH21) having poor reproducibility despite the close similarity of all the run details (see Table 5.3). The reactor was evacuated over the weekend in Run HH21208 and overnight for

HH21209. Normally this should not make any difference because TIBA was used to scavenge residual impurities in the reactor (after each evacuation). Also, venting and evacuating the reactor to almost the same final pressure in both cases removed the residual TIBA. There was no difference in polymerization temperature or pressure to account for the 50% decrease in activity seen in Figure 5.20. The similarity in shapes of the two profiles suggests that some of the catalyst used in Run HH21209 was deactivated prior to the commencement of polymerization. This could happen during the 40-60 min delay (reactor scavenging/venting period) from the time the catalyst was taken out of glove box to its injection, or during the catalyst injection. Leakage into the reactor post scavenging would result in the above observation. Irreproducibilities in catalyst injection, discussed in more details below, could also account for the differences in observed rates.

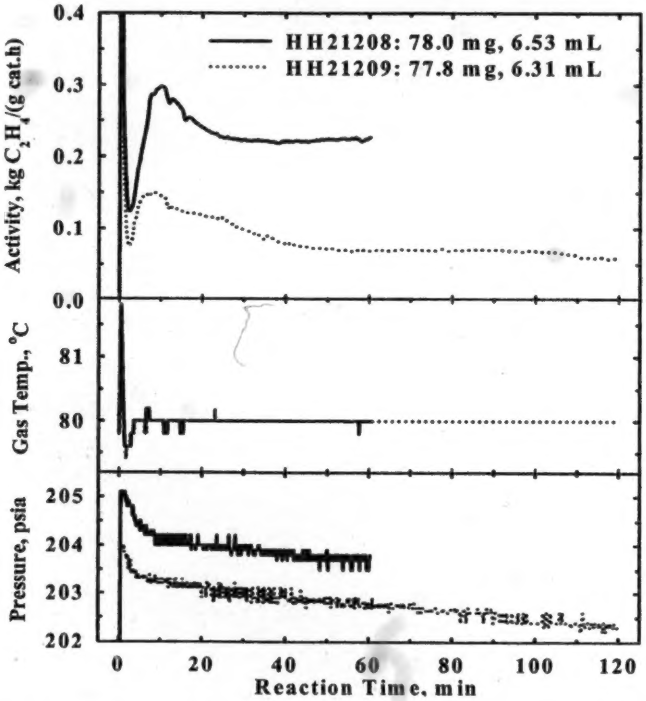

Figure 5.20 Ethylene/1-hexene copolymerization with poor reproducibility in the absence of residual TIBA

Leakage into the reactor after scavenging would have the most dramatic effect on the catalyst because even at < 1 ppm moisture and oxygen levels, the partial pressure of ~10^{-3} torr would permit rapid surface reactions (Oleshko *et al.*, 2002). It is possible to have leakage across closed valves due to marks made on valve seats or o-rings by solid particles. This observation prompted the replacement of the more vulnerable 5-way valve by 2-way valves during test runs on the new reactor. The o-ring sealed Nupro valves used on the catalyst injector are disassembled and cleaned after each polymerization run.

Occasionally helium leak checks were performed on the reactor system after observation of anomalous behavior; these checks some times turned out negative. Nonetheless to avoid any possibility of leaks in the reactor after TIBA scavenging, polymerization Run HH21210 (Table 5.3) was performed with the same amount of catalyst and TIBA as the runs in Figure 5.20 but the residual TIBA was not evacuated from the reactor. The resulting high activity resulted in poor temperature control (Figure 5.21). The high activity in Run HH21210 suggests the possibility of reactor contamination after scavenging during the runs in Figure 5.20. Lower amount of 1-hexene in Run HH21210 is also a factor in the resulting high activity (Chapter 7).

The temporary, but sharp dip in activity observed in Figure 5.21 was likely due to the high rate of gas temperature increase. Under this condition, the increase in reactor pressure due to temperature rise could be greater than the decrease in pressure due to monomer consumption; hence the rapid drop in activity (actually, ethylene feed rate). Note that the temperature peak in Figure 5.21 (middle panel) leads the activity dip (top panel) by about 24 s, and the later in turn leads the pressure dip (bottom panel) by 6 s. The observed behavior could also be due to the nonlinearity in the flow meter response.

Irrespective of the cause, the observed dip is not due to catalyst deactivation; the activity profile subsequently returns to its normal path. Such dips occurred at high rates of temperature rise for other catalysts as well.

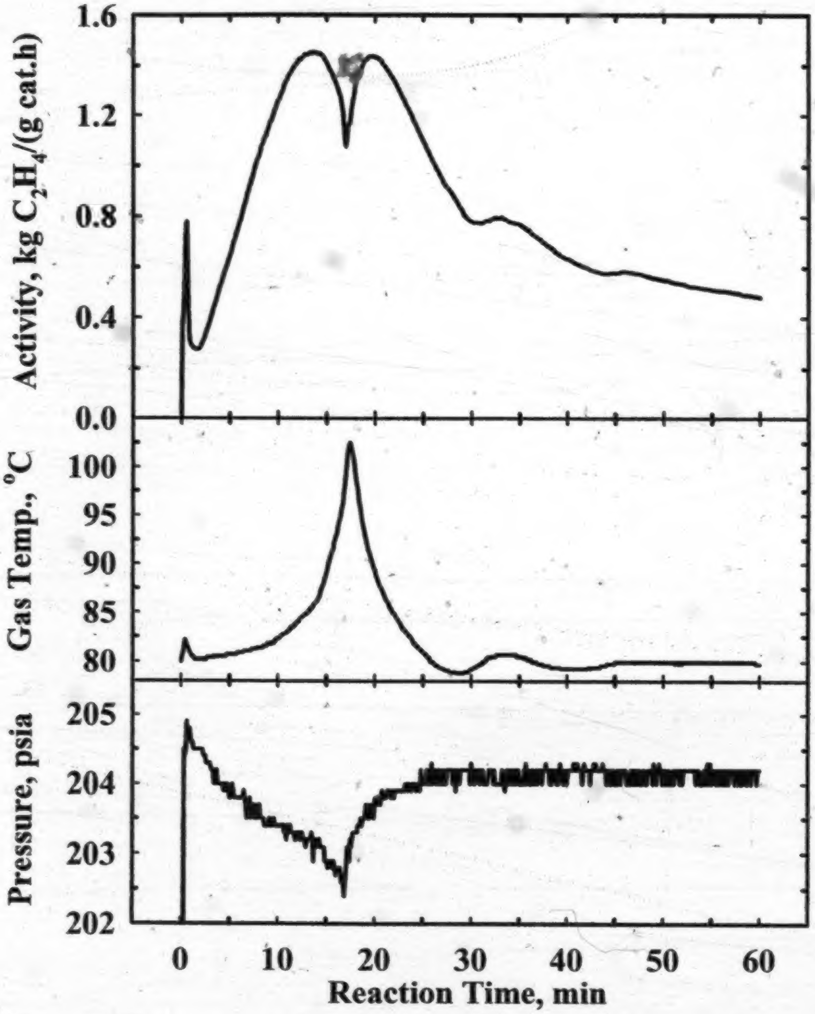

Figure 5.21 Ethylene/1-hexene copolymerization run HH21210 with 0.20 mmol residual TIBA and 4.5 mL 1-hexene.

Catalyst HH21 was used for other sets of reproducibility runs with the residual TIBA left in the reactor (i.e. the reactor was not evacuated after scavenging, Table 5.4). The activity profiles in Figure 5.22 show slightly improved reproducibility, but Run

Table 5.4. Reproducibility of gas-phase polymerization runs with temperature control

Run		Amount in reactor			Temperature[a], °C		Total Rates[b], g C_2H_4/h		Average[c] Activity g PE/(g cat·h)
Number	Date	Cat. mg	1-C_6H_{12}, mL	TIBA, mmol Al	Max	Avg.	Max	Avg.[c]	
HH21211	09/14/02	47	4.58	0.28	80.0	80.0	14.2	9.5	203
HH21212	09/15/02	49	4.57	0.28	80.2	80.0	10.3	6.3	130
HH21213	09/20/02	47	4.58	0.28	80.0	80.0	15.8	10.0	214
HH21216	09/23/02	49	4.57	0.30	80.0	80.0	27.5	16.3	334
HH21217	09/28/02	60	4.51	0.57	80.7	80.0	3.6	87.4	1,457
HH21218	09/29/02	52	4.59	0.59	81.1	80.1	94.5	70.0	1,341
HH21219	09/30/02	52	4.57	0.59	81.8	80.2	102.4	82.7	1,599
HH21220	10/01/02	54	4.67	0.65	80.5	80.0	84.9	64.7	1,200
HH21222	10/06/02	41	4.50	0.59	80.4	80.0	79.1	66.2	1,615
HH21223	10/07/02	42	4.50	0.59	80.2	80.0	73.7	54.8	1,308
HH21224	10/12/02	40	4.58	0.59	80.4	80.0	63.0	43.2	1,072
HH21225	10/14/02	41	4.74	0.59	80.7	80.0	76.3	48.8	1,183
HH21226	10/15/02	42	4.51	0.59	80.4	80.0	80.9	62.7	1,505
HH17230	11/01/02	82	4.50	trace	80.2	80.0	33.5	22.9	279
HH17231	11/02/02	81	4.50	trace	80.2	80.0	34.0	22.9	283
HH17232	11/03/02	83	4.51	trace	80.2	80.0	26.3	18.7	227
HH17233	11/04/02	82	4.50	trace	80.2	80.0	54.1	32.0	392
HH17234	11/08/02	82	4.51	trace	80.2	80.0	48.4	30.6	375
HH07235	11/09/02	100	–	trace	80.5	80.0	42.1	18.0	179
HH07236	11/10/02	102	–	trace	80.2	80.0	28.8	11.2	110
HH07237	11/11/02	100	–	trace	80.0	80.0	28.8	13.5	134

a–Temperature from Thermocouple 1 (T1), initial 2 – 4 min temperature spike ignored; average T i.e., $\sum T_i/N$ where N is the number of equally spaced measurements (usually 600 for a 1 h run); b–maximum rates calculated from ethylene flow reading; c–average determined gravimetrically from polymer yield and total polymerization run time

HH21216 unexplainably had much higher activity. Note that both the catalyst and TIBA amounts were reduced compared to Run HH21210 for better temperature control. All the runs in Figure 5.22 were done over a span of 10 days (see Table 5.3) in the order indicated by the run numbers. Therefore, the observed behavior does not appear to be catalyst deactivation due to aging.

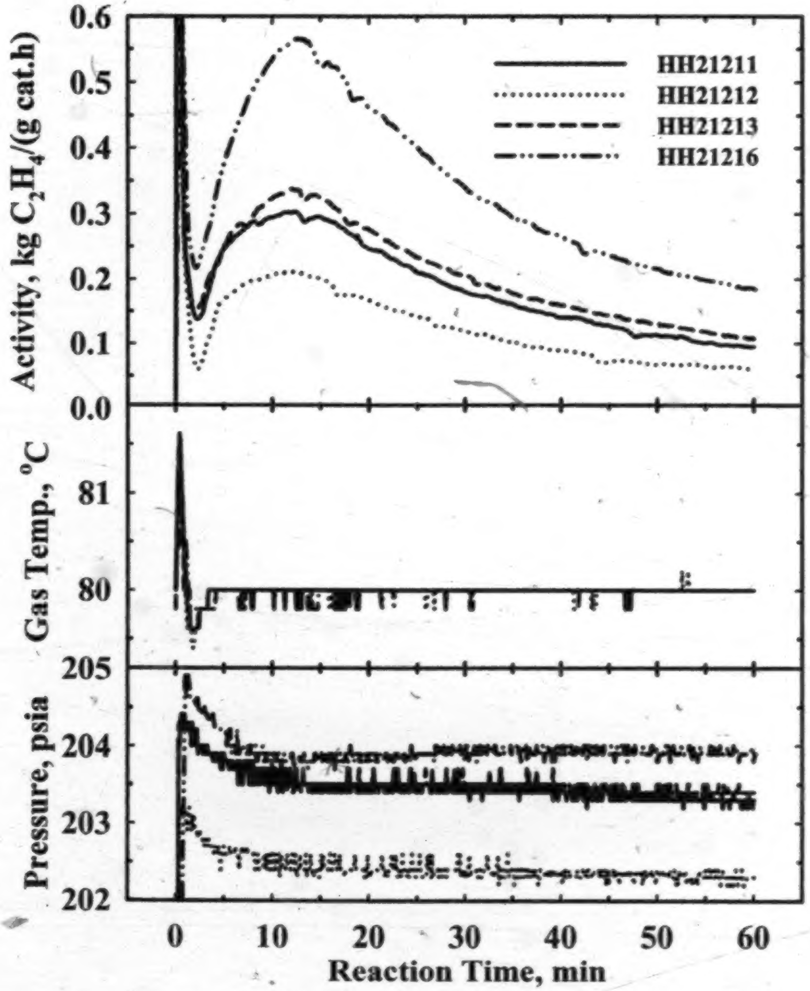

Figure 5.22 Reproducibility runs of ethylene/1-hexene copolymerization with catalyst HH21 in the presence of ~0.3 mmol residual TIBA. Catalyst 47–49 mg; TIBA 0.28-0.30 mmol; 1-hexene 4.6 mL.

Considerable fluctuation in polymerization activity would be expected if the amounts of scavenger used were close to the threshold needed to scavenge impurities. To avoid this, Runs HH21217 to HH21220 in Figure 5.23 were conducted with twice the amount of TIBA, and with slightly more catalyst than the runs in Figure 5.22. The resulting average activities (Figure 5.23) were higher by a factor of six –higher maximum activity and less deactivation. This suggests the TIBA used in the previous runs was inadequate. For most catalysts, reactor scavenging with 0.2 mmol TIBA leaves sufficient residual TIBA to cause delay in catalyst activation (Figure 5.19). Catalyst HH21 has Al:Zr ratio of 150; this is close to, but lower than all the other catalysts used in this work except HH22. Catalyst HH22 with low Al:Zr ratio of 110 had its highest activity only in the presence of 0.59 mmol TIBA (see Chapter 6).

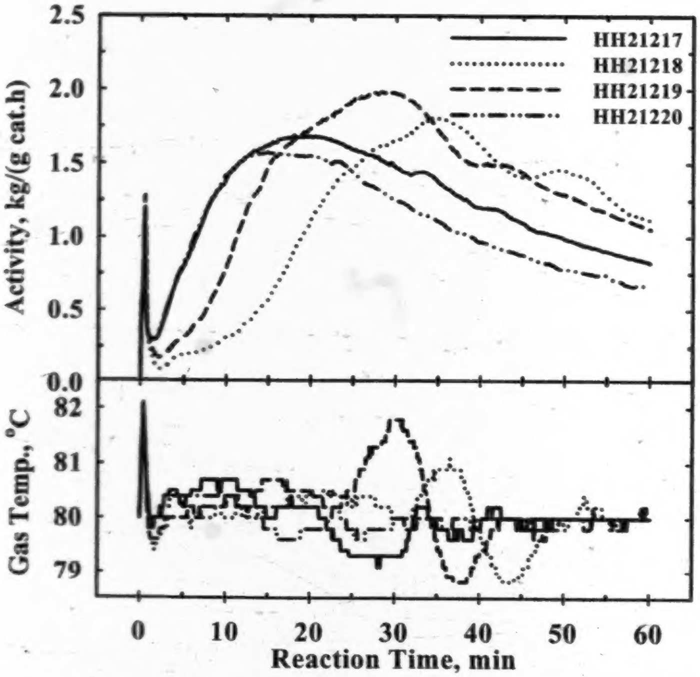

Figure 5.23 Reproducibility of ethylene/1-hexene copolymerizations with catalyst HH21 in the presence of ~0.6 mmol residual TIBA. Catalyst 52–60 mg; TIBA 0.57-0.65 mmol; 1-hexene 4.6 mL.

Seedbed of NaCl was used in the gas-phase reactor to disperse the catalyst and improve heat transfer. Inside the glove box, the weighed catalyst was also sandwiched between two layers of heat-treated sodium chloride in the catalyst holder for better dry catalyst injection. Both the seedbed and the catalyst holder salts were tested as possible sources of impurities. The usual procedure for addition of the seedbed was to load 80 g of salt into the reactor (from an unsealed bottle on lab bench) before the latter was assembled for overnight heating and evacuation at ~90°C. To test the effect of salt drying, NaCl heated at 140-190°C for 30 h (and stored under N_2) was used as the seedbed; it was loaded into the reactor under dry nitrogen flow. Prior to loading the pre-treated salt, the reactor was heated/evacuated at 90°C and 23 mtorr for 8 h. After loading the salt the reactor was further heated/evacuated at the same conditions for 10 h before it was used in polymerization. Figure 5.24 shows the activity profiles of runs made by the normal procedure with those using the treated salt. Run HH21223 (treated seedbed) shows greater delay in activity growth compared to HH21222 (normal seedbed and catalyst holder salt). The delay is indicative of a cleaner reactor with more residual TIBA to complex with active site (see Chapter 6). Further delay was observed when both the seedbed and the catalyst holder salt bed were treated (Run HH21224).

3

The last two observations suggest that treating the salt beds reduces the impurity levels in the reactor. However, Run HH21225 (normal seedbed) exhibited greater delay than HH21223 (treated seedbed) while HH21226 (treated catalyst holder salt) had almost the same profile as HH21222 (normal seedbed and catalyst holder salt). Note that the delay in Run HH21225 could not be due to the slightly higher (0.24 mL) amount of 1-hexene in the run; similar (0.16 mL) difference in the amount of 1-hexene did not make any difference in previous runs with the same catalyst (cf. Runs HH21217 and HH21220 in Figure 5.23). Therefore, there is no observable benefit of any extra treatment of either the seedbed or the catalyst holder salt compared to the normal procedure. The average activities of the polymerization runs shown in Figure 5.24 varied by 36% due largely to variation in the initial rate of catalyst activation.

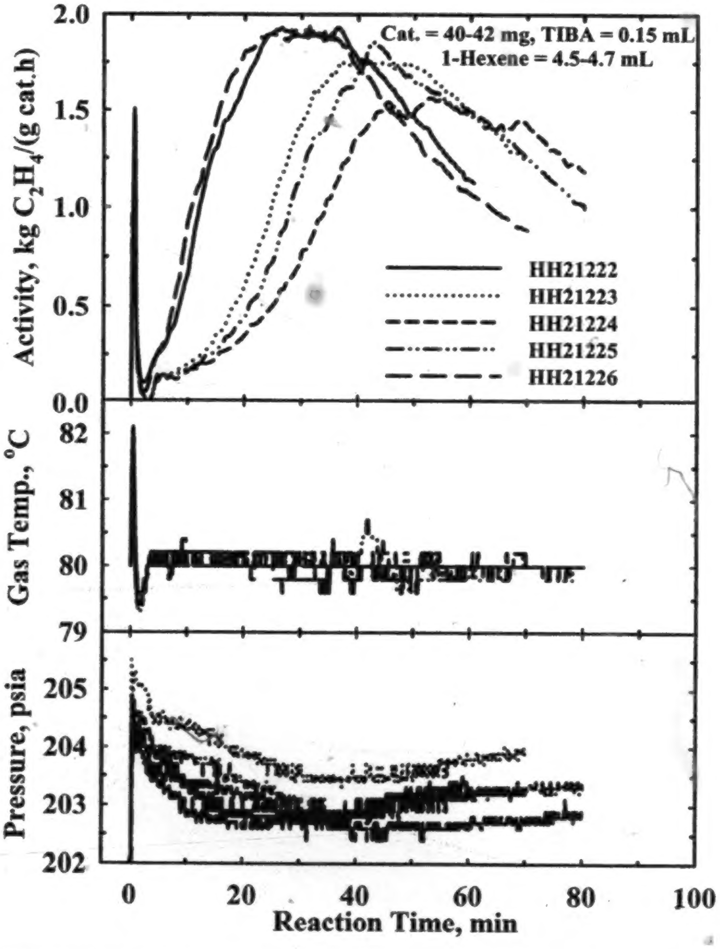

Figure 5.24 Ethylene/1-hexene copolymerization with differently treated seedbed and catalyst transfer salt. Catalyst 40–42 mg; TIBA 0.59 mmol; 1-hexene 4.5–4.7 mL.

The type and amount of aluminum alkyl used in the reactor greatly affects the polymerization activity. More detailed investigation of this effect is reported in Chapter 6 and published elsewhere (Hammawa *et al*., 2004).

During the dry catalyst injection, some catalyst particles remain on the walls of the catalyst injector probably due to electrostatic attraction. This was noticeable by plugs of polymer formed on the part of the catalyst injector inside the reactor, and by the small amounts of polymer formed in the catalyst compartment. There is limited monomer available in the cavity of the catalyst injector compartment after catalyst injection; both ends are shutoff with the Nupro valves immediately after catalyst injection. Figure 5.25 shows polymer plugs formed on the catalyst injector during polymerization with four different catalysts.

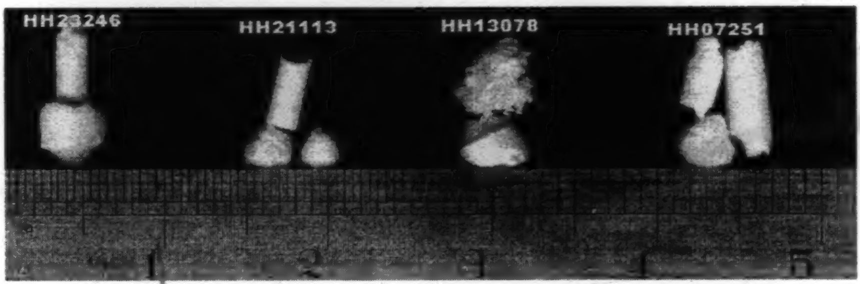

Figure 5.25 Plugs of polyethylene formed on the catalyst injector (inside the reactor)

The extent of the above problem mainly depended on the nature of the catalyst (support and particle size), but it also varied from one polymerization run to another with the same catalyst. EDX analysis of some polymer plugs revealed no detectable aluminum while SEC showed similar molar mass as the rest of the polymer produced in that run. This signifies that the catalyst clinging to the injector could not have significant influence on the activity profiles, i.e. polymerization over such catalyst is similar to that in the mixed bed.

Polymerization occurs on catalyst particles blown into the port cavities (in the top flange) and the upper parts of the reactor resulting in the plugging of those cavities. This could plug off the monomer feed, GC sampling valve, or cause cleaning difficulty. To avoid this, it is desirable to temporarily stop the stirrer during catalyst injection. The duration of this stop influences the activity and reproducibility for some catalysts. Figure 5.26 shows a set of five ethylene/1-hexene copolymerization runs with catalyst HH17 in which the idle time of stirrer was varied.

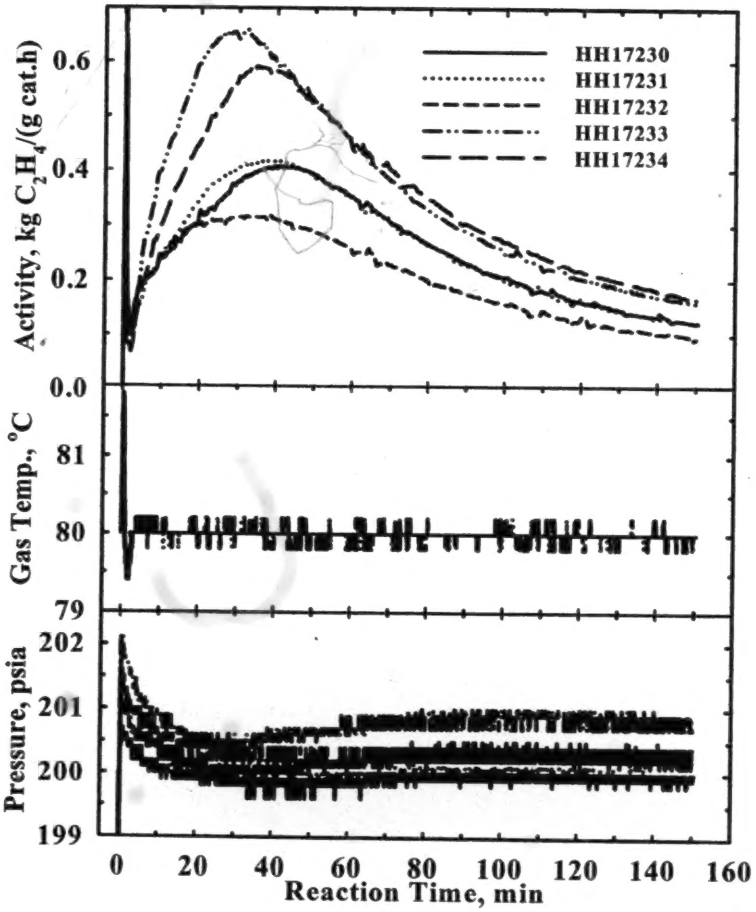

Figure 5.26 Influence of stirrer start-up on activity profile and reproducibility of ethylene/1-hexene copolymerization over catalyst HH17 with the residual TIBA vented. Catalyst 81–83 mg; 1-hexene 4.5 mL.

In Runs HH17230-HH17232 (Figure 5.26) sufficient time (10-15 s) was allowed for the reactor to attain the set pressure following catalyst injection before the stirrer was switched on again. The three runs, particularly HH17230 and HH17231 showed good reproducibility; however, a lump of fused polymer particles (2 – 4 g) formed in all the three runs (see Figure 5.27). These were likely initiated during the 10-15 s fill-up period that the injected catalyst was not stirred. On the other hand, the stirrer was switched on just 1-2 s after catalyst injection in runs HH17233 and HH17234; both runs showed reproducibly higher activity, and had no lumps of fused polymer particles. This problem was not observed on many other catalysts at the 10-15 s delay before stirrer start-up. It is also important to note that for runs HH17230-HH17234, the residual TIBA (in 100 psi N_2) was vented after scavenging and the remaining N_2 displaced by ethylene prior to catalyst injection.

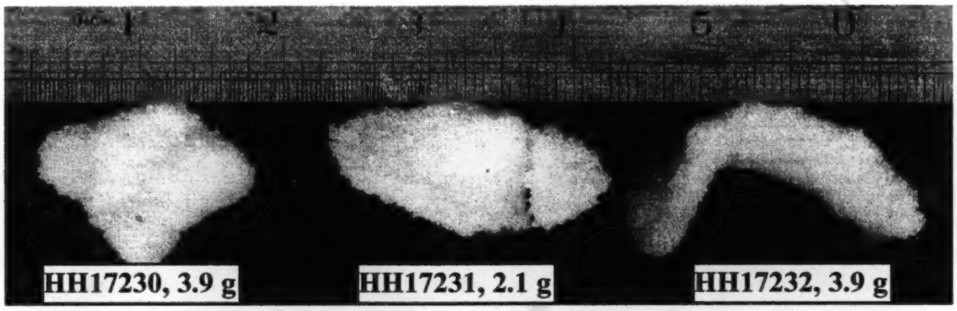

Figure 5.27 Lumps of polymer formed in the reactor due to delay in stirrer start-up after catalyst injection

The above venting procedure proved to be more reproducible for gas-phase polymerizations in the absence of residual TIBA. Therefore, this procedure was adapted for all subsequent gas-phase polymerizations without residual aluminum alkyl in the reactor, e.g. in the polymerization runs to study the temperature and pressure effects. During such series of polymerizations, repeat runs were often made to confirm observations. Figures 5.28 – 5.30 show such tests on other catalysts under different conditions. Catalyst HH07 (Figure 5.28) is prone to the electrostatic effect and is often incompletely injected. On the contrary, catalysts HH18 and HH09 (Figures 5.29 and 5.30 respectively) show excellent reproducibility; average activities agree within 5%.

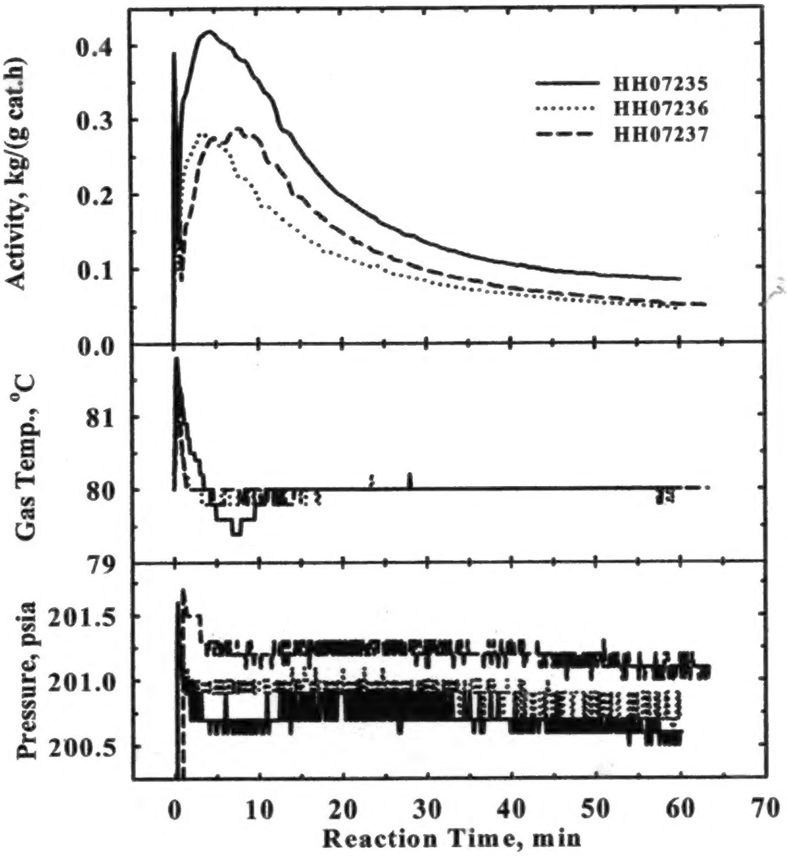

Figure 5.28 Reproducibility of ethylene homopolymerization using 100 mg of catalyst HH07 and the TIBA venting mode.

The molar masses of the ethylene homopolymers and ethylene/1-hexene copolymers produced during the reproducibility runs shown in Figures 5.22 to 5.28 are within 2 to 7 % of the mean values for each set (see Appendix B, Tables B-1 and B-2 for the polymerization conditions and product properties respectively). The molar mass variations are less than the corresponding variations in polymerization activities; hence, the molar masses are less prone to irreproducibility than polymerization activities. This suggests that the irreproducibility is primarily due to deactivation of some active sites rather than a change in the chemical environment of the sites.

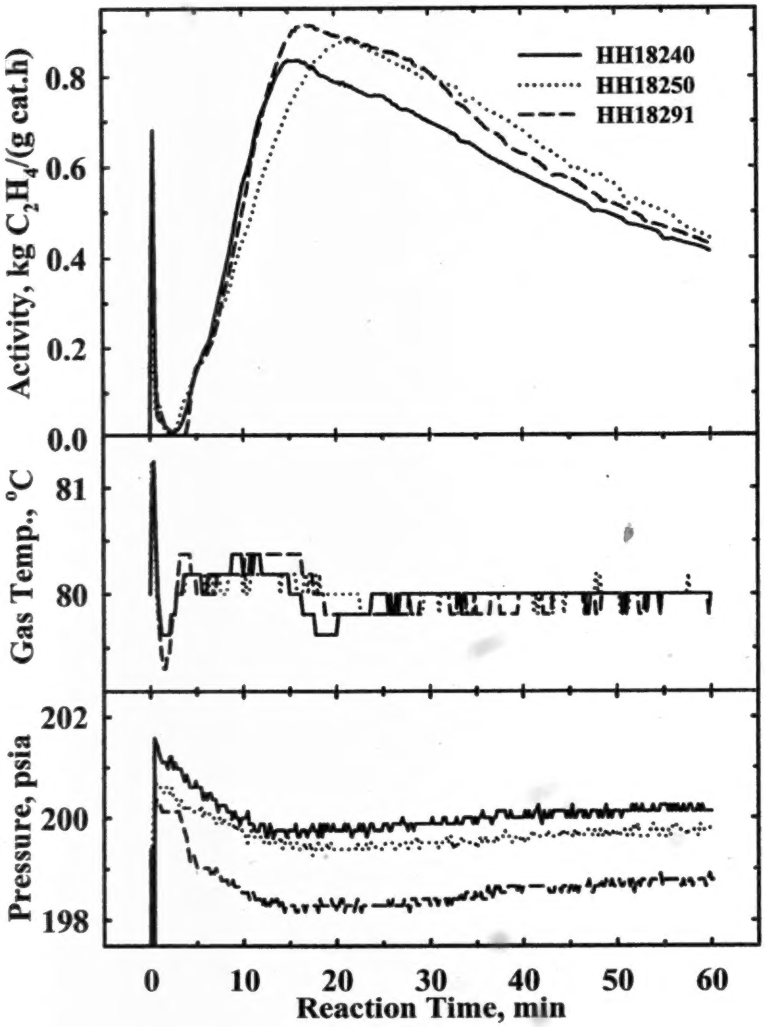

Figure 5.29 Reproducibility of ethylene/1-hexene copolymerization with catalyst HH18

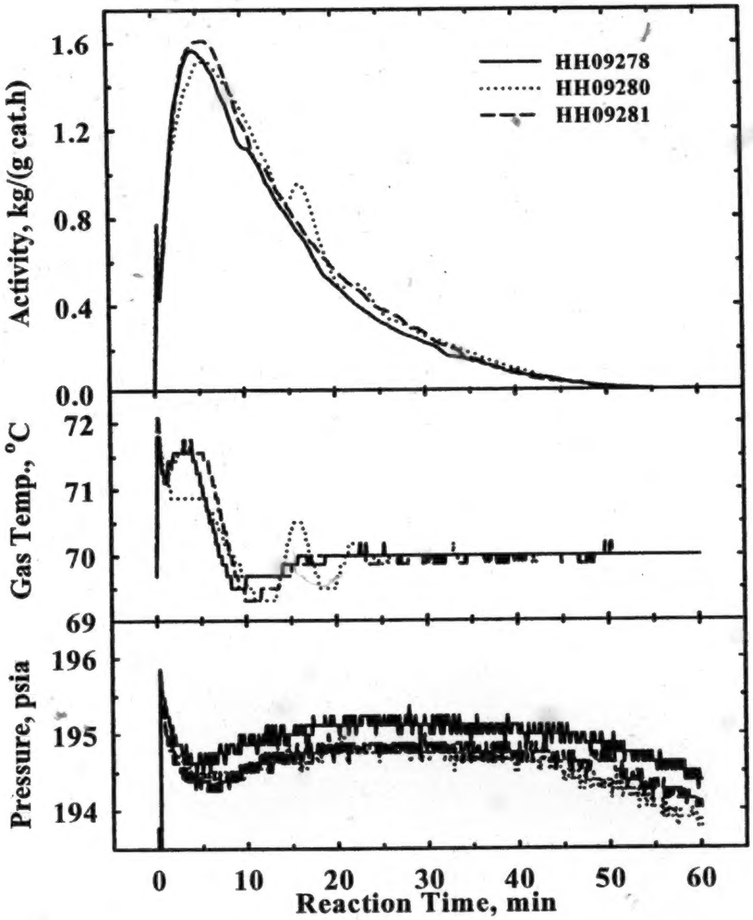

Figure 5.30 Reproducibility of ethylene homopolymerization with catalyst HH09

Ethylene polymerization reaction is highly exothermic, and polymerization catalysts tend to deactivate faster with increasing temperature. Figure 5.31 shows the influence of varying the amount of catalyst HH08 on the total polymerization rate (top panel) and polymerization activity (middle panel). At higher catalyst loading (Runs HH08051 and HH08052), the gas phase temperature increased by 18°C above the 80°C set point (bottom panel of Figure 5.31). Due to poor gas-solid heat transfer, the temperature of the polymerizing particles would be considerably higher than the gas temperature (Webb *et al.*, 1991); hence, rapid catalyst deactivation resulted. Several investigations revealed increased rate of catalyst deactivation with temperature for both metallocene and Ziegler-Natta catalysts (Charpentier *et al.*, 1997; Samson *et al.*, 1998; Samson *et al.*, 1999; Chung and Hsu, 2002; Pater *et al.*, 2003; Kumkaew *et al.*, 2003b). The rate of heat generation per particle (or unit mass of catalyst) is proportional to activity, but if the total rate is low, the gas phase temperature will be low affording better heat transfer with the active particles.

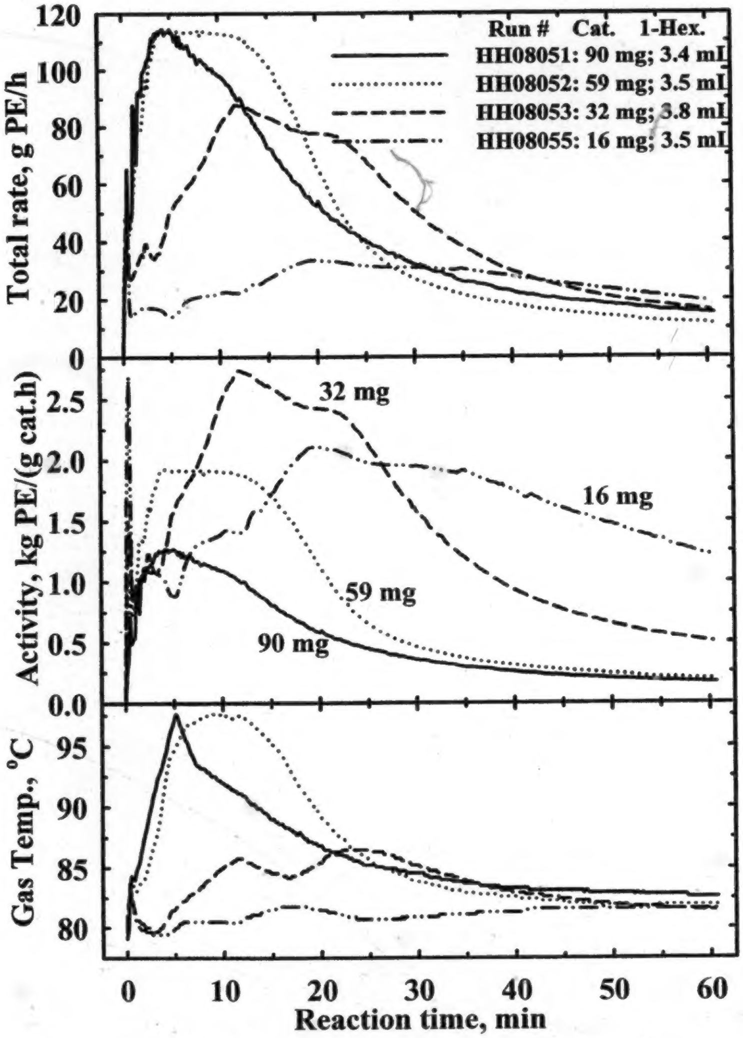

Figure 5.31 Influence of the amount of catalyst charged to the reactor on reproducibility.

During rapid increase in reactor temperature, as in Runs HH08051 and HH08052, the temperature control system, i.e. the controller PID settings, coolant temperature, cooling water temperature and flow rate, could influence the initiation of thermal runaway. It was difficult to obtain good reproducibility under such situations.

Gas-phase polymerization with dry catalyst injection is more prone to irreproducibility than when the catalyst is injected as a suspension in a hydrocarbon. In dry injection, the highly reactive catalytic sites are directly exposed to the impurities present in the system. On the contrary, suspending the heterogeneous catalyst in a hydrocarbon diluent provides some protection. Thus Kumkaew *et al.* (2003b) reported irreproducibility associated with introducing small amounts (less than ~50 mg) of catalyst by dry injection while Weickert *et al.* (1995), injected suspensions of 1 – 4 mg of catalyst in pentane into the polymerization reactor quite reproducibly. When this method is used for gas-phase polymerization, the solvent is removed either by evacuation (Chung and Hsu, 2002) or purging (Samson *et al.*, 1996, 1999) before the introduction of monomer feed. While this approach may be suitable for heterogeneous Ziegler-Natta catalysts, it may not be so for the supported metallocene systems; exposing the catalyst to reactor environment would lead to deactivation even in the absence of polymerization (Hammawa *et al.*, 2004).

Summary of the reactor fabrication and its performance in gas-phase polymerization

A new 2-L gas-phase polymerization reactor capable of ethylene homopolymerization and ethylene/α-olefin copolymerization has been fabricated. The new reactor controlled the gas-phase temperature well even at total polymerization rates of 3 moles ethylene per hour. Drilling channels in the sidewall and inserting static mixers in the channels (to improve heat transfer) enhanced the reactor temperature control capability. High stirring rate, anchor type impeller, and high amount of NaCl seedbed improved temperature control.

The new reactor has unique gas sampling valve and an associated GC system that allowed analyses of ethylene/hydrogen, and ethylene/α-olefin mixtures rapidly. The reactor was successfully operated with batch wise and continuous additions of 1-hexene. The reactor operating procedure, residual impurities, residual aluminum alkyls, and the amount (and activity) of catalyst in the reactor affect reproducibility of the gas-phase polymerizations.

High polymerization rates and rapid increases in initial activity resulted in large changes in bulk gas-phase temperature (> 3 to 4°C). This caused significant increases in the rate of catalyst deactivation; hence, it is necessary to measure gas-phase temperature in the reaction zone. Decreasing the amount of catalyst in the reactor can decrease temperature excursions, but this caused irreproducibilities due to errors in the amount of catalyst injected and/or catalyst deactivation due to impurities.

6. Exploratory Experiments II: Effects of Aluminum Alkyls[*]

Aluminum alkyls are widely used as impurity scavengers in slurry or gas-phase olefin polymerization with supported metallocene/MAO or Ziegler-Natta catalysts. In Ziegler-Natta systems, the aluminum alkyls are also cocatalysts primarily responsible for the generation of active sites. The latter role has also been reported in the polymerization of ethylene and α-olefins using supported as well as homogeneous metallocene/MAO catalysts (e.g., see Ribeiro *et al.*, 1997; Pryzbyla *et al.*, 1999; Hlatky, 2000). Different investigators have observed widely varying and often (apparently) contradicting influences of aluminum alkyls on the polymerization activity and polymer properties. For example, increasing TIBA concentration was reported to increase (Panin *et al.*, 2001) as well as decrease (Petoff *et al.*, 1999) the molar masses of polypropylenes produced with metallocene catalysts. The investigations in this chapter were prompted by the observation of the influence of aluminum alkyls on the gas-phase polymerizations discussed in Chapter 5. Therefore, this chapter presents results of a more detailed and systematic study of the effect of aluminum alkyls on the activity of gas-phase ethylene/α-olefin polymerization. The influences on the polyolefin properties are discussed in Chapter 8.

6.1 Sensitivity of catalysts to TIBA

Table 6.1 summarizes the catalysts used in studying the effects of aluminum alkyls on the gas-phase polymerization of ethylene and 1-hexene. Catalyst HH05 was prepared using Type-4 modified MAO as described in Chapter 3. No support was used in catalyst HH23; the MAO solids served as the support. The polymerization runs used to test the sensitivity of different catalysts to TIBA are summarized in Table 6.2.

---

[*] A version of the chapter has been published in the *Journal of Applied Polymer Science*, **92**, 3549-3560, 2004.

Table 6.1. Description of polymer-supported $(n\text{-BuCp})_2ZrCl_2$/MAO catalysts

Catalyst ID	Support	Amount used		Zr content		Al:Zr ratio
		Support, g	MAO[a], mL	Mass %	μmol/g	
HH05	Poly(DVB /HEMA/STY)	2.01	17.8	0.10	11.40	563
HH06	Poly(DVB/HEMA/STY)	1.50	10.5	0.15	16.66	260
HH09	Poly(DVB/HEMA)	1.50	5.0	0.06	6.69	375
HH14	Poly(DVB/HEMA)	1.00	15.0	0.24	25.76	215
HH15	Poly(DVB/HEMA)	2.00	27.0	0.19	20.50	209
HH16	Poly(EGDM)	1.51	10.0	0.13	14.36	285
HH17	Poly(DVB/EGDM)	1.50	10.0	0.10	11.18	376
HH19	Poly(DVB/NVP)	1.51	11.0	0.16	17.98	230
HH20	Poly(DVB/AN)	1.50	11.5	0.18	19.84	220
HH22	Poly(DVB)	2.00	4.9	0.11	12.28	110
HH23	-	-	22.8	0.80	88.13	166

a – Volume of MAO solution (10 mass % MAO in toluene); MMAO-4 solution in toluene (6.92 mass % Al) used in HH05.

Table 6.2. Effect of Al alkyls on polymerization activity

Run Number[a]	Amount charged to reactor			Activity[c], g PE/(g cat·h)		t_{Rmax}[d], h
	Catalyst[b], mg	TIBA, mmol	$1\text{-}C_6H_{12}$, mL	Avg.	Max.	
HH05039	100	0.39	3.2	36.1	NA	NA
HH05040	106	trace	3.0	72.5	79.7	1.78
HH05041	101	none	3.0	66.1	78.1	1.08
HH06043	102	none	3.1	131.3	flat	0.78
HH06044	113	trace	3.0	335.7	500.0	0.23

a – first four characters, e.g. HH05 represents catalyst number; composition in Table 6.1
b – includes mass of support, MAO, and the metallocene compound
c – average activity obtained gravimetrically; maximum from ethylene mass flow rate
d – time to attain maximum polymerization activity
NA – not attained

Figure 6.1 shows the variation of activity profiles for polymerization runs with Catalyst HH05. The run that used no scavenger had similar activity profile with the one in which residual TIBA was evacuated after scavenging impurities (cf. Runs HH05041 and HH05040). This indicates the reactor is very clean or the catalyst is not sensitive to the traces of impurities in the reactor. The initial delay in Run HH05041 is likely due to reactor overpressure (see lower panel of Figure 6.1) rather than induction period of the catalyst. Addition of 0.4 mmol TIBA in the reactor changed the activity profile to a ramp type that did not attain maximum value during the 1.5 h run.

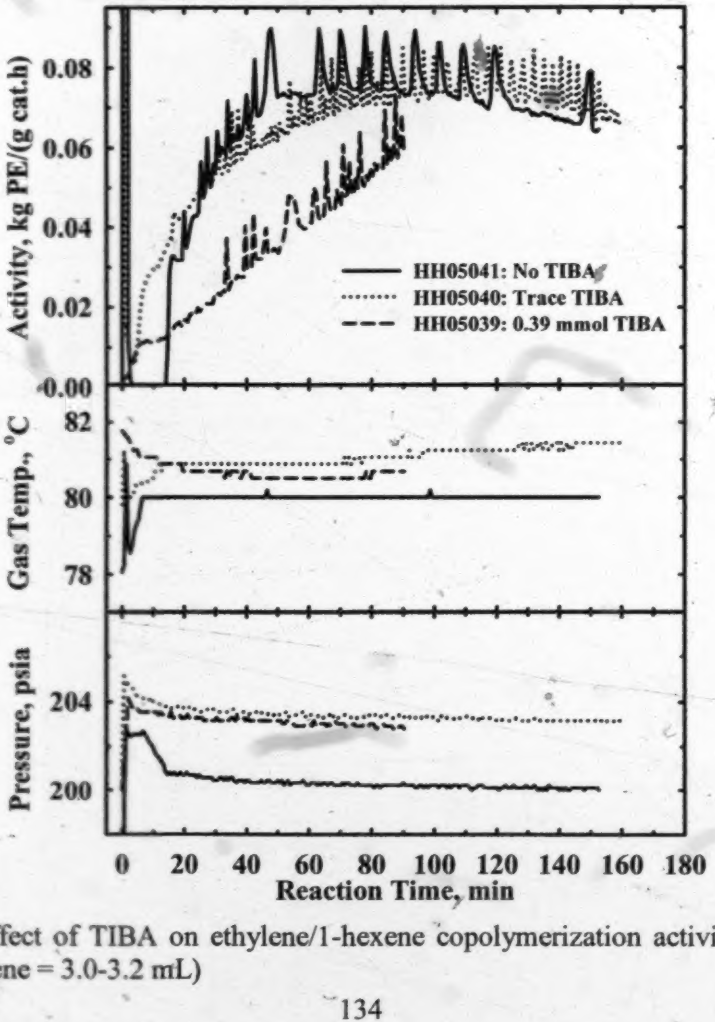

Figure 6.1 Effect of TIBA on ethylene/1-hexene copolymerization activity for catalyst HH05 (1-hexene = 3.0-3.2 mL)

In contrast, scavenging the reactor (followed by evacuating residual TIBA) increased the average activity of Catalyst HH06 almost three fold, Figure 6.2. The two polymerization runs in Figure 6.2 were done under similar conditions to Runs HH05041 and HH05040 (Figure 6.1) in which Catalyst HH05 was used. The higher Al:Zr ratio (Al/Zr = 560) in Catalyst HH05 could be responsible for protecting the active sites from rapid deactivation by traces of impurities in the reactor (cf. Al/Zr = 260 in catalyst HH06).

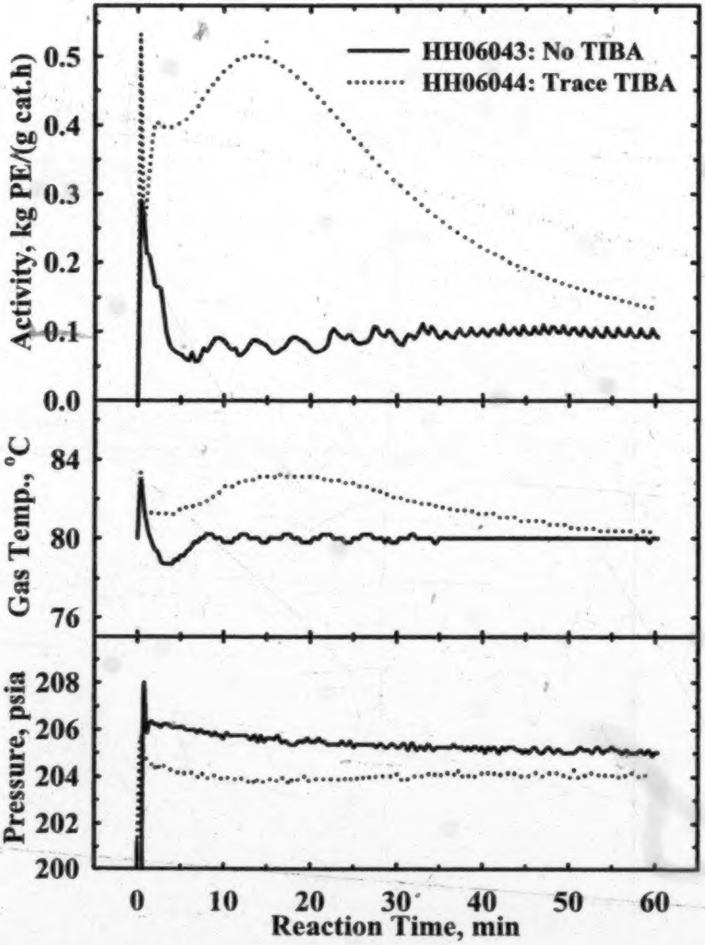

Figure 6.2 Effect of TIBA on ethylene/1-hexene copolymerization activity for catalyst HH06 (1-hexene = 3.0 mL)

6.2 Effect of aluminum alkyl type and concentration

Table 6.3 describes the polymerization runs used to investigate the influence of the type and amount of aluminum alkyl on activity profiles of different supported catalysts. The table shows that the Al alkyls tend to prolong the activity growth period during ethylene homopolymerization and ethylene/1-hexene copolymerization at constant initial ethylene/1-hexene ratio in the reactor (except for Catalyst HH20).

Table 6.3. Effect of Al alkyls on polymerization activity at 80°C, 1.4 MPa and 80g NaCl

Run Number[a]	Al Alkyl Used	Amount charged to reactor			Activity[c], (g PE/g cat·h)		t_{Rmax}[d], h
		Catalyst[b] mg	Al Alkyl[e], mmol	$1\text{-}C_6H_{12}$, mL	Avg.	Max.	
HH09259	TIBA	49.9	0.59	–	1286.6	1736.2	0.46
HH09263	TIBA	40.5	trace	–	696.3	1968.9	0.08
HH14128	TIBA	60.0	trace	–	235.5	1593.9	0.04
HH14129	TEA	60.3	0.26	4.3	955.2	1556.7	0.63
HH14131	TIBA	60.6	trace	4.5	690.9	750.0	0.45
HH14149	TIBA	60.3	0.20	4.5	835.8	1305.0	0.50
HH14159	TIBA	61.4	0.20	–	388.7	1034.3	0.32
HH15093	TIBA	50.0	trace	4.3	1318.6	1971.9	0.23
HH15117	TIBA	59.7	0.20	4.3	1196.0	1882.7	0.36
HH19107	TIBA	76.3	trace	2.3	496.7	635.0	0.51
HH19108	TIBA	76.9	trace	4.7	548.7	727.2	0.65
HH19124	TIBA	77.7	0.12	4.3	364.6	440.7	0.48
HH19122	TIBA	78.7	0.28	4.3	228.4	322.6	1.35
HH19123	TEA	80.2	0.29	4.3	143.5	246.7	2.18
HH19125	TNOA	76.3	0.22	4.3	456.1	631.5	0.88
HH20111	TIBA	77.4	trace	4.5	396.6	466.7	0.61
HH20198	TIBA	77.5	0.20	4.6	407.7	557.1	0.61
HH22200	TIBA	89.6	trace	4.6	69.8	89.1	0.50
HH22201	TIBA	86.7	0.20	4.7	146.5	174.6	0.71
HH22202	TIBA	87.5	0.35	4.9	144.5	183.8	0.47
HH22203	TIBA	88.7	0.59	4.9	734.2	932.6	0.70
HH22205	TIBA	88.6	0.79	4.8	606.5	962.4	0.75
HH23150	TIBA	10.3	0.20	–	1264.1	2552.4	0.61
HH23152	TIBA	10.1	trace	–	1321.3	4016.0	0.05

a–d: same as in Table 6.2

e: Aluminum alkyl, AlR_3 (TEA: R = ethyl; TIBA: R = *i*-butyl; TNOA: R = *n*-octyl)

The Al alkyl effects in the above table originated from its influence on activity profiles as explained below for some selected catalysts. Figure 6.3 shows the effect of residual TIBA on ethylene polymerization with catalysts HH14. The presence of residual TIBA (after scavenging with 0.2 mmol) considerably suppressed the initial activity and broadened the activity profile. The activity of Run HH14128 increased to the maximum of 1.6 kg PE/(g cat·h) in 2 min; this raised the gas-phase temperature by 6°C, and was probably associated with an even higher particle temperature rise. It is difficult to control the reactor temperature during such rapid rate increases. Temperature rise in the growing catalyst particle would normally exceed that in the gas-phase substantially due to the poor gas-solid heat transfer, causing particle overheating. The rapid deactivation after 2 min

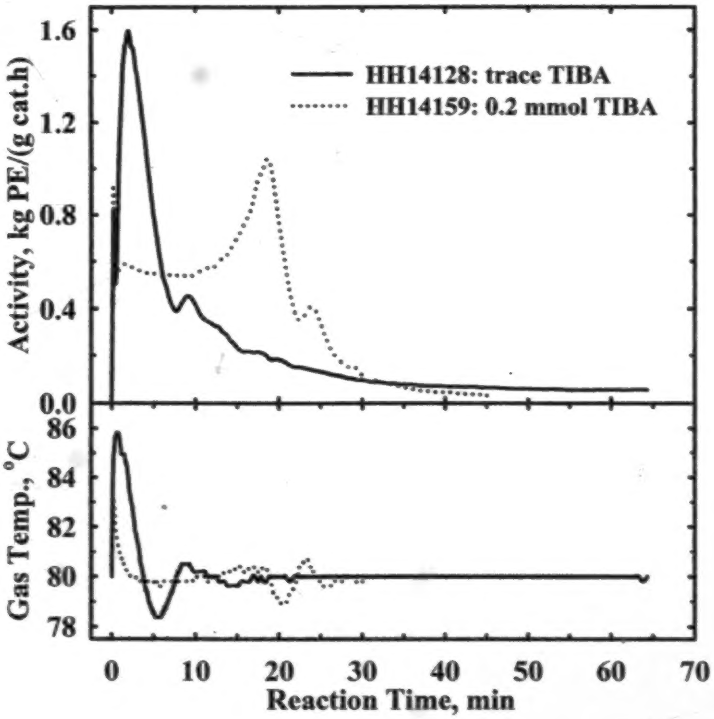

Figure 6.3 Effect of residual TIBA on ethylene homopolymerization activity for catalyst HH14 at 1.4 MPa

reaction time (Figure 6.3) was probably a result of overheating. Deactivation rates of metallocene catalysts were reported to increase with temperature (Kumkaew *et al.*, 2003b; Roos *et al.*, 1997; Fischer and Mülhaupt, 1991).

The effect of residual TIBA on Catalyst HH23 is shown in Figure 6.4. The influence of TIBA was similar to HH14 (Figure 6.3) but both the initial exotherm (<2°C) and the catalyst deactivation rate were lower due to lower heat generation. Although Figure 6.4 shows higher activity values than Figure 6.3, the maximum ethylene consumption rate of Run HH14128 was more than twice that of HH23152. The maximum activity per mole of Zr for Catalyst HH14 (62.2 ton PE/mol Zr·h –trace TIBA, and 40.4 ton PE/mol Zr·h –with 0.2 mmol TIBA) is about 30% higher than the corresponding activities for Catalyst HH23.

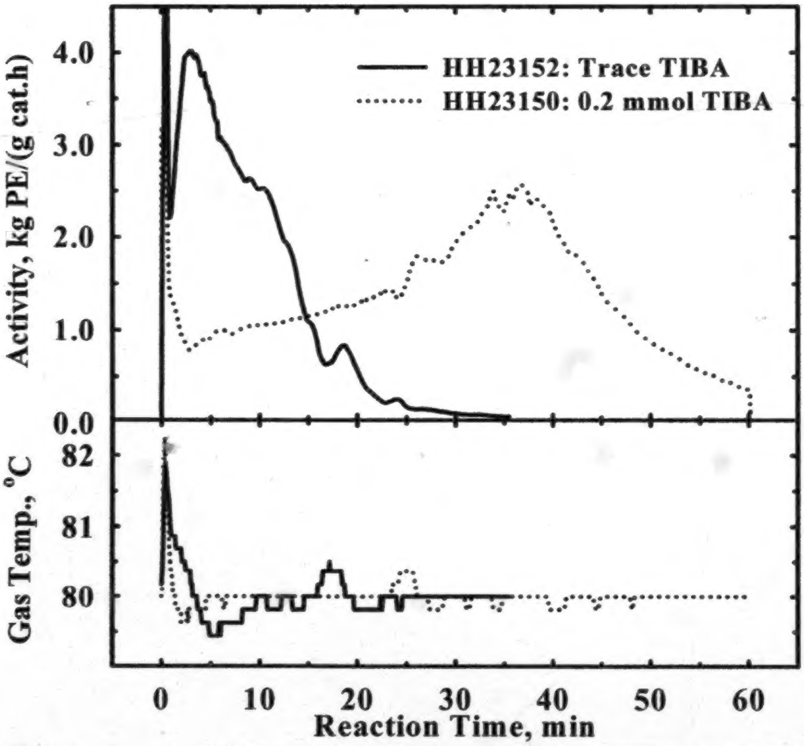

Figure 6.4 Effect of residual TIBA on the activity of Catalyst HH23 at 1.4 MPa C_2H_4

Figure 6.5 shows the effect of higher amount of residual TIBA on ethylene polymerization activity for Catalyst HH09. This catalyst has relatively lower aluminum and zirconium loadings, but higher Al/Zr ratio than HH14 and HH23 (Table 6.1). The presence of residual TIBA delayed the attainment of maximum activity from 5 min to 28 min; however, the average polymerization activity almost doubled due to broadening of the activity profile. The suppression of initial activity (hence, reactor temperature) surge by Al alkyls could be a useful industrial tool for effective temperature control and productivity enhancement. Overheating causes rapid deactivation of catalyst particles.

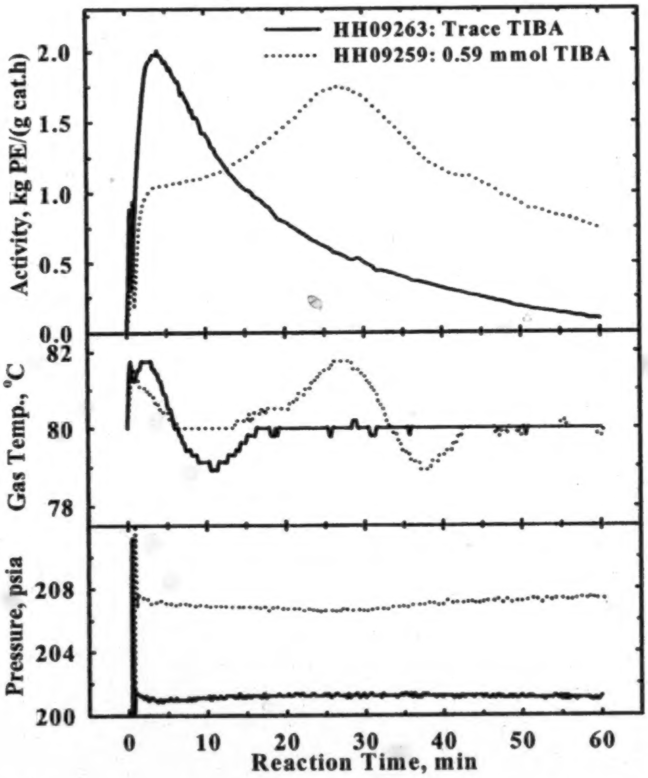

Figure 6.5 Effect of residual TIBA on ethylene homopolymerization activity for catalyst HH09 at 1.4 MPa

The supported metallocene/MAO catalysts are supposedly preactivated i.e. require no induction period in the reactor; hence, the short time (2 – 5 min) required to attain maximum activity for the runs with trace TIBA (Figures 6.3-6.5). The observed delay in attaining the maximum polymerization activity, R_{Pmax}, in the presence of residual TIBA may be due to complexation between the active metallocenium cation and TIBA to form a dormant site. Active metallocenium cations react reversibly with residual and external TMA to form dormant hetero-dinuclear cation $[(Cp_2Zr–Me)\cdot Me_3Al]^+$ (Bochman and Lancaster, 1994). Fischer *et al.* (2000) proposed an equilibrium between such dormant and active sites in propylene polymerization. Depletion of TIBA in the reactor due to reaction with impurities, chain transfer to aluminum, and thermal decomposition favors the conversion of dormant sites to active sites.

The observed effect of aluminum alkyl is not only restricted to ethylene homopolymerization; Figure 6.6 shows the influence of TIBA and TEA on ethylene/1-hexene copolymerization. Comparison of the homopolymerization and the copolymerization runs with trace TIBA (Run HH14128, Figure 6.3 and Run HH14131, Figure 6.6)

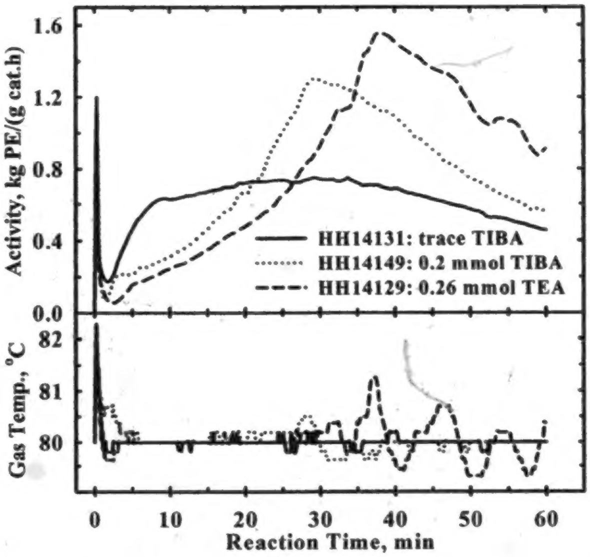

Figure 6.6 Effect of residual TIBA and TEA on copolymerization activity for catalyst HH14 at 1.4 MPa (1-hexene = 5.3-5.5 mL)

shows a significant difference. The maximum copolymerization activity was less than half that of the homopolymerization, but the significantly flat profile of the latter resulted in almost three times the average activity of the former. Residual TIBA and TEA slowed the initial rates (Figure 6.6) with TEA having the greater effect. Unlike ethylene homopolymerization, the maximum activities in the copolymerization runs with residual aluminum alkyls were higher. The average copolymerization activities in Figure 6.6 were all higher than the corresponding homopolymerization ones (Figure 6.3, Table 6.3). This comonomer enhancement is widely reported for both Ziegler-Natta and metallocene catalysts (Wester and Ystenes, 1997; Galland *et al.*, 1999) and will be discussed further in Chapter 7.

The effect of residual TIBA on the copolymerization behavior of Catalyst HH19 is shown in Figure 6.7. Increasing the amount of TIBA from trace to 0.12 and 0.28 mmol, with similar initial amounts of 1-hexene, decreased the maximum activity; however, the t_{Rmax} for Run HH19124 (0.12 mmol TIBA) was lower than that of run HH19108 (trace TIBA). This anomaly may lie in the difficulty of injecting (completely) the small volume (0.03 mL) of TIBA. The difference observed in Figure 6.7 cannot be due to the small variations in the amount of 1-hexene in the reactor; doubling the amount of 1-hexene only resulted in a small difference in activity (cf. Runs HH19107 and HH19108).

Figure 6.8 shows the effect of aluminum alkyl type on copolymerization activity of Catalyst HH19. The three runs had similar amounts of 1-hexene; the different aluminum alkyls used were at approximately the same concentration (Table 6.3). TEA had the strongest effect; it delayed the occurrence of the maximum activity by more than 2 h after catalyst injection. The 10 min induction period of Run HH19123 (with TEA)

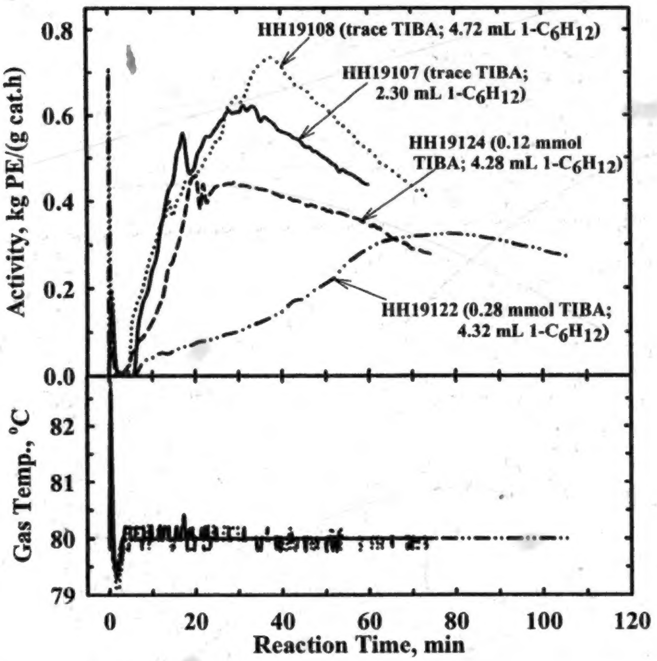

Figure 6.7 Effect of the amount of TIBA and 1-hexene on copolymerization activity for catalyst HH19 at 1.4 MPa

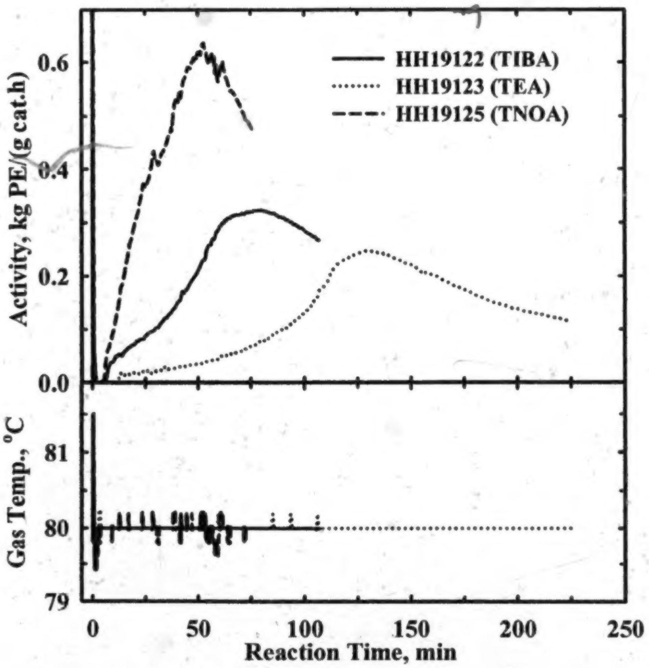

Figure 6.8 Effect of aluminum alkyl type on copolymerization activity of catalyst HH19 at 1.4 MPa (1-hexene = 4.3 mL)

was higher than the induction periods of Run HH19122 with TIBA (6 min), or HH19125 with TNOA (5 min). Of the three aluminum alkyls, TEA has the smallest molar mass (size) and it is the strongest Lewis acid; hence, it can diffuse and react faster than TIBA and TNOA. Run HH19125, with TNOA (higher molar mass) had t_{Rmax} of 0.88 h compared to 0.56 h for Run HH19108 with trace TIBA; the average and maximum activity values for these two runs were also similar (within 15%). Both the delay in t_{Rmax}, and the similarity in activity profiles and average activity for TNOA and trace TIBA runs support the reactivity and/or diffusivity effect stated earlier.

The diffusion and reactivity of aluminum alkyls have a strong effect on the rate of activation of $MgCl_2$-supported Ziegler-Natta catalyst. Nooijen (1994), reported decreased rate of catalyst activation with increasing alkyl aluminum size for TEA, TIBA, TNOA, and IPRA at constant Al/Ti ratio in slurry. The trend was opposite to that observed in the current work with the supported metallocene/MAO catalyst (Figures 6.6 and 6.8 above) because in Ziegler-Natta systems the alkyl aluminums are responsible for the generation of active sites (Zakharov *et al.*, 1983). Also, the cocatalyst diffusion in the gas phase is much faster than in the liquid present in slurry polymerizations. Although alkyl aluminums are responsible for the generation of active sites in Ziegler-Natta systems, they could also be a source of catalyst deactivation due to over-reduction of active titanium species (Doi *et al.*, 1982; Keii *et al.*, 1982). Thus, Lynch et al. (1991), observed increased polymerization activity with alkyl aluminum size for $SiO_2/MgCl_2$-supported $TiCl_4$ catalyst in the gas-phase.

Runs HH22200-HH22205 examine the effect of residual TIBA concentration on the ethylene/1-hexene copolymerization activity of Catalyst HH22. This catalyst had

Al/Zr ratio of 110 compared to Al/Zr ratios >210 for the other supported catalysts in Table 6.1. Run HH22200, with trace TIBA had low polymerization activity; using 0.2 mmol and 0.35 mmol TIBA increased the activity only slightly, Figure 6.9. Further increase of TIBA in the reactor to 0.59 mmol resulted in a surprisingly large increase in polymerization activity, average and maximum activities increased more than five fold (cf. Figures 6.9 and 6.10). There seem to be a threshold amount of TIBA between 0.35 – 0.59 mmol below which the activity remained low.

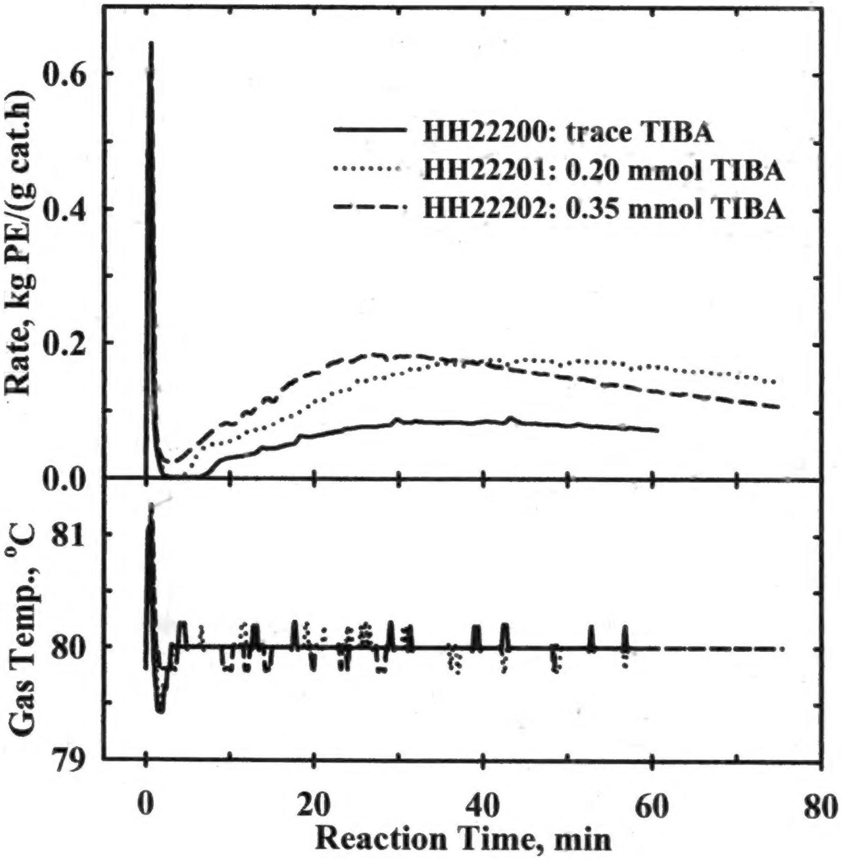

Figure 6.9 Effect of TIBA amount on copolymerization activity of catalyst HH22 at 1.4 MPa (1-hexene = 4.6-4.9 mL)

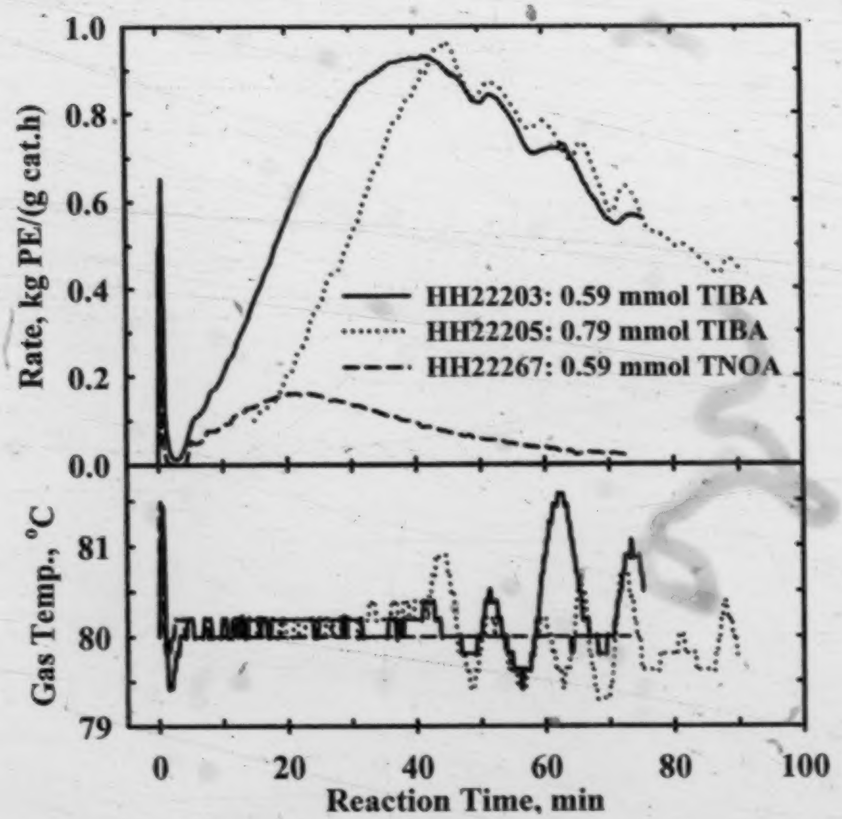

Figure 6.10 Effect of higher TIBA and TNOA concentration on copolymerization activity of catalyst HH22 at 1.4 MPa (1-hexene = 4.8 mL)

The behavior of Catalyst HH22 is the reverse of that observed with the previous catalysts. This seemingly contradictory behavior could well be explained by the formation of dormant metallocene complexes in Catalyst HH22. Density functional theory calculations for Cp_2ZrMe_2/MAO solutions showed that an Al/Zr ratio ≥ 275 ensures the disappearance of the free Cp_2ZrMe_2, the homodinuclear $[Cp_2ZrMe{-}(\mu\text{-}Me){-}ZrMeCp_2]^+[MeMAO]^-$, and the weak $Cp_2ZrMe_2{\cdot}MAO$ complex (Zurek and Ziegler, 2002). The homodinuclear cation (see Equation 6.1), favored by high metallocene concentration, is inactive in olefin polymerization, Bochman and Lancaster (1994).

$$[Cp_2Zr{-}X]^+ + Cp_2ZrX_2 \rightleftharpoons [Cp_2Zr(X)\text{-}\mu X\text{-}Zr(X)Cp_2]^+;\ (X = Cl^- \text{ or } CH_3^-) \qquad (6.1)$$

During the drying step in the catalyst preparation (Section 3.2), the metallocene/MAO solution is concentrated in the catalyst pores. If Al/Zr ratio of 110 is not high enough to prevent interaction between the metallocene molecules, the inactive homodinuclear species $[Cp_2Zr(X)\text{-}\mu X\text{-}Zr(X)Cp_2]^+$ could form. The poly(DVB) support used to make HH22 has no functional groups that would chemically react with MAO. Therefore, the support merely acts as container for the catalyst precursors. Increasing TIBA concentration in the reactor favors the formation of the dormant metallocenium-ion/TIBA complex (Equation 6.2) at the expense of the formation of the inactive homodinuclear complex in Equation 6.1. The dormant complex reactivates as TIBA gets depleted during polymerization.

$$[Cp_2Zr{-}Me]^+ + i\text{-}Bu_3Al \rightleftharpoons [(Cp_2Zr{-}Me)\cdot i\text{-}Bu_3Al]^+ \qquad (6.2)$$

Among all the catalysts used in this work, only Catalyst HH22 had Al/Zr ratio significantly lower than the 275 range reported by Zurek and Ziegler (2002). The similarity in activity between the three runs with trace to 0.35 mmol TIBA (Figure 6.9) and Run HH22267 with 0.59 mmol TNOA (Figure 6.10) suggest that TNOA could not diffuse and react effectively with the inactive complex. This further supports the role of diffusivity and reactivity of aluminum alkyl in influencing the activity profile.

6.3 Effect of inert gas and the contact mode of catalyst with TIBA

The polymerization runs described in Table 6.4 were used to investigate the effects of inert gas and contact mode of catalyst with TIBA. Catalyst HH16 was made using poly(EGDM) support with no DVB component. In all polymerizations where the catalysts were contacted with TIBA in the reactor before introducing ethylene, 0.35-MPa nitrogen was used to inject the catalysts. Comparative runs were also conducted with the same nitrogen partial pressure in the reactor. Runs HH16097 (no N_2) and HH16170 (0.35 MPa N_2) in Figure 6.11 show the effect of nitrogen on ethylene homopolymerization; the ethylene pressure in both runs was 1.4 MPa, Table 6.4. The presence of 0.35 MPa of nitrogen did not have a significant effect on either the activity profile or the average polymerization activity; there was less than 10% variation between these runs. The catalyst was moderately active and did not deactivate rapidly during ethylene homopolymerization.

Table 6.4 Description of ethylene homopolymerization runs to determine effect of inert gas and the contact order and concentration of TIBA

Run Number	Amount in reactor		Pressure, MPa		t_{mix}, min	t_{Rmax}, h	Activity, g PE/(g cat.h)	
	Catalyst, mg	TIBA, mmol	N_2	Total			Avg.	Max.
HH16097	80.4	trace	0.0	1.38	0.0	0.36	243.3	315.9
HH16199	87.9	trace	0.35	1.73	1.0	0.11	84.2	117.3
HH16170	84.6	trace	0.35	1.73	0.0	0.47	262.9	288.9
HH16168	84.5	0.28	0.35	1.73	0.0	0.96	222.5	317.5
HH16169	85.7	0.28	0.35	1.73	0.0	1.09	235.2	358.5
HH16195	92.0	0.28	0.35	1.73	1.0	0.10	42.4	73.5
HH09259	49.9	0.59	0.0	1.38	0.0	0.45	1286.6	1734.8
HH09254	50.1	0.59	0.35	1.73	0.0	0.61	970.7	1167.1
HH09258	49.8	0.59	0.35	1.73	3.0	0.53	759.0	1000.7
HH09255	50.2	trace	0.35	1.73	0.0	0.07	369.7	1506.0
HH09257	50.0	trace	0.35	1.73	3.0	0.07	327.8	1155.9

t_{mix} = time catalyst was in reactor (at 80°C and 450 rpm) before starting ethylene feed
t_{Rmax} = time to attain maximum polymerization rate from the start of ethylene feed

Exposing Catalyst HH16 to nitrogen and low (trace) TIBA concentration while stirring at 80°C, for 1 min prior to introducing ethylene resulted in an over three-fold decrease in the average polymerization activity (cf. Runs HH16199 to HH16170 in Figure 6.11). This suggests catalyst deactivation by impurities prior to ethylene feed.

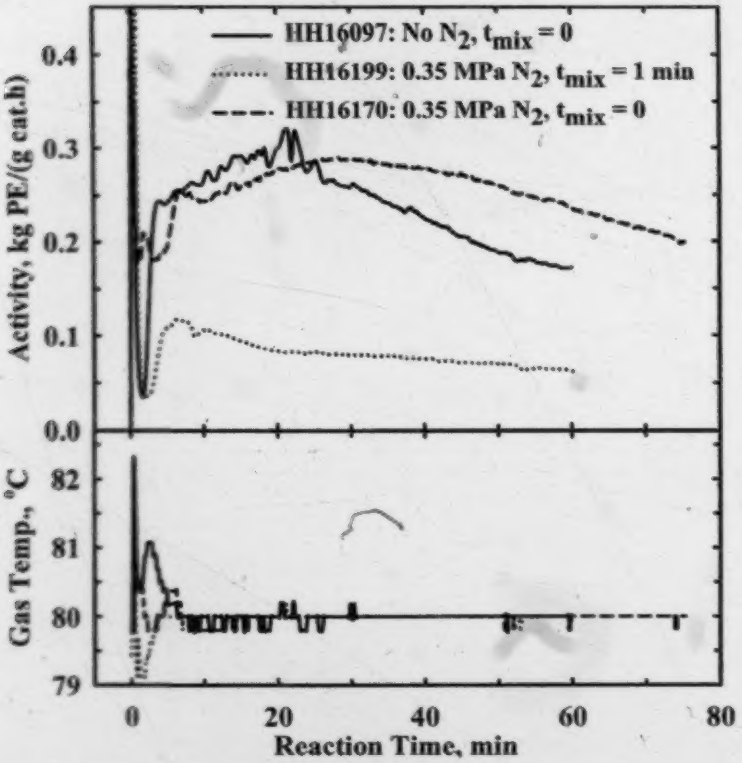

Figure 6.11. Effect of pre-exposure of catalyst HH16 to (trace) TIBA and the presence of N_2 on ethylene homopolymerization activity.

Results of polymerizations run similar to HH16170 and HH16199 (Figure 6.11) but at higher TIBA concentration are shown in Figure 6.12. Injecting the catalyst (with ethylene) into nitrogen, TIBA, and ethylene environment in the reactor resulted in gradual activity growth t_{Rmax} ~ 1 h (Runs HH16168 and HH16169). Run HH16169 is a replicate of HH16168, and it shows good reproducibility. The two profiles are similar to those observed earlier for polymerization in the presence of TIBA. Stirring the catalyst for 1 min at 80°C in the nitrogen and TIBA environment before introducing ethylene resulted in an over five-fold decrease in activity (cf. Runs HH16195 to HH16168/-HH16169 in Figure 6.12). Catalyst HH16 was deactivated by 1 min exposure to nitrogen, and trace or 0.28 mmol TIBA environment at 80°C in the absence of ethylene. This deactivation seems irreversible because no increase in activity was observed in Runs HH16199 and HH16195, Figures 6.11 and 6.12 respectively. TIBA and/or high temperature played a role in the deactivation. Note: The catalyst is stable to prolonged storage under nitrogen. In addition to the low activity, t_{Rmax} for the catalyst pre-exposed for 1 min in the absence of ethylene was <10 min compared to 30 to 65 min for the same catalyst run without the pre-exposure step.

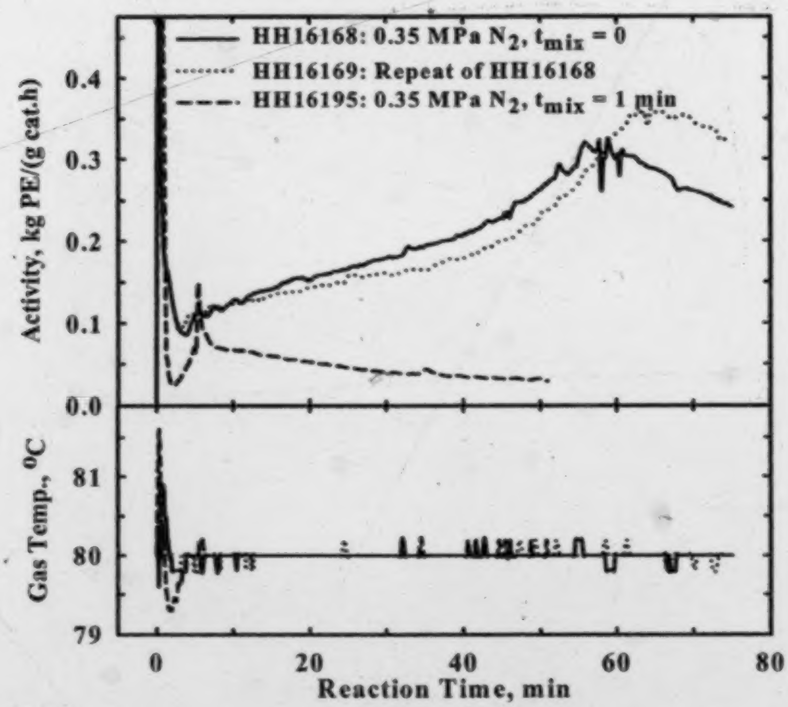

Figure 6.12. Effect of pre-exposure of catalyst HH16 to (0.28 mmol) TIBA and the presence of N_2 on ethylene homopolymerization activity.

Catalyst HH09, with lower Al and Zr loading but higher activity than HH16 was used for experiments similar to those described above with HH16. Runs HH09259 and HH09254 (Figure 6.13) show the effect of nitrogen; the two runs only differed by the presence of 0.35 MPa nitrogen in HH09254. Contrary to Catalyst HH16, the presence of 0.35 MPa nitrogen reduced the maximum and average polymerization activity of Catalyst

HH09 by 25% and 30% respectively. The same conditions resulted in <10% decrease in maximum activity of Catalyst HH16; the one-hour average activity was even 10% higher in the presence of nitrogen.

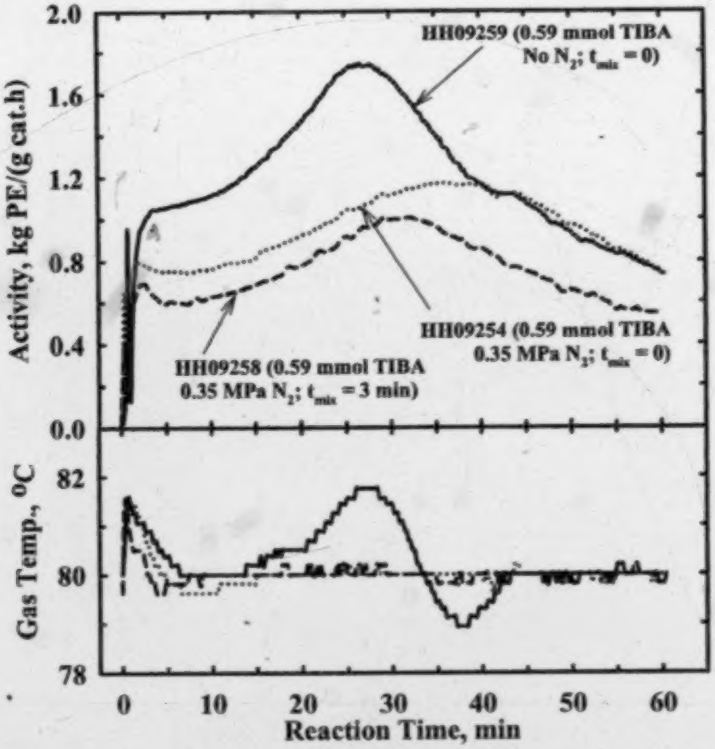

Figure 6.13. Effect of pre-exposure of catalyst HH09 to (0.59 mmol) TIBA and the presence of N_2 on ethylene homopolymerization activity.

The difference in the effect of nitrogen observed between Catalysts HH09 and HH16 could be due to the difference in their activities. The homopolymerization activity depends on catalyst friability (see Chapter 8). Weickert *et al.* (1999) predicted a non-linear decrease in polymerization activity in the presence of gaseous or liquid inert components in the reactor due to an 'enrichment effect' of the inerts. At high polymerization activities in the gas-phase, monomer transport into the porous polymerizing particle is largely by convection, contrary to the widely assumed diffusive transport in the multi-grain models, MGM, (Floyd *et al.*, 1986) and polymeric flow models, PFM, (Schmeal and Street, 1971; Singh and Merrill, 1971) commonly used in describing the growth of polymer particles. Kittilsen *et al.* (2001b), and Veera *et al.* (2002), have modeled this convective monomer transport during olefin polymerization. High ethylene consumption rate in the polymerizing particles creates a pressure drop in the particles. This pressure drop causes flow of the bulk gas (ethylene and nitrogen) into the polymerizing particle. The inert nitrogen exits the particles only by diffusion; hence, the particle pores get 'enriched' with nitrogen. This nitrogen 'enrichment' will continue until the partial pressure of nitrogen in the particle provides sufficient concentration gradient (with the bulk gas) to maintain equal inward (convective and diffusive) and outward (diffusive) nitrogen flow. Catalyst HH16 had lower polymerization activity (low convective flow of monomer); therefore, the presence of nitrogen did not influence the activity significantly.

In Run HH09258 (Figure 6.13), Catalyst HH09 was contacted with nitrogen at 80°C for 3 min in the reactor containing 0.59 mmol TIBA while stirring prior to introducing ethylene. This led to a 20% reduction in the average activity (see Table 6.3) but the activity profiles of these two runs were quite similar. This similarity suggests either a single site type or all the different sites were uniformly affected by the TIBA. Figure 6.14 shows that pre-exposing Catalyst HH09 in the reactor as above, but without TIBA resulted in an 11% reduction in the average activity compared to the run (HH09255) without pre-exposure (Table 6.3). The 11% loss in activity occurred in the first 12 min, the two activity profiles were essentially the same after the first 12 minutes. The difference in activity between the two runs in Figure 6.14 could be due to exposure of the catalyst to TIBA or it could be due to irreproducibility, likely caused by temperature variations in the growing particle. In this work 10 to 20% variation in activity was frequently observed for catalysts with moderate to high initial activity (see Chapter 5). Regardless of the cause, the decrease in polymerization activity caused by the exposure of Catalyst HH09 to nitrogen and TIBA in the absence of ethylene was small compared to similar exposure for Catalyst HH16. The different responses by these two catalysts may be due to the different supports used in the catalysts or the difference in their Al/Zr ratios. The Al/Zr ratio of 373 for Catalyst HH09 seems to provide greater catalyst protection from impurities than the Al/Zr ratio of 163 for Catalyst HH16.

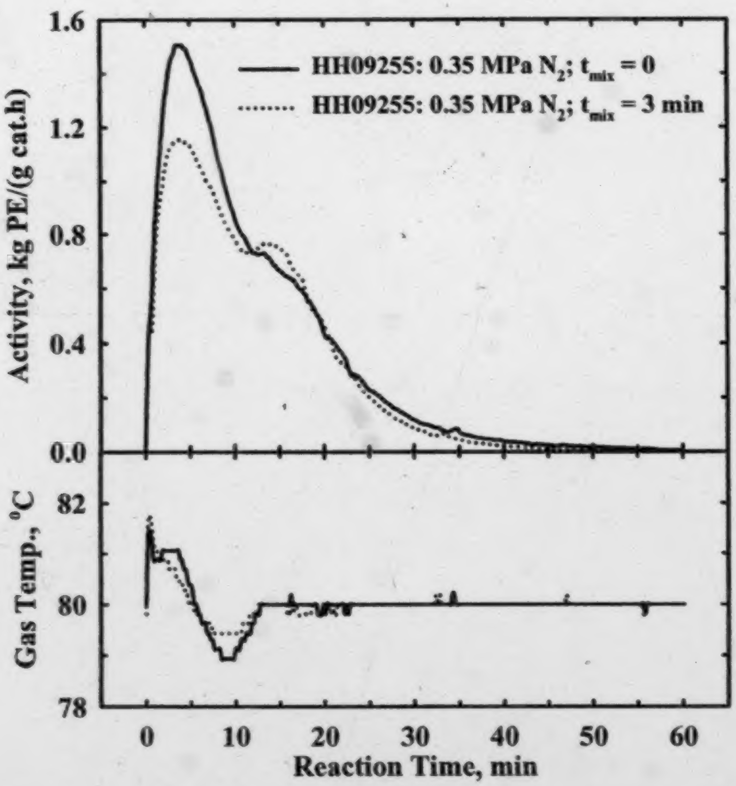

Figure 6.14. Effect of pre-exposure of catalyst HH09 to (trace) TIBA and the presence of N_2 on ethylene homopolymerization activity.

Summary of the effects of aluminum alkyls

Catalysts with high Al:Zr ratio are less sensitive to traces of impurities in the polymerization reactor. Residual aluminum alkyl in the reactor suppressed the initial activity, but broadens the rate profile for both polymer-supported $(n\text{-BuCp})_2\text{ZrCl}_2$/MAO catalyst and solid $(n\text{-BuCp})_2\text{ZrCl}_2$/MAO complex. The broadening of rate profiles due to residual aluminum alkyls often led to higher average activities for 1 h runs. The effectiveness of aluminum alkyls in inhibiting the initial activity decreases with increasing size of the alkyl group i.e., TEA > TIBA > TNOA. Residual TIBA significantly increased the productivity of supported catalyst with low Al:Zr ratio. The sensitivity towards aluminum alkyls differs from one catalyst to another, but more investigation is required to understand the cause of this observation.

7. Rates of ethylene/α-olefin Polymerizations Over Polymer-supported $(n\text{-BuCp})_2ZrCl_2$/MAO Catalysts in the Gas-phase

The productivity of polymerization catalyst as determined by the rate versus time profile is the most important parameter in evaluating the commercial suitability of the catalyst. The rate profile of a catalyst is affected by the catalyst preparation procedure and the polymerization conditions (dos Santos *et al.*, 1999b; Tait *et al.*, 2000). In this chapter, the supported catalysts are evaluated based on their polymerization activity and the total Al and Zr content; no distinction is made between active and inactive Zr in the catalyst.

The composition of the supported catalysts deviate from the expected values based on the amount of metallocene and MAO used in the catalyst preparation (see Section 4.4). Differences were also observed between different batches of otherwise identical catalysts. Both the support-type and the catalyst composition influence the catalyst behavior. To minimize confounding the two effects, the influence of typical variations in the Zr loadings and the Al:Zr ratios for catalysts prepared using the same support is first discussed in Section 7.1. This is followed by the effects of chemical structure and morphology of support on the catalyst activity in Section 7.2. Sections 7.3 to 7.6 discuss the influence of temperature, monomer pressure, and hydrogen respectively on the polymerization rate profiles. The comonomer effects are presented in Chapter 8.

Due to the number, and the interdependence of morphological characteristics of the supports, it was not feasible to investigate the morphological effects in the classic way of varying one parameter at a time. Even the techniques of experimental design are not feasible due to the large number of variables involved. Each support has different microstructure and morphology. For example, different poly(HEMA/DVB) supports have in common only the cross-linker and functional group types. The crosslink density, pore size, pore size distribution, surface area, and fragility of each support may differ. The later properties depend on the preparation conditions for the support (see Sherrington, 1998 and Santora *et al.*, 2001); details of these are outside the scope of this work.

7.1 Influence of typical variation in zirconium loading and Al:Zr ratio

The composition of all catalysts is presented in Table 7.1; the top seven catalysts were used to investigate the effect of typical composition variation. Table 7.2 summarizes the relevant polymerization runs. Figure 7.1 presents the ethylene polymerization rates of Catalysts HH25, HH26, and HH27, all made from the same batch of poly(DVB/N-Vinyl-2-pyrrolidinone) support. Although the activities are different, the three catalysts showed low ethylene homopolymerization activity (average activity 3 – 22 g PE/g cat·h).

Table 7.1 Typical variations in catalyst compositions (continued next page)

Support	Catalyst ID	Measured composition, mass %		Al:Zr ratio
		Aluminum	Zirconium	
Poly(DVB/N-V-2-P)	HH19	11.2	0.164	230
	HH25	11.7	0.161	246
	HH26	11.4	0.181	212
	HH27	16.7	0.202	279
Poly(HEMA/DVB)	HH13	15.2	0.285	181
	HH14	14.9	0.235	215
	HH15	11.6	0.187	209
	HH15A*	20.0	0.414	163
	HH01	Not determined	Not determined	–
	HH02	13.1	0.181	245
Poly(HEMA/PTMA)	HH03	12.3	0.152	273
Poly(HEMA/STY/DVB)	HH04	15.8	0.159	336
	HH05	17.3	0.104	563
	HH06	11.7	0.152	260
Poly(EGDM)	HH07	16.5	0.128	435
Poly(DVB)	HH08	16.4	0.209	265

Table 7.1 Typical variations in catalyst compositions (cont'd)

Support	Catalyst ID	Measured composition, mass % Aluminum	Measured composition, mass % Zirconium	Al:Zr ratio
Poly(HEMA/DVB)	HH09	6.69	0.061	373
	HH10	11.4	0.138	278
	HH11	9.38	0.093	342
Poly(STY/DVB)	HH12	7.73	0.119	220
Poly(EGDM)	HH16	11.1	0.131	286
Poly(DVB/EGDM)	HH17	11.4	0.102	376
Poly(DVB/4-V-Py)	HH18	10.1	0.162	209
Poly(DVB/Acrylonitrile)	HH20	11.8	0.181	220
Poly(DVB/PEI)	HH21	8.38	0.189	150
Poly(DVB)	HH22	3.69	0.112	111
None	HH23	39.5	0.804	166
None	HH24	42.2	0.836	171
Poly(DVB/N-V-2-P)	HH28	15.6	0.138	382
Poly(STY/DVB)	HH29	7.06	0.128	186

* – agglomerated particles separated from HH15 not used in polymerization

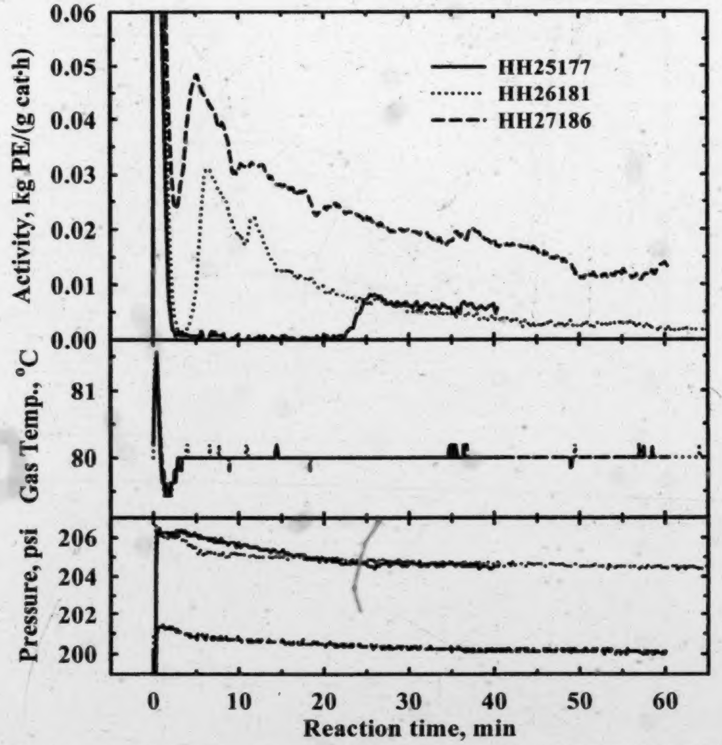

Figure 7.1 Ethylene polymerization activity with poly(DVB/N-V-2-P)-supported (*n*-BuCp)$_2$ZrCl$_2$/MAO catalyst in presence of trace TIBA.

Table 7.2 Influence of typical variations in the Zr loading and Al:Zr ratio on polymerization activity at 80°C and 1.4 MPa.

Catalyst ID	Run #	Amount charged in reactor			Activity, g PE/(g cat·h)		t_{Rmax}[a], min
		Catalyst, mg	1-hexene[b], mL	TIBA[c], mmol	Avg.[d]	Max.[e]	
HH25	HH25177	75.0	–	trace	3.2	8.3	26
	HH25178	75.9	4.54	trace	85.0	109.1	10
	HH25187	101.2	4.39	0.20	180.0	211.1	17
HH26	HH26180	75.7	4.84	trace	50.0	50.0	11
	HH26181	75.0	–	trace	9.1	30.7	6
	HH26188	105.3	4.41	0.20	172.0	192.2	59
HH27	HH27184	75.9	4.29	trace	76.8	111.6	4
	HH27185	101.0	4.34	trace	91.4	91.4	6
	HH27186	100.0	–	trace	22.4	48.4	5
	HH27189	100.4	4.51	0.20	330.0	377.3	22
HH19	HH19108	76.9	4.72	trace	547.2	735.7	37
	HH19109	77.2	–	trace	41.9	72.6	4
HH13	HH13074	40.6	4.31	trace	970.0	1612.1	9
HH14	HH14084	47.0	4.34	trace	534.0	605.6	26
	HH14085	103.0	4.31	trace	482.7	647.8	11
	HH14130	60.2	–	0.20	384.4	989.7	26
	HH14131	60.6	4.45	trace	690.9	749.7	29
	HH14149	60.3	4.50	0.20	835.8	1307.1	29
HH15	HH15089	42.6	4.32	trace	1324.0	2047.1	13
	HH15095	69.5	–	0.28	552.8	920.4	37
	HH15117	59.7	4.28	0.20	1196.0	1897.2	21

a: acceleration period, i.e., time to attain maximum activity
b: injected once before the start of polymerization; 1 mL $\approx$ 3.52 mol/m^3
c: trace denotes residual TIBA was removed after reactor scavenging
d: calculated gravimetrically from recovered polymer
e: calculated from measured ethylene flow rate

The apparent induction period of about 23 min observed for Run HH25177 is likely due to the reactor overpressure during catalyst injection. At low activity, it takes longer to deplete the reactor pressure (by polymerization) to the point that induces flow in the ethylene mass flow meter. The order of the average activities for the three runs in

Figure 7.1 follows that of mass % Zr in the catalysts; however, at such low activities it is difficult to conclude with certainty that the trend is due to the Zr content.

The activity profiles for ethylene/1-hexene copolymerization (trace TIBA) with Catalysts HH25-HH27 are shown in Figure 7.2. The order of the average activities (HH25 > HH27 > HH26) did not follow any pattern of catalyst composition, neither Al:Zr ratio nor mass % Al or Zr. The 10% range on the amount of 1-hexene injected into the reactor would not have significant effect on the activity profile. Only little changes in the 1-hexene concentrations in the reactor occurs during low activity runs. The activity profiles in Figures 7.1 and 7.2 suggest that the observed composition variation of the catalysts (5 mass % in Al loading, 0.04 mass % in Zr loading, and 67 in Al:Zr ratio) did not significantly affect the activity behavior.

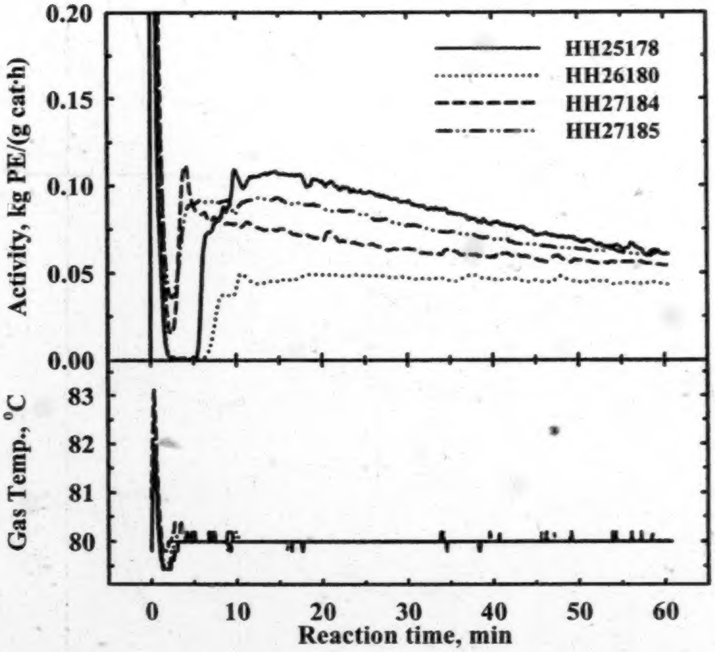

Figure 7.2 Ethylene/1-hexene (4.48 ± 0.23 mL) copolymerization activity with poly(DVB/N-Vinyl-2-pyrrolidinone)-supported $(n\text{-BuCp})_2ZrCl_2$/MAO catalyst in presence of trace TIBA.

Catalysts HH25–HH27 show higher ethylene/1-hexene copolymerization activity in the presence of residual TIBA than with only trace amount of TIBA in the reactor. In this case the order of average activities follow that of Al:Zr ratio of the catalysts (Figure 7.3). Catalyst HH27 has the highest Al loading, Zr loading, and Al:Zr ratio of the three. It also showed the highest activity and deactivation rate (Run HH27189). Repeats for Runs HH26188 and HH27189 showed consistent behavior (see Runs HH26182 and HH27183, respectively in Table B-1).

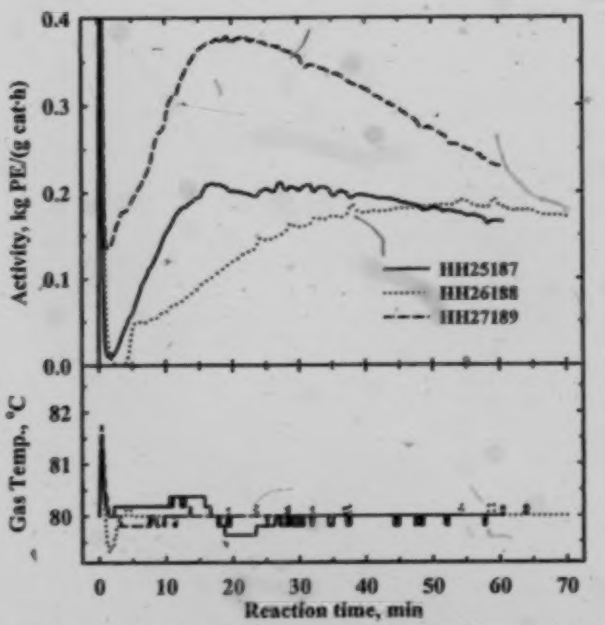

Figure 7.3 Ethylene/1-hexene (4.4–4.5 mL) copolymerization activity with poly(DVB/N-Vinyl-2-pyrrolidinone)-supported (n-BuCp)$_2$ZrCl$_2$/MAO catalyst in presence of 0.20 mmol TIBA.

The activity increase observed in Figure 7.3 over Figure 7.2 (due to residual TIBA in reactor) suggests partial deactivation of the catalyst during catalyst injection or prior to that. Residual TIBA in the reactor reactivated the deactivated catalyst (see Section 5.3). Thus, with only trace amount of TIBA in the reactor, the activity remained low and the maximum activities were attained faster. On the contrary, gradual reactivation of the catalysts by residual TIBA in the reactor (Chapter 6) results in higher activity and longer activation period (Figure 7.3).

Catalyst HH19 was prepared from the same batch of support as HH25 - HH27, and using similar amounts of MAO and zirconocene as HH25 and HH26. Expectedly, HH19 has similar Al and Zr loadings as HH25 and HH26 (Table 7.1). However, HH19 was six to eight times more active than Catalysts HH25 and HH26 in copolymerization in the presence of trace amount of TIBA (cf., Runs HH25178 and HH26180 in Figure 7.2 to HH19108 in Figure 7.4). To a lesser extent, Catalyst HH19 was also more active in ethylene homopolymerization (trace TIBA) and in ethylene/1-hexene copolymerization (in the presence of residual TIBA) than Catalysts HH25 and HH26.

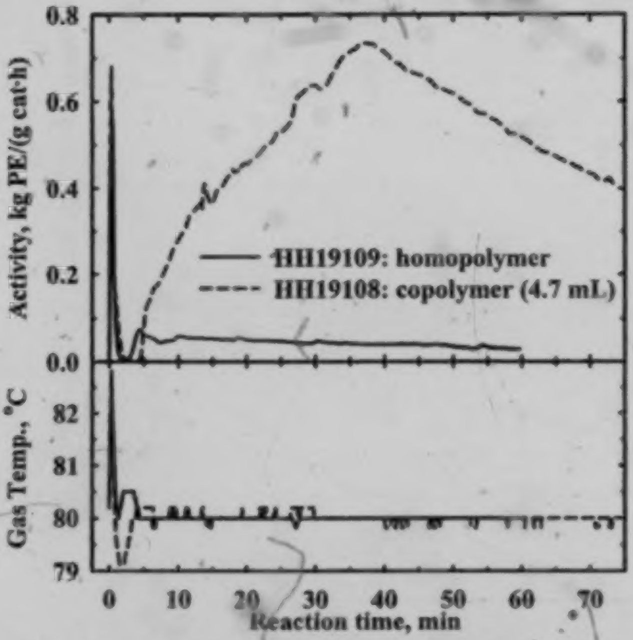

Figure 7.4 Polymerization activity of poly(DVB/N-Vinyl-2-pyrrolidinone)-supported (*n*-BuCp)$_2$ZrCl$_2$/MAO catalyst in presence of trace TIBA (1-hexene comonomer).

The reason for higher activity of Catalyst HH19 over Catalysts HH25-HH27 is not apparent. Although the support evacuation temperature was 5-15°C lower for Catalyst

HH19 (see Appendix A, Table A-1) due to higher draft in the fume hood during the support heating/evacuation process. This temperature difference is usually insignificant in catalyst preparation. Catalyst HH19 has higher surface area and slightly different pore size distribution than HH25-HH27 (cf. Figure 4.8c to Figure 4.12a)

In heterogenizing metallocene/MAO catalysts over inorganic supports such as silica, the support dehydroxylation temperature determines the type and the amount of hydroxyl functional groups on the silica surface (Unger, 1979). The resulting hydroxyl content influences the performance of the silica-supported catalysts (Quijada *et al.*, 1997; dos Santos *et al.*, 1999a, 1999b; Tait *et al.*, 2000). The support used in making Catalysts HH19 and HH25 - HH27 contains functional groups from the N-vinyl-2-pyrrolidinone, but these are unlikely to influence the catalyst behavior due to the low support evacuation temperature and the catalyst preparation method (treating support with MAO before metallocene). No mass loss was observed upon heating and evacuating the above polymeric support at the catalyst preparation conditions.

Poly(HEMA/DVB) support with different morphology than the commercial Hayesep-R (used in Catalysts HH19 and HH25 – HH27) was synthesized in our laboratory and used in Catalysts HH13 – HH15. The same amounts of MAO solution (per gram of support) were used in preparing Catalysts HH13 and HH15 (Table A-1), but HH13 shows higher aluminum and Zr content because about 1.4 g of agglomerated particles were separated from the bulk of Catalyst HH15 used in the polymerization runs. The agglomerated particles contain higher amounts of Al and Zr (20 mass %, and 0.414 mass % respectively) than HH15 (Table 7.1).

The copolymerization (trace TIBA) activity profiles of Catalysts HH13-HH15 are shown in Figure 7.5. A consistently lower activity was observed for HH14 compared to HH13 and HH15. The lower activity of HH14 cannot be explained by the amount of catalyst or the amount of 1-hexene charged into the reactor. The gas-phase temperature of Run HH14084 was higher than the rest (lower panel, Figure 7.5) because the temperature controller was turned off during this run. The reactor was cooled by circulating the silicone oil (coolant) at 80°C to compare with the temperature control of the 1-L reactor of Lynch and Wanke (1991) immersed in isothermal oil bath. Although Catalyst HH14 has lower activity, its activity profiles were broader and more stable to deactivation. Particle overheating was unlikely during the copolymerization runs with Catalyst HH14.

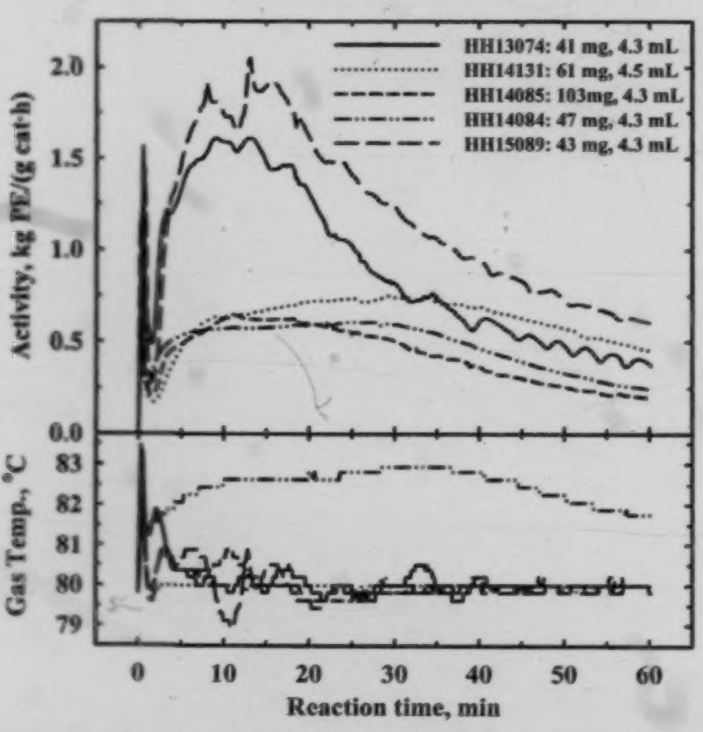

Figure 7.5 Ethylene/1-hexene copolymerization activity with poly(DVB/N-Vinyl-2-pyrrolidinone)-supported $(n\text{-BuCp})_2ZrCl_2$/MAO catalyst in presence of trace TIBA (run details are in Table 7.3).

The activity profiles of Catalysts HH14 and HH15 in the presence of residual TIBA are compared in Figure 7.6 (ethylene homopolymerization) and Figure 7.7 (ethylene/1-hexene copolymerization). The shapes of the activity profiles are similar for both catalysts; the observed difference in R_{Pmax} and t_{Rmax} is mainly due to the TIBA difference in the reactor (see Chapter 5). In spite of the consistently lower copolymerization activity of Catalyst HH14 in runs with trace TIBA, it has similar homopolymerization activity as HH15 in presence of residual TIBA. In addition, the copolymerization activity of HH14 in presence of residual TIBA is 30% higher than the average copolymerization activity with trace TIBA. This implies a significant fraction of the Zr in HH14 that was initially inactive has been reactivated by residual TIBA in the reactor during polymerization (Chapter 6)

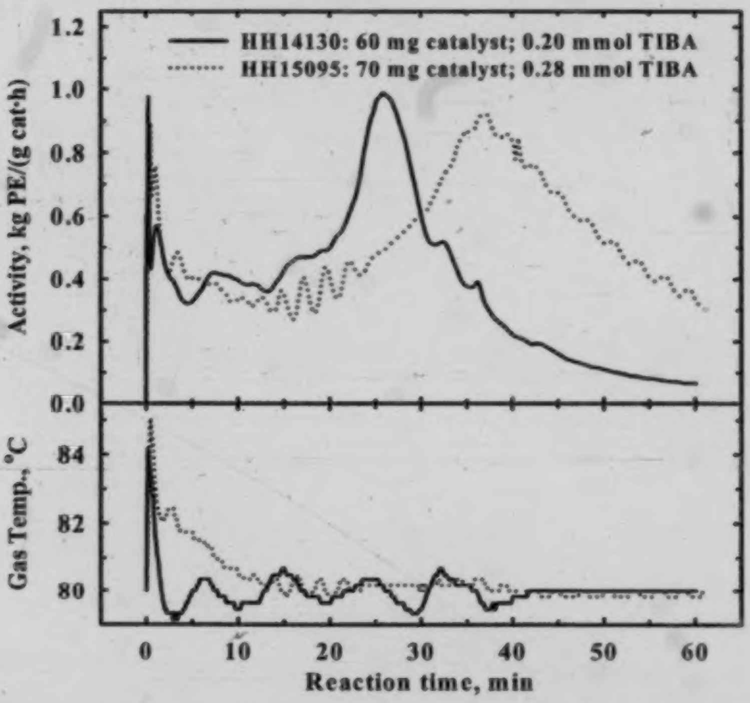

Figure 7.6 Ethylene homopolymerization activity over poly(HEMA/DVB)-supported (n-BuCp)$_2$ZrCl$_2$/MAO catalyst.

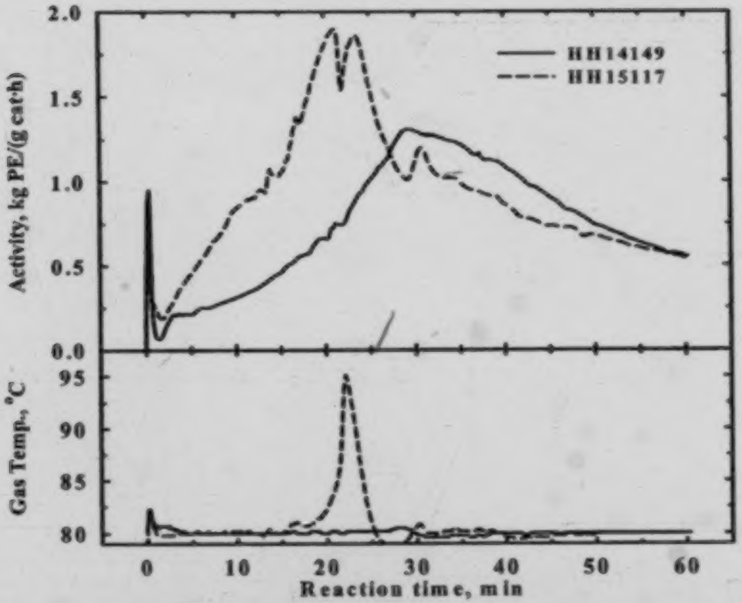

Figure 7.7 Ethylene/1-hexene copolymerization activity with poly(HEMA/DVB)-supported $(n\text{-BuCp})_2ZrCl_2$/MAO catalyst in presence of 0.20 mmol TIBA.

The typical variation in Zr loading and Al:Zr ratio in Table 7.1 did not have any consistent effect on the catalyst performance. Thus, moderate differences in polymerization activity could result from catalysts prepared in a similar manner from the same support. The gas-phase polymerization activity per gram of supported catalyst does not necessarily increase with catalyst precursor loading. This signifies that caution should be exercised when drawing conclusions from single catalyst preparation or from polymerizations run at single conditions. However, when results from several catalysts and/or polymerization runs are put together, clear patterns do emerge. The latter approach was used in the following sections.

7.2 Effects of chemical structure and morphology of support

The nature of the polymeric supports necessitates the collective discussion of the effects of chemical structure and morphology. The relevant polymerization runs are summarized in Table 7.3. Figures 7.8 and 7.9 show the rate profiles of ethylene and ethylene/1-hexene polymerizations (respectively) with Catalysts HH10, HH11, and HH14. These catalysts are all (n-BuCp)$_2$ZrCl$_2$/MAO supported on three different poly(HEMA/DVB) supports. The HEMA/DVB content for the supports used in Catalysts HH10, HH11, and HH14 is 50/50, 80/20, and 50/50 mass % respectively.

Table 7.3 List of runs for the effects of support structure and morphology.

Run #	Amount charged in reactor			Activity, g PE/(g cat·h)		t_{Rmax}[a], min
	Cat., mg	1-hexene[b], mL	TIBA[c], mmol	Avg.[d]	Max.[e]	
HH10060	50.7	–	trace	24	30	4
HH11126	76.1	–	trace	149	(329) 390	(14) 2
HH14128	60.0	–	trace	236	1602	2
HH10059	50	3.9	trace	416	511	29
HH11063	60	4.0	trace	117	366	7
HH14085	103	4.3	trace	483	648	11
HH12127	84.9	–	trace	176	(274) 218	(2) 16
HH29294	63	–	trace	59	177	6
HH12067	71	4.3	trace	423	572	15
HH29296	64.5	4.0	trace	129	183	7
HH08054	32.0	–	trace	882	3591	1
HH22148	60.0	–	trace	47	77	(7) 66
HH08055	15.9	3.5	trace	1706	2110	20
HH22147	82.5	4.3	trace	313	440	50
HH16097	80.4	–	trace	243	320	21
HH17101	84.0	–	trace	230	284	22
HH16096	76.5	4.2	trace	542	808	14
HH17102	80.0	4.3	trace	348	507	21
HH07049	107	–	trace	232	291	15
HH21113	75.4	–	trace	212	507	4
HH07050	104	3.3	trace	678	1042	17
HH21112	85.2	4.3	trace	621	920	13
HH21115	78.0	2.4	trace	577	827	9

a–e: see notes of Table 7.2; some profiles have two activity maxima; support composition in Table 3.1

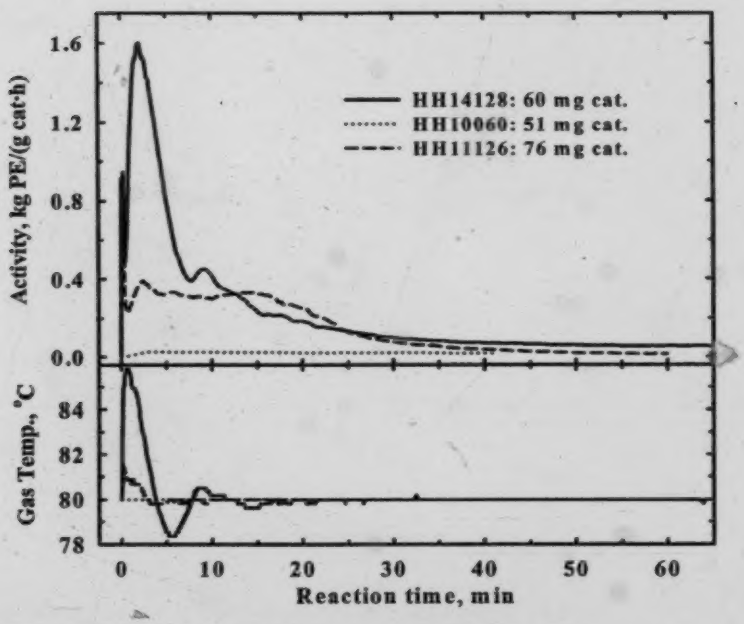

Figure 7.8 Kinetic profiles of ethylene homopolymerization (trace TIBA) with poly(HEMA/DVB)-supported (n-BuCp)$_2$ZrCl$_2$/MAO catalyst.

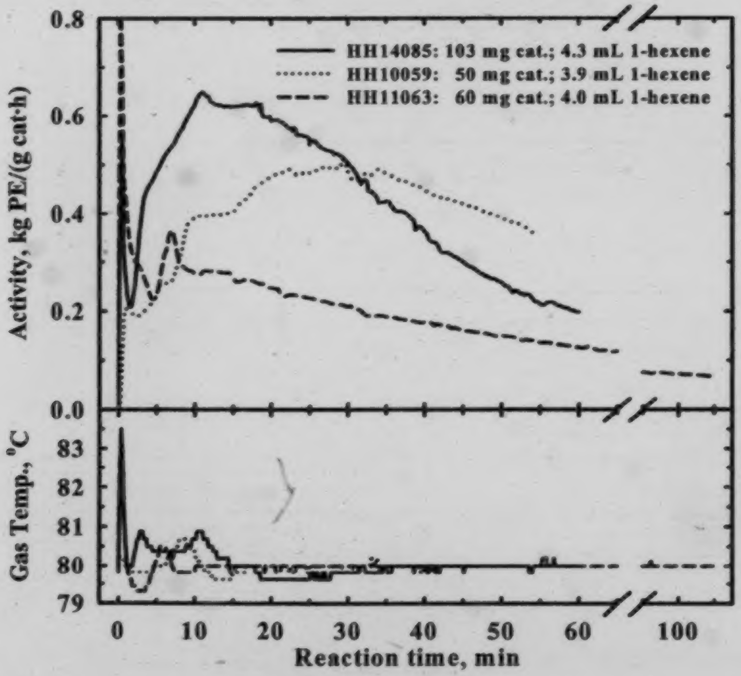

Figure 7.9 Rate profiles of ethylene/1-hexene copolymerization (trace TIBA) with poly(HEMA/DVB)-supported (n-BuCp)$_2$ZrCl$_2$/MAO catalyst.

The supports used in Catalyst HH10 and HH14 (PE971204 and PE971124, respectively) were made from equal amounts of HEMA, DVB, and AIBN initiator, but with different proportions of porogens (toluene and PTMG) used. The emulsion polymerization used in the support synthesis lasted for ~24 h, during this period most of the monomers and the initiator reacted, i.e. the two supports have similar HEMA content and crosslink density. In spite of this similarity, Catalysts HH10 and HH14 behaved quite differently; therefore, neither the HEMA content nor the crosslink density has controlling effect on the observed difference in activity.

HEMA has electron-donating functional groups (Figure 3.1) that are potentially reactive towards the $(n\text{-BuCp})_2ZrCl_2$ and the MAO. However, these functional groups did not influence the catalyst activity because the supports were first reacted with MAO before metallocene addition during the catalyst preparation (Scheme 1, Section 3.2). Thus, the MAO shields the metallocene from reactive interaction with the support surface.

Further test on the influence of morphology was conducted with Catalysts HH08, HH12, HH22, and HH29. The four catalysts were made from four different supports that possess no reactive functional groups (Tables 3.2 and 3.1). Summary of the polymerization runs are included in Table 7.3. The homo- and copolymerization activities of Catalysts HH12 and HH29 are shown in Figures 7.10 and 7.11 respectively. These catalysts are both Poly(STY/DVB) supported. The 50%-DVB support of Catalyst HH12 has a surface area of 7.0 m^2/g. On the contrary, the support for Catalyst HH29 contains only 1% DVB, it is a swellable gel-type support with negligible porosity in the dry state.

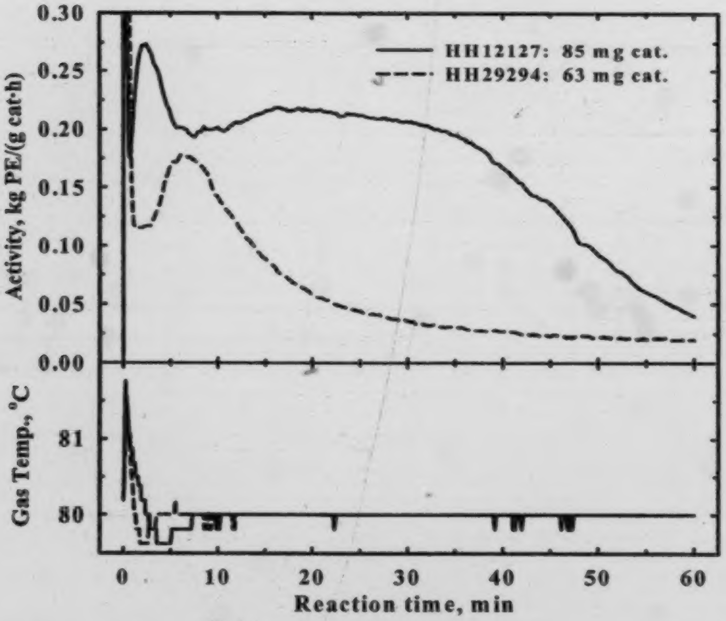

Figure 7.10 Activity profiles of ethylene homopolymerization (trace TIBA) with poly(DVB)-supported $(n\text{-BuCp})_2ZrCl_2/MAO$ catalyst.

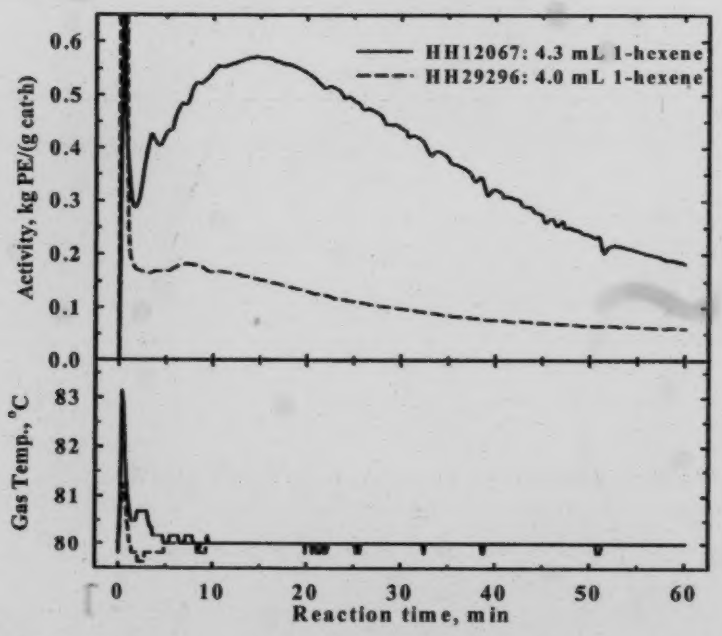

Figure 7.11 Activity profiles of ethylene/1-hexene copolymerization (trace TIBA) with poly(DVB)-supported $(n\text{-BuCp})_2ZrCl_2/MAO$ catalyst.

For both Catalysts HH12 and HH29, the ethylene homopolymerization activities are lower than the ethylene/1-hexene copolymerization (cf. Figures 7.10 to 7.11), and Catalyst HH29 attains maximum activity faster than Catalyst HH12. Inadequate porosity of Catalyst HH29 in the dry state may be the cause of this behavior. When the catalyst is exposed to monomer, mass transfer limitation restricts the polymerization to the outer surface of the catalyst only. This creates polyethylene shell around the catalyst particles that further limits monomer diffusion to the catalyst core, a phenomenon similar to the "filter effect" proposed by Pryzbyla *et al.* (1999). Uneven growth rate across the polymerizing particle results in heavily warped polymer particles, Figure 7.12 (a) and (b). The catalyst (support) matrix is only lightly cross-linked by 1% DVB. During ethylene/1-hexene copolymerization, the morphology of the polymer particles evolve differently, Figure 7.12 (c) and (d). This is further discussed in Chapter 8.

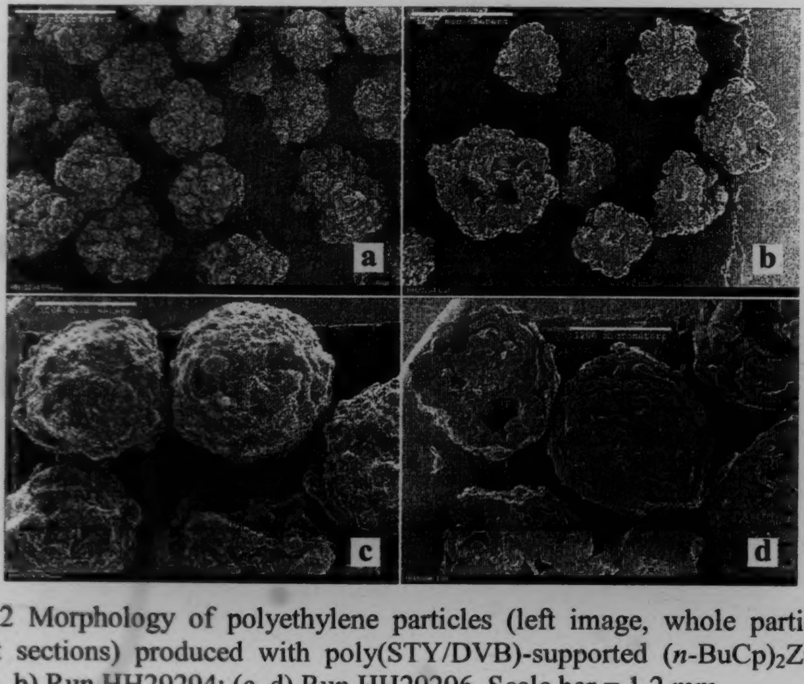

Figure 7.12 Morphology of polyethylene particles (left image, whole particles; right image, cut sections) produced with poly(STY/DVB)-supported $(n\text{-BuCp})_2ZrCl_2$/MAO catalyst; (a, b) Run HH29294; (c, d) Run HH29296. Scale bar = 1.2 mm.

Catalysts HH08 and HH22 are both poly(DVB)-supported, but the two supports have different morphologies. The activity profiles of Catalysts HH08 and HH22 (trace TIBA) are compared in Figures 7.13 and 7.14. The activity of Catalyst HH08 increased to the maximum value rapidly (t_{Rmax} < 2 min) while Catalyst HH22 maintained lower but relatively constant activity for ~80 min before deactivating steadily for 1.5 h. Catalyst HH22 has only about one fifth the Al content and one half the Zr content of HH08. However, this is not a major factor in causing the sharp activity difference shown in Figure 7.13 because Catalyst HH22 has seven times higher activity in copolymerization than homopolymerization at the same conditions (cf. Run HH22148 in Figure 7.13 to Run HH22147 in Figure 7.14). Higher residual TIBA (~0.6 mmol) in the reactor further increased the average ethylene/1-hexene copolymerization activity of Catalyst HH22 to one half the activity of HH08 (Figure 7.15).

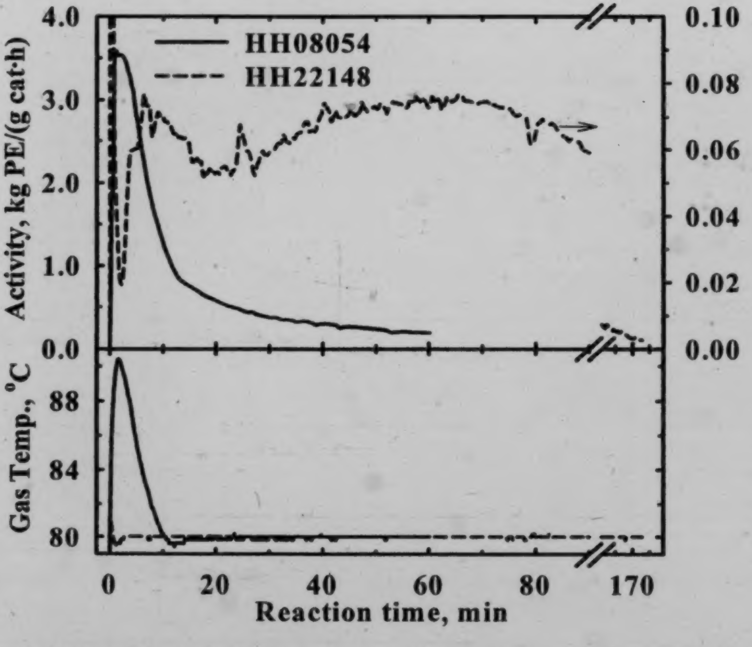

Figure 7.13 Activity profiles of ethylene homopolymerization (trace TIBA) with different poly(DVB)-supported $(n\text{-BuCp})_2ZrCl_2$/MAO.

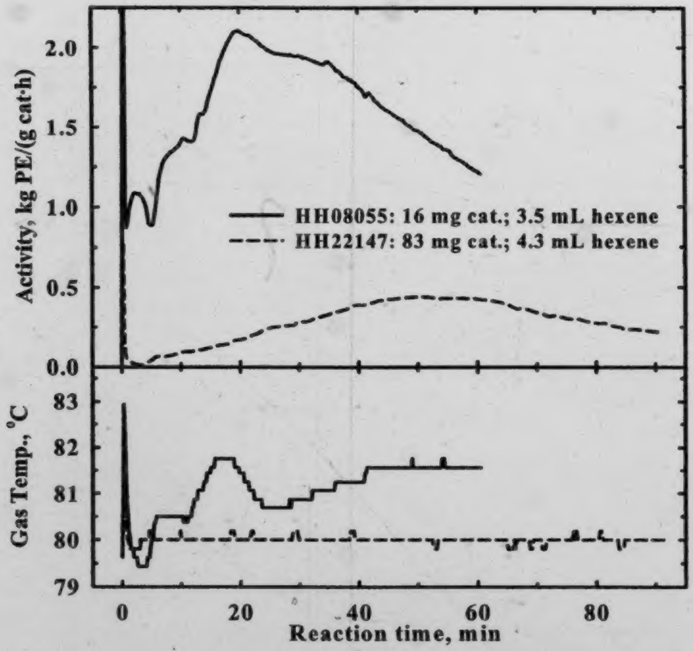

Figure 7.14 Kinetic profiles of ethylene/1-hexene copolymerization (trace TIBA) with (n-BuCp)$_2$ZrCl$_2$/MAO catalysts supported on different poly(DVB).

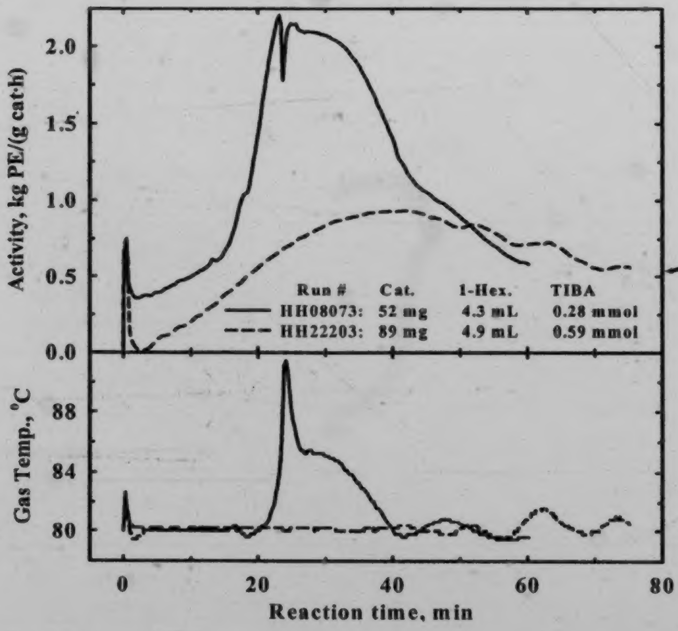

Figure 7.15 Kinetic profiles of ethylene/1-hexene copolymerization (in presence of TIBA) with (n-BuCp)$_2$ZrCl$_2$/MAO catalyst supported on different poly(DVB).

The lower MAO requirement of Catalyst HH22, the activity increases upon TIBA addition to the reactor, and the gradual activity build-up (reducing the possibility for thermal runaway in the reactor) are beneficial for industrial application.

The influence of support crosslink type was investigated using Catalysts HH22, HH17, and HH16 supported on poly(DVB), poly(DVB/EGDM), and poly(EGDM) respectively. The crosslink type varies from the aromatic DVB-based to the linear EGDM segments. Ethylene homopolymerization profiles (trace TIBA) for the three catalysts above are shown in Figure 7.16. The ethylene homopolymerization activity of Catalysts HH16 and HH17 (supports contain EGDM) show higher activity than Catalyst HH22. Catalyst HH22 (DVB-supported) has lower Al loading than HH16 and HH17; however, several other DVB cross-linked supports with Al and Zr loadings similar to HH16 and HH17 (see Section 7.5) also had low ethylene homopolymerization activity.

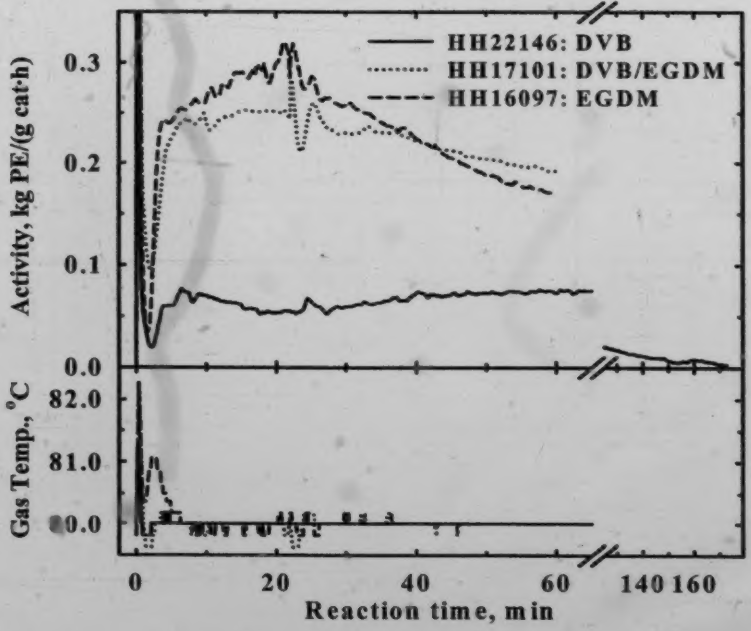

Figure 7.16 Ethylene homopolymerization activity with polymer- supported (n-BuCp)$_2$ZrCl$_2$/MAO catalyst (trace TIBA).

It is also clear that the crosslink type alone is not the cause of low activity of Catalyst HH22 since Catalyst HH08 (also DVB-supported) has high ethylene homopolymerization activity (see Runs HH08054, and HH08055, Table 7.3). Thus, supported catalysts made with commercial DVB-cross-linked supports such as poly(DVB), poly(DVB/N-V-2-P), poly(DVB/Acrylo-nitrile), and poly(DVB/4-V-Py) that have no linear crosslink segments all show low ethylene homopolymerization activity. On the contrary, supports that consist of linear crosslink segments, EGDM (partly or entirely) show moderate ethylene homopolymerization as well as ethylene/1-hexene copolymerization activities (Figures 7.16 and 7.17). The latter observation is not only restricted to EGDM; Catalyst HH21 made using DVB/Polyethylenimine (PEI) support also shows a similar behavior. Rate profiles of Catalyst HH21 are compared to those of another poly(EGDM)-supported catalyst (HH07) in Figures 7.18 and 7.19. The crosslink nature in the DVB/PEI support is not known, but solid PEI particles are commercially produced by cross-linking during ethylenimine polymerization (Roark *et al.*, 2002).

It is not clear whether the observed effect on polymerization activity is caused by the cross-link type or the support friability because the catalysts with low ethylene homopolymerization activity are also made with low friability supports (Table 4.2). The fracture mechanism of the catalyst particles might have contributed to the above influence. This is discussed further in Chapter 8.

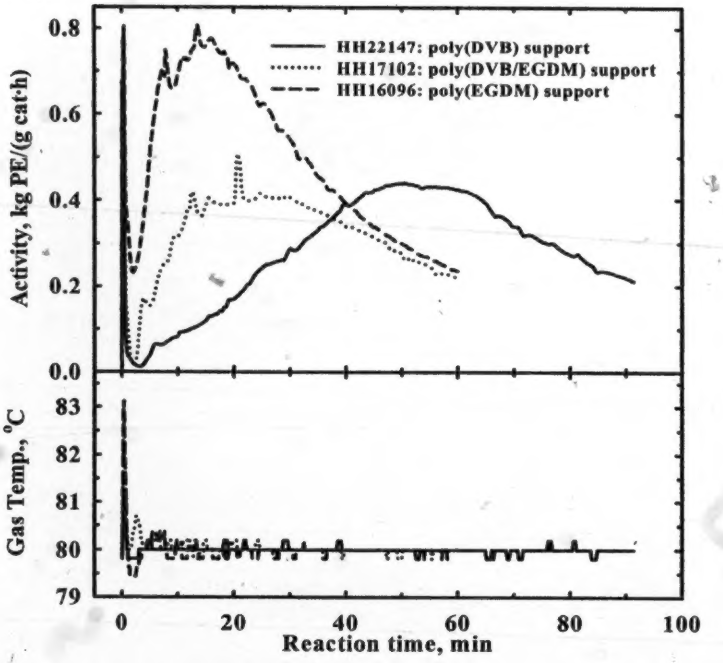

Figure 7.17 Ethylene polymerization activity with supported $(n\text{-BuCp})_2ZrCl_2$/MAO catalyst in presence of trace TIBA.

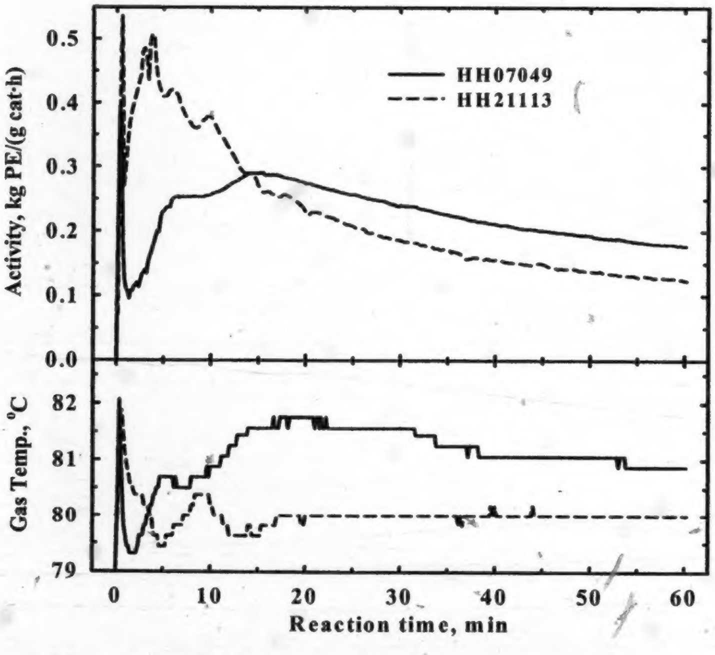

Figure 7.18 Ethylene polymerization activity with poly(DVB/N-Vinyl-2-pyrrolidinone)-supported $(n\text{-BuCp})_2ZrCl_2$/MAO catalyst in presence of trace TIBA.

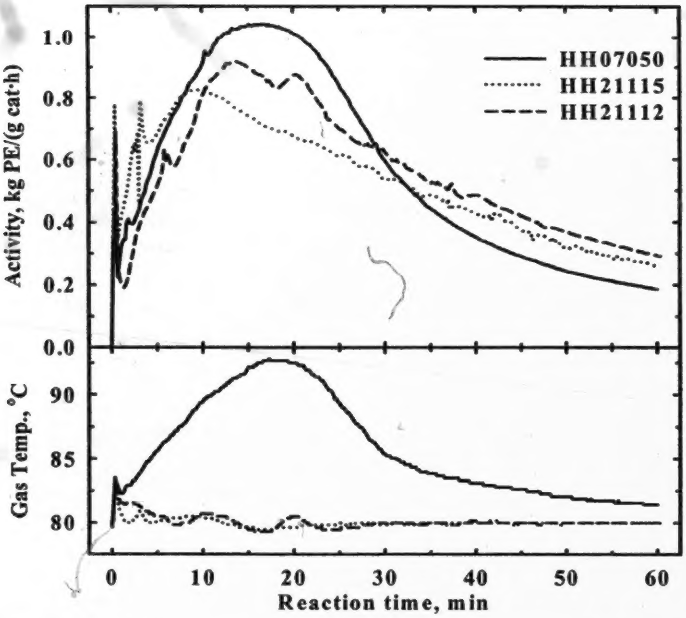

Figure 7.19 Ethylene polymerization activity over poly(DVB/N-Vinyl-2-pyrrolidinone) supported $(n\text{-BuCp})_2ZrCl_2$/MAO catalyst in presence of trace TIBA.

7.3 Effects of polymerization temperature on rate profiles

Polymerization temperature affects both the catalyst activity and the product properties. Table 7.4 summarizes the polymerization runs used to investigate the temperature effect. During these runs, monomer pressure was adjusted (according to ideal gas law) to maintain nearly the same gas-phase monomer concentration as the runs at 80°C and 1.4 MPa.

Monomer pressure adjustment during temperature investigations is seldom reported in literature. Normalizing polymerization activity by monomer pressure will not yield activity profiles that are independent of monomer concentration for polymerization-rate order different from unity. Rate orders different from unity have been reported for polymerization over supported metallocene/MAO (Chien *et al.* 1998) and Ziegler-Natta (Kissin *et al.* 1999; Wu *et al.* 1999) catalysts.

Table 7.4 Summary of the influence of polymerization temperature on activity.

Catalyst ID (mass % Zr; Al:Zr ratio)	Run #	Amount in reactor		Gas temp., °C	PE yield, g	Activity, g PE/(g cat·h)		t_{Rmax}[a], min
		Catalyst, mg	1-hexene[b], mL			Avg.[d]	Max.[e]	
HH07	HH07	101.0	–	50	2.3	23	29	~60
(0.128; 435)	HH07	103.4	–	60	9.6	92	124	23
	HH07	102.8	–	70	19.6	185	254	16
	HH07	100.4	–	80	13.5	134	287	8
	HH07	100.5	–	90	13.8	137	350	5
	HH07	107.5	–	100	13.0	121	383	2
HH09	HH09	51.5	–	50	13.1	255	488	10
(0.061; 373)	HH09	49.8	–	60	25.6	515	1056	9
	HH09	45.7	–	70	21.0	459	1565	5
	HH09	36.5	–	70	17.8	489	1514	6
	HH09	42.7	–	70	20.8	486	1613	6
	HH09	40.5	–	80	28.2	696	2006	4
	HH09	39.0	–	90	17.9	460	1746	3
HH18	HH18	83.1	4.65	60	11.0	133	154	29
(0.162; 376)	HH18	81.5	4.77	70	23.0	282	401	22
	HH18	80.8	4.66	80	55.0	681	913	17
	HH18	80.2	4.76	90	73.8	921	1170	25
	HH18	74.5	4.65	100	23.0	309	324	40
	HH18	77.4	4.83	100	30.6	395	429	34

a–e: see notes of Table 7.2

The influence of temperature on ethylene homopolymerization rates of Catalysts HH09 and HH07 are shown in Figures 7.20 and 7.21 respectively. Catalyst HH09 generally has higher homopolymerization activity than HH07. Catalysts HH07 is poly(EGDM)-supported (Porapak-T) while Catalyst HH09 is poly(HEMA/DVB)-supported (PE971124). The two supports have quite different friability and pore size distributions (see Table 4.2 and Figures 4.9a and 4.11a). The rate profiles consist of initial acceleration to the maximum rate R_{pmax} at time t_{Rmax} followed by activity decay phase. Increasing polymerization temperature generally increased R_{pmax} and reduced t_{Rmax}, i.e. both activation and deactivation rates increase with temperature. R_{pmax} was not attained during the 1-h run at 50°C with the lower activity Catalyst HH07. The lower

R_{pmax} at 90°C (compared to 80°C) for Catalyst HH09 is likely due to thermal deactivation (see, Figure 5.31). At high polymerization temperature, the rapid initial activity and poor heat removal from the catalyst particle resulted in particle overheating and strong deactivation. Kumkaew *et al.* (2003a, 2003b) also observed this reduction in R_{pmax} during gas-phase polymerization over $(n\text{-BuCp})_2ZrCl_2$/MAO catalyst supported on mesoporous molecular sieves.

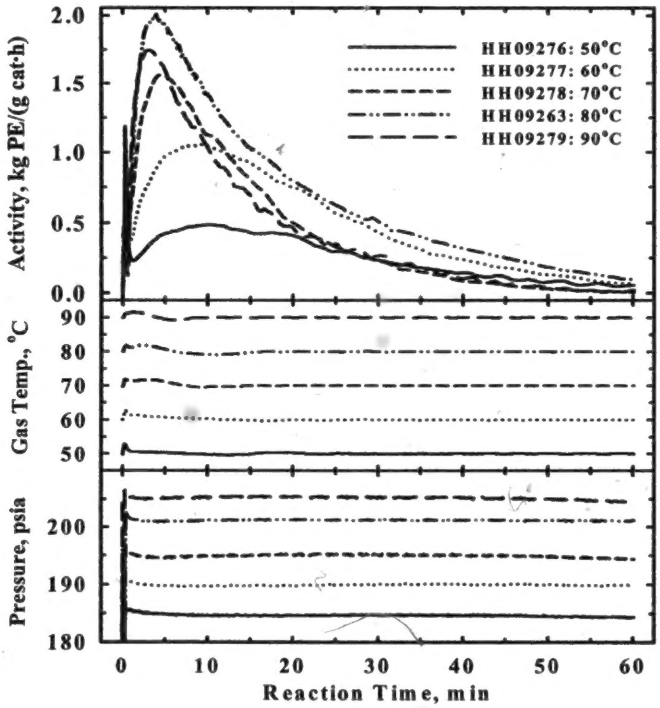

Figure 7.20 Influence of polymerization temperature on ethylene polymerization activity of Catalyst HH09.

The optimum polymerization temperature depends on the catalyst and polymerization conditions such as monomer pressure, and the type and amount of comonomer. These influence the fracture mechanism of the catalyst particles as well as the activation/deactivation rates of the catalyst. Figure 7.22 shows the variation of average activity with temperature for Catalysts HH07, HH09, and HH18. The longer acceleration period for the ethylene/1-hexene copolymerization with Catalyst HH18 (Figure 7.23) is partly due to polymer sintering that results in greater mass transfer resistance (Chakravarti and Ray, 2001). Note that beyond 80°C, t_{Rmax} increased with polymerization temperature (Table 7.4) for the copolymerization runs with Catalyst HH18.

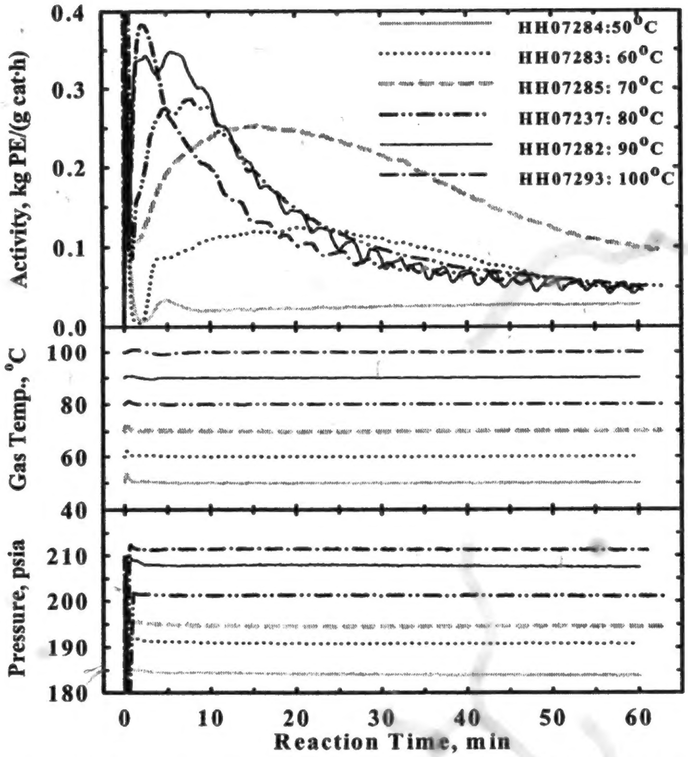

Figure 7.21 Influence of polymerization temperature on the ethylene homopolymerization activity of Catalyst HH07 in the presence of trace TIBA.

The observed temperature dependence is consistent with other findings in gas-phase, slurry, and solution polymerizations for metallocene/MAO (Xu *et al.*, 2001; Chakravarti and Ray, 2001a) as well as Ziegler-Natta (Wu *et al.*, 1999) catalysts. Korber *et al.* (2001) reported similar behavior for bulk phase propylene polymerization with silica-supported $Me_2Si[R^1Ind]_2ZrCl_2$/MAO catalyst. The effect of temperature on polymer molar mass is discussed in Chapter 9.

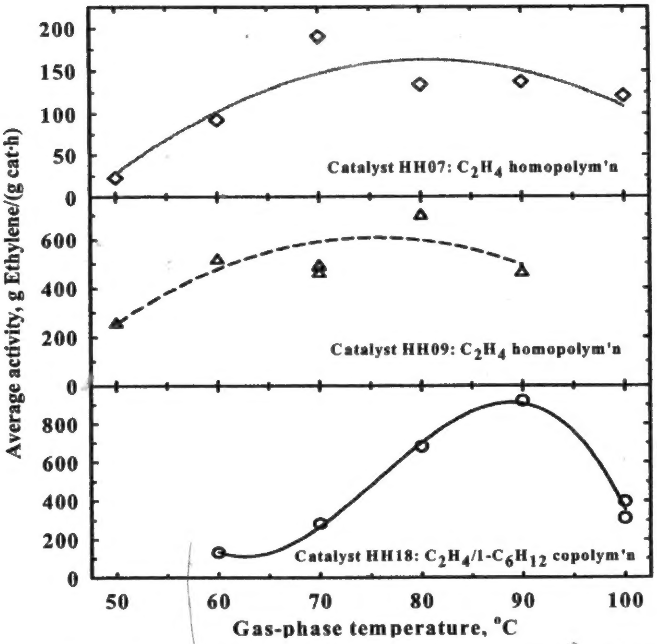

Figure 7.22 Temperature dependence of the average polymerization activity of (*n*-BuCp)$_2$ZrCl$_2$/MAO catalyst heterogenized on different supports.

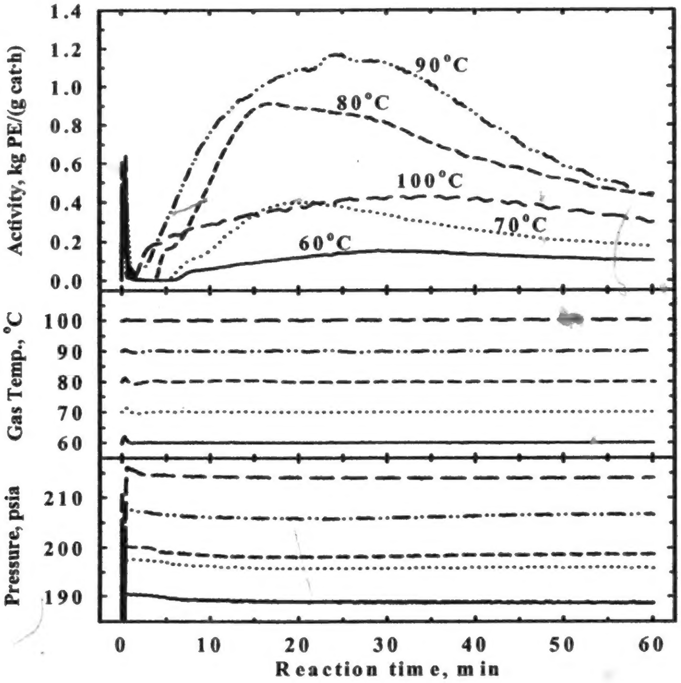

Figure 7.23 Effect of temperature on ethylene/1-hexene copolymerization over poly(DVB/PEI)-supported (*n*-BuCp)$_2$ZrCl$_2$/MAO catalyst.

The observed rate profiles of the polymer-supported $(n\text{-BuCp})_2ZrCl_2$/MAO catalysts are generally described by an initial acceleration period t_{Rmax} during which the activity increases to the maximum value (R_{pmax}), followed by activity decay phase. The observed acceleration period varies from ~1 min to more than 1 h for different catalysts.

The acceleration period has been attributed to different induction times of individual catalyst particles caused by inhomogeneous MAO loadings (Knoke *et al.*, 2003). Without mass transfer resistance, it is not likely that inhomogeneous MAO loading could result in the initial activity-growth phase. Different particles could have different specific activities, but the activity of each particle should be highest at polymerization start-up if the catalyst is pre-activated. Another reason for acceleration phase is the gradual exposure of active sites due to shell wise catalyst fragmentation (Bonini *et al.*, 1995). In Chapter 6, it was shown that the residual aluminum alkyl in the reactor strongly influences the acceleration period. The rate profiles presented earlier also indicate shorter acceleration period in homopolymerization than in copolymerization runs, and the acceleration period tends to increase with the amount of comonomer in the reactor.

The simple acceleration-decay type rate profiles of the gas-phase polymerization with supported metallocene/MAO catalyst can be modeled by the lumped semi-empirical model shown in the scheme below (Meier *et al.*, 2001).

$$\begin{array}{c} C \xrightarrow{k_i} C^* \xrightarrow{k_p} C^* - P_j \\ \downarrow k_d \qquad \downarrow k_d \\ \textit{Deactivated catalyst} \end{array}$$

where C is the potential site, C^* and $C^*\text{–}P_j$ are active sites (assumed to deactivate independently of the length j of the growing chain), k_i, k_p, and k_d are rate constants defined by the Arrhenius law $k_x = k_{x,0} e^{-E_{act,x}/RT}$ for the catalyst activation, the propagation, and the deactivation respectively. E_{act} are the corresponding activation energies.

It is shown in Section 7.4 below that the polymerization activities are not linearly dependent on monomer concentration (pressure). However, the nonlinearity can be explained by temperature or fragmentation (mass transfer resistance) effects. Therefore, the intrinsic polymerization kinetics is assumed first order with both the active site, and the monomer concentrations. The polymerization rate R_p (kg PE/g cat·h) from the above scheme becomes (Meier *et al.*, 2001):

$$R_p = k_p C_m C_0 \frac{k_i}{k_d - k_i} \left(e^{-k_i t} - e^{-k_d t} \right) \qquad (7.1)$$

where C_m is the monomer concentration, and C_0 the initial amount of potential sites.

The above model was fitted to experimental data under the following conditions: The gas-phase ethylene concentration (kg/m^3) was used for C_m, and moles Zr per gram catalyst used for C_0. Ideally, C_m should be the sorbed monomer concentration in the polymer, but this needs the polymer crystallinity (not known). The use of gas-phase monomer concentration for C_m will overestimate k_p because C_m is usually higher than the gas-phase concentration. Use of "correct" ethylene concentration is essential in the deduction of kinetic constants (Jejelowo *et al.*, 1991). The ethylene homopolymerization data of Catalyst HH09 (Figure 7.20) was used in fitting Equation (7.1) because the activity profiles of this catalyst are least influenced by the physical process of catalyst fragmentation. Support PE971124 used for this catalyst is highly friable (Table 4.2). In addition, Catalyst HH09 has low Al and Zr loadings; hence, it has relatively high surface area and pore volume. Figure 7.24 compares experimental data to the model fit at four different temperatures. The rate constants obtained using nonlinear regression are summarized in Table 7.5. Catalyst HH09 has 0.061 mass % zirconium (C_0 = 6.687 μmol Zr/g cat). The activation energies obtained from the Arrhenius plot (Figure 7.25) are

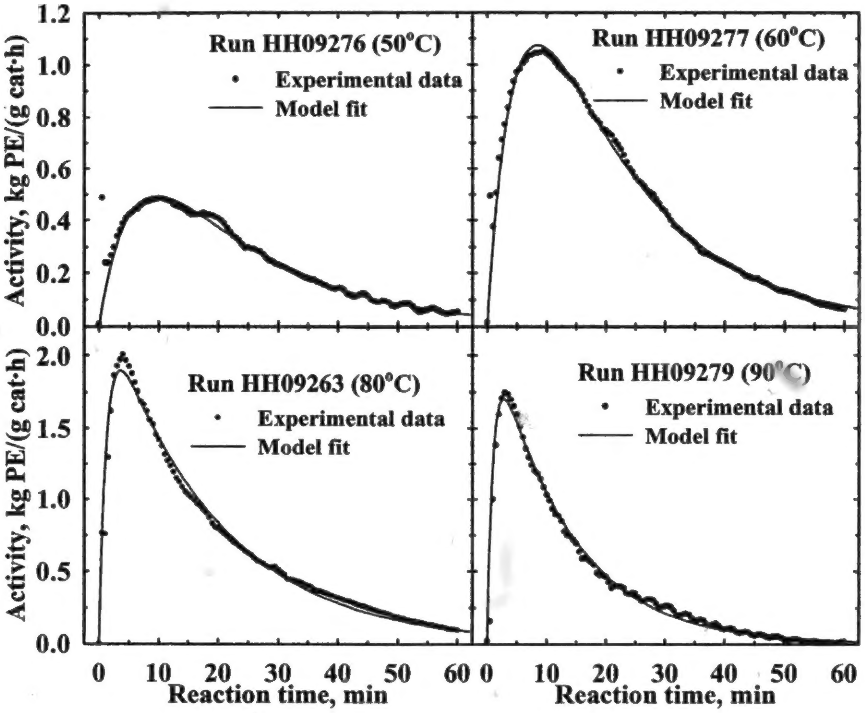

Figure 7.24 Fit of ethylene homopolymerization data of Catalyst HH09 to Equation 7.1 at different polymerization temperatures.

Table 7.5 Parameters from the fit of Equation 7.1

Run #	Gas temp., °C	C_m, kg/m^3	k_p, m^3/(mol·h)	$10^3 \times k_i$, min^{-1}	$10^3 \times k_d$, min^{-1}	R^2
HH09276	50	13.252	9260 ± 60	178.2 ± 2.1	52.53 ± 0.44	0.993
HH09277	60	13.203	19900 ± 80	207.9 ± 1.6	57.74 ± 0.29	0.997
HH09278	70	13.158	26000 ± 65	426.4 ± 2.7	86.07 ± 0.28	0.999
HH09280	70	13.158	28070 ± 183	307.9 ± 4.0	86.61 ± 0.71	0.995
HH09281	70	13.158	27650 ± 116	379.1 ± 3.7	85.57 ± 0.46	0.997
HH09263	80	13.180	26140 ± 85	810.5 ± 14.1	54.24 ± 0.25	0.995
HH09279	90	13.074	24330 ± 75	975.8 ± 17.0	79.38 ± 0.35	0.997

$E_{act,\ i}$ = 46.2 kJ/mol; $E_{act,\ p}$ = 22.3 kJ/mol; $E_{act,\ d}$ = 7.8 kJ/mol. Deviation of $ln(k_p)$ and $ln(k_d)$ from linearity is quite apparent for temperatures greater than 70°C. Considering only the 50 – 70°C runs, the corresponding E_{act} values are 35.8, 47.4, and 24.5 kJ/mol respectively. The $E_{act,\ p}$ value of 47.4 kJ/mol signifies that the propagation rate is a chemical reaction controlled process. On the contrary, in the 70-90°C range, the $E_{act,\ p}$ is essentially zero (Figure 7.25); hence, the propagation rate is controlled by a physical (i.e. ethylene diffusion) process. Meier *et al.* (2001) observed similar deviations in *ln(k)* values for high activity (gas-phase) propylene polymerization in the presence of hydrogen, but not during lower activity runs in the absence of hydrogen. They concluded particle overheating is not responsible for this observation since both the non-prepolymerized, and the prepolymerized silica-supported metallocene catalysts showed this behavior. The deviation in Figure 7.25 is opposite what it would be due to particle overheating; hence, mass transfer limitation of ethylene is the likely cause.

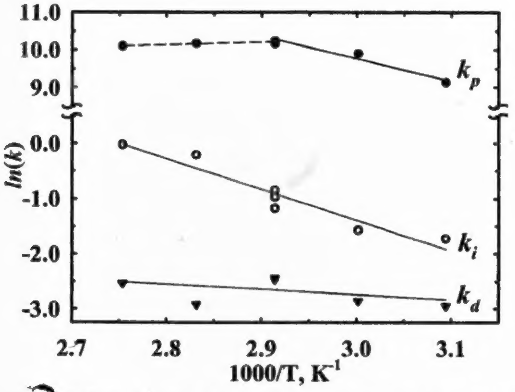

Figure 7.25 Arrhenius plots of rate constants in Equation 7.1.

7.4 Effects of monomer pressure on polymerization rate

The effect of ethylene pressure (0.69–2.76 MPa, 100–400 psi) on the activity of Catalysts HH07, HH09, and HH23 is presented in Table 7.6. The supports of Catalysts

HH07 and HH09 have different microstructure/morphology, and Catalyst HH23 is (unsupported) solid $(n\text{-BuCp})_2\text{ZrCl}_2$/MAO complex.

Table 7.6 Summary of the influence of ethylene pressure on polymerization activity.

Catalyst	Run #	Catalyst, mg	Reactor pressure, MPa	PE yield, g	Activity, g PE/(g cat·h MPa)		t_{Rmax}[a], min
					Avg.[d]	Max.[e]	
HH07	HH07253	100.0	0.70	3.3	47.4	132.9	1.2
	HH07235	100.4	1.38	18.0	129.5	303.4	4.5
	HH07236	102.0	1.39	11.2	79.4	204.1	3.5
	HH07237	100.4	1.39	13.5	96.4	206.8	7.8
	HH07251	99.7	2.07	26.0	125.8	243.2	11.9
	HH07252	100.0	2.76	18.6	67.3	173.6	1.6
HH09	HH09260	50.0	0.69	13.1	380.1	927.9	7.1
	HH09263	40.5	1.38	28.2	505.6	1455.3	3.9
	HH09261	39.8	2.07	22.0	227.0	1253.8	2.8
	HH09262	30.7	2.76	25.8	304.1	1305.4	2.2
HH23	HH23243	10.0	0.70	1.0	142.2	658.1	4.1
	HH23244	10.0	0.69	0.9	138.6	812.4	1.2
	HH23241	10.0	1.39	13.3	962.9	1861.2	10.1
	HH23242	10.1	2.07	7.8	375.3	1892.8	1.7
	HH23246	10.1	2.07	10.4	497.3	1856.0	1.6
	HH23245	10.1	2.76	51.8	1855.6	2320.3	2.1

a–e: see notes of Table 7.2

Figure 7.26 shows the pressure-normalized activity profiles of catalyst HH07. The pressure effect is clearly nonlinear with Run HH07251 having the highest average activity. Since the gas-phase temperature was well controlled (lower panel of Figure 7.26), it is also expected that the particle temperature did not rise significantly above the 80°C set point. Thus, the observed activity difference was not caused by catalyst deactivation due to particle overheating. It is likely due to the fracture mechanism of Catalyst HH07; this is discussed in Chapter 8.

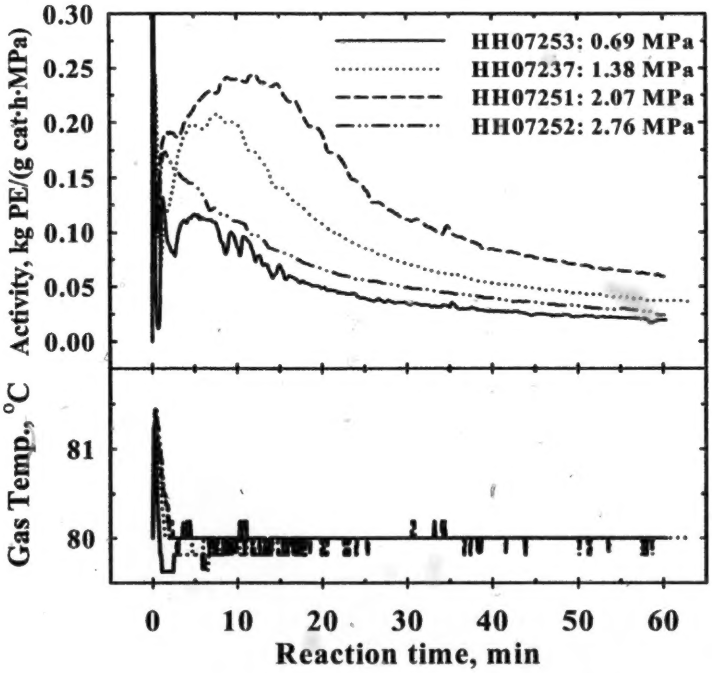

Figure 7.26 Influence of ethylene pressure on the rate profile of Catalyst HH07

Catalyst HH09 (Figure 7.27) responded differently to increases in ethylene pressure than HH07. The high initial activity of Catalyst HH09 resulted in 2-4°C increases in the gas-phase temperature (except Run HH09260, 0.69 MPa). The initial exotherm of the catalyst particles must be higher, resulting in thermal deactivation of the catalyst particles. Thus, higher monomer pressure caused particle overheating; hence, more rapid deactivation as seen in Figure 7.27. Note that Catalyst HH09 fractures differently from HH07 during ethylene homopolymerization.

Figure 7.28 shows the pressure-normalized activity profiles of Catalyst HH23. The normalized activity of the run at 2.76 MPa is more than 13 times the activity at 0.69 MPa. The observed behavior may be due to the combination of catalyst encapsulation by polymer and the catalyst fracture during polymerization.

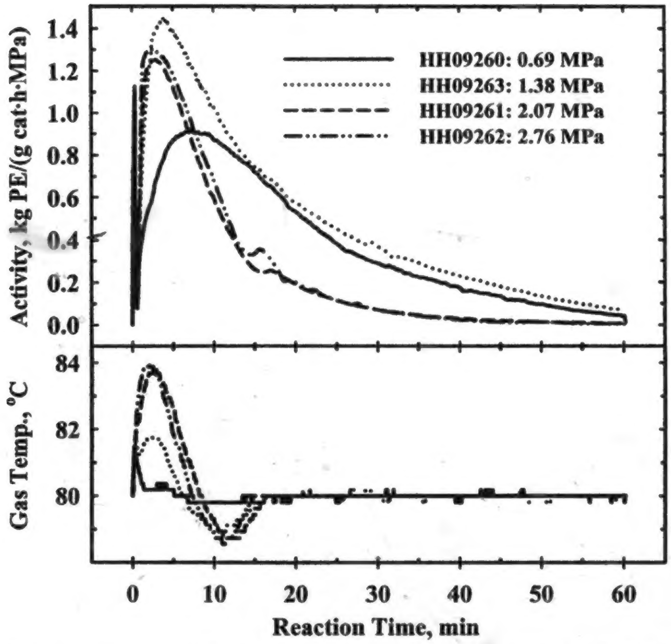

Figure 7.27 Influence of ethylene pressure on the rate profile of Catalyst HH09

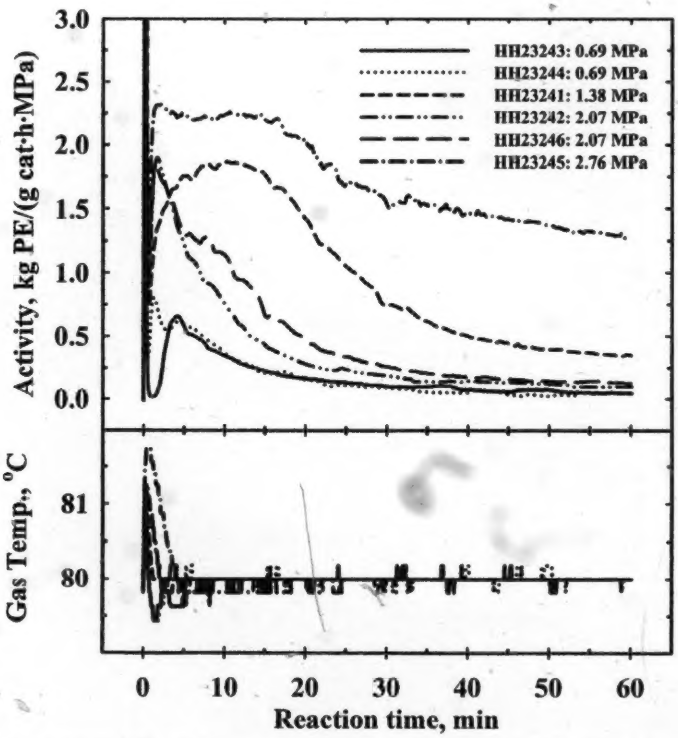

Figure 7.28 Influence of ethylene pressure on the rate profile of Catalyst HH23

7.5 Influence of hydrogen on rate profile

Figure 7.29 shows the effect of hydrogen on ethylene polymerization activity of Catalyst HH15. The presence of H_2 (70 molar ppm) in the reactor reduced the initial activity and prolonged the activity growth period; however, the maximum activity value increased slightly. Both the initial rate depression and the delay of maximum activity increased with the amount of H_2 in the reactor, but the dependence seems nonlinear. The effect of increasing H_2 from 70 to 500 ppm is less than the effect of changing from 0 to 70 ppm. The maximum activity values seem independent of the amount of H_2 in the reactor, suggesting that the observed effect of H_2 is reversible.

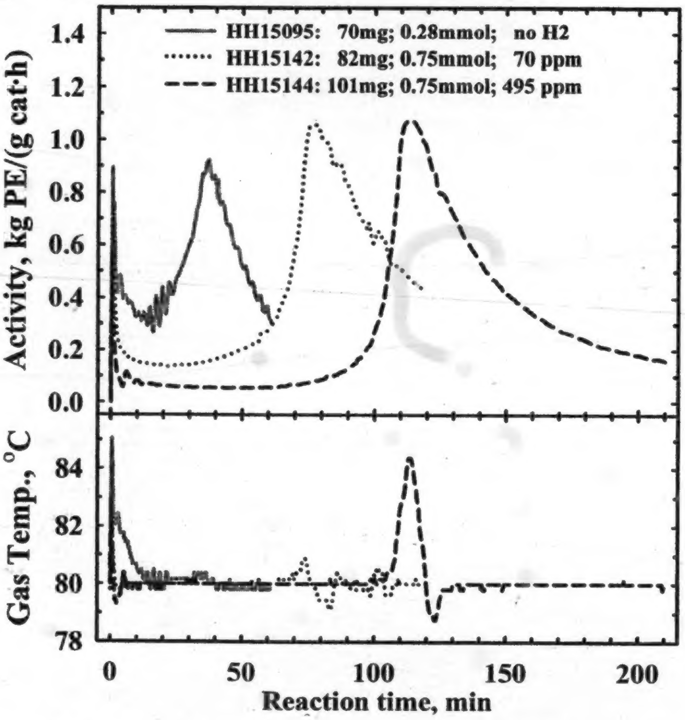

Figure 7.29 Influence of hydrogen on the rate profile of Catalyst HH15

The reversibility of the H_2 effect was checked as follows: Ethylene polymerization was initiated in the presence of H_2 (70 molar ppm), after 12 min of polymerization, the ethylene/hydrogen mixture was replaced with only ethylene. The resulting rate profile (Run HH15141, Figure 7.30) shows that full activity was restored after H_2 removal. The shape of the hydrogen-free part of the activity profile is similar to Run HH15095 (in which no H_2 was used), but the activity is even higher; compare Figure 7.30 to Run HH15095 in Figure 7.29. The maximum activity occurred 10 min earlier in Figure 7.29 probably because residual TIBA was also removed from the reactor (Chapter 6) together with the ethylene/hydrogen mixture.

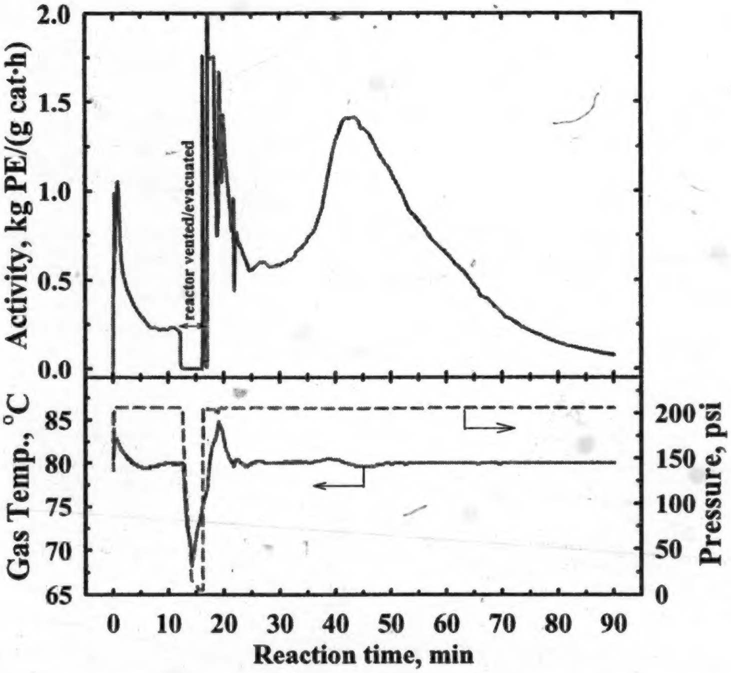

Figure 7.30 Reversible effect of hydrogen during ethylene homopolymerization activity of Catalyst HH15.

The reversible rate-depressing effect of hydrogen is known in Ziegler-Natta (Kissin, 1999) as well as metallocene/MAO (Kaminsky and Lüker 1984; Chu *et al.*, 1999) catalysts. Kissin (1999) observed this effect with silica-supported $TiCl_4$ catalyst of Mink and Nowlin (1995), and attributed it to the formation of the more stable Ti-C_2H_5

group following ethylene insertion into the Ti-H group. For metallocene/MAO catalysts, the observed results vary with the metallocene type, and the polymerization conditions. Chu *et al.* (2000) reported increase in polymerization activity upon H_2 removal similar to the above for in situ-supported Silica-MAO/Cp_2ZrCl_2 catalyst in hexane; however, under identical conditions, Silica-MAO/Et[Ind]$_2$ZrCl$_2$ catalyst behaved oppositely.

The initial activity depression by hydrogen (Figure 7.30) could be due to Zr-C_2H_5 species as with Ti-C_2H_5 suggested by Kissin (1999), while absence of H_2 in the subsequent part of the polymerization may explain the rapid activity rise to maximum. Due to high reactivity of metallocene/MAO catalysts toward hydrogen, the latter can be consumed in a short time during polymerization (Blom, 1999; Andersen, 2001). In spite of this, it is noteworthy that Chu *et al.* (2000) have polymerized ethylene in presence of significant mounts of H_2.

The rate of H_2 consumption during polymerization with Catalyst HH23 [solid (*n*-BuCp)$_2$ZrCl$_2$/MAO complex] at 80°C and 400 psi was monitored by online GC measurement (Chapter 3). The activity of this support-free catalyst was also depressed by H_2, Figure 7.31. After the initial drop, the activity continuously increased with decreasing H_2 concentration during the 1 h run. Catalyst HH23 is surprisingly less sensitive to H_2 than Catalyst HH15. In the presence of 5.6 mol % hydrogen, Catalyst HH15 was completely inactive for ~ 1 h, then it polymerized ethylene at < 5 g PE/(g cat·h) for more than 20 min before the reaction was terminated (Run HH15140, Table B-1). In addition to being support-free, Catalyst HH23 has higher Al (39.5 mass %) and Zr (0.804 mass %) content, but lower Al:Zr ratio (166) than Catalyst HH15 (11.6 mass %, 0.187 mass %, and 209 respectively).

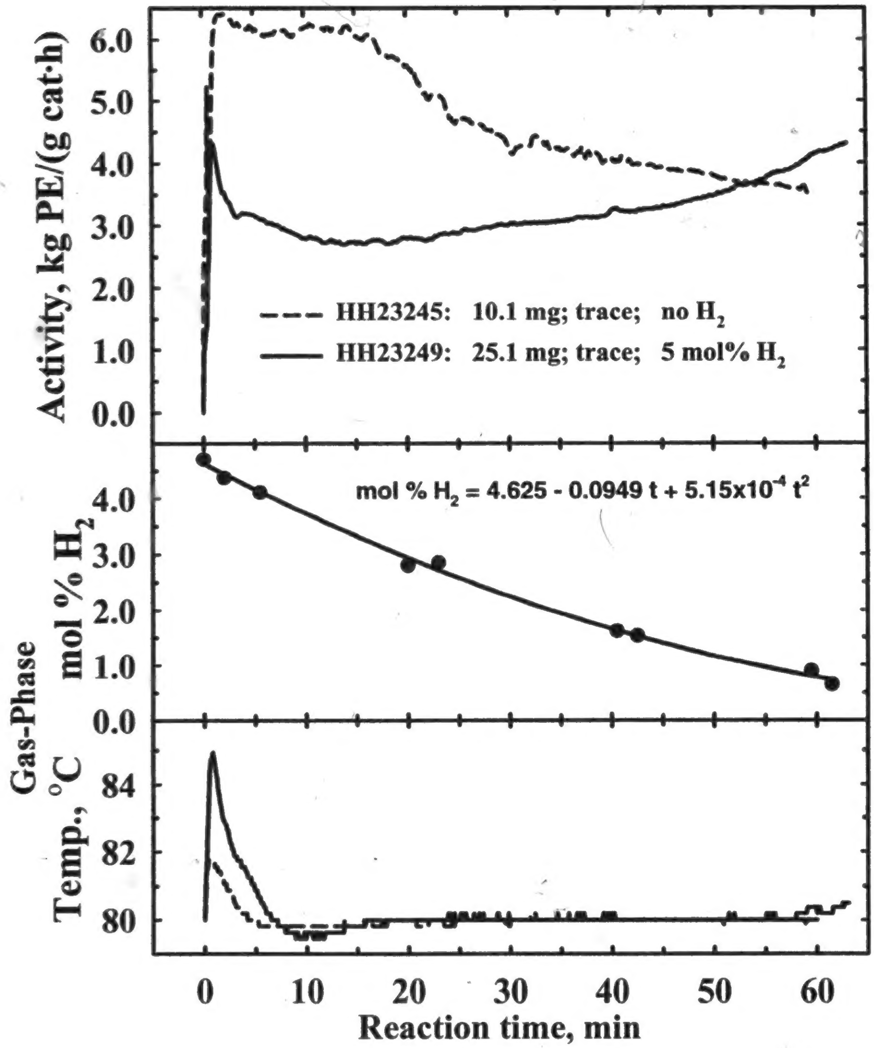

Figure 7.31 Depletion of hydrogen in the reactor (gas phase) during ethylene homopolymerization with Catalyst HH23.

Small amounts of hydrogen increased the gas-phase ethylene polymerization activity similar to homogeneous (Kaminsky and Lüker, 1984) and slurry (Andersen *et al.*, 2001) polymerizations. This increase could be due to activation of dormant sites, since the presence of dormant sites is enhanced by high metallocene concentration and low Al:Zr ratio catalysts (see Chapter 6).

Summary of the polymerization rate behavior of polymer-supported catalysts

Moderate differences in polymerization activity occurred with supported catalysts prepared under similar conditions, but the small variations in Zr loading and Al:Zr ratio of these catalysts showed no consistent effect on activity. The differences may have originated from the catalyst preparation since the activities of the catalysts did not follow any composition pattern.

The polymerization rates of the supported catalysts were affected by the support type, but the observed effect is probably due to physical rather than chemical differences between the supports. Commercial polymeric supports crosslinked by linear segments had better ethylene homopolymerization activity than catalysts supported on commercial DVB crosslinked supports. This effect could also be due to the catalyst friability. Polymerization activity generally improved with the support friability and the surface area and pore volume of catalyst. Functional groups of supports did not have significant effect on catalyst activity because MAO shields the metallocene from interacting with the functional groups. In a contrary finding for supported Ziegler-Natta catalyst, Ivanchev *et al.* (1980) reported that the chemical nature of supports rather than their structures had primary influence on polymerization activity and polyethylene properties.

All the tested catalysts exhibited the acceleration-decay type of activity profiles. In the absence of significant monomer transport resistance, the activity profiles are adequately described by a simple lumped parameter model with exponential activation and deactivation. Both the activation and deactivation rates increase with the polymerization temperature. Optimum polymerization temperature is catalyst dependent, and varies with other polymerization conditions; maximum rates occurred in the 70 –

90°C range. A nonlinear dependence of polymerization activity on monomer pressure was observed. The nonlinearity is mainly due to the changing effects of temperature and mass transport resistance with the monomer pressure.

The supported catalysts in this thesis work had good activity in gas-phase ethylene homopolymerization and ethylene/α-olefin copolymerization. Most of the catalysts had average polymerization activities greater than 10,000 kg PE/(mol Zr·h). The overall average activity is about 30,000 kg PE/(mol Zr·h); this is in the "very high" activity catalyst rating according to the classification of Britovsek *et al.* (1999). Catalysts HH08 and HH09 had average polymerization activities up to 110,000 and 190,000 kg PE/(mol Zr·h) respectively. The overall average activity value is higher than the values for the same metallocene reported in Table 2.2 from the literature, and higher than the activity of several other supported metallocenes reported in the table.

The supported $(n\text{-BuCp})_2ZrCl_2$ catalysts are highly sensitive to hydrogen. The polymerization activity is considerably depressed by the presence of <100 ppm (molar) hydrogen in the reactor. The hydrogen effect is reversible since the catalyst activity was restored after the hydrogen in the reactor was depleted.

8. Influence of Comonomer on Activity Profiles and Product Morphology for Gas-phase Polymerization Over Polymer-supported $(n\text{-BuCp})_2ZrCl_2$/MAO Catalysts

Numerous ethylene/1-hexene copolymerization activity profiles had been presented in Chapters 5 – 7. In this chapter the influence of comonomer on the gas-phase ethylene/α-olefin polymerization over several polymer-supported catalysts is discussed. In this investigation, the amounts of 1-hexene injected into the reactor were varied at relatively constant total reactor pressure. 1-Hexene was mostly used because it is commercially the most important comonomer in LLDPE production (Wester and Ystenes, 1997). Propylene and 1-decene were also used in some experiments to gain more insight into the influence of comonomer size on the catalyst fracture mechanism.

Several inferences made in this chapter are based on SEM images of cross-sections of polymer particles. Therefore, it is important to note that a wide variation in product morphology can be obtained from a single polymerization run. Even different parts of a single polymer particle can exhibit different morphologies. Both the inter- and intra-particle morphology differences can originate from the preparation and handling of support and the catalyst. Since each catalyst particle is an independent micro reactor, they can behave quite differently during polymerization. In preparing SEM samples, the anomalous particles are usually over represented because of curiosity. The inferences presented in this chapter are based on more SEM images than the ones shown.

8.1 Influence of 1-hexene on polymerization rates and product morphology

For most of the supported catalysts, the copolymerization activity profiles remarkably differed from those of ethylene homopolymerization, with copolymerization usually having higher activity. The influence of 1-hexene on the polymerization behavior of the catalysts generally fall into one of the following three groups:

- Group-1: Low ethylene homopolymerization activity catalysts which exhibit several times higher activity during ethylene/1-hexene copolymerization.
- Group-2: Moderate ethylene homopolymerization activity catalysts that show only moderate activity increase in ethylene/1-hexene copolymerization.
- Group-3: High ethylene homopolymerization catalysts which show no clear activity enhancement or which even decrease in activity in the presence of 1-hexene.

8.1.1 Effect of 1-hexene on activity of Group-1 catalysts

Table 8.1 summarizes the effects of 1-hexene on Group-1 catalysts. The presence of 1-hexene resulted in the increases of the average activity, maximum activity, and the activity growth period. This is due to the 1-hexene influence on activity profile as shown in Figures 8.1 and 8.2 for Catalysts HH10 and HH22, respectively.

Table 8.1 Influence of 1-hexene on the activity of Group-1 catalysts.

Run number	Amount charged in reactor			Initial $1\text{-}C_6H_{12}$ content mol. %	Activity, g PE/(g cat·h)			t_{Rmax}[a], min
	1-hexene[b] mL	Catalyst, mg	TIBA[c], mmol		Avg.[d]	Max.[e]	A_C/A_H[f]	
HH10059	3.9	50.0	Trace	3.0	416	511	17.3	29
HH10060	–	50.7	Trace	–	22	22	–	24
HH10061	4.9	52.0	0.28	3.7	410	579	17.1	44
HH22147	4.3	82.5	Trace	3.3	313	440	6.7	50
HH22148	–	82.3	Trace	–	47	77	–	66
HH18103	2.3	76.0	Trace	1.7	479	537	4.8	31
HH18104	–	76.7	Trace	–	100	117	–	5
HH18105	4.6	76.4	Trace	3.4	855	1095	8.6	28
HH18106	7.2	77.2	Trace	5.5	363	387	3.6	40

a: time to attain maximum activity; b: injected once before the start of polymerization
c: Trace denotes residual TIBA was evacuated after reactor scavenging
d: calculated from the product recovered (gravimetric); e: based on measured ethylene flow rate only; f: ratio of average copolymerization to homopolymerization activities

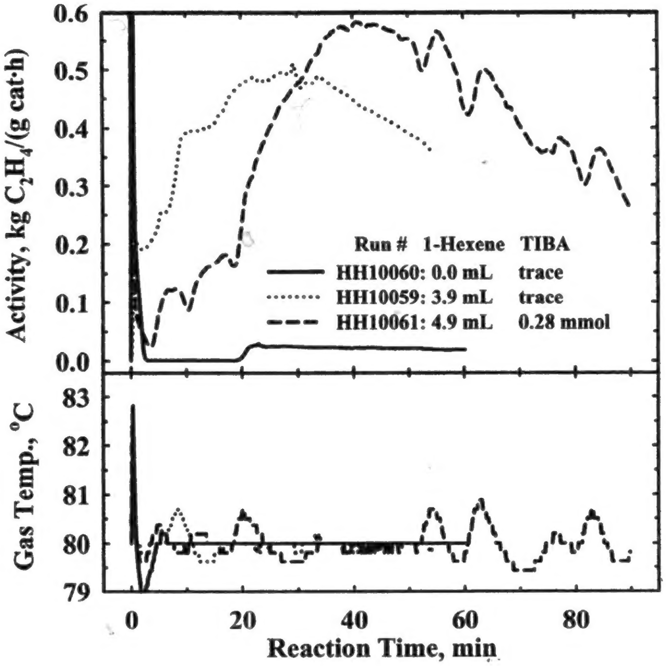

Figure 8.1 Influence of 1-hexene on the polymerization activity of Catalyst HH10

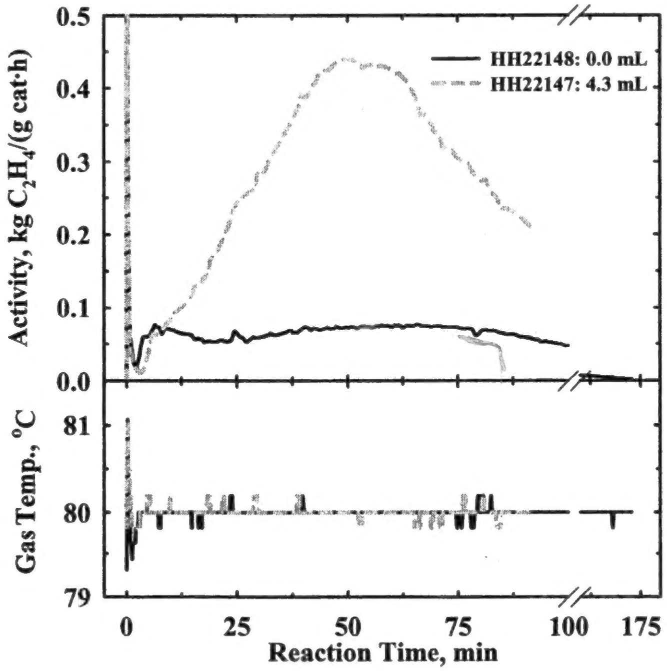

Figure 8.2 Influence of 1-hexene on the polymerization activity of Catalyst HH22

1-Hexene influences similar to the above were also observed for Catalyst HH18 (see Figure 8.3). Further, the activity of Catalyst HH18 increased with increase in the amount of 1-hexene to a maximum value and decreased on further 1-hexene addition; other catalysts behaved similarly (e.g., see Figure 8.4). These activity maxima are consistent with others reported for ethylene/1-hexene copolymerization over supported metallocene catalysts (Pryzbyla *et al.*, 1999; Chu *et al.*, 1999). The reported maximum activities occurred at higher concentration ratios of 1-hexene/ethylene than those in Table 8.1 for slurry polymerization with bridged metallocenes because 1-hexene is more reactive with the bridged metallocenes than the unbridged $(n\text{-BuCp})_2ZrCl_2$.

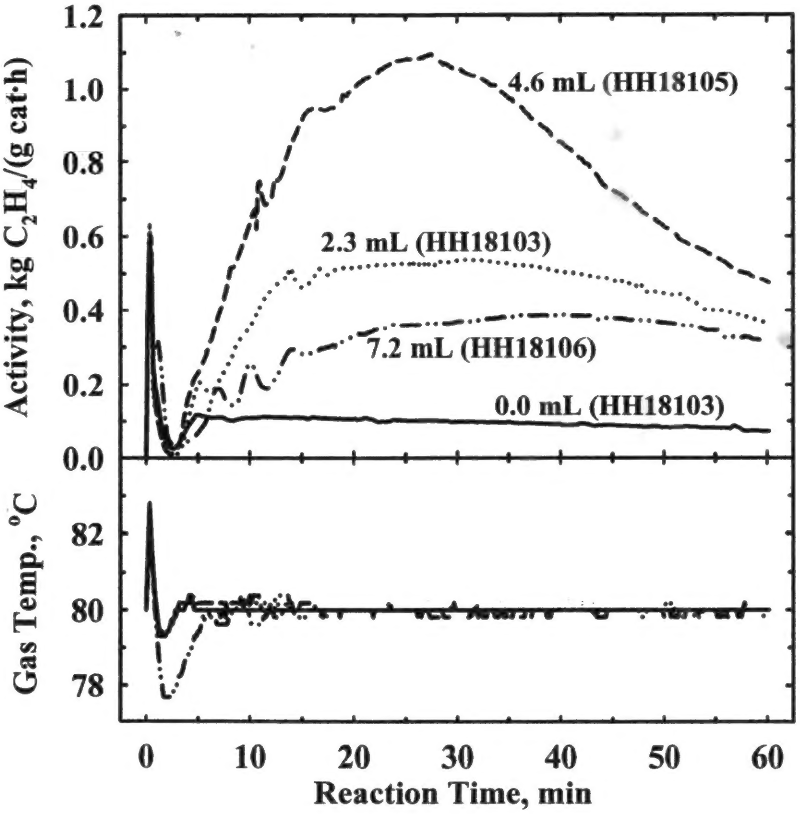

Figure 8.3 Influence of 1-hexene on the polymerization activity of Catalyst HH18

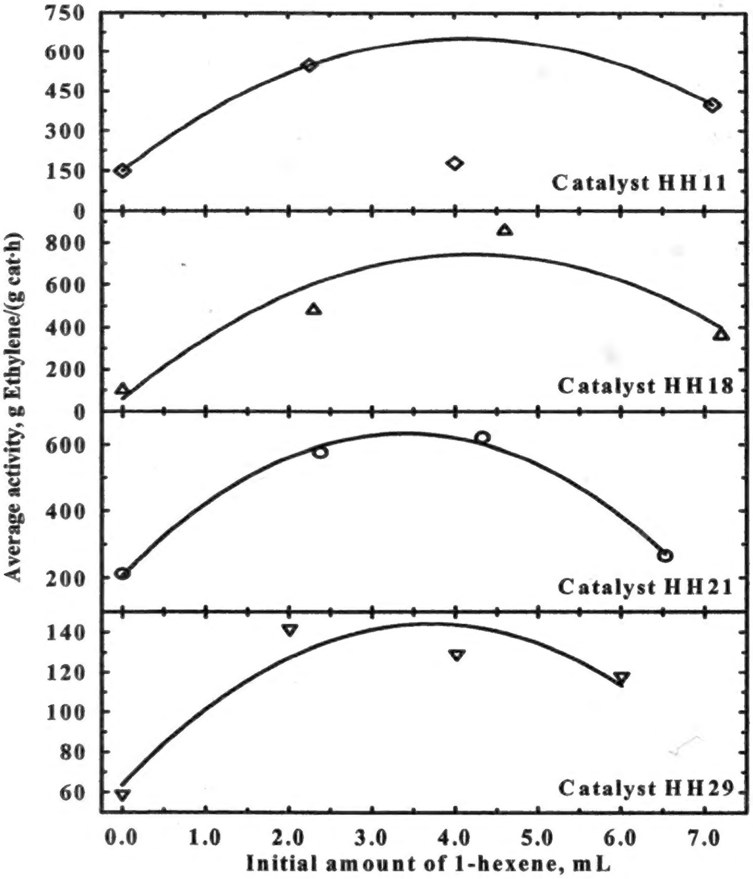

Figure 8.4 Influence of the initial amount of 1-hexene in the polymerization reactor on average activity at 80°C and 1.4 MPa.

The ethylene/α-olefin synergism in polymerization is widely reported for both Ziegler-Natta, and metallocene catalysts (Koivumäki and Seppälä, 1993; Camurati *et al.*, 2001). Physical and chemical effects have both been used to explain this phenomenon (see Section 2.3.4.3). Chakravarti and Ray (2001) similarly observed higher activity and slower activation (longer t_{Rmax}) during gas-phase ethylene/1-hexene copolymerization over (unspecified) non-bridged supported zirconocene. Similar 1-hexene influences had been attributed (at least partly) to physical changes in heterogeneous Ziegler-Natta catalysts (Wester and Ystenes, 1997).

To explore the above physical changes, cross-sections of the product polyethylene particles were examined under SEM (Figures 8.5 to 8.7). The micrographs show completely different internal morphology of the homopolymer compared to copolymer particles. Polymer particles from all the low activity homopolymerization runs have embedded cores that are quite distinct from the surrounding macroporous polyethylene, an artichoke-like structure. EDX line scans across the particles clearly show high Al counts in the cores (Figures 8.8). This shows that the cores predominantly consist of the original catalyst particles and contain very little polyethylene. Zirconium distribution in the catalyst particles could not be assessed because it is below the detection limit of the EDX.

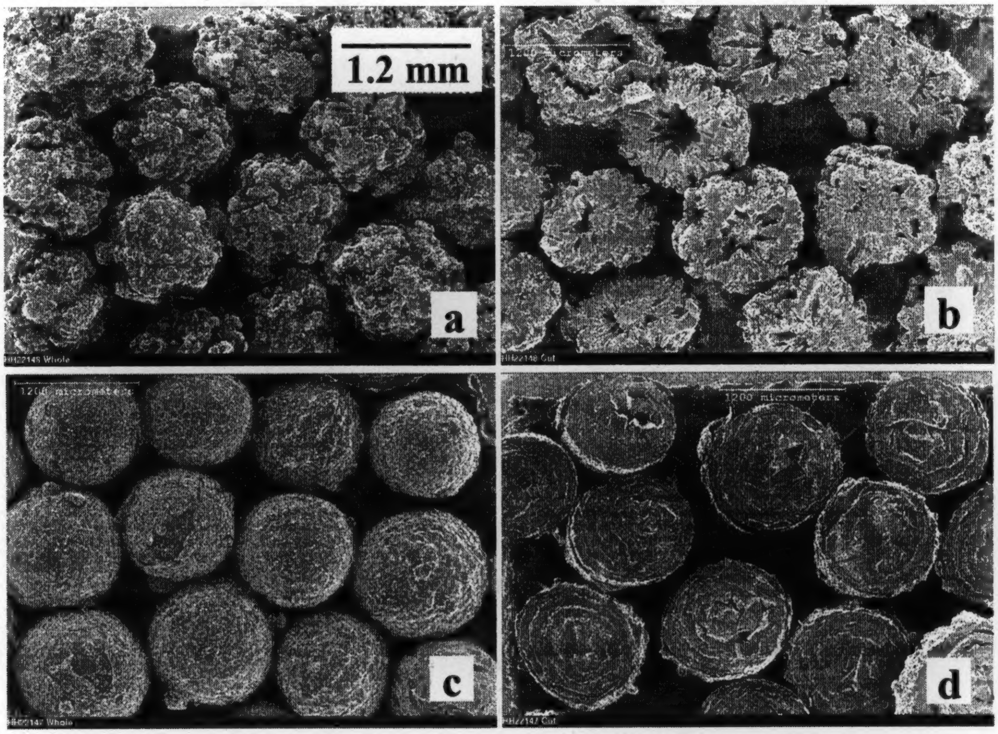

Figure 8.5 External surface (left) and cross-section (right) morphology of polymer particles produced with Catalyst HH22 in Runs (a and b) HH22148, ethylene homopolymer; (c and d) HH22147 ethylene/1-hexene copolymer. See Table 8.1 for run details.

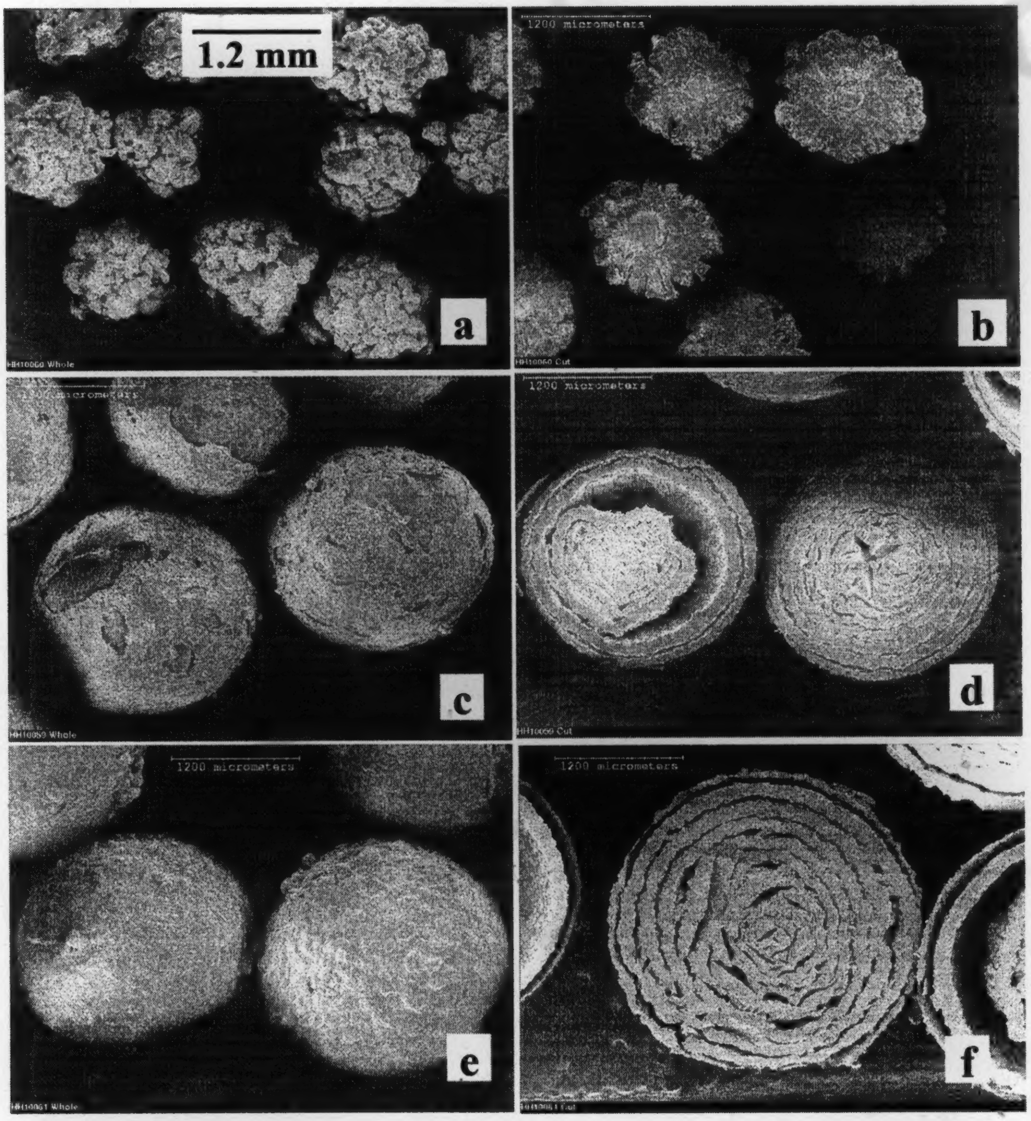
1.2 mm
1200 micrometers
a
HH10060 Whole
b
HH10060 Cut
1200 micrometers
c
HH10059 Whole
1200 micrometers
d
HH10059 Cut
1200 micrometers
e
HH10061 Whole
1200 micrometers
f
HH10061 Cut

Figure 8.6 SEM micrographs of whole (left) and cross-sections (right) of polymer particles produced by Catalyst HH10; (a and b) ethylene homopolymer Run HH10060, and ethylene/1-hexene copolymers with (c and d) 3.9 mL and (e and f) 4.9 mL 1-hexene.

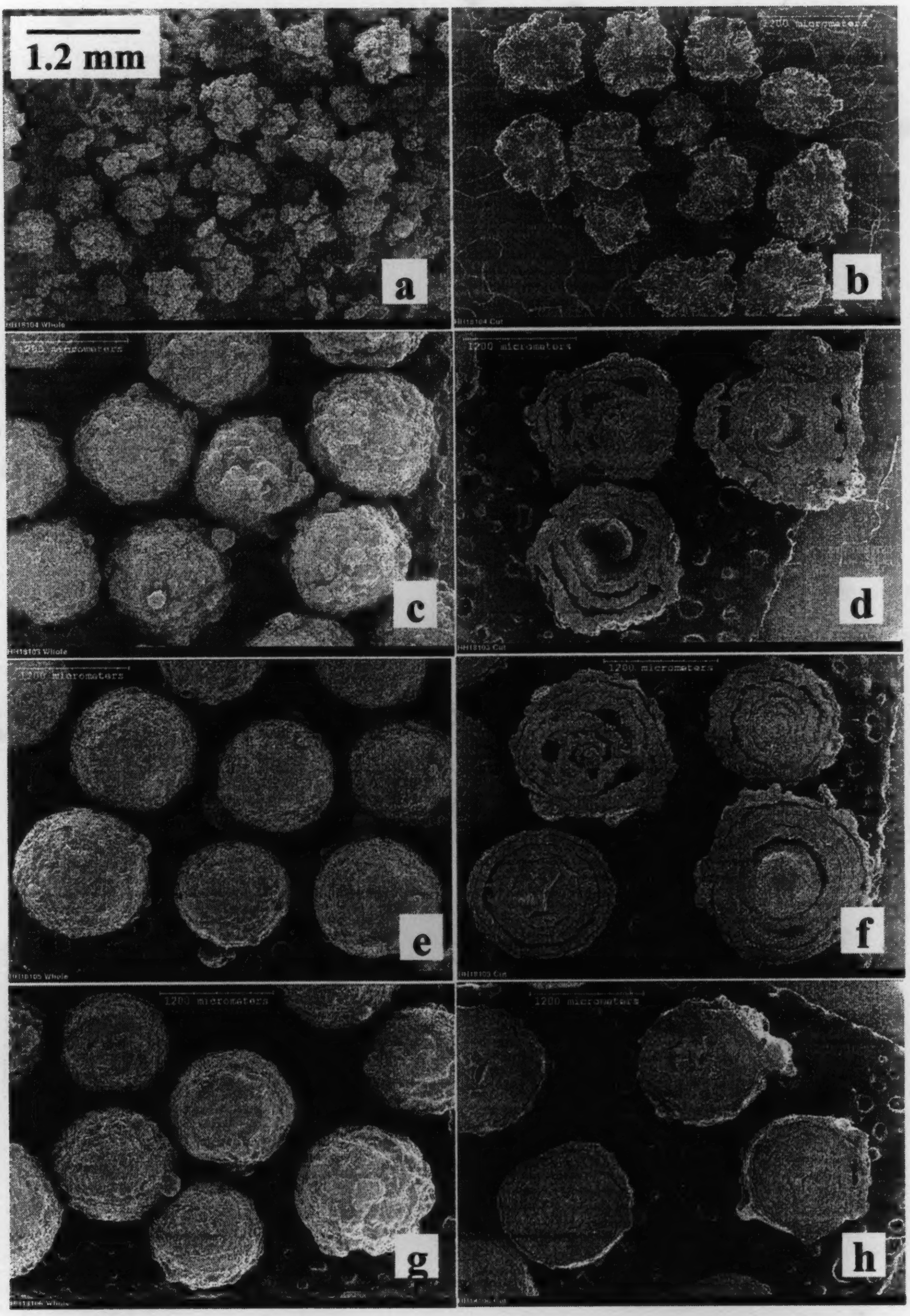
1.2 mm
a
HH18104 Whole
b
HH18104 Cut
1200 micrometers
c
1200 micrometers
d
1200 micrometers
e
1200 micrometers
f
1200 micrometers
g
1200 micrometers
h

Figure 8.7 External surface (left) and cross-section (right) morphology of polymer particles produced with Catalyst HH18 in Runs (a and b) HH18104, (c and d) HH18103, (e and f) HH18105, and (g and h) HH18106. See Table 8.1 for run details.

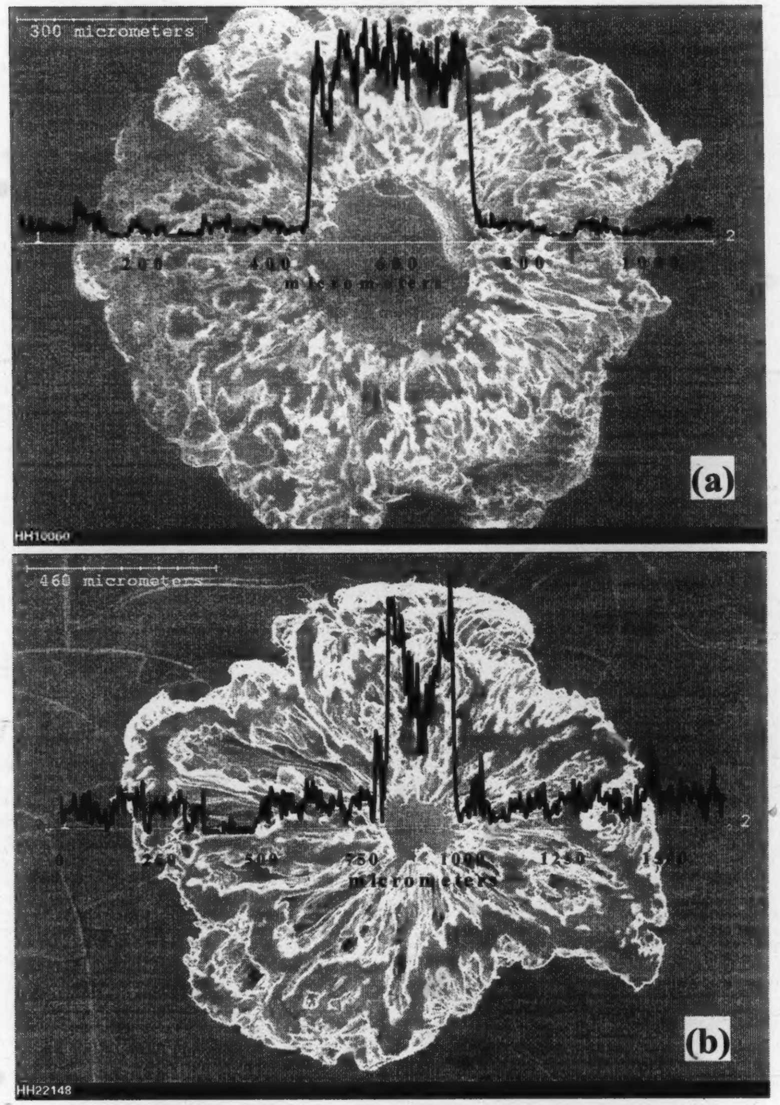

Figure 8.8 EDX line scans (Al) across polyethylene particles reveal unfragmented catalyst cores after polymerization with (a) Catalyst HH10 for 1 h to 23.5 g/g, and (b) Catalyst HH22 for 2.9 h to 136 g/g.

Contrary to the homopolymer particles, the ethylene/1-hexene copolymer particles produced by the same catalysts had no distinct cores; instead, the internal morphology of the copolymer particles consist of several distinct concentric shells forming an onion-ring structure. Aluminum was not detectable across the copolymer particles by the EDX analysis. Similar onion-ring structured morphology was earlier reported for polypropylene particles (Ziegler-Natta catalyst) as a product of sophisticated catalyst "architecture" (Galli *et al*., 1999) that led to the commercial reactor granule technology (RGT) process (Galli and Vecellio, 2001).

8.1.2 Effect of 1-hexene on activity of Group-2 catalysts

A summary of the influence of 1-hexene on the polymerization activity of Group-2 catalysts is given in Table 8.2. The variation of activity profiles for Catalysts HH07, HH17, and HH21 with the initial amount of 1-hexene in the reactor is shown in Figures 8.9 – 8.11 respectively.

Table 8.2 Effect of 1-hexene on the activity of Group-2 catalysts.

Run number	Amount charged in reactor			Initial 1-C_6H_{12} content mol %	Activity, g PE/(g cat·h)			t_{Rmax}[a], min
	1-hexene[b], mL	Catalyst, mg	TIBA[c], mmol		Avg.[d]	Max.[e]	A_C/A_H[f]	
HH07048	5.3	106	Trace	4.0	271	271	1.2	2; 34
HH07049	–	107	Trace	–	232	291	–	15
HH07050	3.3	104	Trace	2.5	678	1042	2.9	17
HH17100	2.1	80	Trace	1.5	346	510	1.5	22
HH17101	–	84	Trace	–	230	284	–	22
HH17102	4.3	80	Trace	3.2	348	507	1.5	21
HH21112	4.3	85	Trace	3.3	621	920	2.9	13
HH21113	–	75	Trace	–	212	507	–	4
HH21115	2.4	78	Trace	1.8	577	827	2.7	9
HH21208	6.5	78	Trace	4.9	265	298	1.3	10

a–f: see notes of Table 8.1

Note that in Figure 8.9, the disparity in the activity between Run HH07050 (3.3 mL 1-hexene) and the other two (0.0 and 5.3 mL 1-hexene) is inflated by the temperature excursion in Run HH07050. This group of catalysts showed similar activity in ethylene homopolymerization (A_H) and ethylene/1-hexene copolymerization (A_C). The range of the activity ratio A_C:A_H is about 1–3 (Table 8.2) compared to A_C:A_H of about 4–17 for Group-1 (Table 8.1). The increase in polymerization activity of Group-2 catalysts with 1-hexene also passes through a maximum at about 2 – 4 mL (7 – 14 mol/m^3) 1-hexene, with the amount of 1-hexene for maximum activity being catalyst specific.

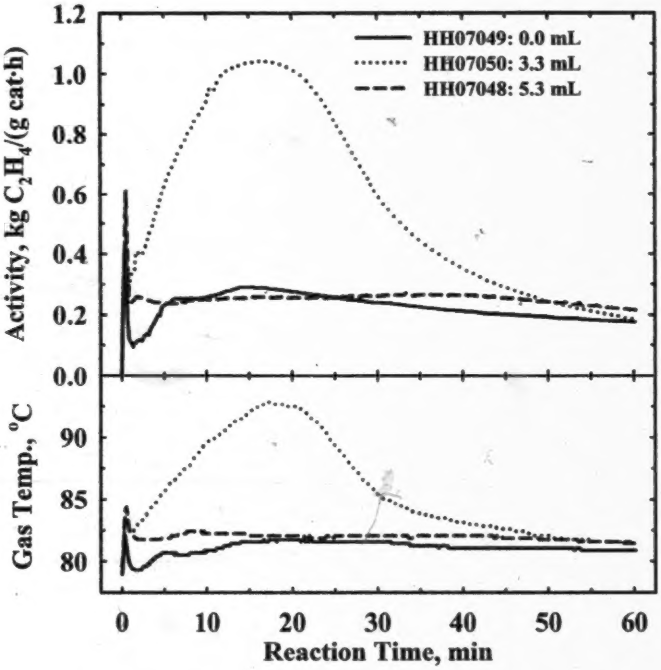

Figure 8.9 Influence of 1-hexene on the polymerization activity of Catalyst HH07

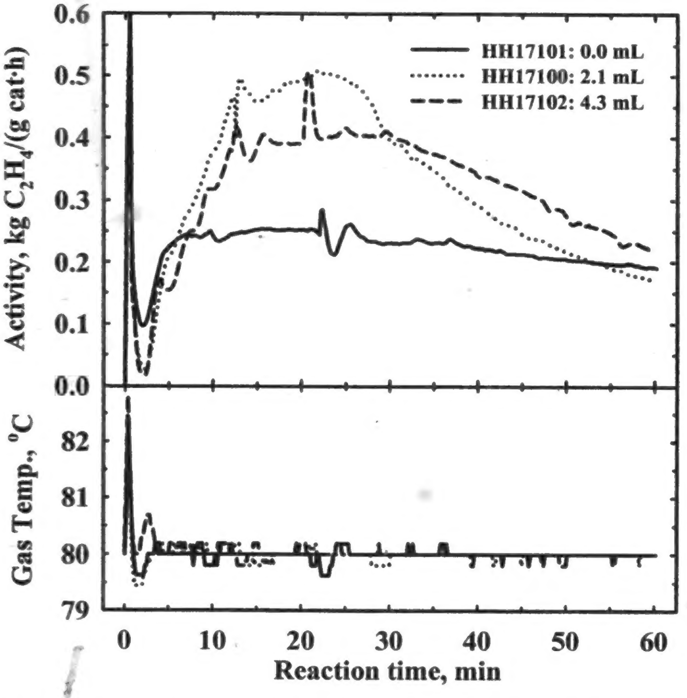

Figure 8.10 Influence of 1-hexene on the polymerization activity of Catalyst HH17

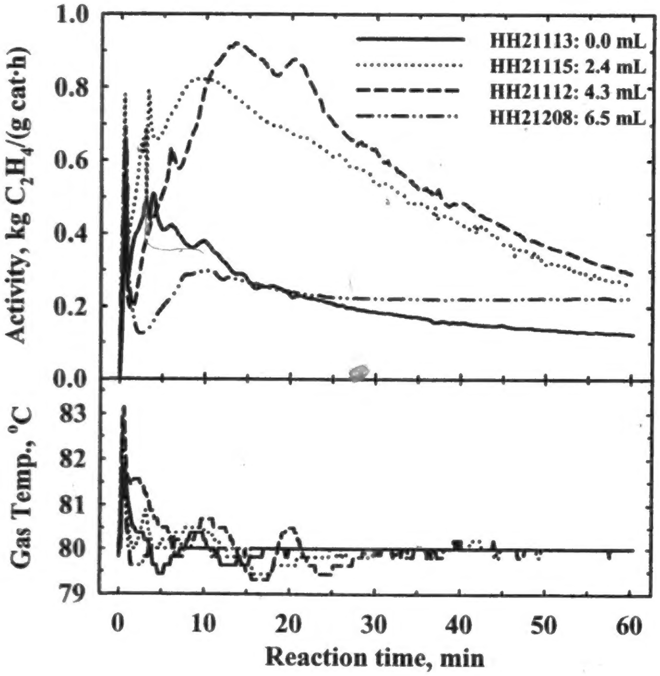

Figure 8.11 Influence of 1-hexene on the polymerization activity of Catalyst HH21

The morphology of the polymer particles produced by Catalysts HH07, HH17, and HH21 above are shown in Figures 8.12 – 8.14 respectively. The homopolymer particles produced by these catalysts consist mostly of hollow shells housing a core. This differs from the artichoke-like morphology of the homopolymer particles of Group-1 catalysts [see Figures 8.5(b), 8.6(b), and 8.7(b)]. Group-2 catalysts rarely produced homopolymer particles with the artichoke-like morphology.

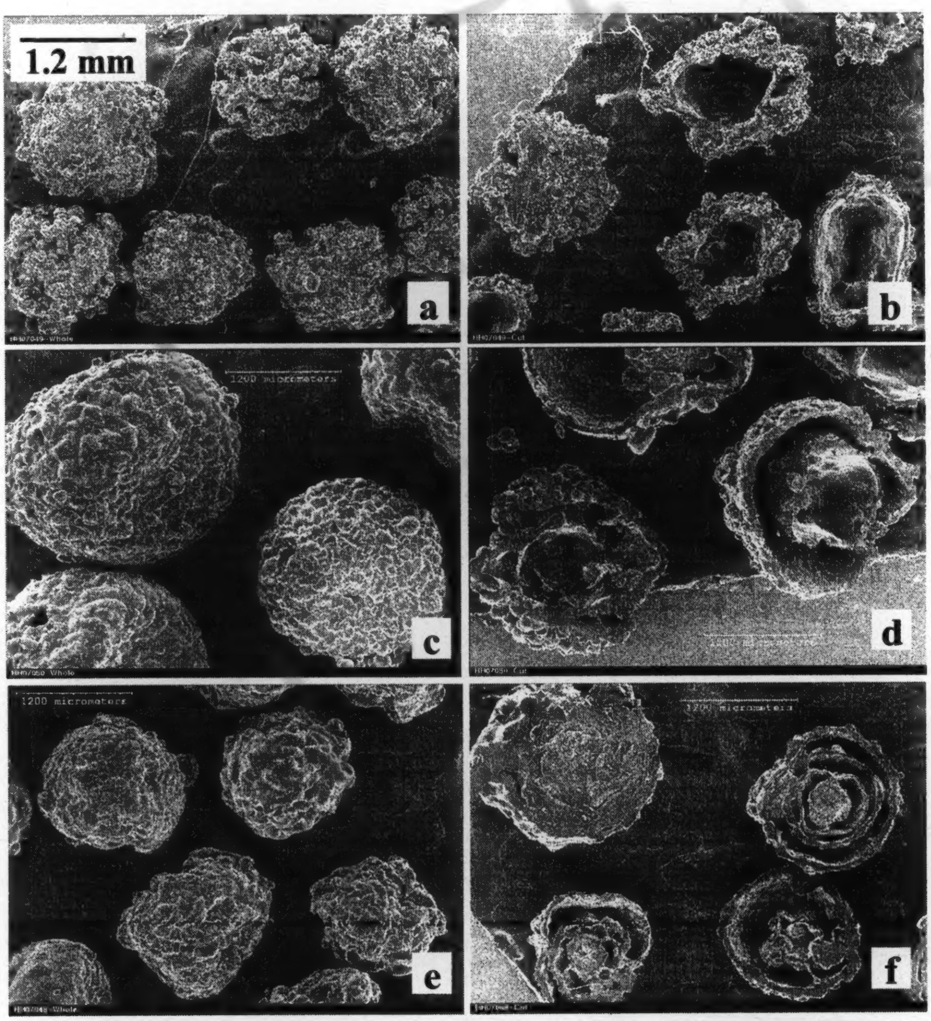

Figure 8.12 SEM micrographs of external surface (left) and cross-section (right) of polymer particles produced by Catalyst HH07 in Runs (a and b) HH07049, (c and d) HH07050, and (e and f) HH07048. See Table 8.2 for run details.

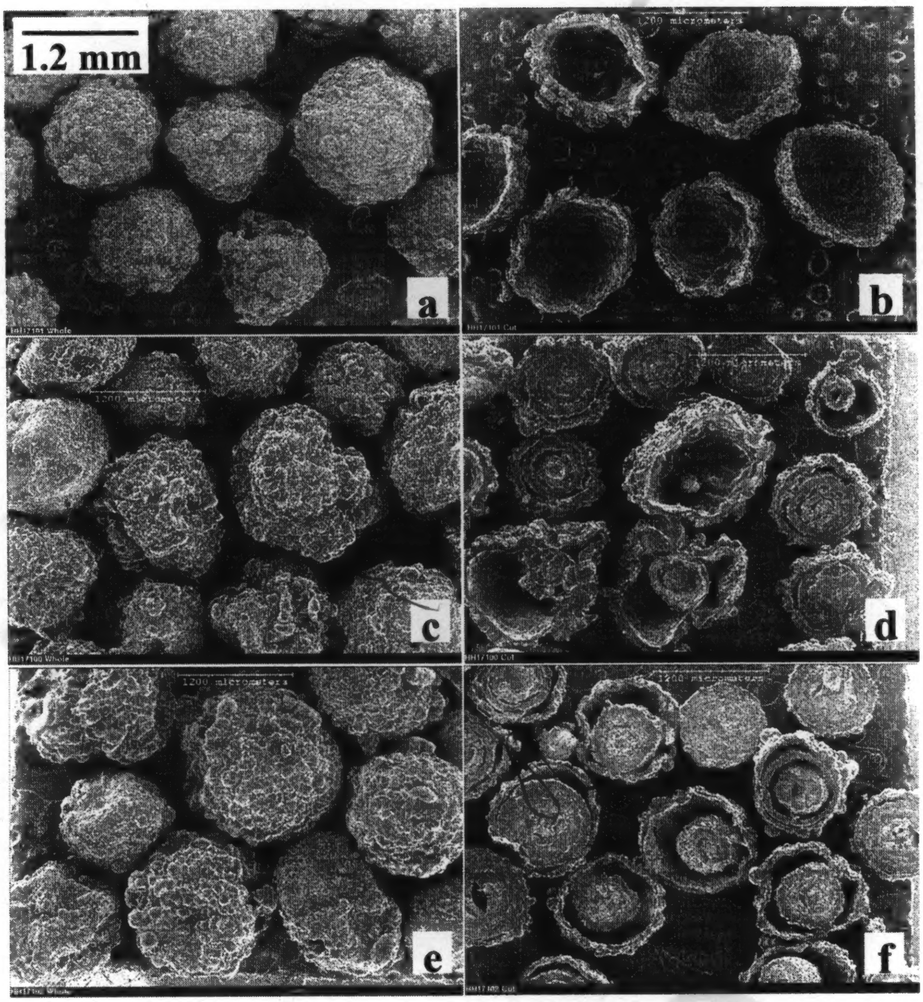

Figure 8.13 SEM micrographs of external surface (left) and cross-section (right) of polymer particles produced by Catalyst HH17 in Runs (a and b) HH17101, (c and d) HH17100, and (e and f) HH17102. See Table 8.2 for run details.

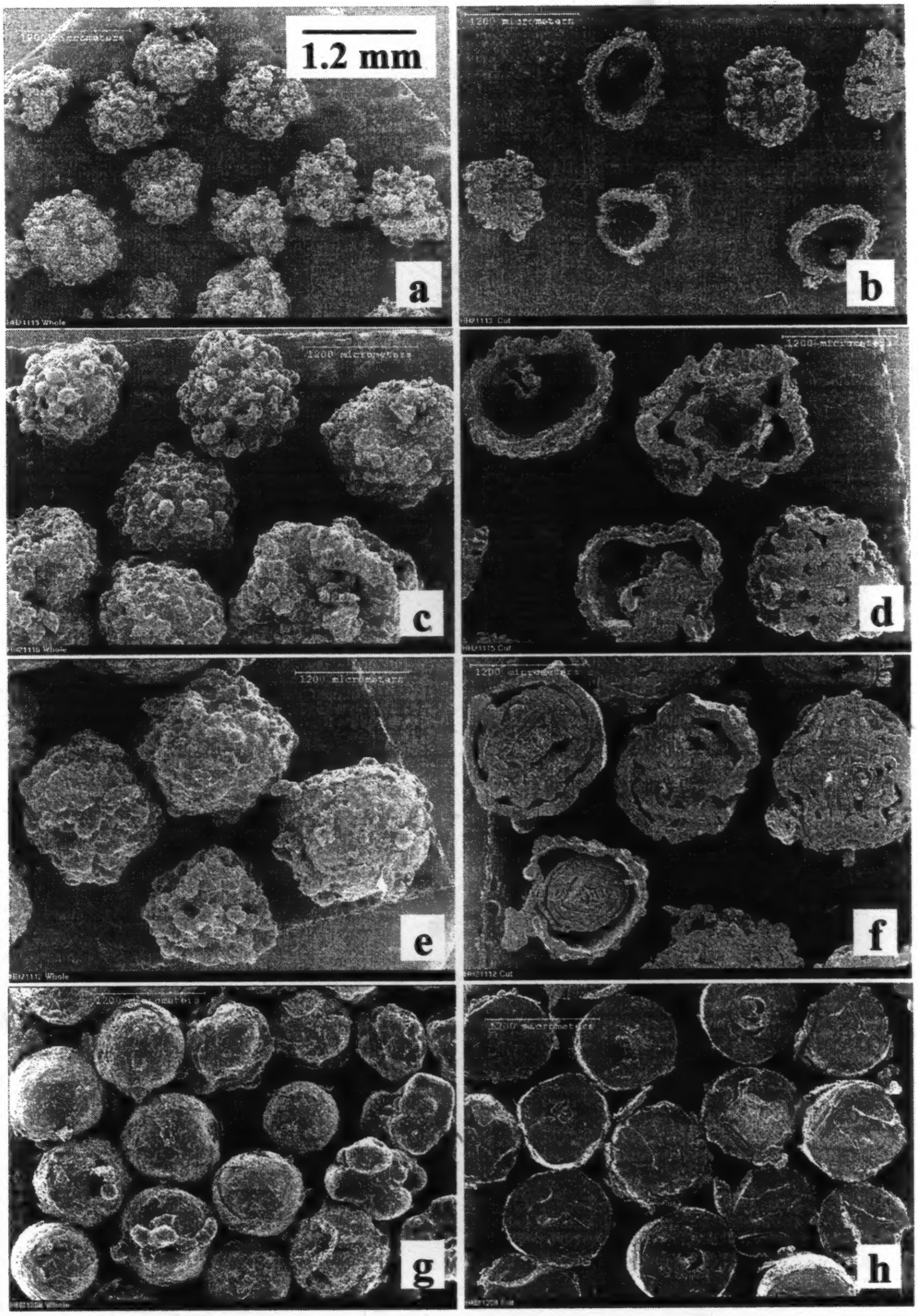
1.2 mm
1200 micrometers
a
b
c
d
e
f
g
h

Figure 8.14 SEM micrographs of external surface (left) and cross-section (right) of polymer particles produced by Catalyst HH21 in Runs (a and b) HH21113, (c and d) HH21115, (e and f) HH21112, and (g and h) HH21208. See Table 8.2 for run details.

8.1.3 Effect of 1-hexene on activity of Group-3 catalysts

The catalysts in Group-3 (Table 8.3) tend to have lower copolymerization to homopolymerization activity ratios (A_C:A_H ~ 0.4–2) than the previous two groups. In addition, the maximum ethylene homopolymerization activity is attained more rapidly (t_{Rmax} ~ 1–4 min) with these catalysts. Figures 8.15–8.17 show activity profiles of three representative catalysts of Group-3. The presence of 1-hexene suppresses the initial activity; hence, the higher average copolymerization activities are mainly due to the broadening of the activity profiles. Maximum copolymerization activity is often lower than the maximum homopolymerization activity. Run HH08062 (Figure 8.16) has higher maximum copolymerization activity because the residual TIBA in the reactor was not evacuated (Table 8.3).

Table 8.3 Influence of 1-hexene on the polymerization activity of Group-3 catalysts.

Run number	Amount charged in reactor			Initial $1\text{-}C_6H_{12}$ content, mol %	Activity, g PE/(g cat·h)			t_{Rmax}[a], min
	1-hexene[b], mL	Catal., mg	TIBA[c], mmol		Avg.[d]	Max.[e]	A_C/A_H[f]	
HH06044	3.0	113	Trace	2.3	351	502	1.7	13
HH06046	6.0	113	Trace	4.5	258	287	1.3	39
HH06047	0.0	112	Trace	0.0	205	928	–	2
HH08054	0.0	32	Trace	0.0	882	3591	–	1
HH08062*	3.4	26	0.28	2.6	2524	4354	2.8	42
HH08073*	4.3	52	0.28	3.3	1465	2153	1.7	25
HH09056	3.6	103	Trace	2.7	736	1107	1.1	11
HH09057	0.0	31	Trace	0.0	661	2671	–	3
HH09072	4.3	41	Trace	3.2	266	427	0.4	15
HH09263	0.0	41	Trace	0.0	696	2006	–	4

a–f: see notes of Table 8.1

* The presence of residual TIBA in the reactor resulted in higher average activity

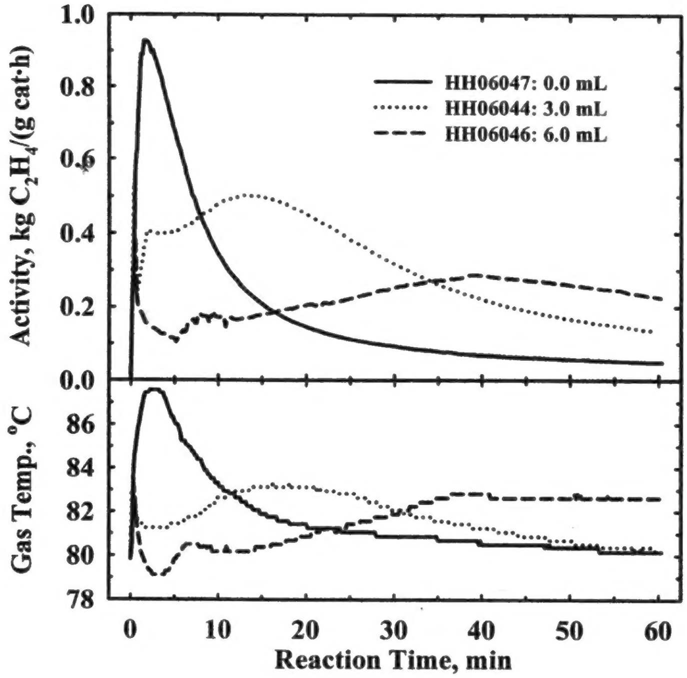

Figure 8.15 Influence of 1-hexene on the polymerization activity of Catalyst HH06

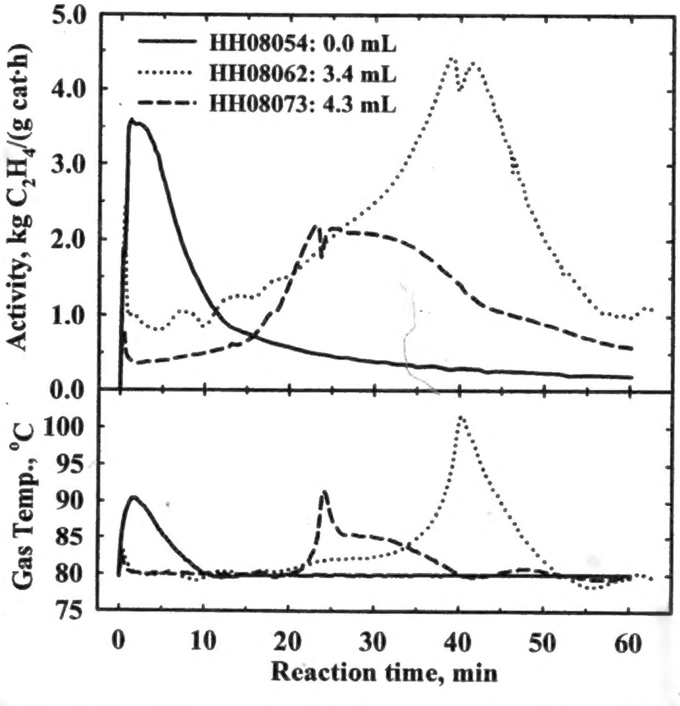

Figure 8.16 Influence of 1-hexene on the polymerization activity of Catalyst HH08

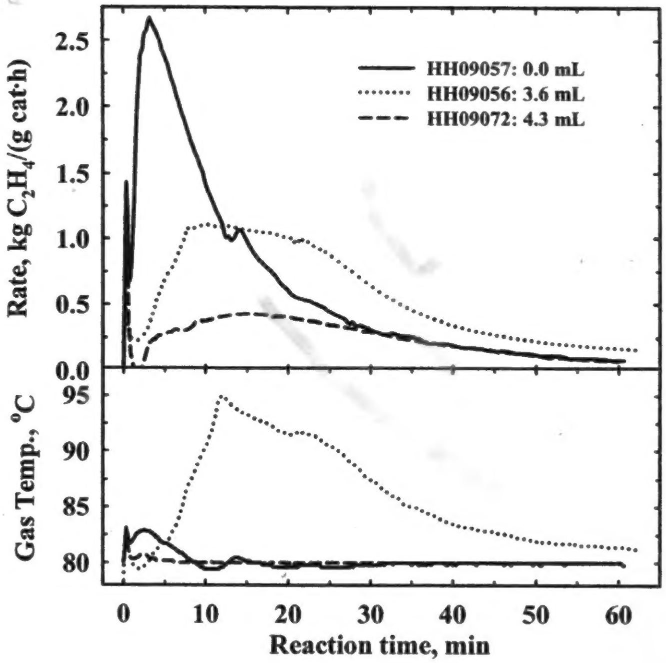

Figure 8.17 Influence of 1-hexene on the polymerization activity of Catalyst HH09

Figures 8.18 – 8.20 show the morphology of the polymer particles produced in the polymerization runs shown in Figures 8.15 – 8.17 respectively. Spherical and highly porous polymer particles were obtained. The spherical shape is a direct replication of the catalyst particles (see Figures 4.12 and 4.13). Scanning electron micrographs of cross-sections of the particles reveal a uniformly porous internal morphology for the homopolymer particles [Figures 8.18(b), 8.19(b), and 8.20(b)]. This morphology is quite different from the artichoke-like morphology of homopolymer particles of Group-1 catalysts, and the hollow-shell morphology of the Group-2 catalysts. Figures 8.18–8.20 show that all the three catalysts (HH06, HH08, and HH09) have increasing tendency to produce copolymer particles with the concentric-shell morphology as the amount of 1-hexene in the reactor was increased. However, polymer particles with uniform internal morphology predominate up to 4 mL (14 mol/m^3) 1-hexene initially present in the reactor. The Group-1 and Group-2 catalysts produced the onion-ring morphology with lower amount of 1-hexene in the reactor. Thus, Group-3 catalysts have lower tendency of producing the layered copolymer particle morphology than the catalysts in Group-1 and Group-2.

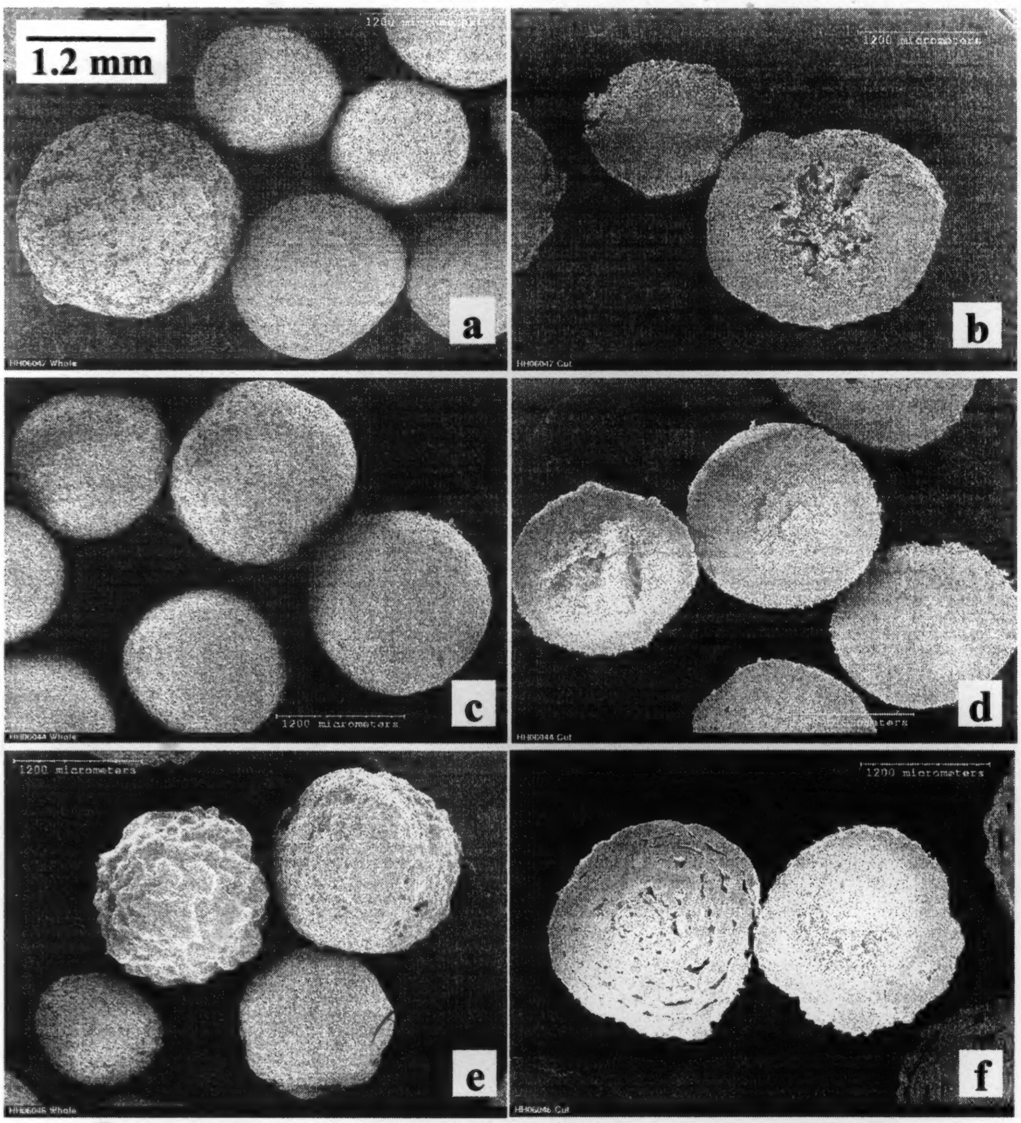
1.2 mm
1200 micrometers
a
HH06047 Whole
1200 micrometers
b
HH06047 Cut
1200 micrometers
c
HH06044 Whole
d
HH06044 Cut
1200 micrometers
e
HH06046 Whole
1200 micrometers
f
HH06046 Cut

Figure 8.18 SEM micrographs of external surface (left) and cross-section (right) of polymer particles produced by Catalyst HH06 in Runs (a and b) HH06047, (c and d) HH06044, and (e and f) HH06046. See Table 8.3 for run details.

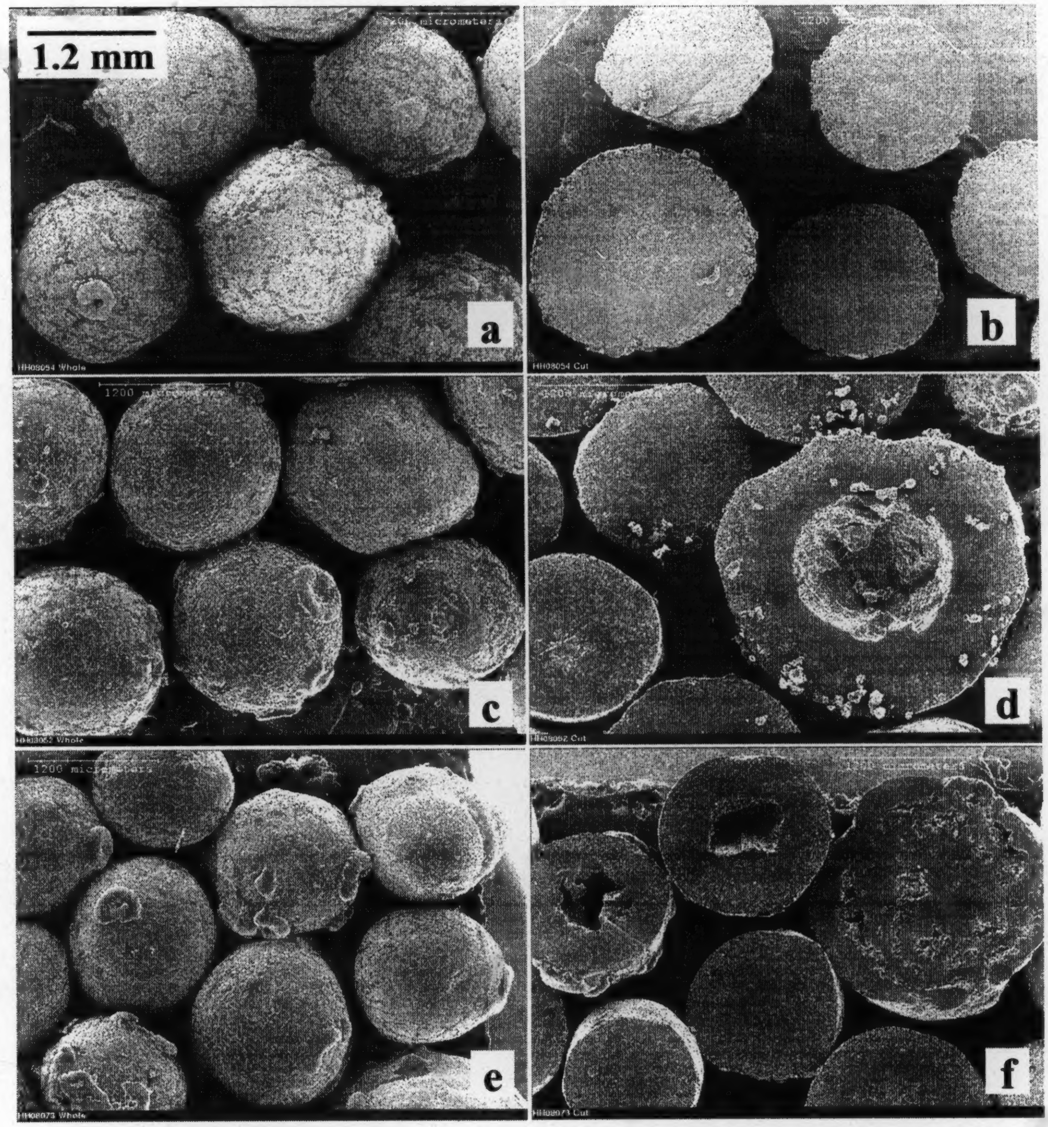
1.2 mm
1200 micrometers
a
HH08054 Whole
b
HH08054 Cut
c
HH08052 Whole
d
HH08052 Cut
e
HH08073 Whole
f
HH08073 Cut

Figure 8.19 SEM micrographs of external surface (left) and cross-section (right) of polymer particles produced by Catalyst HH08 in Runs (a and b) HH08054, (c and d) HH08052, and (e and f) HH08073. See Table 8.3 for run details.

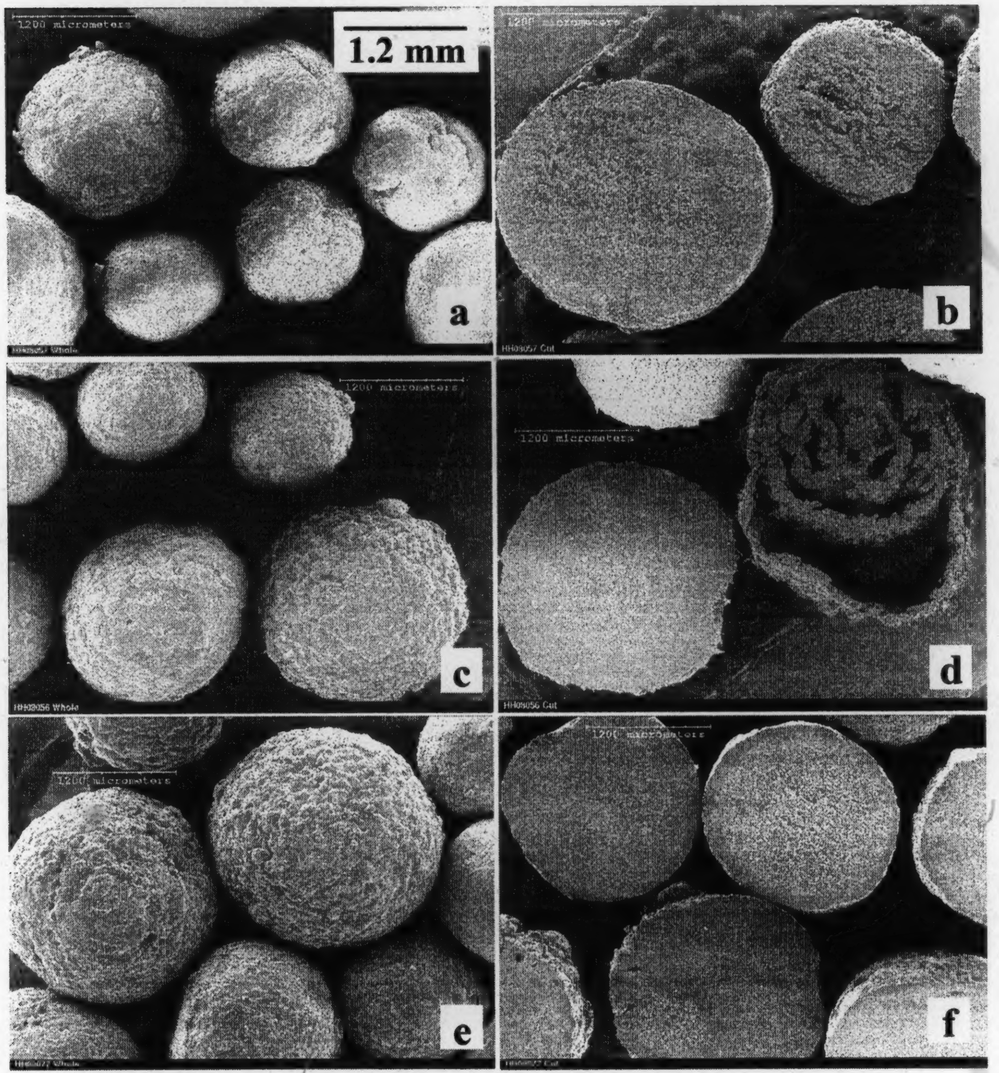
1200 micrometers
1.2 mm
a
HH09057 Whole
1200 micrometers
b
HH09057 Cut
1200 micrometers
c
HH09056 Whole
1200 micrometers
d
HH09056 Cut
1200 micrometers
e
HH09072 Whole
1200 micrometers
f
HH09072 Cut

Figure 8.20 SEM micrographs of external surface (left) and cross-section (right) of polymer particles produced by Catalyst HH09 in Runs (a and b) HH09057, (c and d) HH09056, and (e and f) HH09072. See Table 8.3 for run details.

The criteria of average copolymerization to homopolymerization activity ratios and where available the polymer particles morphology were used as in the above to classify the remaining catalysts (used in this work but not listed in Tables 8.1 – 8.3) in Table 8.4. The polymerization behavior was affected more significantly by the support rather than the Al and Zr loadings of the catalysts. Catalysts HH09 and HH13–HH15 used a common support (PE971124); the four catalysts behaved as Group-3 in spite of the composition differences. Similarly, Catalysts HH19 and HH25–HH27 (HayeSep-R supported) all exhibited the characteristics of Group-1.

Table 8.4 Classification of catalysts into Groups 1-3 according to polymerization activity (approximate run conditions: trace TIBA, 80°C, 1.4 MPa, and 15 mol/m^3 1-C_6H_{12})

Catalyst	Group assigned (approx.)	Average polymerization activity, kg ethylene/(g cat·h)			Comment
		Homopol.	Copolym.	Ratio	
HH01	–	–	35-480	–	No comparative homopol. run
HH02	–	–	–	–	Not active
HH03	2	10.0	9.5	1.0	Homopol. Run with TIBA
HH04	–	–	–	–	Not active
HH05	1	7.7	66.1	8.6	160g NaCl used in homopol. run
HH06	3	205.6	257.7	1.3	6 mL hexene; at 3 mL ratio = 1.6
HH11	3	148.6	177.1	1.2	4 mL 1-hexene
HH12	2	175.6	422.5	2.4	4.33 mL
HH13	3	–	100-1702	–	No homopolymerization run
HH14	3	570.5	835.8	1.5	4.5 mL
HH15	3	552.8	1196.0	2.2	4.3 mL with TIBA
HH16	2	243.3	541.8	2.2	
HH19	1	41.9	548.7	13.1	4.72 mL
HH20	1	60.4	396.6	6.6	4.5 mL
HH23	–	1264.1	5549.0	4.4	4.5 mL unsupported complex
HH24	–	1803.0	2606.2	1.4	4.5 mL unsupported complex
HH25	1	3.2	84.6	26.4	4.5 mL
HH26	1	9.1	180.8	19.9	4.9 mL
HH27	1	22.4	90.3	4.0	Ratio with TIBA is 14.7
HH28	–	49.0	–	–	No homopolymerization run
HH29	2	59.0	129.1	2.2	

The above observations strongly suggest that the support/catalyst properties affected the polymerization activity of the polymer-supported catalysts. The presence of 1-hexene modifies the polymerization activity and the morphology of the resulting polymer particles. Further investigation on the mechanism of supported-catalyst/comonomer interaction was performed using additional comonomers and polymerization conditions and presented below.

8.2 Interaction between support fragility and comonomer in the development of product morphology during gas-phase polymerization

8.2.1 Catalyst fracture during ethylene homopolymerization

The morphology of polymer particles observed in Section 8.1 did not vary appreciably with polymerization conditions. Figures 8.21 and 8.22 show the morphology of ethylene homopolymer (Catalyst HH07) and ethylene/1-hexene copolymer (Catalyst HH18) particles produced at different temperatures. The morphology of polymer particles produced with Catalyst HH07 at different ethylene pressures is shown in Figure 8.23. The size of the catalyst cores in the low- and moderate-activity homopolymer particles are within the size range of the catalyst particles; hence, there is no conclusive evidence of fracturing of the catalyst particles based on the core size. The outer polymer shell or the artichoke-like polymer layer could have (at least partly) formed from the layer of metallocene/MAO left on the surface of the catalyst particle during the catalyst-drying step. This hypothesis is further supported by the fact that Catalysts HH07 and HH16 that have the metallocene/MAO film developed the hollow-shell polymer morphology. However, Catalysts HH10 and HH18 with no apparent films [Figures 4.13(f) and 4.14(d)] developed the artichoke-like morphology, Figures 8.5(b) and 8.6(b).

In addition to the outer polymer shell, most of the product particles from Group-2 catalysts have second polymer layers that did not separate from the catalyst core, see Figure 8.21(d and f). It is likely that this second polymer layer and the polymer layer from Group-1 catalysts are due to the initiation of a sequential shell-by-shell fragmentation of the catalyst particles from the outer surface to the center as proposed by Bonini *et al.*, (1995). However, the fragmentation process stops before any noticeable reduction in the size of the catalyst core was achieved.

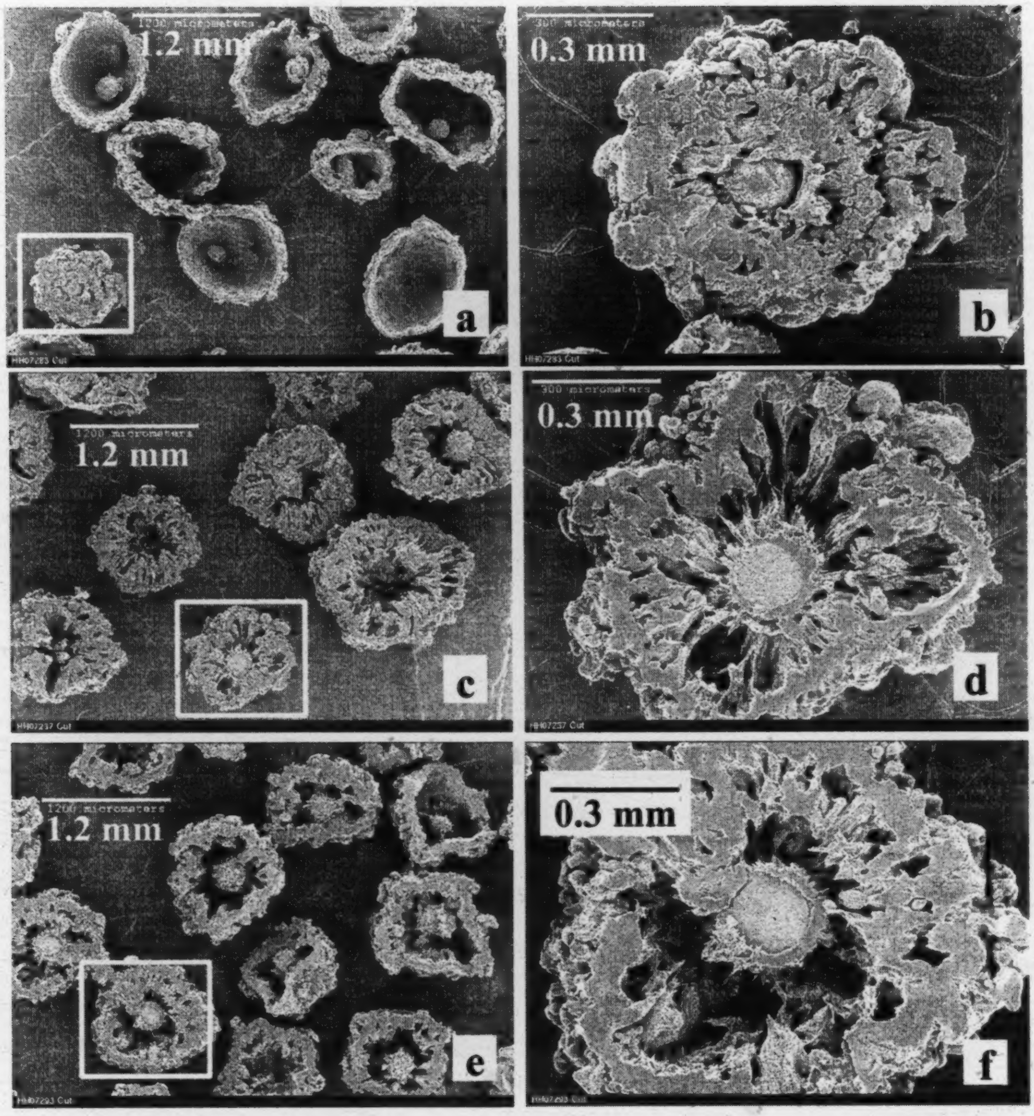
1200 micrometers
1.2 mm
a
HH07283 Cut
300 micrometers
0.3 mm
b
HH07283 Cut
1200 micrometers
1.2 mm
c
HH07237 Cut
300 micrometers
0.3 mm
d
HH07237 Cut
1200 micrometers
1.2 mm
e
HH07293 Cut
0.3 mm
f
HH07293 Cut

Figure 8.21 Morphology of cross-sections of ethylene homopolymer particles produced with Catalyst HH07 in Runs (a and b) HH07283 at 60°C, (c and d) HH07237 at 80°C, and (e and f) HH07293 at 100°C gas-phase temperature.

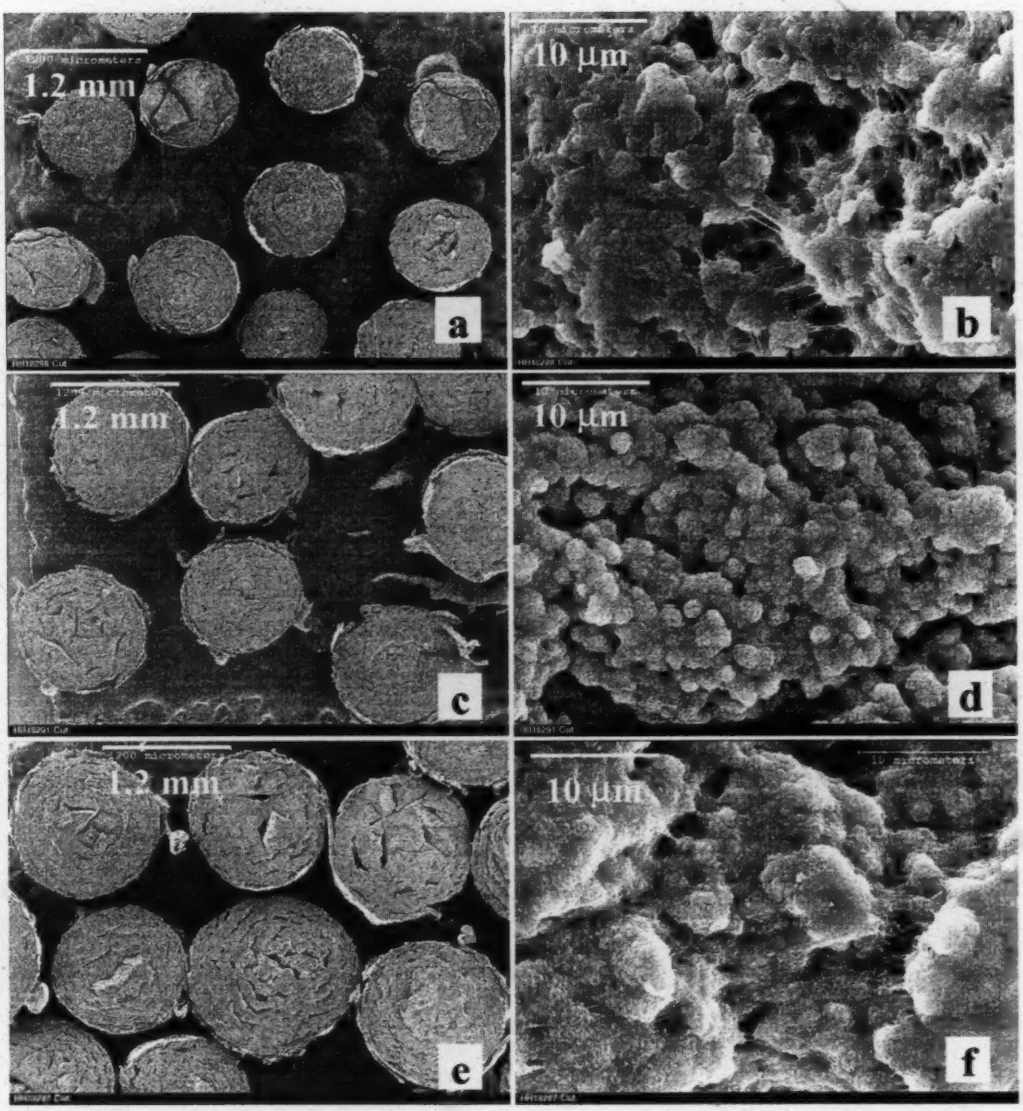
1.2 mm
a
10 µm
b
1.2 mm
c
10 µm
d
1.2 mm
e
10 µm
f

Figure 8.22 Morphology of cross-sections of ethylene/1-hexene copolymer particles produced with Catalyst HH18 in Runs (a and b) HH18288 at 70°C, (c and d) HH18291 at 80°C, and (e and f) HH18287 at 90°C gas-phase temperature.

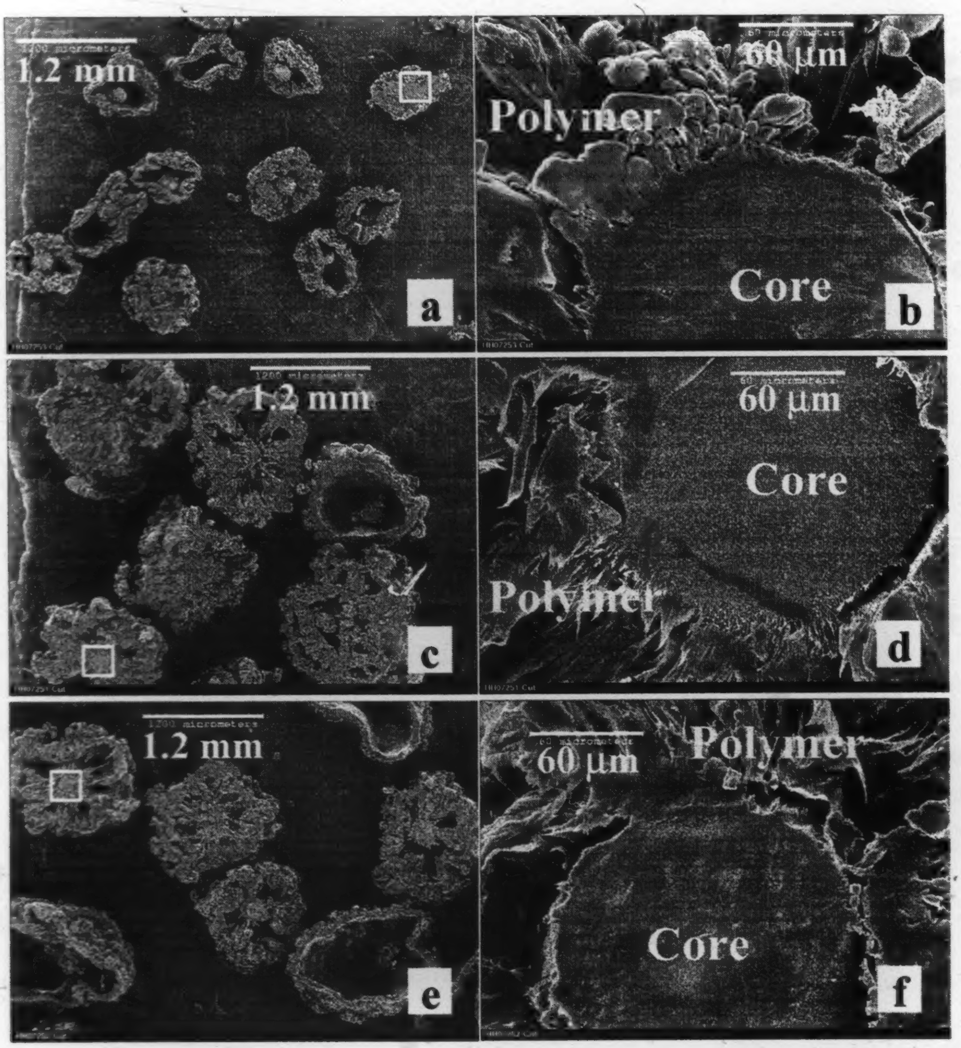
1200 micrometers
1.2 mm
a
60 micrometers
60 µm
Polymer
Core
b
1200 micrometers
1.2 mm
c
60 micrometers
60 µm
Core
Polymer
d
1200 micrometers
1.2 mm
e
60 micrometers
60 µm
Polymer
Core
f

Figure 8.23 Morphology of ethylene homopolymer particles (cross-sections) produced with Catalyst HH07 in Runs (a and b) HH07253 at 1.4 MPa, (c and d) HH07251 at 2.1 MPa, and (e and f) HH07252 at 2.8 MPa ethylene, and 80°C gas-phase temperature.

A closer examination of cross-sections of the homopolymer particles (low and moderate activity) suggest that when the catalyst particles are exposed to ethylene in the reactor, the polymerization starts and the outer shells of the catalyst particles fragment into chunks of polymer globules. Unlike the model of Bonini *et al.* (1995) where initially only the outer shell of catalyst is active, in the current postulate, the initial polymer formation occurs throughout the catalyst particle. However, the growing polymer that holds the fragmented chunks together also fills the pores in the unfragmented catalyst cores. The pore fill-up by high density (high crystallinity) polyethylene significantly reduces monomer access to active sites while the strength of the catalyst matrix prevents further fragmentation of the catalyst particles; poor break-up catalysts are more prone to mass transfer resistance at the microparticle level (Floyd *et al.*, 1987). Subsequently, the polymerization rate remains very low for want of monomer (Webb *et al.*, 1991; McKenna and Mattioli, 2001) as observed with silica-supported Phillips catalysts (McDaniel, 1981; Dalla Lana *et al.*, 1992). Webb *et al.* (1991) noted that polymer yield of 0.1 g/g-cat rendered the active sites on a silica-supported chromium oxide catalyst inaccessible to ethylene.

Polymer continues to grow slowly on the fragmented catalyst layer above. This growth pushes the fragmented chunks apart, thereby stretching the interconnecting polymer to cold-drawn fibrils (see Figure 8.24). Formation of stretched fibers due to growth of polyethylene particles was reported for conventional Ziegler-Natta (Muñoz-Escalona *et al.*, 1984) and supported metallocene catalysts (Janiak and Rieger, 1994).

The fracture of the outer shell of catalyst into fragments of polymer globules, and the pore fill-up in the resulting fragments was inferred from observation of the particle morphology. The fill-up of pores in the unfragmented catalyst core cannot be similarly inferred; however, the surface area of the low yield polymer particles were too low to be measured reliably by nitrogen adsorption. This implies that the (initially high) surface area of the catalyst was lost during the low yield polymerization. Since the catalyst cores are not sealed by the attached polymer layer (Figure 8.23), the observed loss of surface area could only be explained by plugging of the catalyst pores by polymer. In addition, the catalyst cores were easily hand-sectioned with a scalpel, an action that would normally crumble the original catalysts particles. Thus, the assemblage of particles that formed the support/catalyst particle is held together by the elastic polymer formed in the interstitial space between them.

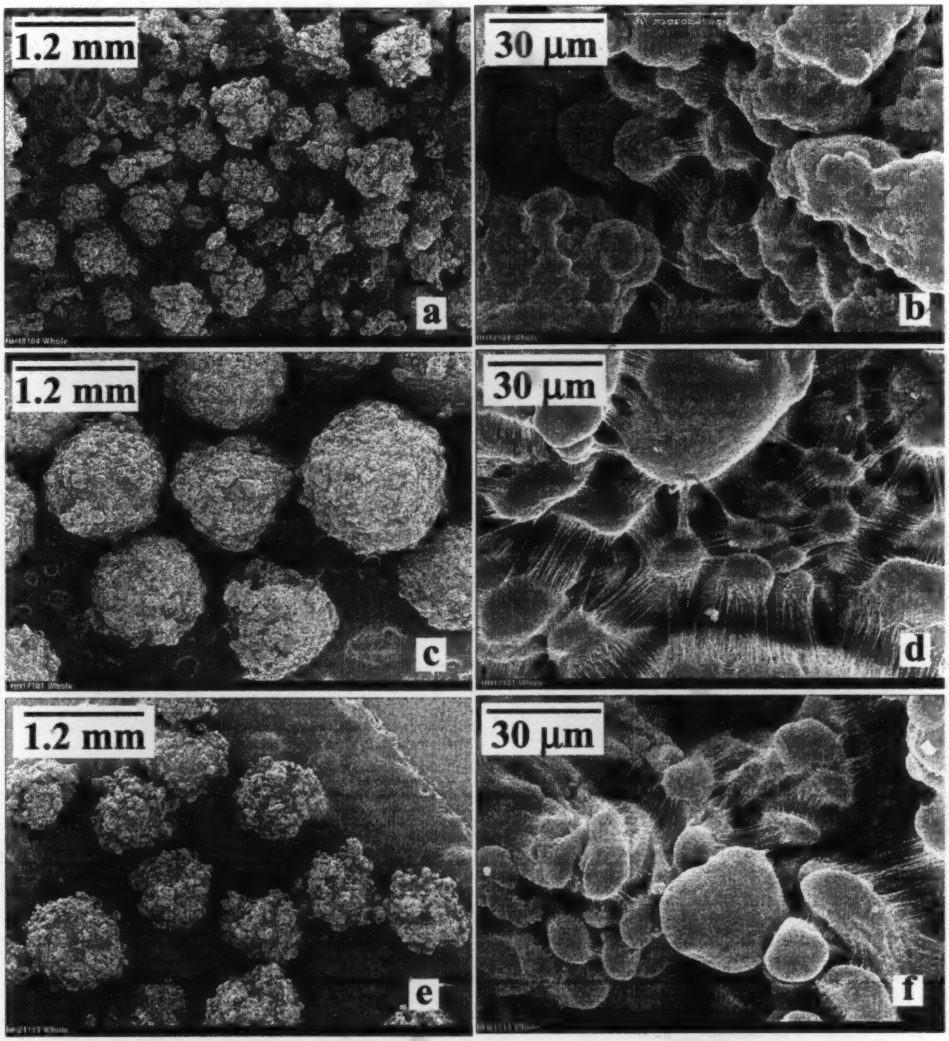

Figure 8.24 External surface morphology of ethylene homopolymer particles produced at 200 psi and 80°C with Catalysts (top) HH18 100g/g, (center) HH17 230 g/g, and (bottom) HH21 210g/g

Once the ethylene transport hindrance (by the high crystallinity polymer plugging the pores of the catalyst cores) is established, remedial actions such as manipulating polymerization conditions are ineffective. Ethylene homopolymerization at 2.8 MPa showed no activity [kg-C_2H_4·(g cat·h)$^{-1}$] improvement over the run at 1.4 MPa (cf. Runs HH18247 and HH18104). Although the two runs were performed more than one year apart, catalyst deactivation due to aging is not likely responsible for the observed low activity because ethylene/1-hexene copolymerization around the same time yielded higher activity. In addition, injecting 1-hexene after 15 min of ethylene homopolymerization with Catalyst HH19 did not improve the polymerization activity (Run HH19173).

The high ethylene homopolymerization activity catalysts (Group-3 in Section 8.1) fracture differently from the above during ethylene homopolymerization. The morphology of these catalysts is a (relatively) loose aggregation of interconnected globules. The identity of the globules is conspicuous (Figure 8.25). This type of support morphology is usually obtained with high monomer/porogen compatibility in the support preparation recipe (Sherrington, 1998). The monomer/porogen compatibility and the high fraction of porogens used during the support preparation ensured wide pore size distribution and good pore volume. Therefore, this group of catalysts is more friable than the ones in Group-1 and Group-2 (see Sections 4.1 and 4.6).

When the Group-3 catalysts are exposed to ethylene in the reactor, polymerization and catalyst fragmentation commences throughout the catalyst particle as in the widely used multigrain model, MGM (Hutchinson *et al.*, 1992). The high friability of these catalysts enables the fragmentation process to keep pace with the polymerization rate;

hence, polymer grows evenly in the polymerizing particle and the particle macroporosity is maintained. At high polymerization rates, ethylene transport into the particle occurs by both convection and diffusion. Thus, the presence of nitrogen (inert gas) influenced the polymerization activity due to the enrichment effect (see Figure 6.13).

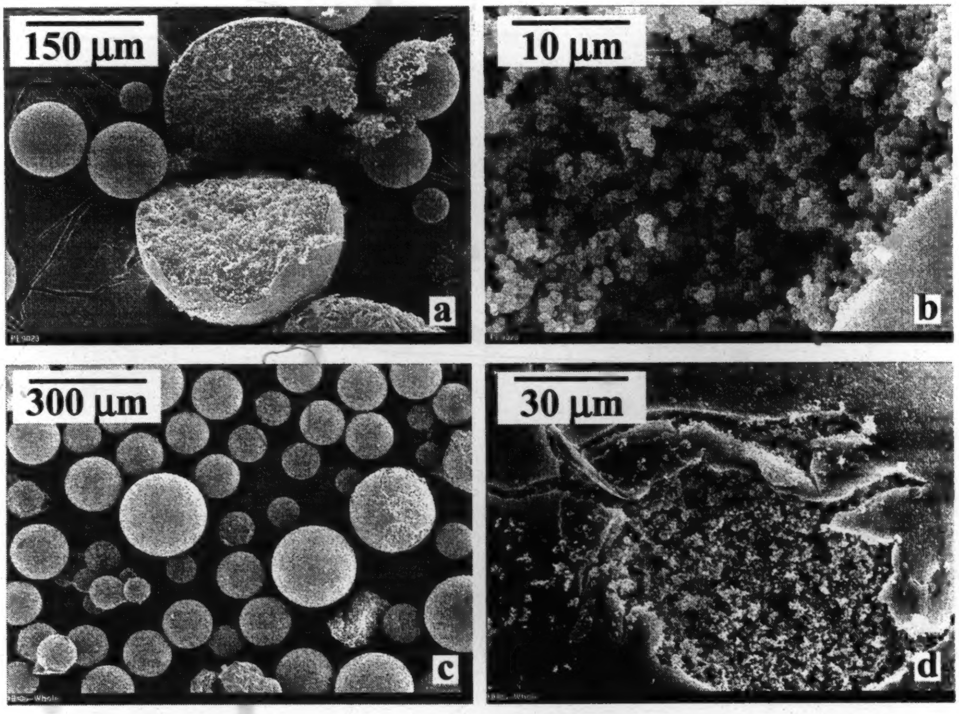

Figure 8.25 Morphology of the high friability (a and b) support –PE9023, and (c and d) the corresponding catalyst HH06

8.2.2 Catalyst fracture during ethylene/α-olefin copolymerization

Fragmentation of catalyst particles during ethylene/α-olefin copolymerization over the Group-1 and Group-2 catalysts (Section 8.1) starts like the fragmentation during ethylene homopolymerization. However, instead of the drop in activity due to pore fill-up and lack of catalyst fracture observed in homopolymerization, the shell-by-shell fragmentation continues until the catalyst particle is fully fragmented. The major difference with the model proposed by Bonini *et al.* (1995) is that each polymer shell physically separates from the remaining catalyst core. This mechanism results in the concentric-shell morphology of the polymer particles.

The separation of the polymer shells from the catalyst core is due to the differential growth rates of the inner and outer parts (induced by mass transfer limitation) in the polymerizing particles. The differential growth rate builds up localized stress in the affected parts of the polymerizing particle. When the resulting elastic tension exceeds the yield point of the material, the outer shell separates, thereby relaxing the tension (Kittilsen *et al.*, 2001).

The shell-by-shell fragmentation takes place over a few minutes. Figure 8.26(a) shows that several polymer layers have already formed during 1 min of copolymerization with Catalyst HH10, but the catalyst core remains. The shell formation was completed within 10 min of polymerization (Figure 8.27a), but the polymer shells are still thin. Further polymerization increased the shell thickness through polymer accumulation (Figure 8.28a).

Observation of the surfaces of the inner polymer shells at higher magnification gives more insight into the fragmentation mechanism. The surfaces of the inner shells of the polymer particles are not affected by the continuous impact with other polymer particles, reactor wall/internals, or the seedbed (NaCl) particles during polymerization. Therefore, these surfaces retain the memory of the fracture mechanism. Figure 8.26 (b) shows the early catalyst fracture (possibly) into chunks of several globules. As the polymerization proceeds, further fracturing of the fragmented chunks and the catalyst core takes place, and spherical globules begin to emerge (Figure 8.27 b and 8.28 b).

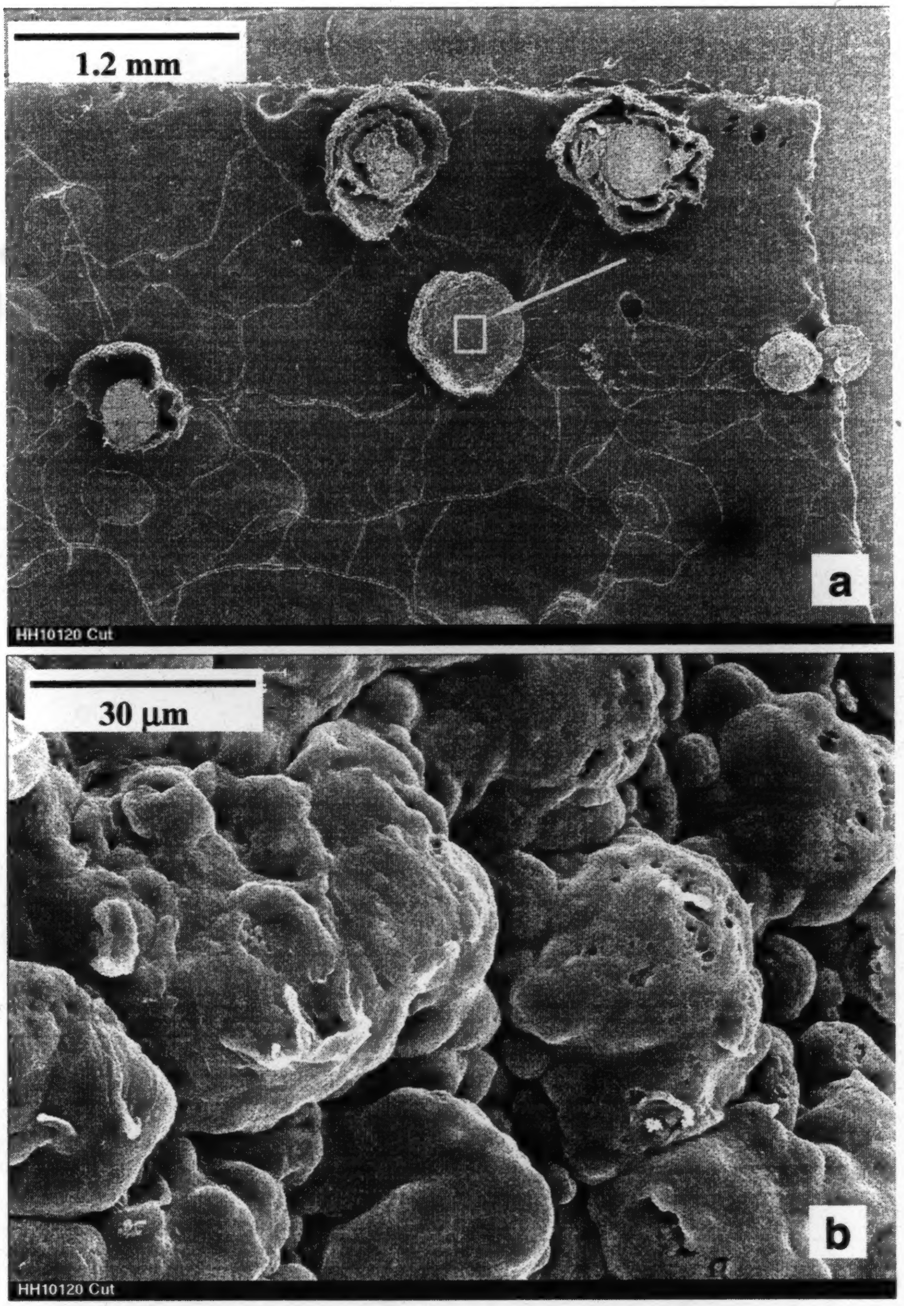
1.2 mm
a
HH10120 Cut
30 µm
b
HH10120 Cut

Figure 8.26 Morphology of Catalyst HH10 particle after 1 min copolymerization (Run HH10120). Arrow shows the section of micrograph (a) magnified in (b).

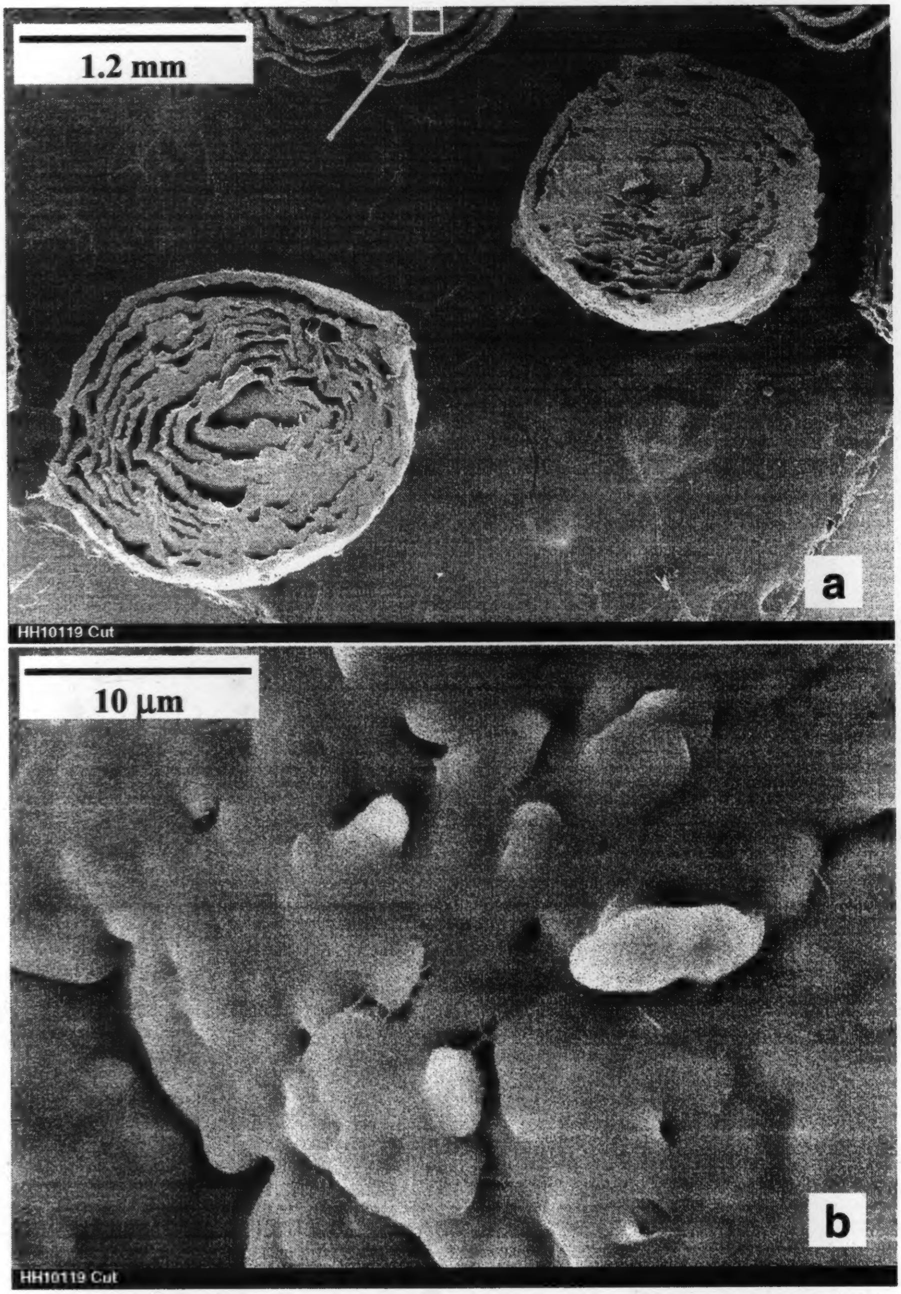
1.2 mm
a
HH10119 Cut
10 µm
b
HH10119 Cut

Figure 8.27 Morphology of Catalyst HH10 particle after 10 min copolymerization (Run HH10119). Arrow shows the section of micrograph (a) magnified in (b).

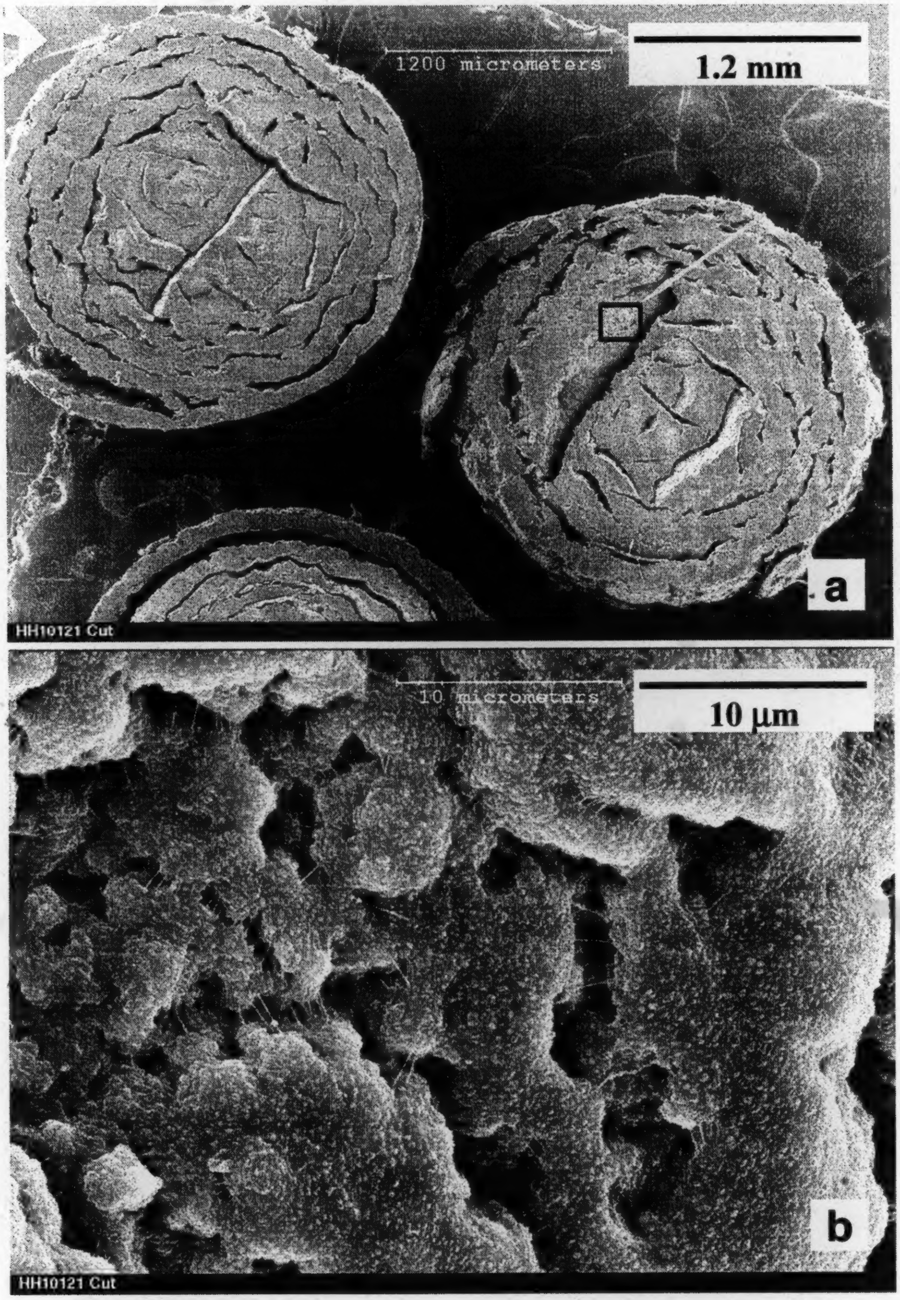
1200 micrometers
1.2 mm
a
HH10121 Cut
10 micrometers
10 µm
b
HH10121 Cut

Figure 8.28 Morphology of Catalyst HH10 particle after 1.75 h copolymerization (Run HH10121). Arrow shows the section of micrograph (a) magnified in (b).

The presence of comonomer at the beginning of polymerization drives the sequential fracturing of the catalyst particles to completion during ethylene/α-olefin copolymerization. As the outer polymer shell is formed, diffusion of ethylene and to a lesser extent, the α-olefin in the amorphous phase of the copolymer (formed in the pores of the catalyst core) maintains adequate monomer/comonomer access to the active sites. This continues the polymerization reaction and fracturing of the next polymer shell. As each shell separates from the catalyst core, the newly generated surfaces become exposed to the bulk monomer concentration because the shells are porous. At high yields, the Group-1 and Group-2 catalyst particles are completely fragmented and the secondary particles (globular morphology) are quite distinct (see Figure 8.29 a and b). This globular morphology is similar to the globular structure observed in the homo- and copolymer particles of Group-3 catalysts (see Figure 8.29 c and d).

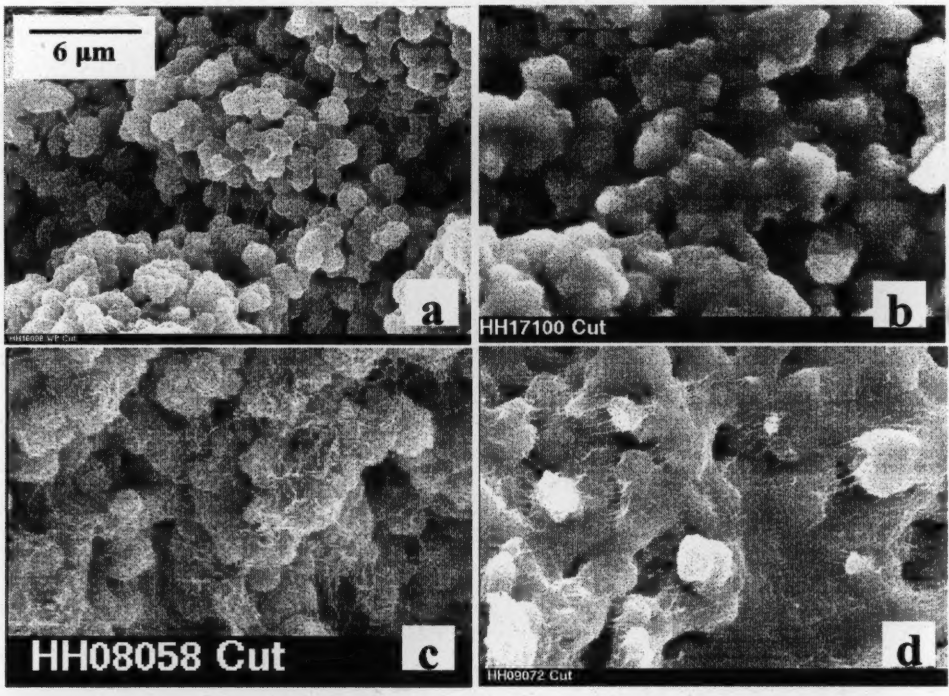

Figure 8.29 Morphology of ethylene/1-hexene copolymers of (a) Group-1 and (b) Group-2 catalysts, and the homo- and copolymer of Group-3 catalysts (c and d respectively) showing the globular structure.

The morphology of catalysts in Group-1 to Group-3, and the friabilities of the corresponding supports are compared in Table 8.5. The main difference between Group-3 catalysts and the Groups-1 and 2 is the support morphology. Group-3 catalysts are generally more fragile. Although Group-3 catalysts tend to have lower total pore volume and larger average pore size, the difference is too small for reliable conclusions. During polymerization, the ease of catalyst fracturing enhances transport of monomer/

Table 8.5 Support friability and the morphology of supported catalysts

Catalyst		Catalyst Morphology			Support Friability, %
Class	Number	Surface Area, m^2/g	Pore volume, cm^3/g	Pore radius, nm	
Group-1	HH05	23	0.04	2.56	ND
	HH10	237	0.68	6.87	ND
	HH18	258	0.38	7.15	19.4
	HH19	204	0.57	5.31	18.1
	HH20	210	0.44	9.42	15.3
	HH22	443	0.54	3.43	23.7
	HH25	217	0.38	4.72	18.1
	HH26	279	0.38	5.18	18.1
	HH27	136	0.20	6.44	18.1
	HH28	194	0.27	5.65	18.1
Group-2	HH03	0.0	0.01	–	–
	HH07	112	0.26	4.31	16.0
	HH12	11	0.10	7.07	43.0
	HH16	86	0.28	6.93	ND
	HH17	145	0.37	6.16	27.3
	HH21	303	0.34	4.39	22.1
	HH23	10	<0.01	1.83	–
	HH24	ND	ND	–	–
	HH29	low	–	–	ND
Group-3	HH06	15	0.14	18.30	43.8
	HH08	90	0.13	2.96	49.7
	HH09	74	0.33	6.82	66.0
	HH11	low	0.05	39.61	ND
	HH13	15.3	0.14	6.00	66.0
	HH14	80	0.22	5.28	66.0
	HH15	72	0.50	7.07	66.0

ND – not determined

comonomer molecules by convection and diffusion thereby maintaining a more homogeneous growth rate over the entire particle. This minimizes the shell formation (Figures 8.18-8.20). However, even for these catalysts, high loading of the active precursor may result in the concentric-shell morphology for the following reasons: Rapid polymerization rate in the catalyst particle creates radial monomer concentration gradient, this will be further exacerbated by the increased pore blockage by the catalyst components (Figure 4.11). Thus, Catalyst HH15 has higher tendency to form the concentric-shell particles than Catalyst HH09 made with the same support.

The polymerization runs summarizing further effects of comonomer on polymerization activity and polymer morphology are given in Table 8.6. In addition to 1-hexene, propylene and 1-decene were used because the molar mass and diffusivity of 1-hexene lies between those of propylene and 1-decene.

Table 8.6 Influence of comonomer on activity of catalysts.

Run number	Amount charged in reactor				Initial comono. content, mol. %	Activity, g Polymer/(g cat·h)			t_{Rmax}[a], min
	Comonomer[b]		Catal., mg	TIBA[c], mmol					
	Type	mL[g]				Avg.[d]	Max.[e]	A_C/A_H[f]	
HH26181	–	–	75.0	Trace	–	9	31	–	6
HH26182	1-C_6H_{12}	5	100.3	0.20	4	181	214	19.8	58
HH26194	C_3H_6	33	101.0	0.20	17	472	627	51.6	71
HH26272	C_3H_6	153	82.0	0.59	100	35	–	–	–
HH15095	–	–	69.5	0.28	–	553	921	–	37
HH15192	C_3H_6	10	61.1	0.28	5	419	1648	0.8	2.5
HH15193	C_3H_6	32	63.0	0.28	16	1755	1800	3.2	10
HH15117	1-C_6H_{12}	4	59.7	0.20	3.2	1196	1897	2.2	21.2
HH15162	1-$C_{10}H_{20}$	7	60.3	0.20	3.7	542	663	1.0	42

a–f: see notes of Table 8.1; g: amount of propylene in psia

Figure 8.30 compares the activity of Catalyst HH26 in ethylene homopolymerization to ethylene/propylene, and ethylene/1-hexene copolymerization. The activity of Catalyst HH26 (Group-1 type) increased 20 times in the presence of ~4 mol percent (initial) 1-hexene in the reactor. The activity increase is even higher (50 times) with 17 mol percent propylene initially present in the reactor. For all the catalysts tested, decrease in activity with increasing amounts of 1-hexene in the reactor occurs at much lower concentration than the 17 mol percent observed with propylene. Surprisingly, the catalyst exhibited low activity during propylene homopolymerization (Run HH26272, Table 8.6). The propylene homopolymerization was run at a lower pressure and higher amount of residual TIBA, but these are not likely the cause of the observed activity difference.

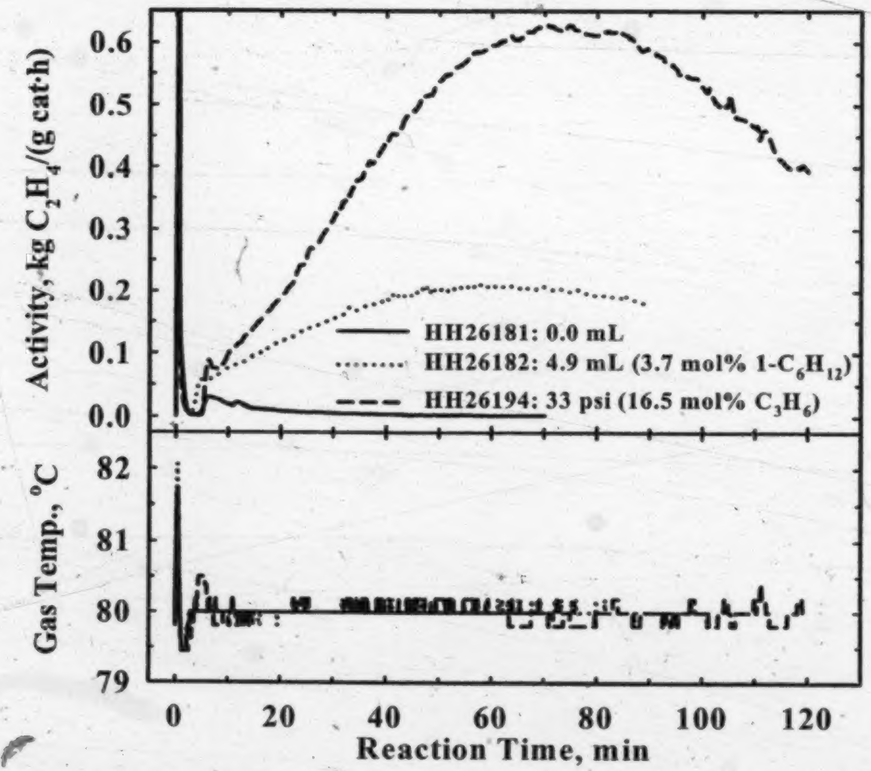

Figure 8.30 Effect of comonomer on the polymerization activity of Catalyst HH21 (total pressure ≈ 1.4 MPa)

Catalyst HH15 was prepared using the same support as HH09 (Group-1 type), but with higher Al and Zr loadings, and lower Al:Zr ratio than HH09. Figure 8.31 shows that the presence of propylene resulted in marked change in the activity profile of Catalyst HH15 relative to ethylene homopolymerization. The high polymerization activity observed at relatively high mole fraction of propylene supports the ease of ethylene insertion in a growing chain Polymer–Zr. The rapid increase in initial activity could be due to physical enhancement of monomer access to the catalyst sites, or chemical

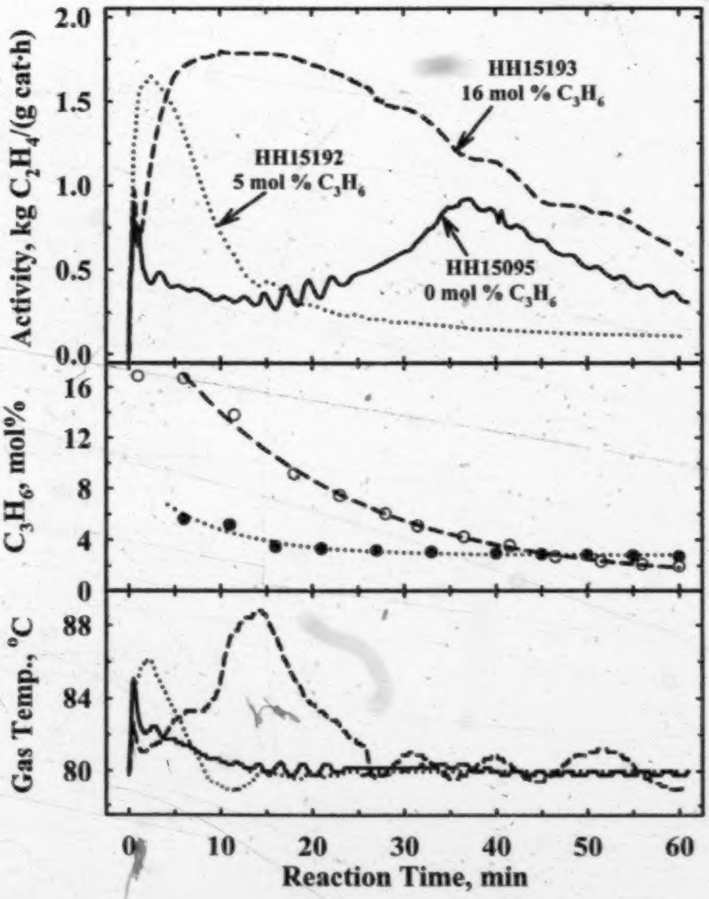

Figure 8.31 Effects of propylene on ethylene/propylene copolymerization activity of Catalyst HH15 (total pressure ≈ 1.4 MPa).

activation of some sites that were initially dormant towards ethylene. Note that despite the higher Zr loading of Catalyst HH15 over HH09, it is less active than the latter. It is possible that, higher Zr loading and lower Al:Zr ratio resulted in the formation of the dormant homodinuclear metallocene complex in Catalyst HH15. Regardless of the reason for increased activity in the presence of propylene, the activity decreases with the depletion of propylene in the reactor (see the middle panel of Figure 8.31).

The morphologies of ethylene homopolymer, and ethylene/propylene copolymers of Catalyst HH15 are compared in Figure 8.32; while the ethylene homopolymer has

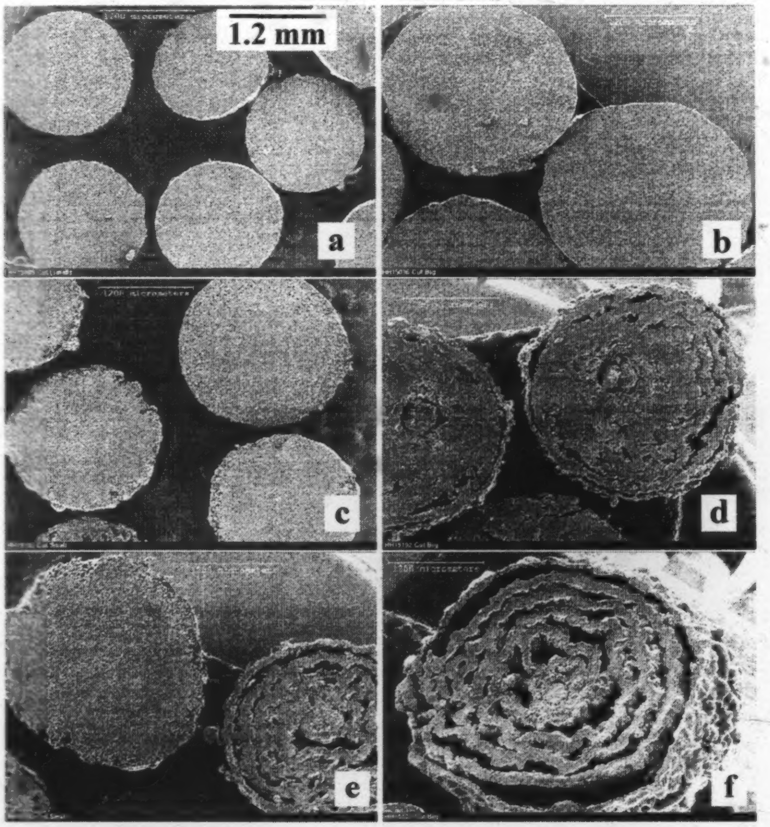

Figure 8.32 Influence of propylene on polymer particle morphology (a and b) Run HH15095, no comonomer; (c and d) Run HH15192, 5 mol % C_3H_6; (e and f) Run HH15193, 16 mol % C_3H_6.

uniform particle morphology (Figure 8.32 a and b), the copolymer with propylene showed increasing tendency of forming the concentric shells structure with increasing size of catalyst particle [Figure 8.32(c vs. d), and (e vs. f)] and amount of propylene in the reactor [Figure 8.32(c, d vs. e, f)]. The morphology of ethylene/propylene copolymer of Catalyst HH26 (Run HH26194, Figure 8.33) shows the formation of the onion-ring structure, but this is not well defined as in ethylene/1-hexene copolymers.

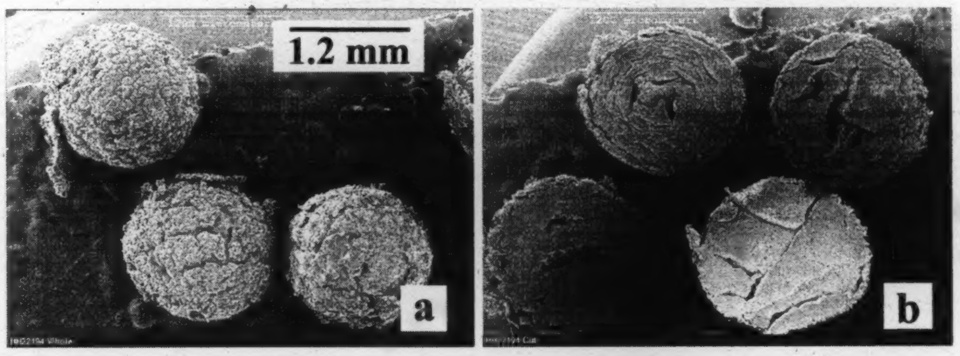

Figure 8.33 Morphology of ethylene/propylene copolymer particles produced with Catalyst HH26 in Run HH26194 (a) external surface, and (b) cross-section.

Figure 8.34 shows that 1-hexene also enhances the activity of Catalyst HH15, but the activation is delayed relative to propylene (cf. Figure 8.31). Poor temperature control contributed to the observed high activity of Run HH15117. The activity profile of ethylene/1-decene copolymerization resembles that of homopolymerization, but is slightly less active (Run HH15162). The lower activity is likely due to hindered ethylene access to the active sites by films of liquid 1-decene on the catalyst surface. At the 80°C reactor temperature, the vapor pressure of 1-decene is less than 1 psi; hence, most of the 7 mL of 1-decene injected in the reactor did not vaporize.

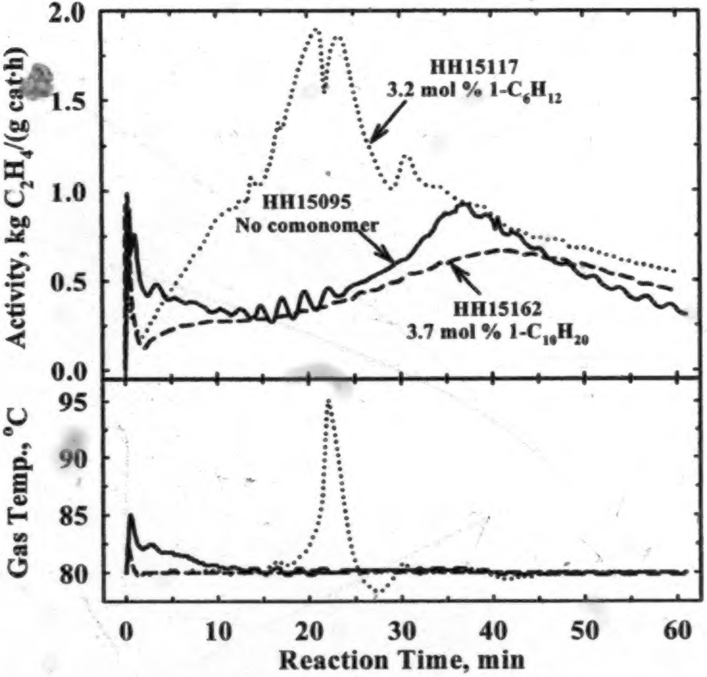

Figure 8.34 Influence of 1-hexene and 1-decene on the activity of Catalyst HH15 at 80°C and 1.4 MPa.

Ethylene/1-hexene copolymer particles form more shells than the ethylene/ propylene particles [cf. Figures 8.35a to 8.32(d and f)]. The smaller size of propylene enables it to diffuse more competitively with ethylene in the polymer matrix. This reduces the extent of differential growth across the particle, and hence the shell development. The larger 1-decene molecules behave differently from propylene and 1-hexene. In ethylene/1-decene copolymer particles, the shells are more developed in the smaller particles than the larger ones, Figure 8.35 (b and c). In the larger particles, shell formation occurs on the outer parts of the particle only. The morphology of the inner core resembles that of ethylene homopolymer particles. It is likely that the 1-decene could not diffuse fast enough to reach the inner core of the particles. This 'filtering effect' resulted in copolymer product of wide chemical composition distribution; TREF profile of the ethylene/1-decene copolymer revealed the presence of both short chain branched copolymer and homopolymer fractions (see Chapter 9).

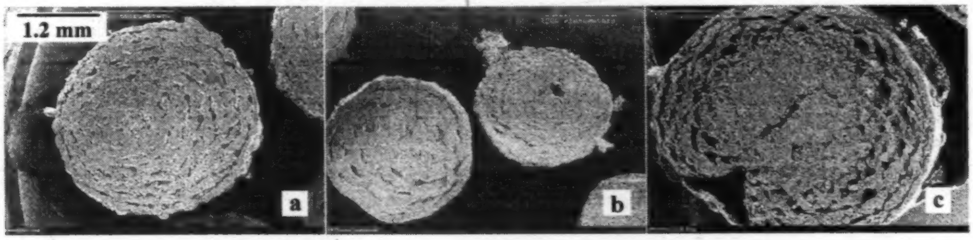

Figure 8.35 Influence of comonomer on particle morphology (a) Run HH15093, 3.2 mol% 1-hexene, (b and c) Run HH15162, 3.7 mol% 1-decene. Scale bar = 1.2 mm

Summary of the influence of comonomer on catalyst activity and product morphology

The influence of 1-hexene on polymerization activity of the supported catalysts depended on the supports. The polymerization activities of catalysts supported on low friability supports were significantly improved by the presence of 1-hexene. The supports cross-linked by linear segments such as EGDM, which also have slightly better friability show only moderate activity improvement in ethylene/1-hexene copolymerization compared to ethylene homopolymerization. The high friability supports produced catalysts with high ethylene homopolymerization activity. These catalysts show little or no activity enhancement by 1-hexene.

The following catalyst fracture mechanism was proposed based on the observed morphology of the polymer particles: For low friability catalysts, lack of fracturing causes the catalyst pores to be filled up by high crystallinity polyethylene at the beginning of the polymerization (Figure 8.36a). This severely limits ethylene diffusion into the catalyst macroparticles; hence, polymerization activity remains low. The rapid catalyst fragmentation rate of high friability catalysts ensures adequate porosity in the polymerizing particles; hence, high ethylene homopolymerization activity and uniform fracturing of the catalyst particles result (Figure 8.36b). During ethylene/α-olefins polymerization, moderate monomer diffusion rate in the low crystallinity LLDPE results in differential expansion rate of the polymerizing particle. This leads to a layer-by-layer fragmentation of the catalyst particle (Figure 8.36c) that results in the onion-rings like morphology of the polymer particle. The tendency of the catalyst particles to form the onion-rings like structure decreased with increasing catalyst (support) friability.

The activity enhancement by comonomer reaches a maximum that is catalyst specific, beyond the optimum amount of comonomer, activity decreased. Polymerization activity enhancement by comonomer decreased with increasing comonomer size due to the diffusivity and the reactivity of the comonomers.

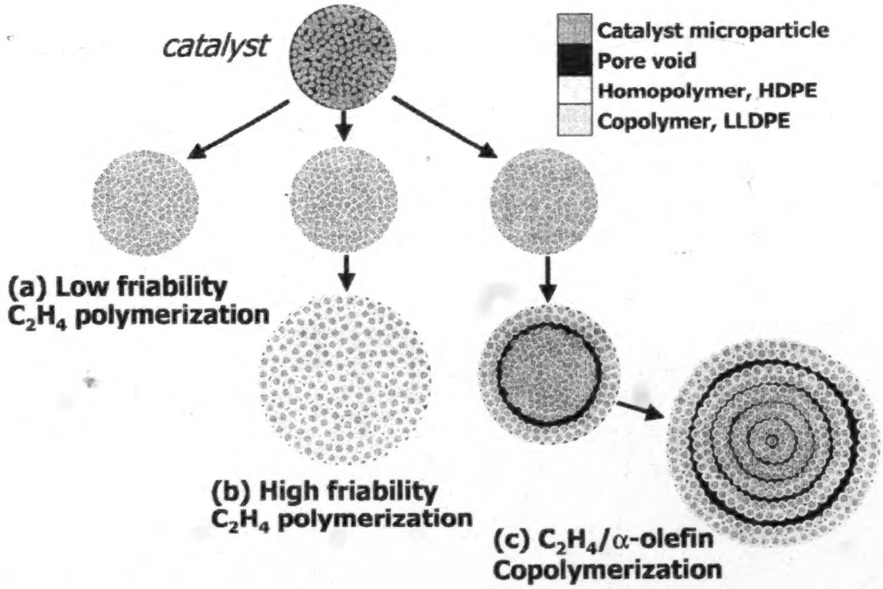
catalyst
Catalyst microparticle
Pore void
Homopolymer, HDPE
Copolymer, LLDPE
(a) Low friability
C₂H₄ polymerization
(b) High friability
C₂H₄ polymerization
(c) C₂H₄/α-olefin
Copolymerization

Figure 8.36 Proposed fracture mechanism of low and high friability polymer-supported metallocene/MAO catalyst particles during gas-phase olefins polymerization.

9. Properties of the Polyolefin Products

The morphology and bulk density of nascent polymer particles are very important for stable operation of fluidized bed polymerization reactors and in the post-reactor handling of the polyolefin product. The polymer microstructure determines the suitable processing method and end use application of the product. This chapter discusses the effects of support and reaction conditions on the nascent morphology and the microstructure of the resulting polymers.

Several polymerization runs produced polyolefin particles with differences in physical appearance as well as microstructure. The discussions in this chapter are based on the representative product properties. The differences between polymer particles produced in single polymerization runs are also discussed.

9.1 Morphology and bulk density of polyolefin particles

The friability of catalyst particles plays a vital role in the particle replication process from catalyst to polymer. It was shown in Chapter 8 that support friability also affected the catalyst activity. Polyolefin products from homogeneous process or heterogeneous process with poor catalyst-to-polymer replication often possess low bulk density and irregular particle sizes and shapes. The bulk densities of polyolefin products made with several supported catalysts are summarized in Table 9.1.

The average bulk density of ethylene homopolymer particles produced with the catalysts supported on the in-house supports (0.372 g/mL) is higher than the corresponding value for particles produced with the catalysts supported on the commercial supports (0.305 g/mL). The average bulk densities of ethylene/α-olefin copolymers are similar for both in-house (0.394 g/mL) and commercial supports (0.386

g/mL). For ethylene homopolymers, the bulk density difference is mainly due to the low-density artichoke-like morphology or the hollow shell morphology of polyethylene produced by catalysts supported on the commercial supports; these catalysts did not fracture during ethylene homopolymerization. In addition, the in-house supports have wider particle size distribution resulting in higher bulk density products (smaller particles fit in the interstices between larger ones). The latter effect is not significant since the bulk densities of copolymers are less dependent on the nature of the supports.

Table 9.1 Bulk densities of nascent polyolefin products.

Catalyst ID	Bulk density of polyolefin product*, g/mL							
	Ethylene homopolymer				Ethylene/1-hexene copolymer			
	No. of runs	Average	Lowest	Highest	No. of runs	Average	Lowest	Highest
HH06	1	0.400	–	–	4	0.450	0.421	0.496
HH08	2	0.411	0.408	0.413	10	0.412	0.362	0.455
HH09	20	0.396	0.350	0.449	2	0.411	0.393	0.428
HH10	1	0.313	–	–	5	0.312	0.246	0.368
HH11	1	0.290	–	–	3	0.362	0.334	0.399
HH12	1	0.307	–	–	2	0.360	0.334	0.385
HH13	–	–	–	–	9	0.424	0.356	0.451
HH14	12	0.401	0.340	0.460	6	0.406	0.384	0.441
HH15	4	0.393	0.364	0.404	10	0.412	0.360	0.455
HH15**	4	0.441	0.420	0.456	–	–	–	–
HH23	8	0.302	0.270	0.330	1	0.380	–	–
HH23**	2	0.380	0.350	0.410	–	–	–	–
HH24	1	0.290	–	–	1	0.410	–	–
HH07	12	0.281	0.247	0.310	2	0.311	0.273	0.348
HH16	9	0.238	0.180	0.310	4	0.268	0.250	0.300
HH17	1	0.240	–	–	10	0.325	0.260	0.360
HH18	2	0.298	0.285	0.310	13	0.421	0.393	0.480
HH19	–	–	–	–	11	0.417	0.364	0.444
HH20	1	0.257	–	–	3	0.349	0.314	0.380
HH21	1	0.320	–	–	21	0.373	0.310	0.444
HH22	3	0.363	0.294	0.436	8	0.397	0.363	0.450
HH25	–	–	–	–	3	0.443	0.440	0.450
HH26	1	0.350	–	–	3	0.460	0.450	0.480
HH27	1	0.310	–	–	4	0.403	0.370	0.430
HH28	–	–	–	–	2	0.445	0.430	0.460
HH29	1	0.390	–	–	3	0.400	0.360	0.42

*– Bulk densities of individual runs are given in Appendix B, Table B-2

**– Different amounts of hydrogen (chain transfer agent) used in these runs

?

Neither the polymerization temperature, T_p nor ethylene concentration, P_{Et} had any consistent effect on the bulk density, ρ_b of ethylene homopolymer products. For example: ρ_b increased with T_p for Catalysts HH07 and HH09 but not HH23; ρ_b decreased with increase in P_{Et} for Catalysts HH07 and HH23, but not HH09; there was no apparent effect of T_p on ρ_b of ethylene/1-hexene copolymer produced with Catalyst HH18.

There was excellent morphology replication from catalyst to polymer particles except for the ethylene homopolymer particles produced with the low friability commercial supports. The artichoke-like and the hollow shell morphologies above resulted in granular particles of non-uniform surface (see Chapter 8).

The morphology of ethylene/1-hexene copolymer particles of Run HH19123 (Figure 9.1 a and b) is different from all the other polymer particles (made with the same or different catalysts). About 0.29 mmol TEAL in 0.06 mL *n*-hexane, and 4.25 mL 1-hexene were used in Run HH19123 that lasted for 3.5 h. The same catalyst (HH19, in presence of 0.22 mmol TNOA and 4.32 mL 1-hexene) copolymerized ethylene/1-hexene at higher activity in Run HH19125, but with the usual product morphology (Figure 9.1 c and d). Catalyst HH01 (in-house support PE971124) also produced ethylene/1-hexene copolymer with the usual particle morphology in a 3.5 h run using 1.25 mmol TEAL and 3.1 mL 1-hexene (Run HH01015, Figure 9.1 e and f). Therefore, it is difficult to attribute the morphology of the particles produced in Run HH19123 to the run time, polymerization activity, or the TEAL scavenger. Note that organoaluminum compounds were reported to improve the bulk density of polyethylenes produced by Ziegler-Natta catalysts (Muñoz-Escalona *et al.*, 1984).

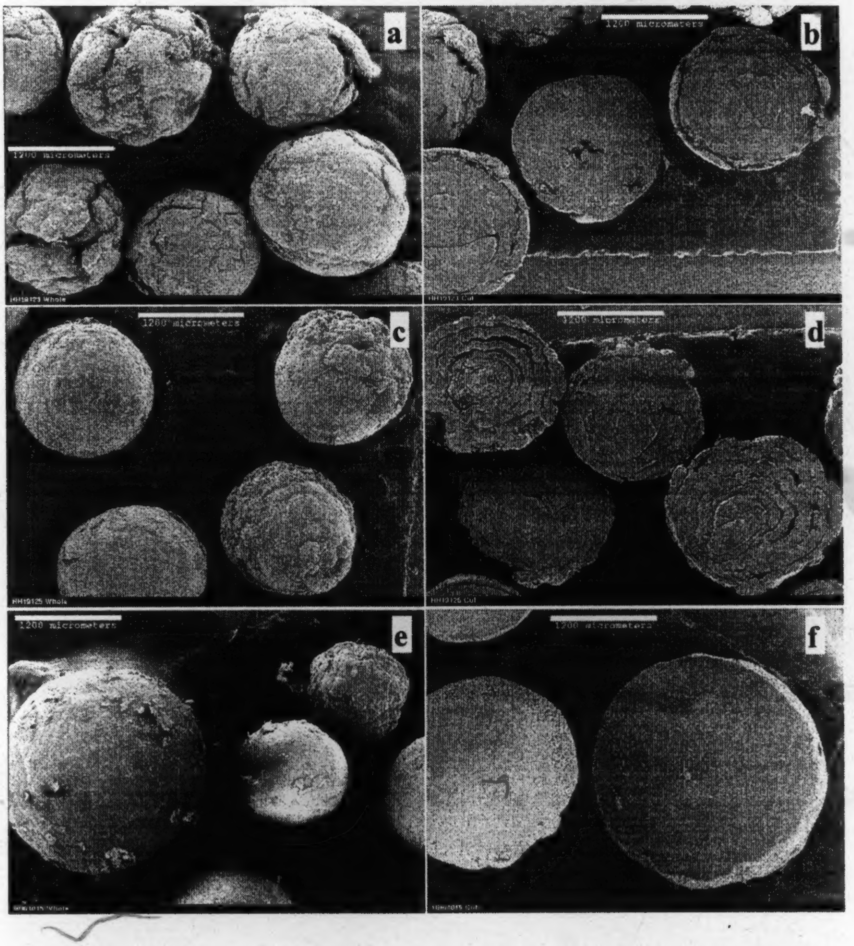
a
1200 micrometers
b
1200 micrometers
c
1200 micrometers
d
1200 micrometers
e
1200 micrometers
f
1200 micrometers

Figure 9.1 External surface (left) and cross-section (right) morphologies of ethylene/1-hexene copolymer particles produced in (a and b) Run HH19123, (c and d) Run HH19125, and (e and f) Run HH01015. Scale bar = 1.2 mm.

Ethylene homopolymerization in the presence of hydrogen resulted in higher bulk density product for both supported catalyst (HH15) and the solid ($(n\text{-BuCp})_2ZrCl_2$/MAO complex (HH23). This may be due to increase in crystallinity of the lower molar mass product; greater mobility of these molecules would result in higher molecular order in the final product (the polyethylene formed in Run HH23249 softened in the reactor). However, further investigation is necessary to ascertain how the presence of hydrogen affected the polymer bulk density.

9.2 Molar mass and polydispersity index

The polyolefin molar masses were affected by polymerization temperature, monomer pressure, particle size, and the concentration of chain transfer agents.

9.2.1 Influence of particle size and monomer pressure on molar mass

The influence of particle size on polymer molar mass for ethylene homopolymers of Catalyst HH09 was investigated at four different ethylene pressures. Catalyst HH09 had a wide particle size distribution (approximately 60 – 300 μm). Three size-groups of the polyethylene particles (large, medium, and small) produced with Catalyst HH09 were selected from each run as shown in Figure 9.2. The molar masses of these size groups are shown in Figure 9.3.

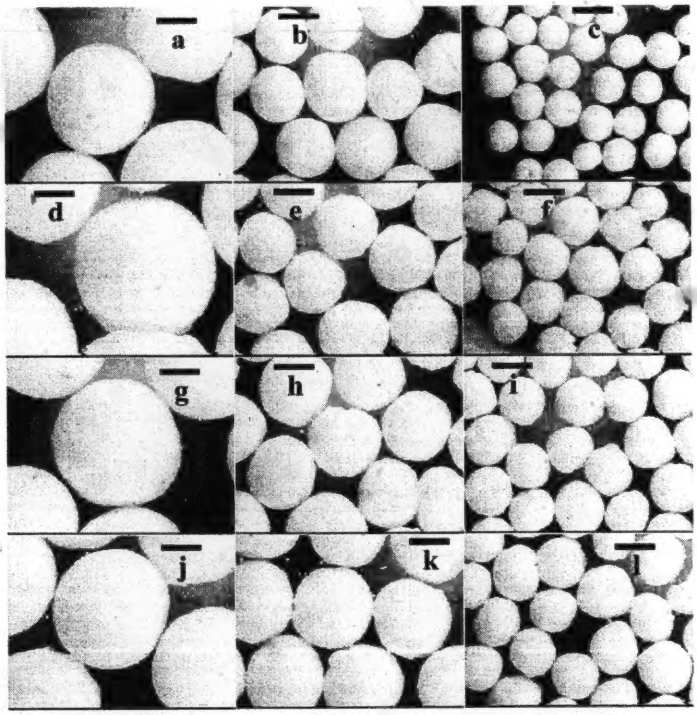

Figure 9.2 Optical images of the three size-groups of ethylene homopolymer particles produced with Catalyst HH09 at 80°C gas-phase temperature and (a-c) 0.7 MPa, (d-f) 1.4 MPa, (g-i) 2.1 MPa, and (j-l) 2.8 MPa ethylene. Scale bar = 1.0 mm.

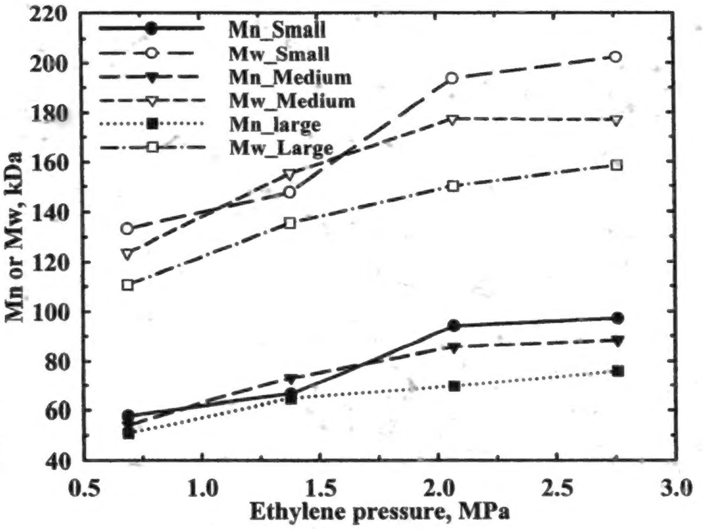

Figure 9.3 Influence of particle size and ethylene pressure on molar masses of polyethylenes produced with Catalyst HH09 (80°C, trace TIBA)

The molar masses of all sizes increased with ethylene pressure. Both the number average and the mass average molar masses decreased with increasing particle size for all runs except for the run at 1.4 MPa. Przybyla *et al.* (1999) attributed both decrease in molar mass and polymerization activity with increasing catalyst particle size for silica-supported *rac*-$Me_2Si[IndR_2]_2ZrCl_2$/MAO system to uneven MAO loading (similar to Figure 4.16a) on the larger catalyst particles. The particles size of Catalyst HH09 (about 60 – 300 μm) are mostly larger than those of Przybyla *et al.* (10 – 80 μm); however, uneven MAO distribution is not likely in Catalyst HH09 because Catalyst HH08 with support of similar morphology to the support of HH09 (cf. Figures 4.5a and 4.13a) did not show the unevenness in MAO distribution (see Figure 4.17 b) even at twice the MAO loading of Catalyst HH09.

Floyd *et al.* (1987) attributed decrease in molar mass with increasing size of Ziegler-Natta catalyst particles to greater mass transfer resistance of monomer relative to hydrogen. This is not applicable to the observed influence of particle size in Figure 9.3 because no hydrogen was used. Monomer diffusion resistance would result in lower molar mass product in the large catalyst particles if chain transfer to monomer were not the predominant chain termination reaction; however, this would also be accompanied by high polydispersity indices. Bulls and Huggins (1970) predicted polydispersity values up to 10 due to monomer concentration variation in catalyst particles. The average polydispersity values of Catalyst HH09 (2.12 ± 0.12) suggest no significant monomer mass transfer resistance. Therefore, the molar mass decreases were likely due to particle overheating. Higher monomer pressure increases the polymerization rate per unit mass of catalyst. This could result in particle overheating and decrease in molar mass; polymer molar mass decreases with increasing polymerization temperature (see Section 9.2.2).

Janiak and Rieger (1994) similarly reported small but consistent decrease in molar mass with increase in particle size for a single batch of polyethylene produced over silica-supported Cp_2ZrCl_2/MAO catalyst slurry in n-heptane at 80°C; however, the polydispersity also decreased with the molar masses. Macroparticle mass transfer resistance is normally negligible for gas-phase processes (Floyd *et al.*, 1986) but the low thermal capacity of gases and the poor gas to solid heat transfer coefficients make particle overheating likely. On the contrary, slurry processes are characterized by better heat transfer and poorer mass transfer than the gas-phase processes.

The tendency for particle overheating increases with the size of the catalyst particle because larger catalyst particles have lower heat transfer surface per unit volume. In this regard it is interesting to note that the size of the large polymer particles produced in Runs HH09261 (2.1 MPa) and HH09262 (2.8 MPa) are smaller than in Run HH09263

(1.4 MPa) (see Figure 9.2). The productivities of the last two runs were 840 g-PE/g-cat and 696 g-PE/g-cat respectively. This suggests that most of the productivity gain at the higher ethylene pressure of 2.8 MPa was due to the medium and small catalyst particles; this is further supported by the particle size distribution shown in Figure 9.4. The large particles deactivated more rapidly due to higher initial overheating.

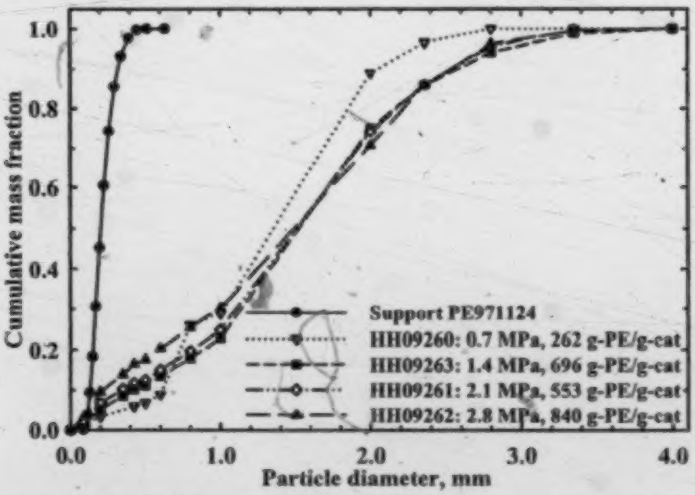

Figure 9.4 Comparison of particle size distribution of Support PE971124 to polyethylene produced at different yields and ethylene pressures (for support ordinate is cumulative volume fraction).

For a single site metallocene catalyst, monomer concentration (pressure) is related to the number average chain length r_n as follows:

$$r_n = \frac{M_n}{M_0} = \frac{k_p C_m}{k_{tm} C_m + k_\beta + k_{tAl} C_{Al} + k_{tH} C_H} \tag{9.1}$$

where M_n is the number average molar mass, M_0 is the molecular weight of the monomer, k_p is the propagation rate constant, and k_{tm}, k_{tAl}, k_{tH}, and k_β are termination rate constants by chain transfer to monomer, chain transfer to Al, chain transfer to hydrogen, and β-hydride elimination respectively. C_m, C_{Al}, and C_H are the concentrations of monomer, Al, and hydrogen respectively. The ethylene (monomer) concentration in the amorphous polymer is related to the ethylene pressure in the reactor by Henry's law (Equation 9.2)

$$C_m = H \times P_{Ethylene} \tag{9.2}$$

lumping all the termination rates (other than by chain transfer to monomer) into k'_β simplifies Equation 9.1 to the following:

$$\frac{1}{r_n} = \frac{M_0}{M_n} = \frac{k'_\beta}{k_p} \cdot \frac{1}{C_m} + \frac{k_{tm}}{k_p} \tag{9.3}$$

Figure 9.5 shows plots of Equation 9.3 for ethylene homopolymerization with Catalysts HH07, HH09, and HH23. C_m was estimated from Equation 9.2 using an extrapolated H value [$7.26\text{x}10^{-3}$ g C_2H_4/(g-amPE·MPa)] from the data of Moore and Wanke (2001) for a HDPE sample of 70% crystallinity. The fitting parameters for the three catalysts and the corresponding values of k_{tm}/k'_β are summarized in Table 9.2.

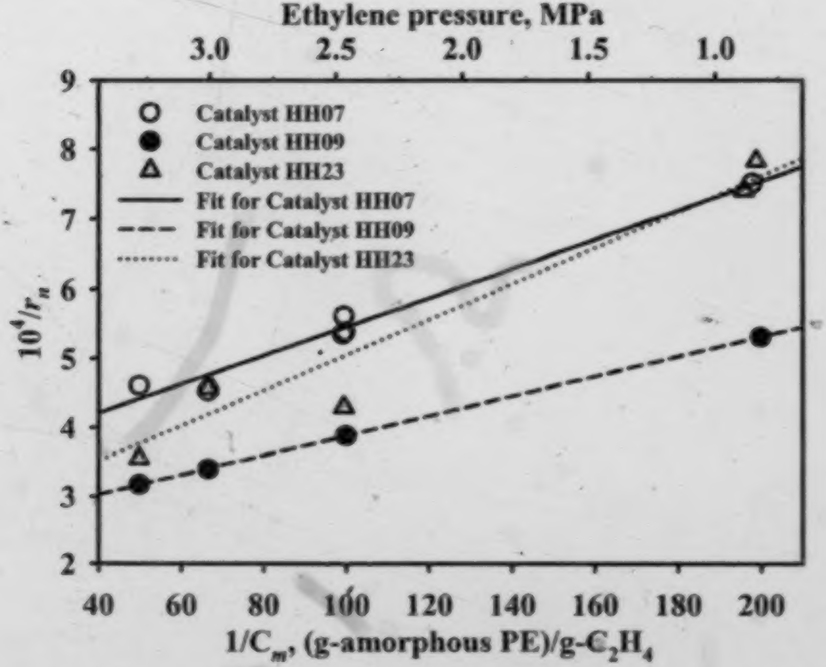

Figure 9.5. Influence of ethylene concentration on number average chain length

Table 9.2 Parameters of Equation 9.3 obtained from the data in Figure 9.5

Parameter	Unit	Catalyst		
		HH07	HH09	HH23
k_{tm}/k_p	–	$3.382 \cdot 10^{-4}$	$2.460 \cdot 10^{-4}$	$2.490 \cdot 10^{-4}$
k'_β/k_p	g-C_2H_4/g-amorphousPE	$2.079 \cdot 10^{-6}$	$1.426 \cdot 10^{-6}$	$2.560 \cdot 10^{-6}$
k_{tm}/k'_β	g-amorphousPE/g-C_2H_4	162.7	172.5	97.3
R^2	–	0.977	1.000	0.938

The increases in molar mass with ethylene pressure show that chain transfer to monomer is not a dominant chain termination reaction. Among the other transfer processes lumped in k'_β, β-hydride elimination is likely the dominant process because of the low aluminum alkyl concentration, and the absence of hydrogen in the reactor. With in the ethylene concentration range shown in Figure 9.5, the two terms in the right hand side of Equation 9.3 are similar in magnitude; hence, the observed molar mass dependence on ethylene pressure (concentration). At much higher ethylene pressures, there would be less dependence of molar mass on ethylene pressure because the contribution of the first term in Equation 9.3 will diminish. The observed difference between the three catalysts in Figure 9.5 may be due to difference in Al:Zr ratio or the catalyst morphology; these would affect the relative contribution of the two terms in Equation 9.3.

9.2.2 Effect of polymerization temperature on molar masses

It was shown in the last section that both chain transfer to monomer and β-hydride elimination have significant influence on the polyethylene molar masses ($k_{tm}C_m \approx k'_\beta$); hence, the influence of polymerization temperature on molar mass cannot be analyzed by the simple approximation $r_n = k_p/k_{tm}$. Figure 9.6 shows the dependence of molar masses on polymerization temperature for ethylene homopolymerization with Catalysts HH07 and HH09, and for ethylene/1-hexene copolymerization with Catalyst HH18. Molar masses decrease with increasing polymerization temperature. The copolymerization data shows weaker temperature dependence because the molar masses are influenced by the continuously changing 1-hexene concentrations in the reactor. The decrease in molar masses with increasing polymerization temperature is due to higher activation energy of chain transfer than chain propagation reactions, this is observed with both Ziegler-Natta (Hutchinson and Ray, 1991) and metallocene (Eskelinen and Seppälä, 1996) systems.

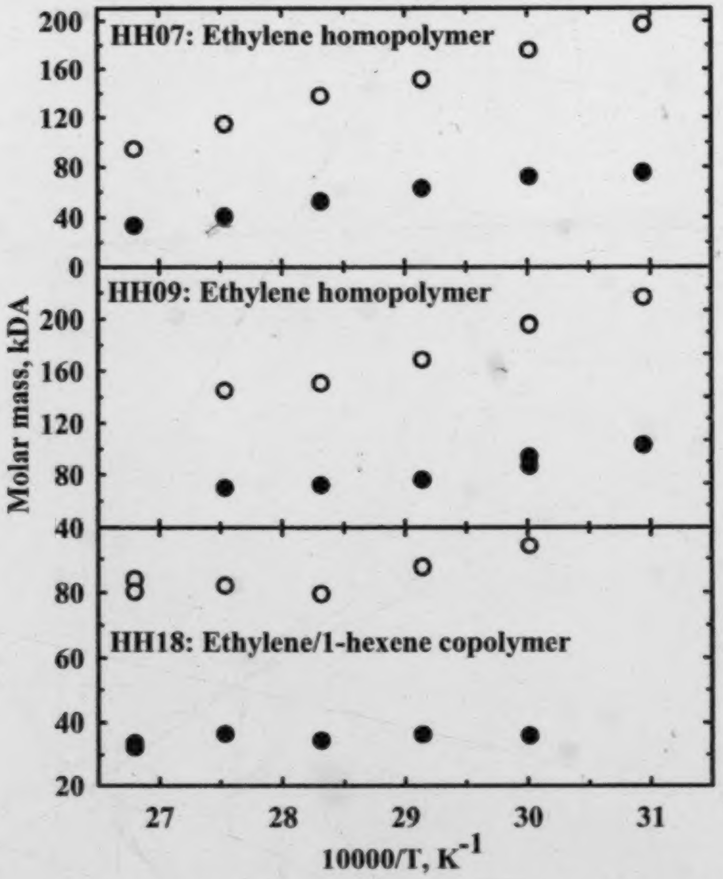

Figure 9.6 Dependence of polymer molar mass on the polymerization temperature (● = M_n and ○ = M_w)

9.2.3 Influence of hydrogen on molar mass and polydispersity

Hydrogen is a highly effective chain transfer agent for metallocene/MAO catalysts (see Section 7.5). It was shown in Figure 7.31 that most of the hydrogen initially fed into the reactor was consumed during the 1-h polymerization of Run HH23249. The rapid hydrogen consumption resulted in significant reduction in the molar masses of the ethylene homopolymers produced with the supported catalysts and the unsupported (*n*-BuCp)$_2$ZrCl$_2$/MAO complex (see Table 9.3). Figure 9.7 shows the variation of molar mass distribution of ethylene homopolymers of Catalyst HH23 with the initial amount of hydrogen charge in the reactor.

Table 9.3 Influence of hydrogen on molar mass of ethylene homopolymers

Catalyst ID	Run #	Initial amount, psi		Yield, g PE	$10^{-3}\cdot$Mn	$10^{-3}\cdot$Mw	PDI
		C_2H_4	H_2				
HH23	HH23245	401	0	51.8	79.0	184.2	2.3
	HH23248	399	2.4	32.3	3.4	15.4	4.5
	HH23249	381	20.0	84.3	1.2	11.2	9.7
HH15	HH15095	204	0	38.4	78.0	169.1	2.2
	HH15141	206	145*,a	43.5	77.2	168.6	2.2
	HH15142	205	70*	76.8	71.2	155.5	2.2
	HH15144	202	495*	111.2	51.0	122.0	2.4

* – Amount of hydrogen in ppm (molar); a – H_2/C_2H_4 mixture replaced by C_2H_4 after 12 min polymerization

The presence of 0.6 mol% hydrogen in the initial (ethylene + hydrogen) gas mixture in the reactor resulted in the decrease of M_n and M_w values by 10 and 20 fold respectively (cf. Runs HH23245 and HH23248 in Table 9.3). The shifts in the molar mass distribution plots indicate the effectiveness of hydrogen as a chain transfer agent. The low molar mass tail in the GPC traces are due to the polymer fraction formed early in the reaction when hydrogen concentration was highest, polymer of higher molar mass subsequently forms as the hydrogen depletes. Thus, the increase in polydispersity in the presence of hydrogen was due to the large variation in the hydrogen concentration. Blom and Dahl (1999) reported polydispersity of 32 in the presence of hydrogen for $Cp_2ZrCl_2/MAO/SiO_2$ system in *i*-butane at 80°C. The response of different metallocenes to hydrogen can vary considerably (e.g. see Chu *et al.*, 2000b; Blom and Dahl, 1999). The polyethylenes produced with Catalyst HH15 in the presence of 70 – 500 ppm hydrogen have no low molar mass tails.

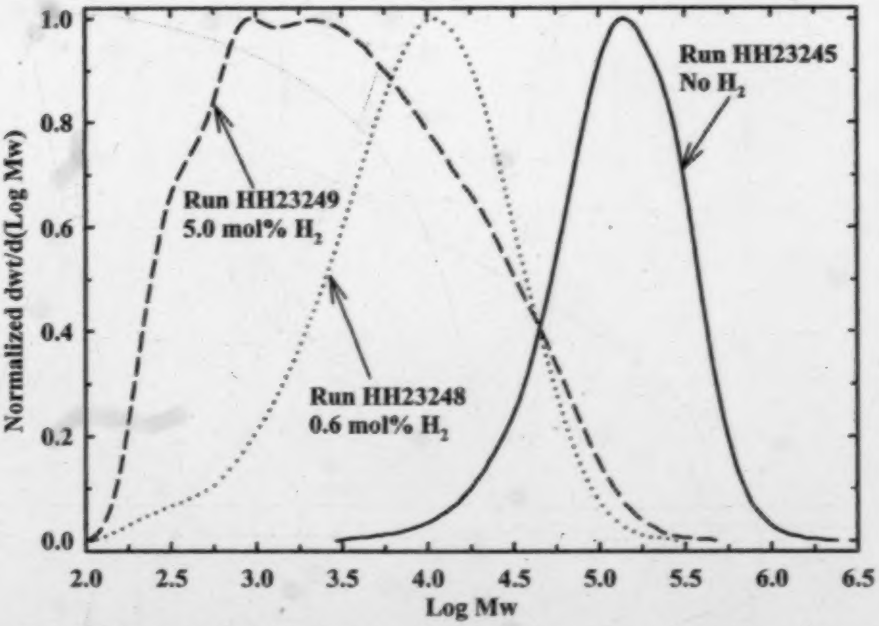

Figure 9.7 Influence of hydrogen on the molar masses of ethylene homopolymers produced with Catalyst HH23 at 80°C and 2.76 MPa (400 psi) reactor pressure.

9.2.4 Influence of 1-hexene on molar mass and polydispersity

The molar masses of ethylene homopolymers are significantly higher than the molar masses of ethylene/1-hexene copolymers for all the supported catalysts tested in this work. Table 9.4 lists the molar masses of ethylene homopolymers and ethylene/1-hexene copolymers produced (~80°C, ~4.5 mL 1-hexene, 1.4 MPa) with catalysts from each of the four support-groups in Table 3.1. There is variation of molar mass with the catalysts, but further tests are needed to confirm whether the observed differences are due to the supports or other factors such as aluminum loading and Al:Zr ratio.

Table 9.4 Molar masses of ethylene homopolymer and ethylene/1-hexene copolymers synthesized with supported catalysts at 80°C and 1.4 MPa.

Catalyst ID	Run Number	Amount of 1-hexene in reactor, mL[a]	Yield, g PE	Molar mass, kDa		Polydispersity index
				Mn	Mw	
HH08	HH08054	–	28.2	73.7	159.8	2.2
	HH08069	4.28	12.7	40.2	114.6	2.9
HH12	HH12067	4.33	30.0	26.9	93.5	3.5
	HH12127	–	14.9	56.8	151.8	2.7
HH29	HH29294	–	3.7	42.5	147.9	3.5
	HH29296	4.02	8.3	22.9	101.3	4.4
HH09	HH09057	–	20.3	82.6	168.6	2.0
	HH09072	4.31	10.8	49.6	123.9	2.5
HH14	HH14128	–	15.3	81.8	185.1	2.3
	HH14131	4.45	41.9	37.0	87.7	2.4
HH10	HH10060	–	1.2	76.2	201.9	2.7
	HH10118	4.25	18.2	39.7	106.4	2.7
HH17	HH17101	–	19.3	53.7	150.0	2.8
	HH17102	4.29	27.8	37.7	97.9	2.6
HH18	HH18104	–	7.7	70.9	201.6	2.8
	HH18238[b]	12.06	42.6	31.6	82.4	2.6
	HH18240	4.6	47.3	32.2	81.5	2.5
HH20	HH20111	4.47	30.7	35.5	97.1	2.7
	HH20114	–	4.6	86.2	236.1	2.7
HH07	HH07048	5.29	28.9	25.6	101.7	4.0
	HH07050	3.26	70.5	36.6	94.0	2.6
	HH07235	–	18.0	52.0	135.8	2.6
HH16	HH16096	4.21	41.5	35.3	94.4	2.7
	HH16097	–	19.6	55.1	149.5	2.7

a – 1 mL of 1-hexene ≡ 3.52 mol/m^3 in the gas-phase

b – Constant 1-hexene/ethylene ratio maintained by continuous 1-hexene addition

The presence of 1-hexene resulted in considerable molar mass decreases for all the catalysts, but the sensitivity of molar mass to 1-hexene is catalyst dependent. For example, Catalyst HH18 is less responsive to 1-hexene than Catalyst HH07 (Table 9.4); the molar masses of ethylene/1-hexene copolymers of Runs HH18238 and HH18240 differed only slightly in spite of the higher amount of 1-hexene used in the former to keep constant ethylene/1-hexene ratio.

Figure 9.8 shows the normalized GPC traces of ethylene/1-hexene copolymers produced with Catalyst HH29. Addition of 2.0 mL 1-hexene to the polymerization reactor reduced the polymer molar mass appreciably. Subsequently, using higher amounts of 1-hexene only increased the relative amount of the low molar mass polymer fraction; this suggests high chain transfer rate to 1-hexene.

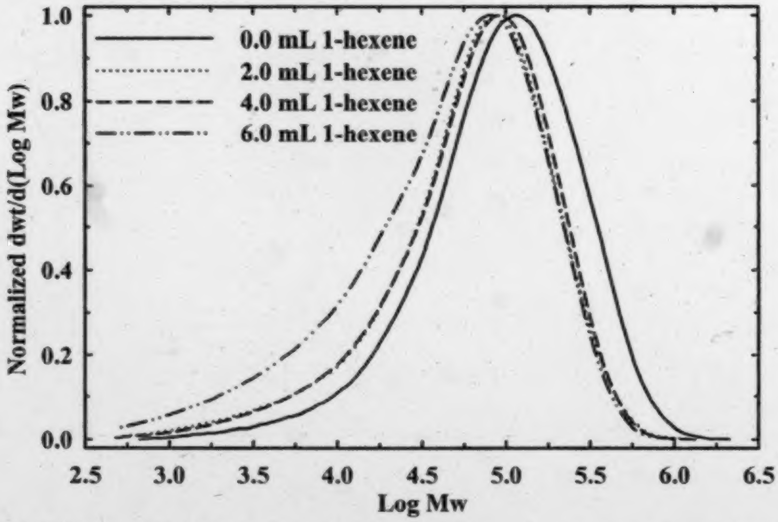

Figure 9.8 Effect of 1-hexene on the distribution of molar masses of ethylene/1-hexene copolymers (Catalyst HH29, swellable STY/1%-DVB support) at 80°C and 1.4 MPa.

If chain transfer to 1-hexene dominates the chain transfer to monomer, Equation 9.1 can be approximated to the following:

$$\frac{M_0}{M_n} = A_n \times V_{Hexene} + B_n \tag{9.4}$$

where A_n is a lumped constant consisting of rate constant for chain transfer to 1-hexene, propagation rate constant, and the constant ethylene concentration. B_n is the ratio of the sum of all chain transfer rates (other than chain transfer to 1-hexene) to the propagation rate. V_{Hexene} is the volume of 1-hexene added to the reactor. Figure 9.9 shows the plot of Equation 9.4 for the polymers in Figure 9.8.

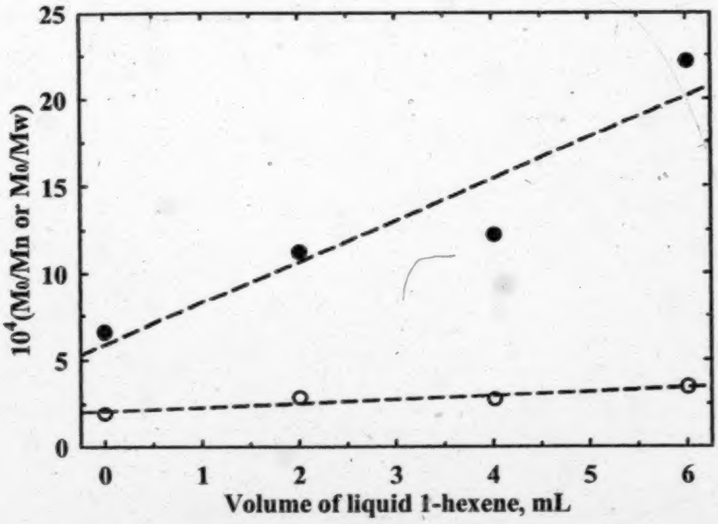

Figure 9.9 Influence of 1-hexene on the molar masses of ethylene/1-hexene copolymers produced by Catalyst HH29 (swellable STY/1%-DVB support) at 80°C and 1.4 MPa (○ = M_0/M_w; ● = M_0/M_n).

The linear trend of the data in Figure 9.9 confirms that chain transfer to 1-hexene plays a significant role in controlling the molar mass. This is consistent with the higher β-hydride elimination rate of 1-hexene reported by Galland *et al.* (1999). However, Galland *et al.* observed decreases in polydispersity with increases of 1-hexene concentration in the reaction slurry (toluene diluent). Polydispersity values less than 2 (most probable value) were observed in the presence of 0.50 mol/L 1-hexene; this could have been due to loss of low molar mass, high 1-hexene-content polymer material during sample work-up after the polymerization (Chien and He, 1991). No such losses occurs in gas-phase polymerization; hence, Figure 9.8 showed increase in low molar mass fraction with the amount of 1-hexene added to the reactor; hence, the polydispersity also increased with the amount of 1-hexene in the reactor.

9.3 Comonomer incorporation

The incorporation of 1-hexene in ethylene/1-hexene copolymers was measured by TREF. Polymer molecules with higher short chain branching (low ability to crystallize) elute at lower temperature. The average concentration of short chain branches, C_N (CH_3 groups per 1000 carbon atoms) was calculated from the TREF profiles using Equation 9.5 below (Kumkaew *et al.*, 2003a)

$$C_N = \frac{\int_{T_0}^{T_f} (IR)_{signal} [CH_3]_T \, dT}{\int_{T_0}^{T_f} (IR)_{signal} \, dT} \tag{9.5}$$

where $(IR)_{signal}$ is the baseline-corrected output of the IR cell (a measure of the polymer, i.e. the $–CH_2–$, concentration in the eluted stream, see Section 3.4.5), $[CH_3]_T$ is the dependence of the concentration of CH_3 groups per 1000 carbon atoms on elution temperature (Equation 9.6; with temperature T in °C) obtained from previous calibration (Zhang, 1999; Kumkaew *et al.*, 2003). T_0 and T_f are the temperature limits of the integration, normally 0 to 101.2°C.

$$[CH_3]_T = \frac{CH_3\ groups}{1000\,Carbons} = 76.37 - 1.20T + 4.4\times10^{-3}T^2 \tag{9.6}$$

The broadness of the short chain branching distribution was obtained from the ratio C_W/C_N, where C_W was obtained from the first and the second moments of the short chain branching distribution (Equation 9.7).

$$C_W = \frac{\int_{T_0}^{T_f} (IR)_{signal} [CH_3]_T^2 \, dT}{\int_{T_0}^{T_f} (IR)_{signal} [CH_3]_T \, dT} \tag{9.7}$$

Figure 9.10 shows some TREF profiles of polyethylenes made with Catalyst HH18 with different amounts of 1-hexene in the reactor. The short chain branching distributions of several polymer products were calculated from the TREF profiles using Equations 9.5 to 9.7; the results are summarized in Table 9.5. The amount of 1-hexene reacted is given by $0.006C_N \times$Yield.

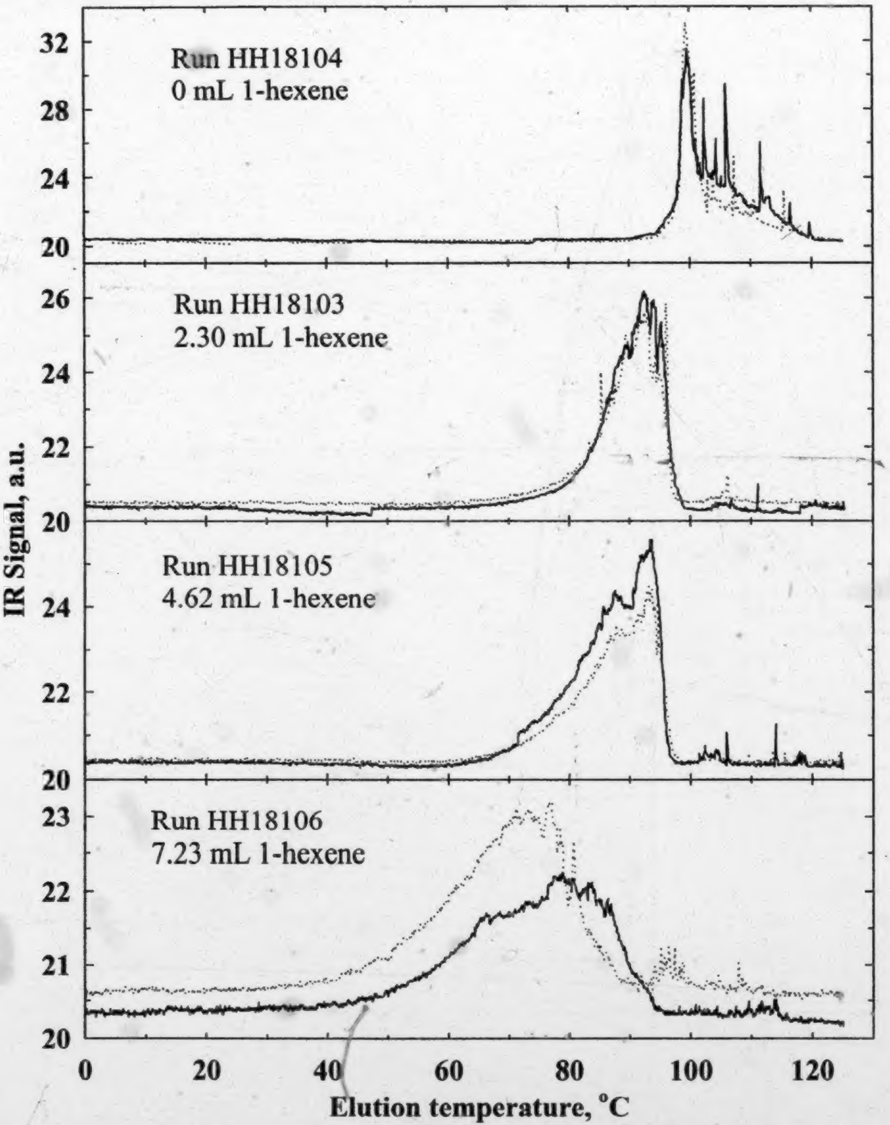

Figure 9.10 TREF profiles of ethylene homopolymer and ethylene/1-hexene copolymers produced with Catalyst HH18 at 80°C and 1.4 MPa (Repeat analyses shown for each sample).

Table 9.5 Short chain branching distribution of ethylene/1-hexene copolymers

Run #	1-C_6H_{12} mL	Yield, g PE	C_N	C_W	C_W/C_N	Fraction 1-C_6H_{12} reacted	Comments
HH10119	4.36	2.1	8.27	8.88	1.07	0.04	10 min run
HH14129	4.25	57.6	7.05	10.44	1.48	0.85	0.04 mL TEAL
HH14131	4.45	41.9	5.38	7.48	1.39	0.45	
HH15090	4.32	62.8	5.08	6.65	1.31	0.66	
HH23151	4.50	56.6	6.22	9.41	1.51	0.70	Unsupported cat.
Industrial	NA	NA	11.57	23.03	2.16	NA	Ziegler-Natta cat.
HH16098	2.52	16.5	13.69	23.58	1.72	0.80	60°C, 104 psi run
HH17100	2.10	27.7	5.85	12.27	2.10	0.70	
HH17102	4.30	27.8	9.68	14.88	1.54	0.56	
HH17230	4.50	57.2	3.86	6.83	1.77	0.44	2.5 h run
HH17233	4.50	80.1	3.68	17.86	4.85	0.58	2.5 h run
HH18103	2.30	36.4	4.75	6.58	1.39	0.67	
HH18105	4.62	65.3	6.13	9.27	1.51	0.77	
HH18106	7.23	28.1	13.88	20.48	1.48	0.48	
HH18240	4.60	47.3	6.37	10.16	1.59	0.58	
HH18238*	12.06	42.6	14.27	18.68	1.31	0.45	
HH19107	2.30	37.9	4.54	6.25	1.38	0.67	Trace TIBA
HH19108	4.70	52.0	8.16	25.82	3.17	0.81	Trace TIBA
HH19122	4.30	31.9	11.05	28.60	2.59	0.73	0.07 mL TIBA
HH19123	4.30	40.3	7.27	10.57	1.46	0.61	0.04 mL TEAL
HH19124	4.30	35.4	8.22	16.01	1.95	0.61	0.03 mL TIBA
HH19125	4.30	43.5	7.18	15.54	2.17	0.64	0.10 mL TNOA
HH22147	4.33	38.7	9.50	16.82	1.77	0.76	
HH22200	4.60	6.3	12.30	16.46	1.34	0.15	
HH22201	4.72	15.9	9.58	12.44	1.30	0.29	
HH22202	4.88	15.8	11.57	14.44	1.25	0.33	
HH22203	4.85	81.4	4.91	9.15	1.86	0.73	
HH22205	4.80	80.6	4.95	9.58	1.94	0.74	
HH25178	4.54	6.4	11.70	16.10	1.38	0.15	
HH25187	4.40	18.2	10.37	18.74	1.81	0.38	
HH27184	4.30	5.8	12.63	15.91	1.26	0.15	

* 1-hexene/ethylene mole ratio kept constant by continuous addition of 1-hexene during the run (see Figure 5.7)

For all catalysts, 1-hexene incorporation in the polymer chains increased with increasing amounts of 1-hexene charged to the reactor e.g. compare Runs HH17100 and H17102; HH18103, HH18105 and HH18106; HH19107 and HH19108 in Table 9.5. Polymerization runs in which the fractions of 1-hexene reacted are small (due to low activity, short run time or high amount of 1-hexene) showed low C_W/C_N values due to relatively constant 1-hexene/ethylene ratios in the reactor (cf. Runs HH10119; HH22200, HH25178, and HH27184 with HH18238 in Table 9.5). 1-Hexene was continuously added in Run HH18238 (see Figure 5.7)

The fraction of 1-hexene incorporated in the polymer chains and the broadness of the short chain branching distributions depended on the amount of 1-hexene charged to the reactor and the total polymer yield (g PE). Figure 9.11 shows the dependence of C_N on yield for the runs that utilized 4.2 to 4.88 mL 1-hexene in Table 9.4. Different symbols represent different catalysts in Figure 9.11.

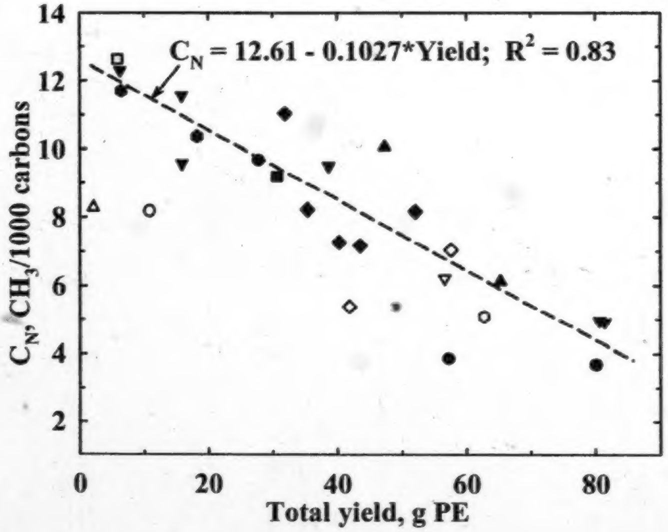

Figure 9.11 Dependence of C_N on the total polymer yield for $(n\text{-BuCp})_2ZrCl_2$/MAO catalysts supported on different low friability commercial supports (solid symbols) and high friability in-house support (open symbols).

The supported (n-BuCp)$_2$ZrCl$_2$/MAO catalysts showed a linear C_N vs. yield dependence in spite of the differences in the catalyst properties (support morphology, Zr loading and Al:Zr ratio). Thus, the support morphology did not significantly influence the average reaction rate of 1-hexene in polymerizations that lasted 1 h or more. This is probably because during ethylene/1-hexene copolymerization, the catalyst particles always fractured completely, and the fracturing process is completed early in the reaction ($t_{polymerization} >> t_{fracturing}$). Once the fracturing is completed, the concentration gradients in the polymerizing particle are small.

Possible effects of comonomer concentration gradients were investigated on copolymer particles produced with Catalyst HH14 (15 mass % Al, 0.235 mass % Zr). TREF profiles of the outer shells and the inner parts of copolymer particles of Run HH14131 are shown in Figure 9.12. The figure suggests decreasing short chain branching towards the particle centre; however, the difference in not appreciable.

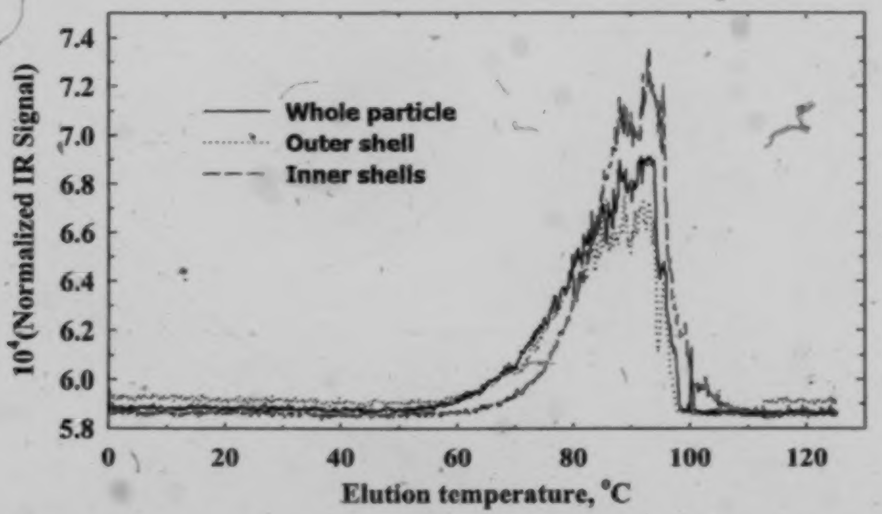

Figure 9.12 TREF profiles of different parts of a polymer particle produced with Catalyst HH14 (Run HH14131: 80°C, 4.6 mL 1-hexene, 1.4 MPa).

The TREF profiles for Catalyst HH18 (Figure 9.10) and for numerous other catalysts showed that the homopolymer-peak commonly observed in copolymers produced by Ziegler-Natta catalysts (Starck, 1996; Xu and Feng, 2000; Huang *et al.*, 1997) is not prominent with the supported metallocene catalysts studied in this work. Thus, the supported metallocene/MAO catalysts (with batch mode of 1-hexene additions) produced polymers with better 1-hexene distributions than a commercial Ziegler-Natta product (with continuous 1-hexene addition to the reactor). Only the solid (*n*-BuCp)$_2$ZrCl$_2$/MAO complex at a yield of 630 kg-PE/mol-Zr (5.6 kg-PE/g-cat) produced copolymer with similar TREF profile to that of commercial Ziegler-Natta catalyst (Figure 9.13) due to significant depletion of 1-hexene in the reactor.

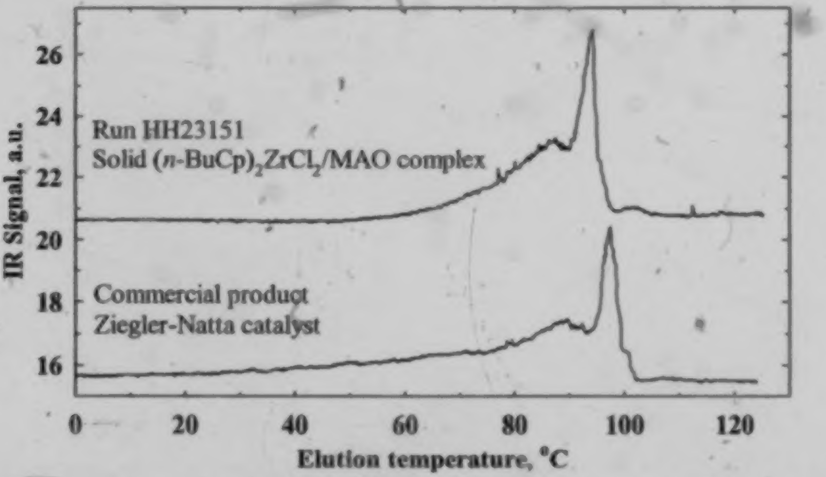

Figure 9.13 TREF profiles of ethylene/1-hexene copolymers showing the homopolymer peak (profiles were off set for clarity).

The type and the amount of aluminum alkyl scavenger used in the polymerization did not influence the short chain branching distribution significantly (cf. Runs HH19108, HH19122-HH19125 in Table 9.5).

The type of comonomer employed in polymerization with ethylene affected the TREF profiles (SCBD). Figure 9.14 shows the TREF profiles of ethylene/ propylene and ethylene/1-decene copolymers produced with Catalyst HH15. The C_N values for these copolymers were not quantified because no $[CH_3]_T$ calibration was available. The broad range of elution temperature (~30 - 103°C) in the TREF profile of the ethylene/1-decene copolymers suggests the presence of substantially branched copolymer and a significant homopolymer fraction. TREF profile of ethylene homopolymer was previously shown in Figure 9.10 (top panel).

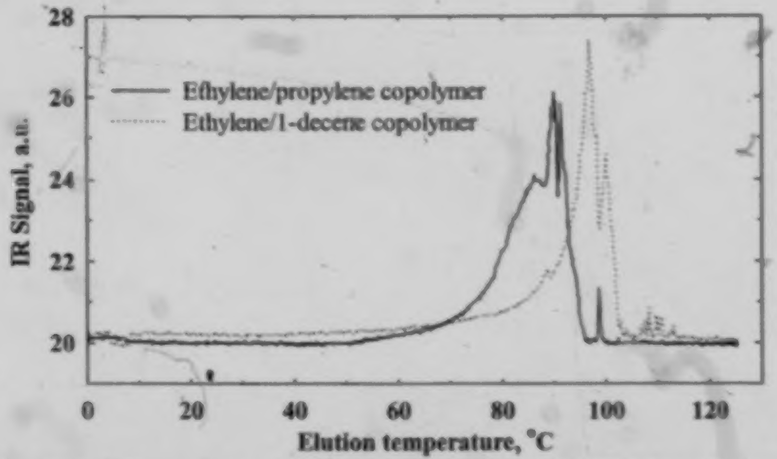

Figure 9.14 TREF profiles of ethylene/propylene and ethylene/1-decene copolymers produced with Catalyst HH15.

Comparison of copolymerization with Catalyst HH16 (Run HH16098) at 60°C to copolymerization with many other catalysts at 80°C but at similar 1-hexene/ethylene mole ratio in the reactor showed higher fraction of 1-hexene reacted in the 60°C run (Table 9.5). The C_N value for Run HH16098 is even higher than that of Run HH16099 at 80°C (with the same catalyst) in which the 1-hexene was prepolymerized for 5 min prior to ethylene feed (Figure 9.15). The increase in 1-hexene incorporation at lower polymerization temperature is likely due to increased 1-hexene solubility. Kumkaew *et* *al.* (2003a) reported higher 1-hexene incorporations at lower polymerization temperatures. For identical temperature decrease, the relative increase in 1-hexene solubility in ethylene/1-hexene copolymer is more than the relative increase for ethylene (Moore and Wanke, 2001).

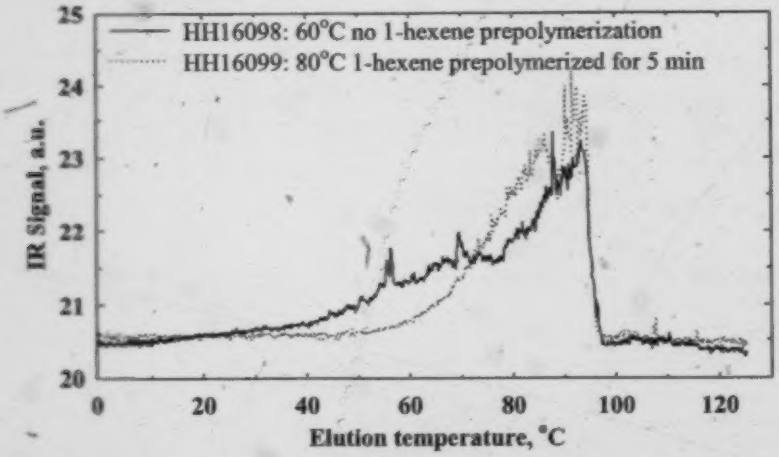

Figure 9.15 Enhancement of 1-hexene incorporation at low polymerization temperature.

Summary of the effects of catalyst and polymerization conditions on polymer properties

The polymer-supported $(n\text{-BuCp})_2ZrCl_2$/MAO catalysts exhibited excellent morphology replication from catalyst to polymer particles. The particle replication for the catalysts supported on the in-house supports was superior to that of catalysts supported on commercial supports in ethylene homopolymerization; the commercial supports are mechanically stronger than the in-house ones. For the same supported catalyst, the bulk densities of ethylene/1-hexene copolymers are higher than that of ethylene homopolymers. Hydrogen improved the bulk density of ethylene homopolymers produced by supported catalyst as well as the solid $(n\text{-BuCp})_2ZrCl_2$/MAO complex.

Molar masses of ethylene homopolymers increased with ethylene pressure, and decreased with increasing catalyst particle size (due to particle overheating), and polymerization temperature. The molar masses of ethylene/1-hexene copolymers decreased with the amount of 1-hexene in the reactor, while the polydispersity increased. Addition of small amounts of hydrogen (~0.5 mol %) results in significant reduction in polyethylene molar mass.

The short chain branching content of polymers increase with the amount of 1-hexene in the reactor. High catalyst productivity reduces the average branch content and broadens the short chain branching distribution due to the depletion of 1-hexene in the reactor. The polymer-supported $(n\text{-BuCp})_2ZrCl_2$/MAO catalysts exhibited more uniform 1-hexene incorporation than the commercially produced copolymer using Ziegler-Natta catalysts. The type and the amount of aluminum alkyl scavenger used in the gas-phase polymerizations had no significant effect on 1-hexene incorporation.

10. Conclusions and Recommendations for Future Work

The objective of this thesis research was to fabricate a new polymerization reactor with improved temperature control and investigate the influence of the properties of polymeric supports on gas-phase olefin polymerization over supported ($(n\text{-BuCp})_2ZrCl_2$/ MAO catalysts. This chapter summarizes the important findings in the above two aspects of the work and presents recommendation for future work.

10.1 Summary and conclusions

A new 2-L reactor system with improved temperature control and a unique gas-sampling valve was fabricated and used in gas-phase polymerization of ethylene and α-olefins. The gas sampling and analysis system allowed GC analysis of reactor gas at 3 min intervals.

Heat removal from the new polymerization reactor was achieved by flowing coolant through channels housing static mixers in the sidewalls of the reactor. Good gas-phase temperature control was achieved at polymerization rates up to 80 L (STP) ethylene per hour. High polymerization rates for extended periods and rapid increases in initial activity reduce the temperature control effectiveness of the new reactor.

Increases in bulk gas-phase temperature by about 4°C, and higher, increased the rate of catalyst deactivation and results in irreproducible activity profiles; such increases in bulk gas-phase temperature are probably accompanied by much higher increases in polymerizing particle temperatures.

Supported $(n\text{-BuCp})_2ZrCl_2$/MAO catalysts were prepared using several commercial and in-house polymeric supports of different porosity and composition. The catalysts polymerized ethylene and α-olefins with high activity in the gas-phase. Average copolymerization activities were generally higher than homopolymerization activities.

Residual aluminum alkyls in the polymerization reactor suppressed the initial activity and broadened the activity profiles. This often led to better temperature control and higher average activity values (1-h runs) than in polymerization runs without residual aluminum alkyls. Thus, aluminum alkyls can be used to enhance reactor temperature control without compromising productivity. The effectiveness of aluminum alkyls in suppressing the initial polymerization activities decreased with increasing size of the alkyl group i.e., TEA > TIBA > TNOA.

The small variations in Zr loading and Al:Zr ratio arising from catalyst preparation had no consistent effect on the polymerization activity of the catalysts; the activities did not follow any composition pattern of the catalyst. The support type affected the polymerization rates of the supported catalysts, but the observed effect is probably due to physical (fragmentation) rather than chemical differences between the supports.

Polymeric supports possessing linear crosslink segments resulted in catalysts with better ethylene homopolymerization activity than the DVB crosslinked supports but this effect could be due to the catalyst friability. Polymerization activity generally improved with the support friability, and the surface area and pore volume of catalyst. Functional groups in the supports did not affect catalyst activity significantly because the MAO shielded the metallocene from interacting with the functional groups.

The polymer-supported catalysts that fracture rapidly exhibited the acceleration-decay activity profiles that were adequately described by a simple lumped parameter model with exponential activation and deactivation. Both the activation and deactivation rates increased with polymerization temperature; the highest polymerization activities occurred between 70–90°C gas-phase temperature. The polymerization activity depended nonlinearly on monomer pressure due to the effects of monomer pressure on particle temperature and fragmentation; these affected catalyst deactivation and mass transport resistance, respectively.

The supported $(n\text{-BuCp})_2ZrCl_2$/MAO catalysts are highly sensitive to hydrogen in the gas-phase polymerization. Less than 10 ppm hydrogen in the reactor depressed the polymerization activity considerably and lowered polymer molar mass. The rate depressing effect is reversible because the polymerization activity was restored upon depletion of hydrogen in the reactor by chain transfer reaction or its removal from the reactor by venting.

Catalysts supported on low friability supports had significant polymerization activity improvement in presence of 1-hexene. The supports crosslinked by linear segments such as EGDM, which also have slightly better friability, showed only moderate ethylene/1-hexene synergism. The high friability supports produced catalysts with high ethylene homopolymerization activity; these catalysts showed small or no activity enhancement by 1-hexene. Increasing comonomer/ethylene mole ratios first increased polymerization activities to a maximum followed by activity decline upon further comonomer addition; the optimum activity values are catalyst specific. Polymerization activity enhancement by comonomer decreased with increasing comonomer size due to the diffusivity and the reactivity of the comonomers.

Low friability catalysts did not fracture completely during ethylene homopolymerization. The presence of comonomer drives the fracturing of these catalysts to completion. This was accompanied by the formation of onion-ring like morphology of the polymer particle. The tendency of the catalyst particles to form the onion-ring like structure decreased with increasing catalyst (support) friability.

The spherical morphology of the polymer-supported (*n*-BuCp)$_2$ZrCl$_2$/MAO catalyst particles were replicated in the polymer particles. Catalysts made with the more friable in-house supports had superior particle replication in ethylene homopolymerization. The morphology replication in ethylene/α-olefin copolymerization was equally good for both the higher and the lower friability catalysts. For the same supported catalyst, the bulk densities of ethylene/1-hexene copolymers were higher than ethylene homopolymers. Hydrogen improved the bulk density of ethylene homopolymers produced by supported catalyst as well as the solid (*n*-BuCp)$_2$ZrCl$_2$/MAO catalyst complex.

Molar masses of ethylene homopolymers increased with ethylene pressure, and decreased with increasing catalyst particle size and polymerization temperature. The molar masses of ethylene/1-hexene copolymers decreased with the amount of 1-hexene in the reactor, while the polydispersity increased. Addition of about 0.5 mol % hydrogen results in significant reduction in polyethylene molar mass.

Increasing 1-hexene/ethylene mole ratio in the reactor increased the short chain branching content of polymers. Depletion of 1-hexene in the reactor broadens the short chain branching distribution in the polymer produced. The polymer-supported (*n*-BuCp)$_2$ZrCl$_2$/MAO catalysts exhibited more uniform 1-hexene incorporation than the commercially produced copolymer using Ziegler-Natta catalysts. The type and the amount of aluminum alkyl scavenger used in the gas-phase polymerizations had no significant effect on 1-hexene incorporation.

10.2 Recommendations for future work

The effectiveness of the reactor temperature control decreases for prolonged high rates due to the increase in the cold compartment bath temperature. Using a level-controlled valve to direct the coolant return stream to the appropriate compartment, and increasing the capacity of the cooling coils would minimize temperature increases in the cold compartment.

The 1-hexene dosing pump could be interfaced with the GC analysis system to enable copolymerization at constant comonomer/ethylene ratio without resorting to operating the reactor in the purge mode (Xu *et al.*, 2001). Considerable effort is required for manual control of this ratio and it is less accurate.

The new reactor was only used for conventional gas-phase polymerization. With a depth-to-diameter ratio of two, this reactor may also be used in the super condensed mode. This would be made possible by installing cooling coils close to the top flange. Circulating coolant in these coils at the appropriate temperature would enable the less volatile comonomer (or inert heat transfer agent) to condense and drip back to the reaction zone. This would permit reliable investigation of polymerization kinetics and comonomer incorporation at even higher polymerization rates and comonomer/ethylene ratios than is currently possible with the reactor.

Thermal deactivation is evidently an important factor in the deactivation of the polymer-supported $(n\text{-BuCp})_2\text{ZrCl}_2/\text{MAO}$ catalysts, but the uncertainty in the actual particle temperature limited the analysis of thermal deactivation. More information would be obtained by conducting a series of polymerization runs at different temperatures with high fraction of inerts to suppress possible surges in particle temperature.

Metallocene deactivation in homogeneous systems is believed to be mainly due to the formation of the homodinuclear zirconium species. Using the pore size, pore volume, and surface area of support, it is possible to estimate the surface density of the metallocenium centers in a supported catalysts (see Chien, 1999) and use it to investigate deactivation as function of Al:Zr ratio and Zr loading. Since deactivation via the alkylene Zr dimer does not involve monomer, deactivation by the dimer formation due to catalyst aging could also be studied by keeping freshly prepared catalysts in sealed vials at various conditions for different periods before use in polymerization.

One of the drawbacks of metallocene/MAO-catalyzed polyolefins is poor processability. Long chain branching (LCB) is known to improve this property, but not much work has been done in this regard especially for polymer-supported catalysts in the gas-phase. Therefore, a study of the ability of supported constrained geometry catalysts to form polyolefins with long chain branching in gas-phase polymerization is of industrial and academic significance. There is less steric hindrance at the metal site in bridged (constrained geometry) metallocene catalysts; hence, the bridged metallocenes have greater ability to incorporate vinyl terminated polymer molecules into the growing chain than the unbridged ones. The adsorption and polymerization of olefin end groups was suggested as possible reason for increase in molar mass with yield for chromium catalyst (Whitaker and Wills, 1969).

The catalysts made using low friability supports homopolymerized ethylene to form particles with outer polymer layer and inner catalyst core. It is not clear whether the catalyst particles fractured during the polymerization because the sizes of the catalyst cores are similar to the sizes of the support particles. Washing the supported catalysts (during preparation) would clarify whether the outer polymer layer is due to fracturing of the catalyst or the layer of (n-BuCp)$_2$ZrCl$_2$/MAO complex on the catalyst particles.

Hydrogen seem to have interesting effect on the activity of the polymer-supported (n-BuCp)$_2$ZrCl$_2$/MAO catalysts. More detailed evaluation of the hydrogen effect involving the addition of different amounts to the reactor at different reaction times (before and after attainment of maximum activity) would lead to more conclusive inferences on the effect of hydrogen on active, dormant or deactivated metallocene sites. Hydrogen liberation was observed during ethylene/1-hexene copolymerization (but not during ethylene homopolymerization) with some metallocenes (Karol *et al.*, 1999). This phenomenon could explain the significant drop in polyethylene molar mass caused by 1-hexene, but may contradict the finding of Galland (1996) that 1-hexene incorporation favors termination by β-hydride elimination; formation of unsaturated polymer chain are unlikely in the presence of hydrogen. The new reactor could be used to investigate the above observations during gas-phase polymerization because smaller amounts of hydrogen than those reported by Karol *et al.* can be determined rapidly. Such investigation would further explain the effect of 1-hexene on the molar mass of ethylene/1-hexene copolymer.

Substantial amount of experimental data on gas-phase olefin polymerization rates, product morphology, and polymer properties have been generated in this thesis work.

These data can be used in conjunction with existing morphology development/mass transfer resistance models (Bonini *et al.*, 1995; Kittilsen *et al.*, 2001a; Estenoz *et al.*, 2001; Naik and Ray, 2001) to further understand these mechanisms and to refine the models to better represent experimental observations.

The supports used in this work were not specifically designed for this purpose; therefore, it was not possible to study the influence of the morphological properties of the supports systematically because individual support variables could not be separated for explicit study. More systematic studies would, therefore, start from the support preparation since it is possible to vary many of these parameters individually during the support preparation step (see Sherrington, 1998; Rosenberg and Flodin, 1987a).

References

Alt, H. G., The heterogenization of homogeneous metallocene catalysts for olefin polymerization, *Journal of the Chemical Society, Dalton Transactions*, 1703-1709 (1999).

Andersen, A., Blom, R. and Dahl, I. M., Semi-batch polymerizations of ethylene with metallocene catalysts in the presence of hydrogen, 2 Deduction of kinetic parameters, *Macromolecular Chemistry and Physics*, **202**, 726-733 (2001).

Anwander, R., SOMC@PMS. Surface organometallic chemistry at periodic mesoporous silica, *Chemistry of Materials*, **13**, 4419-4438 (2001).

Arnold, M., Henschke, O. and Knorr, J., Copolymerization of propene and higher α-olefins with the metallocene catalyst $Et[Ind]_2HfCl_2$/methylaluminoxane, *Macromolecular Chemistry and Physics*, **191**, 563-573 (1996).

Atiqullah, M., Hammawa, H., Akhtar, M. N., Khan, J. H. and Hamid, H., Nonisothermal, uncontrolled homo- and copolymerization of ethylene using selected zirconocenes, *Journal of Applied Polymer Science*, **70**, 137-147 (1998).

Barrett, A. G. M. and de Miguel, Y. R., A well-defined metallocene catalyst supported on polystyrene beads, *Chemical Communications*, 2079-2080 (1998).

Barrett, A. G. M. and de Miguel, Y. R., Synthesis and characterization of a new polymer support for a metallocene catalyst, *Tetrahedron*, **58**, 3785-3792 (2002).

Barrett, E. P., Joyner, L. G. and Halenda, P. P., "The determination of pore volume and area distributions in porous substances", *Journal of the American Chemical Society,* **73**, 373 (1953).

Barron, A. R., Alkylalumoxanes: Synthesis, structure and reactivity. In *Metallocene-based polyolefins. Preparations, properties and technology,* Vol 1. John Scheirs and W. Kaminsky Eds. John Wiley & Sons, Ltd. Chichester 2000. p 33–67.

Biffis, A., Corain, B., Cvengrošová, Z., Hronec, M., Jeřábek, K. and Králik, M., "Relationship between physico-chemical properties and catalytic activity of polymer-supported palladium catalysts II. Mathematical model", *Applied Catalysis A: General*, **142**, 327-346 (1996).

Blom, R. and Dahl, I. M., On the sensitivity of metallocene catalysts toward molecular hydrogen during ethylene polymerization, *Macromolecular Chemistry and Physics*, **200**, 442-449 (1999).

Blom, R. and Dahl, I. M., Semi-batch polymerization of ethylene with single-site catalysts in the presence of hydrogen, 1 Modelling of molecular weight distributions, *Macromolecular Chemistry and Physics*, **202**, 719-725 (2001).

Bochman, M. and Lancaster, S. J., Monomer-dimer equilibria in homo- and heterodinuclear cationic alkylzirconium complexes and their role in polymerization catalysis, *Angewandte Chemie International Edition in English*, **33**, 1634-1637 (1994).

Böhm, L. L., The ethylene polymerization with Ziegler catalysts: Fifty years after the discovery, *Angewandte Chemie International Edition*, **42**, 5010-5030 (2003).

Bonini, F., Fraaije, V. and Fink, G., Propylene polymerization through supported metallocene/MAO catalysts: Kinetic analysis and modeling, *Journal of Polymer Science: Part A: Polymer Chemistry*, **33**, 2393-2402 (1995).

Bortolussi, F., Boyer, J-P., Spitz, R. and Boisson, C., Synthesis of silica-supported metallocene catalysts for olefin polymerization, *Macromolecular Chemistry and Physics*, **203**, 2501-2507 (2002).

Braca, G., Sbrana, G., Raspolli-Galletti, A. M., Altomare, A., Arribas, G., Michelotti, M. and Ciardelli, F., Supported transition metal complexes for ethylene polymerization, *Journal of Molecular Catalysis A: Chemical*, **107**, 113-121 (1996).

Britovsek, G. J. P., Gibson, V. C. and Wass, D. F., The search for new-generation polymerization catalysts: Life beyond metallocenes, *Angewandte Chemie International Edition*, **38**, 428-447 (1999).

Broeckhoff, J. P. C. and van Beek, W. P., Scanning studies on capillary condensation and evaporation of nitrogen. Part 2. Analysis of ascending and descending scanning curves with B-type hysteresis loops, *Journal of Chemical Society, Faraday Transactions I*, **75**, 42-55 (1979).

Brunauer, S., Emmett, P. H. and Teller, E., Adsorption of Gases in Multimolecular Layers, *Journal of the American Chemical Society*, **60**, 309-319 (1938).

Busico, V., Cipullo, R., Cutillo, F. and Vacatello, M., Metallocene-Catalyzed Propene Polymerization: From Microstructure to Kinetics. 1. C_2-Symmetric *ansa*-Metallocenes and the "Trigger" Hypothesis, *Macromolecules*, **35**, 349-354 (2002).

Calabro, D. C. and Lo, F. Y., A comparison of the reaction kinetics for the homo- and copolymerization of ethylene and hexene with a heterogeneous Ziegler-Natta catalyst. In *Transition metal catalyzed polymerizations–Ziegler-Natta and metathesis polymerizations*; R.P. Quirk, Ed., Cambridge University Press, Cambridge, 1988; p 729-739.

Campbell, J. A. and Bewick, M. W. M., Neutron Activation Analysis – A Review of the Method and its Present and Potential Uses in Agriculture and Soil Science, *Special Publication No. 7, Commonwealth Bureau of Soils,* Commonwealth Agricultural Bureaux, Slough, (1978).

Camurati, I., Cavicchi, B., Dall'Occo, T. and Piemontesi, F., Synthesis and characterization of ethylene/1-olefin copolymers obtained by "single centre" catalysis, *Macromolecular Chemistry and Physics*, **202**, 701-709 (2001).

Carrado, K. A. and Xu, L., "Materials with controlled mesoporosity derived from synthetic polyvinylpyrrolidinone-clay composites", *Microporous and Mesoporous Materials*, **27**, 87-94 (1999).

Chakravarti, S. and Ray, W. H., Kinetic study of olefin polymerization with a supported metallocene catalyst. II. Ethylene/1-hexene copolymerization in gas phase, *Journal of Applied Polymer Science*, **80**, 1096-1119 (2001).

Charpentier, P. A., Zhu, S., Hamielec, A. E. and Brook, M. A., Continuous solution polymerization of ethylene using metallocene catalyst system, zirconocene dichloride/methylaluminoxane/trimethylaluminum, *Industrial and Engineering Chemistry Research*, **36**, 5074-5082 (1997).

Chatt, A. and Katz, S. A., Neutron Sources for Activation Analysis of Geological Minerals, in Mineralogical Association of Canada: Short Course in Neutron Activation Analysis in the Geosciences, G. K. Muecke (Ed.) p. 49 (1980).

Chien, J. C. W. and He, D., Olefin copolymerization with metallocene catalysts. I. Comparison of catalysts, *Journal of Polymer Science: Part A: Polymer Chemistry,* **29**, 1585-1593 (1991).

Chien, J. C. W. and He, D., Olefin copolymerization with metallocene catalysts. III. Supported metallocene/MAO catalyst for olefin copolymerization, *Journal of Polymer Science: Part A: Polymer Chemistry,* **29**, 1603-1607 (1991b).

Chien, J. C. W. and Nozaki, T., Ethylene-Hexene copolymerization by heterogeneous and homogeneous Ziegler-Natta catalysts and the "comonomer" effect, *Journal of Polymer Science: Part A: Polymer Chemistry,* **31**, 227-237 (1993).

Chien, J. C. W. and Sugimoto, R., Kinetics and stereochemical control of propylene polymerization initiated by ethylene bis(4,5,6,7-tetrahydro-l-lndenyl) zirconium dichloride/ methylaluminoxane catalyst, *Journal of Polymer Science: Part A Polymer Chemistry*, **29**, 459-470 (1991).

Chien, J. C. W. and Wang, B-P., Metallocene-methylaluminoxane catalysts for olefin polymerization. I. Trimethylaluminum as coactivator, *Journal of Polymer Science: Part A: Polymer Chemistry,* **26**, 3089-3102 (1988).

Chien, J. C. W. and Wang, B-P., Metallocene-methylaluminoxane catalysts for olefin polymerization. V. Comparison of Cp_2ZrCl_2 and Cp_2ZrCl_3, *Journal of Polymer Science: Part A: Polymer Chemistry,* **28**, 15-38 (1990).

Chien, J. C. W., Kuo, C.-I. and Ang, T., Magnesium chloride supported high mileage catalysts for olefin polymerization. VI. Definitive evidence against diffusion limitation, *Journal of Polymer Science: Polymer Chemistry Edition*, **23**, 723-729 (1985).

Chien, J. C. W., Supported metallocene polymerization catalysis, *Topics in Catalysis*, **7**, 23-36 (1999).

Choi, K. Y. and Ray, W. H., Polymerization of olefins through heterogeneous catalysis. II. Kinetics of gas phase propylene polymerization with Ziegler-Natta catalysts, *Journal of Applied Polymer Science*, **30**, 1065-1081 (1985).

Chu, K-J., Shan, C. L. P., Soares, B. P. and Penlidis, A., Copolymerization of ethylene and 1-hexene with in-situ supported Et[Ind]$_2$ZrCl$_2$, *Macromolecular Chemistry and Physics*, **200**, 2372-2376 (1999).

Chu, K-J., Soares, J. B. P. and Penlidis, A., Effect of experimental conditions on ethylene polymerization with *in-situ*-supported metallocene catalyst, *Journal of Polymer Science A: Polymer Chemistry*, **38**, 1803-1810 (2000a)

Chu, K-J., Soares, J. B. P. and Penlidis, A., Effect of hydrogen on ethylene polymerization using in-situ supported metallocene catalysts, *Macromolecular Chemistry and Physics*, **201**, 552-557 (2000b).

Chung, J. S. and Hsu, J. C., A kinetic analysis on the gas phase polymerization of ethylene over polymer supported $(CH_3)_2Si[Ind]_2ZrCl_2$ catalyst, *Polymer*, 43, 1307-1311 (2002).

Chung, J.S., Tairova, G., Zhang, Y., Hsu, J. C., McAuley, K. B. and Bacon, D. W., Polymer-supported metallocene catalysts for gas-phase ethylene polymerization, *Korean Journal of Chemical Engineering*, **19**, 597-600 (2002).

Collins, S., Kelly, W. M. and Holden, D. A., Polymerization of propylene using supported, chiral, ansa-metallocene catalysts: Production of polypropylene with narrow molecular weight distribution, *Macromolecules*, **25**, 1780-1785 (1992).

Costa Vaya, V. I., Belelli, P. G., dos Santos, J. H. Z., Ferreira, M. L. and Damiani, D. E., Influence of Acidic support in metallocene catalysts for ethylene polymerization, *Journal of Catalysis,* **204**, 1-10 (2001).

Covezzi, M., The spherilene process: Linear polyethylenes, *Macromolecular Symposium*, **89**, 577-586 (1995).

Cybulski, A. and Werner, K., Static mixers –criteria for applications and selection, *International Chemical Engineering,* **26(1),** 171-180 (1986).

Dalla Lana, I. G., Szymura J. A., and Zielinski, P. A., The role of porosity in ethylene polymerization on Cr/SiO$_2$ catalysts, in New Frontiers in Catalysis; *Proceedings of the 10th International Congress on Catalysis, Budapest, 1992*; L. Guczi, F. Solymosi, and P. Tétényi (Eds.), Akadémiai Kiadó, Budapest, 1993; p. 2329-2332.

Doi, Y., M. Murata, K. Yano and T. Keii, Gas-phase polymerization of propene with the supported Ziegler catalyst: $TiCl_4/MgCl_2/C_6H_5COOC_2H_5/Al(C_2H_5)_3$, *Industrial & Engineering Chemistry Production Research and Development*, **21**, 580-585 (1982).

dos Santos, J. H. Z., Dorneles, S., Stedile, F. C., Dupont, J., Forte, M.M.C. and Baumvol, I.J.R., Silica supported zirconocenes and Al-based cocatalysts: surface metal loading and the catalytic activity, *Macromolecular Chemistry and Physics*, **198**, 3529-3537 (1997).

dos Santos, J. H. Z., Krug, C., da Rosa, M. B., Stedile, F. C., Dupont, J. and Forte, M. de C., The effect of silica dehydroxylation temperature on the activity of SiO_2-supported zirconocene catalysts, *Journal of Molecular Catalysis A: Chemical*, **139**, 199-207 (1999a).

dos Santos, J. H. Z., Larentis, A., da Rosa, M. B., Krug, C., Baumvol, I. J. R., Dupont, J., Stedile, F. C. and Forte, M. de C., Optimization of silica supported bis(butylcyclopentadienyl)-zirconium dichloride catalyst for ethylene polymerization, *Macromolecular Chemistry and Physics*, **200**, 751-757 (1999b).

Eskelinen, M., and Seppälä, J. V., Effect of polymerization temperature on the polymerization of ethylene with dicyclopentadienylzirconiumdichloride/methylalumoxane catalyst, *European Polymer Journal*, **32**, 331-335 (1996).

Estenoz, D. A., Mario, G. and Chiovetta, G., Olefin polymerization using supported metallocene catalysts: Process representation scheme and mathematical model, *Journal of Applied Polymer Science*, **81**, 285-311 (2001).

Ewen, J. A., Mechanisms of stereochemical control in propylene polymerizations with soluble Group 4B metallocene/methylalumoxane catalysts, *Journal of the American Chemical Society*, **106**, 6355-6364 (1984).

Ferreira, M. L. and Damiani, D. E., Catalysts based on supported metallocenes for α-olefin polymerization, *Macromolecular Chemistry and Physics*, **202**, 694-700 (2001).

Ferrero, M. A. and Chiovetta, M. G., Catalyst fragmentation during propylene polymerization: Part I. The effects of grain size and structure, *Polymer Engineering and Science*, **27**, 1436-1447 (1987a).

Ferrero, M. A. and Chiovetta, M. G., Catalyst fragmentation during propylene polymerization: Part II. Microparticle diffusion and reaction effects, *Polymer Engineering and Science*, **27**, 1448-1460 (1987b).

Fischer, D. and Mülhaupt, R., Reversible and irreversible deactivation of propene polymerization using homogeneous Cp_2ZrCl_2/methylaluminoxane Ziegler-Natta catalysts, *Journal of Organometallic Chemistry*, **417**, C7-C11 (1991).

Fischer, D., Jungling, S., Schneider, M. J., Suhm, J. and Mülhaupt, R., Influence of metallocene structures on molecular and supermolecular architectures of polyolfins. In *Metallocene-based polyolefins. Preparations, properties and technology*, Vol 1. John Scheirs and W. Kaminsky Eds. John Wiley & Sons, Ltd. Chichester 2000. p 103–117.

Floyd, S., Choi, K. Y., Taylor, T. W. and Ray, W. H., Polymerization of olefins through heterogeneous catalysis. III. Polymer particle modeling with an analysis of intraparticle heat and mass transfer effects, *Journal of Applied Polymer Science*, **32**, 2935-2960 (1986).

Floyd, S., Heiskanen, T., Taylor, T. W., Mann, G. E. and Ray, W. H., Polymerization of olefins through heterogeneous catalysis. VI. Effect of particle heat and mass transfer on polymerization behavior and polymer properties, *Journal of Applied Polymer Science*, **33**, 1021-1065 (1987).

Galland, G. B., Seferin, M., Mueler, R. S. and dos Santos, J. H. Z., Linear low-density polyethylene synthesis promoted by homogeneous and supported catalysts, *Polymer Internatinal*, **48**, 660-664 (1999).

Galli, P. and Vecellio, G., Technology: driving force behind innovation and growth of polyolefins, *Progress in Polymer Science*, **26**, 1287-1336 (2001).

Galli, P., Cecchin, G., Chadwick, J. C., Del Duca, D. and Vecellio, G., Polypropylene: 44 years young! The challenge for the 21st century, In *Metalorganic Catalysts for Synthesis and Polymerization Recent Results by Ziegler-Natta and Metallocene Investigations*, W. Kaminsky (Ed.), Springer-Verlag, Berlin, PP 14-29 (1999).

Glöckner, G., Polymer Characterization by Liquid Chromatography, Elsevier, New York, p 207-218, (1978).

Goretzki, R., Fink, G., Tesche, B., Rieger, R. and Uzick, W., Unusual ethylene polymerization results with metallocene catalysts supported on silica, *Journal of Polymer Science: Part A: Polymer Chemistry*, **37**, 677-682 (1999).

Gregg, S. J. and Sing, K. S. W., "Adsorption, Surface Area and Porosity", Academic Press, Toronto, 2nd Edition, pp 153-160 (1982).

Grizotto, R. and De Menezes, H. C., Effect of Cooking on the Crispness of Cassava Chips, *Journal of Food Science,* **67(3)**, 1219-1223 (2002).

Hammawa, H., Mannan, T. M., Lynch. D. T. and Wanke, S. E., Effects of aluminum alkyls on ethylene/1-hexene polymerization with supported metallocene/MAO catalysts in the gas-phase, *Journal of Applied Polymer Science*, **92**, 3549-3560 (2004).

Han, T. K., Ko, Y. S., Park, J. W. and Woo, S. I., Determination of the number of active sites for olefin polymerization catalyzed over metallocene/MAO using the CO inhibition method, *Macromolecules*, **29**, 7305-7309 (1996).

Han-Adebekun, C. G., Debling, J. A. and Ray, W. H., Polymerization of olefins through heterogeneous catalysis. XVI. Design and control of a laboratory stirred bed copolymerization reactor, *Journal of Applied Polymer Science,* **64**, 373-382, (1997a).

Han-Adebekun, C. G., Hamba, H. and Ray, W. H., Kinetic study of gas-phase olefin polymerization with a $TiCl_4/MgCl_2$ catalyst I. Effect of polymerization conditions, *Journal of Polymer Science A: Polymer Chemistry*, **35** 2063-2074 (1997).

Harlan, C. J., Bott, S. G. and Barron, A. R., Three-coordinate aluminum is not a prerequisite for catalytic activity in the zirconocene-alumoxane polymerization of ethylene, *Journal of the American Chemical Society*, **117**, 6465-6474 (1995).

Harrison, D., Coulter, I. A., Wang, S., Nistala, S., Kuntz, B. A., Pigeon, M., Tian, J. and Collins, S., Olefin polymerization using supported metallocene catalysts: development of high activity catalysts for use in slurry and gas-phase ethylene polymerizations, *Journal of Molecular Catalysis A: Chemical,* **128**, 65-77 (1998).

Hewitt, G. F., Shires, G. L. and Bott, T. R., Process heat transfer, CRC Press, Boca Raton, p. 937 (1994).

Hlatky, G. G., Heterogeneous single-site catalysts for olefin polymerization, *Chemical Reviews*, **100**, 1347-1376 (2000).

Hsieh, H. L., Olefin polymerization catalysis technology, *Catalysis reviews: science and engineering*, **26 (3 & 4)**, 631-651 (1984).

Huang, J. and Rempel, G. L., Kinetic study of propylene polymerization using $Et(H_4Ind)_2ZrCl_2$/Methylalumoxane catalysts, *Industrial and Engineering Chemistry Research*, **36**, 1151-1157 (1997).

Huang, J. and Rempel, G. L., Ziegler-Natta catalysts for olefin polymerization: mechanistic insights from metallocene systems, *Progress in Polymer Science*, **20**, 459-526 (1995).

Huang, J. C.-K., Lacombe, Y., Lynch, D. T. and Wanke, S. E., Effects of hydrogen and 1-butene concentrations on the molecular properties of polyethylene produced by catalytic gas-phase polymerization, *Industrial and Engineering Chemistry Research*, **36**, 1136-1143 (1997).

Hutchinson, R. A., and Ray, W. H., Polymerization of olefins through heterogeneous catalysis IX: Experimental study of propylene polymerization over a high activity $MgCl_2$-supported Ti catalyst, *Journal of Applied Polymer Science*, **43**, 1271-1285 (1991).

Hutchinson, R. A., Chen, C. M. and Ray, W. H., Polymerization of olefins through heterogeneous catalysis X: Modeling of particle growth and morphology, *Journal of Applied Polymer Science*, **44**, 1389-1414 (1992).

Ivanchev, S. S., Baulin, A. A. and Rodionov, A. G., Promotion by supports of the reactivity of propagating species of Ziegler supported catalytic systems for the polymerization and copolymerization of olefins, *Journal of Polymer Science: Polymer Chemistry Edition*, **18**, 2045-2050 (1980).

Janiak, C. and Rieger, B., Silica gel supported zirconocene dichloride/methylalumoxane catalysts for ethylene polymerization: Effects of heterogenization on activity, polymer microstructure and product morphology, *Die Angewandte Makromolekulare Chemie*, **215**, 47-57 (1994).

Janiak, C., Rieger, B., Voelkel, R. and Braun, H-G., Polymeric aluminoxanes: A possible cocatalytic support material for Ziegler-Natta-type metallocene catalysts, *Journal of Polymer Science: Part A: Polymer Chemistry*, **31**, 2959-2968 (1993).

Jejelowo, M. O., Lynch, D. T. and Wanke, S. E., Comparison of ethylene polymerization in gas-phase and slurry reactors, *Macromolecules*, **24**, 1755-1761 (1991).

Jiang, Y., McAuley, K. B. and Hsu, J. C. C., Heat Removal from Gas-Phase Polyethylene Reactors in the Supercondensed Mode, *Industrial and Engineering Chemistry Research,* **36**, 1176-1180, (1997).

Joshi, P., Nigam, K. D. P. and Nauman, E. B., The Kenics static mixer: new data and proposed correlations, *The Chemical Engineering Journal,* **59,** 265-271 (1995).

Kageyama K, Tamazawa, J-I. and Aida, T., Extrusion polymerization: Catalyzed synthesis of crystalline linear polyethylene nanofibers within a mesoporous silica, *Science*, **285**, 2113-2115 (1999).

Kakugo, M., Sadatoshi, H., Sakai, J. and Yokoyama, M., Growth of polypropylene particles in heterogeneous Ziegler-Natta polymerization, *Macromolecules*, **22**, 3172-3177 (1989b).

Kakugo, M., Sadatoshi, H., Yokoyama, M. and Kojima, K., Transmission electron microscope observation of nascent polypropylene particles using a new staining method, *Macromolecules*, **22**, 547-551 (1989a).

Kallio, K., Wartmann, A. and Reichert, K-H., Effect of light on the activity of metallocene catalysts in the gas-phase polymerization of ethylene, *Macromolecular Rapid Communications*, **22**, 1330-1334 (2001).

Kamfjord, T., Wester, T. S. and Rytter, E., Supported metallocene catalysts prepared by impregnation of MAO modified silica by a metallocene/monomer solution, *Macromolecular Rapid Communications*, **19**, 505-509 (1998).

Kaminsky, W. and Laban, A., Metallocene catalysis, *Applied Catalysis A: General*, **222**, 47-61 (2001).

Kaminsky, W. and Lüker, H., Influence of hydrogen on the polymerization of ethylene with the homogeneous Ziegler system bis(cyclopentadienyl)zirconiumdichloride/alumoxane, *Die Makromolekulare Chemie. Rapid Communications*, **5**, 225-228 (1984).

Kaminsky, W. and Renner, F., High melting polypropenes by silica-supported zirconocene catalysts, *Die Makromolekulare Chemie. Rapid Communications*, **14**, 239-243 (1993).

Kaminsky, W. and Renner, F., High melting polypropylenes by silica-supported zirconocene catalysts, *Macomolecular Rapid Communications*, **14**, 239-243 (1993).

Kaminsky, W. C. and Strübel, C., Hydrogen transfer reactions of supported metallocene catalysts, *Journal of Molecular Catalysis A: Chemical*, **128**, 191-200 (1998).

Kaminsky, W., Highly active metallocene catalysts for olefin polymerization, *Journal of the Chemical Society, Dalton Transactions*, Pages 1413-1418 (1998).

Kaminsky, W., Olefin polymerization catalyzed by metallocenes, *Advances in Catalysis*, **46**, 89-159 (2001).

Kaminsy, W., New polymers by metallocene catalysis, *Macromolecular Chemistry and Physics*, **197**, 3907-3945 (1996).

Karol, F. J. and Kao, S-C., Ligand effects at transition metal centers for ethylene polymerization, *New Journal of Chemistry*, **18**, 97-103 (1994).

Karol, F. J., Kao, S-C., Wesserman, E. P. and Brady, R. C., Use of copolymerization studies with metallocene catalysts to probe the nature of active sites, *New Journal of Chemistry*, **21**, 797-805 (1997).

Karol, F. J., Kao, S-C., Wesserman, E. P. and Yu, Z., Features of cyclopentadienyl metal catalysts for ethylene copolymerization in gas and liquid phase. In *Metalorganic Catalysts for Synthesis and Polymerisation: Recent results by Ziegler-Natta and metallocene investigations*; W. Kaminsky, Ed., Springer, Berlin, 1999; p 629-642.

Kashiwa, N. and Yoshitake, J., The role of ethylbenzoate in the stereospecific propylene polymerization and copolymerization with ethylene using $MgCl_2$ supported $TiCl_4$ catalyst system. In *Transition metal catalyzed polymerizations–Ziegler-Natta and metathesis polymerizations*; R. P. Quirk, Ed., Cambridge University Press, Cambridge, 1988; p 240-254.

Keii, T., Suzuki, E., Tamura, M., Murata, M. and Doi, Y., Propene polymerization with magnesium chloride-supported Ziegler catalyst. 1. Principal kinetics, *Macromolecular Chemie*, **183**, 2285-2304 (1982).

Kissin, Y. V., *Isospecific Polymerization of Olefins with Heterogeneous Ziegler-Natta Catalysts*, Springer-Verlag New York Inc., p. viii (1985).

Kissin, Y. V., Mink, R. I., Nowlin, T. E. and Brandolini, A. J., Kinetics of ethylene polymerization and copolymerization reactions with heterogeneous titanium-based Ziegler-Natta catalysts, In *Metalorganic Catalysts for Synthesis and Polymerization Recent Results by Ziegler-Natta and Metallocene Investigations*, W. Kaminsky, Ed., p 60-75, Springer, Berlin (1999).

Kittilsen, P., McKenna, T. F., Svendsen, H., Jakobsen, H. A. and Fredriksen, S. W., The interaction between mass transfer effects and morphology in heterogeneous olefin polymerization, *Chemical Engineering Science*, **56**, 4015-4028 (2001a).

Kittilsen, P., Svendsen H., and McKenna, T. F., Modeling of transfer phenomena on heterogeneous Ziegler-Natta catalysts. IV. Convection effects in gas-phase processes, *Chemical Engineering Science*, **56**, 3997-4005 (2001b).

Klimesch, R., Littmann, D. and Mähling, F.-O., Polyethylene: High-pressure, in *Encyclopedia of Materials: Science and Technology*, Elsevier Science Ltd. p. 7181-7184 (2001).

Knoke, S., Korber, F., Fink, G. and Tesche, B., Early stages of propylene bulk phase polymerization with supported metallocene catalysts, *Macromolecular Chemistry and Physics*, **204**, 607-617 (2003).

Ko, Y. S. and Woo, S. I., Generation of active site confined inside supercage of NaY zeolite on a nano-scale and its ethylene polymerization, *European Polymer Journal*, **39**, 1553-1557 (2003).

Ko, Y. S., Han, T. K., Park, J. W. and Woo, S. I., Propene polymerization catalyzed over MCM-41 and VPI-5-supported Et(Ind)$_2$ZrCl$_2$ catalysts, *Macromolecular Rapid Communications*, **17**, 749-758 (1996).

Koch, M., Falcou, A., Nenov, N., Klapper, M. and Müllen, K., Reversibly crosslinked networks of nanoparticles in metallocene-catalyzed olefin polymerization, *Macromolecular Rapid Communications*, **22**, 1455-1462 (2001).

Koch, M., Stork, M., Klapper, M. and Müllen, K., Immobilization of metallocenes through noncovalent bonding via MAO to a reversibly cross-linked polystyrene, *Macromolecules*, **33**, 7713-7717 (2000).

Koivumäki, J. and Seppälä, J. V., Observations on the rate enhancement effect with MgCl$_2$/TiCl$_4$ and Cp$_2$ZrCl$_2$ catalyst system upon 1-hexene addition, *Macromolecules*, **26**, 5535-5538 (1993).

Koivumäki, J., Fink, G. and Seppälä, J. V., Copolymerization of ethane/1-dodecene and ethane/1-octadecene with the stereorigid zirconium catalyst systems iPr[FluCp]ZrCl$_2$/MAO and Me$_2$[Ind]$_2$ZrCl$_2$/MAO: Influence of the comonomer chain length, *Macromolecules*, **27**, 6254-6258 (1994).

Korber, F., Hauschild, K. and Fink, G., Reaction calorimetric approach to the kinetic investigation of the propylene bulk phase polymerization, *Macromolecular Chemistry and Physics*, **202**, 3329-3333 (2001).

Kumkaew, P., Wanke, S. E., Praserthdam, P., Danumah, C. and Kaliaguine, S., Gas-phase ethylene polymerization using zirconocene supported on mesoporous molecular sieves, *Journal of Applied Polymer Science*, **87**, 1161-1177 (2003b).

Kumkaew, P., Wu, L., Praserthdam, P. and Wanke, S. E., Rates and product properties of polyethylene produced by copolymerization of 1-hexene and ethylene in the gas phase with (*n*-BuCp)$_2$ZrCl$_2$ on supports with different pore sizes, *Polymer*, **44**, 4791-4803 (2003a).

Lacombe, Y., TREF and SEC Characterization of Ethylene/1-Butene copolymers Produced at Various 1-Butene and Hydrogen Pressures, *M.Sc., Thesis, University of Alberta,* Edmonton, Canada, p 55-69 (1995).

Lahelin, M., Kokko, E., Lehmus, P., Pitkänen, P., Löfgren, B. and Seppälä, J., Propylene polymerization with *rac*-SiMe$_2$(2-Me-4-PhInd)$_2$ZrMe$_2$/MAO: Polymer characterization and kinetic models, *Macromolecular Chemistry and Physics*, **204**, 1323-1337 (2003).

Lasarov, H., Monkkonen, K. and Pakkanen, T. T., Versatile Laboratory-Scale Polymerization Reactor System: Matallocene/MAO-Based Ethylene/Cycloolefin Copolymerizations, *Journal of Applied Polymer Science,* **77,** 2921-2928 (2000).

Lauher, J. W. and Hoffmann, R., Structure and Chemistry of bis(cyclopentadienyl)–ML_n complexes, *Journal of the American Chemical Society*, **98**, 1729-1742 (1976).

Laurence, R. L. and Chiovetta, M. G., Heat and mass transfer during olefin polymerization from the gas-phase. In *Polymer reaction engineering: Influence of reaction engineering on polymer properties*, K. H. Reichert and W. Geiseler (Eds.), Hanser Publishers, Munich, 1983. p. 73-111.

Lee, I-M., Gauthier, W. J., Ball, J-A. M., Iyengar, B. and Collins, S., Electronic effects in Ziegler-Natta polymerization of propylene and ethylene using soluble metallocene catalysts, *Organometallics*, **11**, 2115-2122 (1992).

Leofanti, G., Padovan, M., Tozzola, G. and Venturelli, B., Surface area and pore texture of catalysts, *Catalysis Today,* **41**, 207-219 (1998).

Lippens, B. C. and DeBoer, J. H., Studies on pore systems in catalysts V. The *t* method, *Journal of Catalysis,* **4**, 319-323 (1965).

Liu, C., Tang, T. and Huang, B., Preparation and application of a novel core-shell-particle-supported zirconocene catalyst, *Journal of Polymer Science: Part A: Polymer Chemistry*, **39**, 2085-2092 (2001).

Liu, S., Meng, F., Yu, G. and Huang, B., Preparation of polymer-supported zirconocene catalysts and olefin polymerization, *Journal of Applied Polymer Science*, **71**, 2253-2258 (1999).

Liu, S., Yu G., and Huang, B., Polymerization of ethylene by zirconocene-$B(C_6F_5)_3$ catalysts with aluminum compounds, *Journal of Applied Polymer Science*, **66**, 1715-1720 (1997).

Lynch, D. T. and Wanke, S. E., Reactor design and operation for gas-phase ethylene polymerization using Ziegler-Natta catalysts, *The Canadian Journal of Chemical Engineering*, **69**, 332-339 (1991).

Lynch, D. T., Jejelowo, M. O. and Wanke, S. E., The influence of aluminum alkyls on the polymerization of ethylene with $SiO_2/MgCl_2$-supported $TiCl_4$ catalysts, *The Canadian Journal of Chemical Engineering*, **69**, 657-664 (1991).

Mannan, T. M., Hammawa, H., Lynch, D. T. and Wanke, S. E., A laboratory reactor for gas-phase olefin polymerization, *The Canadian Journal of Chemical Engineering* (in press, September, 2003).

McDaniel, M. P., Fracturing silica-based catalysts during ethylene polymerization, *Journal of Polymer Science: Polymer Chemistry Edition*, **19**, 1967-1976 (1981).

McKenna, T. and Mattioli, V., Progress in describing particle growth for polyolefins: A look at particle morphology, *Macromolecular Symposium*, **173**, 149-162 (2001).

McKenna, T. F. and Soares, J. B. P., Single particle modeling for olefin polymerization on supported catalysts: A review and proposals for future developments, *Chemical Engineering Science*, **56**, 3931-3949 (2001).

Meier, G. B., Weickert, G. and van Swaaij, W. P. M., Gas-phase polymerization of propylene: Reaction kinetics and molecular weight distribution, *Journal of Polymer Science: Part A: Polymer Chemistry*, **39**, 500-513 (2001).

Meng, F., Yu, G. and Huang, B., Polymer-supported zirconocene catalyst for ethylene polymerization, *Journal of Polymer Science: Part A: Polymer Chemistry*, **37**, 37-46 (1999).

Meshkova, I. N., Ushakova, T. M., Ladygina, T. A., Kovaleva, N. Yu. and Novokshonova, L. A., Ethylene polymerization with catalysts on the base of Zr-cenes and methylaluminoxanes synthesized on zeolite support, *Polymer Bulletin*, **44**, 461-468 (2000).

Michelotti, M., Altomare, A., Ciardelli, F. and Roland, E., Zeolite supported polymerization catalysts: Copolymerization of ethylene and α-olefins with metallocenes supported on HY zeolite, *Journal of Molecular Catalysis A: Chemical*, **129**, 241-248 (1998).

Mills, N. J., Plastics: Microstructure & Engineering Applications, Halsted Press, New York (1993) p. 22.

Mink, R. I. and Nowlin, T. E., High activity polyethylene catalysts prepared with alkoxysilane reagents, US Patent 5,470,812 (1995).

Mix, H., Fuhrmann, H., Reihsig, J., Bredereck, H, Oswald, L., Pracht, H. and Haupke, K., High-active Ziegler-Natta catalysts on polymeric supports for the manufacture of injection moulding polyethylene, *Acta Polymerica*, **41**, 601-607 (1990).

Moore, S. J. and Wanke, S. E., Solubility of ethylene, 1-butene and 1-hexene in polyethylenes, *Chemical Engineering Science*, **56**, 4121-4129 (2001).

Moroz, B. L., Semikolenova, N. V., Nosov, A. V., Zakharov, V. A., Nagy, S. and O'Reilly, N. J., Silica supported zirconocene catalysts: Preparation, characterization and activity in ethylene polymerization, *Journal of Molecular Catalysis A: Chemical*, **130**, 121-129 (1998).

Mortara, S., Fregonese, D. and Bresadola, S., Metallocene derivatives as active supports of olefin polymerization catalysts, *Macromolecular Chemistry and Physics*, **202**, 2630-2633 (2001).

Mteza, S. B., Hsu, C. C. and Bacon, D. W., A study of polyethylene-gr-2-tert-butyl amino methacrylate-supported $TiCl_4$ catalyst for ethylene polymerization, *Journal of Polymer Science: Part A: Polymer Chemistry*, **34**, 1693-1702 (1996).

Muñoz-Escalona, A., García, H. and Albornoz, A., Homo- and copolymerization of ethylene with highly active catalysts based on $TiCl_4$ and Grignard compounds, *Journal of Applied Polymer Science*, **34**, 977-988 (1987).

Muñoz-Escalona, A., Hernandez, J. G. and Gallardo, J. A., Catalytic activity and control of the nascent morphology of polyethylenes obtained with first and second generation Ziegler-Natta catalysts, *Journal of Applied Polymer Science*, **29**, 1187-1202 (1984).

Musikabhumma, K., Uozumi, T., Sano, T. and Soga, K., Poly(4-vinylpyridine)-supported cationic bis(cyclopentadienyl)zirconocene catalyst: Development of a new simple method to prepare polymer-supported cationic zirconocene and its application to ethylene polymerization, *Macromolecular Rapid Communications*, **21**, 675-679 (2000).

Naik, S. D. and Ray, W. H., Particle morphology for polyolefins synthesized with supported metallocene catalysts, *Journal of Applied Polymer Science*, **79**, 2565-2579 (2001).

Nishida, H., Uozumi, T., Arai, T. and Soga, K., Polystyrene-supported metallocene catalysts for olefin polymerizations, *Macromolecular Rapid Communications*, **16**, 821-830 (1995).

Nooijen, G. A. H., On the importance of diffusion of cocatalyst molecules through heterogeneous Ziegler-Natta catalysts, *European Polymer Journal*, **30**, 11-15 (1994).

O'Donohue, S. J. and Meehan, E., Polymer Characterization by High Temperature Size Exclusion Chromatography Employing Molecular Weight Sensitive Detectors, in Chromatography of Polymers: Hyphenated and Multidimentional techniques, T. Provder (Ed.), *ACS Symposium Series 731*, American Chemical Society, Washington, DC, p 52-65 (1999).

Oleshko, V. P., Crozier, P. A., Cantrell, R. D. and Westwood, A. D., *In situ* real-time environmental TEM of gas phase Ziegler-Natta catalytic polymerization of propylene, *Journal of Electron Microscopy*, **51(supplement)**, S27-S39 (2002).

Ortega-Rivas, E., Food Powders: Part I, Characterization, Aspen Publishers, Inc., Gaithersburg, MD, p (2001). Reference information taken from a Preprint of the book at www.fcq.uach.mx/licenciaturas/temarios/ procesamiento/tema1.pdf

Oulahna, D., Cordier, F., Galet, L. and Dodds, J. A., Wet granulation: the effect of shear on granule properties, *Powder Technology*, **130**, 238-246 (2003).

Panin, A. N., Dzhabieva, Z. M., Nedorezova, P. M., Tsvetkova, V. I., Saratovskikh, S. L., Babkina, O. N. and Bravaya, N. M., Triisobutylaluminum as cocatalyst for zirconocenes. II. Triisobutylaluminum as a component of a cocatalyst system and as an effective cocatalyst for olefin polymerization derived from dimethylated zirconocenes, *Journal of Polymer Science, Part A: Polymer Chemistry*, **39**, 1915-1930 (2001).

Pasquet, V. and Spitz, R., Irreversible activation effects in ethylene polymerization, *Makromolekulare Chemie*, **194**, 451-461 (1993).

Pater, J. T. M., Weickert, G. and van Swaaij, W. P. M., Propene bulk polymerization kinetics: Role of prepolymerization and hydrogen, *AIChE Journal*, **49**, 180-193 (2003).

Petoff, J. L. M., Myers, C. L. and Waymouth, M., Influence of trialkylaluminum reagents on the propylene polymerization behavior of bridged and unbridged 2-arylidene metallocene polymerization catalysts, *Macromolecules*, **32**, 7984-7989 (1999).

Piccolrovazzi, N., Pino, P., Consiglio, G., Sironi, A. and Moret, M., Electronic effect in homogeneous indenylzirconium Ziegler-Natta catalysts, *Organometallics*, **9**, 3098-3105 (1990).

Pietikäinen, P. and Seppälä, J. A., Low molecular weight ethylene/propylene copolymers. Effect of process parameters on copolymerization with homogeneous Cp_2ZrCl_2 catalyst, *Macromolecules*, **27**, 1325-1328 (1994).

Pnachenko, N. N., Zakharov, V. A., Danilova, I. G., Paukshtis, E. A., Zakharov, I. I., Goncharov, V. G. and Suknev, A. P., "Structure and performance of the solid methylalumoxane at temperatures 20–250°C: Experimental and DFT calculation study", *Journal of Molecular Catalysis A: Chemical*, **174**, 107-117, (2001).

Przybyla, C., Tesche, B. and Fink, G., Ethylene/hexene copolymerization with the heterogeneous catalyst system SiO_2/MAO/*rac*-$Me_2Si[2\text{-}Me\text{-}4\text{-}Ph\text{-}Ind]_2ZrCl_2$: The filter effect, *Macromolecular Rapid Communications*, **20**, 328-332 (1999).

Qin, Y., Tang, T., Zhao, Z. and Huang, B., Ethylene polymerization with porous polystyrene spheres supported Cp_2ZrCl_2 catalyst, *Journal of Polymer Science: Part A: Polymer Chemistry*, **41**, 3313-3319 (2003).

Quijada, R., Rojas, R., Alzamora, L., Retuert, J. and Rabagliati, F. M., Study of metallocene supported on porous and nonporous silica for the polymerization of ethylene, *Catalysis Letters*, **46**, 107-112 (1997).

Quijada, R., Rojas, R., Narvaez, A., Alzamora, L., Retuert, J. and Rabagliati, F. M., The effect of reaction parameters on catalytic activity in the polymerization of ethylene using supported and unsupported metallocene catalysts, *Applied Catalysis A: General*, **166**, 207-213 (1998).

Rahiala, H., Beurroies, I., Eklund, T., Hakala, K., Gougeon, R., Trens, P. and Rosenholm, J. B., Preparation and characterization of MCM-41 supported metallocene catalysts for olefin polymerization, *Journal of Catalysis*, **188**, 14-23 (1999).

Ran, R., Polymer-supported Ziegler-Natta catalyst for the polymerization of isoprene, *Journal of Polymer Science: Part A: Polymer Chemistry*, **31**, 1561-1569 (1993).

Rappé, A. K., Skiff, W. M. and Casewit, C. J., Modeling metal-catalyzed olefin polymerization, *Chemical Reviews*, **100**, 1435-1456 (2000).

Resconi, L., Piemontesi, F., Franciscono, G., Abis, L. and Fioranit, T., Olefin polymerization at bis(pentamethylcyclopentadienyl)zirconium and –hafnium centers: Chain-transfer mechanisms, *Journal of the Americam Chemical Society*, **114**, 1025-1032 (1992).

Ribeiro, M. R., Deffieux, A. and Portela, M. F., Supported metallocene complexes for ethylene and propylene polymerizations: Preparation and activity, *Industrial and Engineering Chemistry Research*, **36**, 1224-1237 (1997).

Roark, D. N., McKusick, B. C. and Steuerle, U., Aziridines, in Ullmann's Encyclopedia of Industrial Chemistry, Wiley-VCH Verlag (Electronic Edition), (2002).

Robinson, S., Breaking the mould, *Chemistry and Industry*, **12**, 377-379 (2001).

Roos, P., Meier, G. B., Samson, J. J. C., Weickert, G. and Westerterp, K. R., Gas phase polymerization of ethylene with a silica-supported metallocene catalyst: influence of temperature on deactivation, *Macromolecular Rapid Communications*, **18**, 319-324 (1997).

Roscoe, S. B., Fréchet, J. M. J., Walzer, J. F. and Dias, A. J., Polyolefin spheres from metallocenes supported on noninteracting polystyrene, *Science*, **280**, 270-273 (1998).

Roscoe, S. B., Gong, C., Fréchet, J. M. J. and Walzer, J. F., Functionalized polystyrene as a versatile support for olefin polymerization catalysts, *Journal of Polymer Science Part A: Polymer Chemistry*, **38**, 2979-2992 (2000).

Rosenburg, J.-E. and Flodin, P., Macroporous Gels. 1. Polymerization of Trimethylolpropane Trimethacrylate in Toluene, *Macromolecules*, **19**, 1543-1546 (1986).

Rosenburg, J.-E. and Flodin, P., Macroporous Gels. 2. Polymerization of Trimethylolpropane Trimethacrylate in Various Solvents, *Macromolecules*, **20**, 1518-1522 (1987a).

Rosenburg, J.-E. and Flodin, P., Macroporous Gels. 3. Copolymerization of Trimethylolpropane Trimethacrylate and Methyl Methacrylate in Toluene or Ethyl Acetate, *Macromolecules*, **20**, 1522-1526 (1987b).

Rytter, E. and Ott, M., Supported metallocene catalysts prepared by impregnation of silica with metallocene/aluminoxane/1-hexene solutions, *Macromolecular Rapid Communi-cations*, **22**, 1427-1431 (2001).

Sacchi, M.C., Zucchi, D., Tritto, I., Locatelli, P. and Dall'Occo, T., Silica-supported metallocenes: stereochemical comparison between homogeneous and heterogeneous catalysis, *Macomolecular Rapid Communications*, **16**, 581-590 (1995).

Samson J. J. C., van Middelkoop, B., Weickert, G. and Westerterp, K. R., Gas-Phase Polymerization of propylene with a Highly Active Ziegler-Nata Catalyst, *AIChE J,* **45,** 1548-1558 (1999).

Samson, J. J. C., Stokman, J., Weickert, G. and Westerterp, K. R., Gas phase polymerization of propylene with a highly active $MgCl_2/TiCl_4$/Ethylbenzoate catalyst, Proceedings of AIChE Conference, Sandiego 1996, p 521-526.

Samson, J. J. C., Weickert, G., Heerze, A. E. and Westerterp, K. R., Liquid-phase polymerization of propylene with a highly active catalyst, *AIChE Journal*, **44**, 1424-1437 (1998).

Santora, B. P., Gagne, M. R., Moloy, K. G. and Radu, N. S., Porogen and cross-linking effects on the surface area, pore volume distribution, and morphology of macroporous polymers obtained by bulk polymerization, *Macromolecules*, **34**, 658-661 (2001).

Satyanarayana, G. and Sivaram, S., An unusually stable supported bis(cyclopentadienyl) titanium dichloride-trialkylaluminum catalyst system for ethylene polymerization, *Macromolecules*, **26**, 4712-4714 (1993).

Schmeal, W. R. and Street, J. R., Polymerization in expanding catalyst particles, *AIChE Journal*, **17**, 1188-1197 (1971).

Selic, E. and Borchard, W., A new apparatus for the characterization of the swelling behavior of micro-gel particles, *Macromolecular Chemistry and Physics,* 202, 516-520 (2001).

Sherrington, D. C., Preparation, structure and morphology of polymer supports, *Chemical Communications*, 2275-2286 (1998).

Singh, D. and Merrill, R. P., Molecular weight distribution of polyethylene produced by Ziegler-Natta catalysts, *Macromolecules*, **4**, 599-604 (1971).

Sinn, H., Proposals for structure and effect of methylalumoxane based on mass balances and phase-separation experiments, *Macromolecular Symposia*, **97**, 27-52 (1995).

Šír, J. and Lecjaks, Z., Pressure drop and homogenization efficiency of a motionless mixer, *Chemical Engineering Communications,* **16,** 325-334 (1982).

Soga, K. and Kaminaka, M., Copolymerization of olefins with SiO_2-supported zirconocene catalysts by common trialkylaluminums, *Makromolekulare Chemie*, **194**, 3499-3504 (1993).

Soga, K., Shiono, T. and Kim, H. J., Activation of SiO_2-, Al_2O_3, and $MgCl_2$-supported metallocene catalysts activated by trialkylaluminums, *Macromolecular Chemistry and Physics*, **195**, 1369-1379 (1994).

Spaleck, W., Küber, F., Winter, A., Rohrmann, J., Bachmann, B., Antberg, M., Dolle, V. and Paulus, E. F., The influence of aromatic substituents on the polymerization behavior of bridged zirconocene catalysts, *Organometallics*, **13**, 954-963 (1994).

Starck, P., Studies of the comonomer distributions in low density polyethylenes using temperature rising elution fractionation and stepwise crystallization by DSC, *Polymer International*, **40**, 111-122 (1996).

Stork, M., Koch, M., Klapper, M., Müllen, K., Gregorius, H. and Rief, U., Ethylene polymerization using crosslinked polystyrene as support for zirconocene dichloride/methylaluminoxane, *Macromolecular Rapid Communications*, **20**, 210-213 (1999).

Sun, L., Hsu, C. C. and Bacon, D. W., Polymer-supported Ziegler-Natta catalysts. I. A preliminary study of catalyst synthesis, *Journal of Polymer Science: Part A: Polymer Chemistry*, **32**, 2127-2134 (1994b).

Sun, L., Hsu, C. C. and Bacon, D. W., Polymer-supported Ziegler-Natta catalysts. II. Ethylene homo- and copolymerization with $TiCl_4/MgR_2$/Poly(ethylene-*co*-acrylic acid) catalyst, *Journal of Polymer Science: Part A: Polymer Chemistry*, **32**, 2135-2145 (1994a).

Tait, P. J. T., Downs, G. W. and Akinbami, A. A., Copolymerization of ethylene and α-olefins: A kinetic consideration. In *Transition metal catalyzed polymerizations–Ziegler-Natta and metathesis polymerizations*; R.P. Quirk, Ed., Cambridge University Press, Cambridge, 1988; p 834-860.

Tait, P. J. T., Monteiro, M. G. K., Yang, M., Richardson, J. and Ediati, R., Advances in supported metallocene catalysis, *Polimery*, **45**, 314-322 (2000).

Tian, J., Wang, S., Feng, Y., Li, J. and Collins, S., Borane-functionalized oxide supports: development of active supported metallocene catalysts at low aluminoxane loading, *Journal of Molecular Catalysis A: Chemical*, **144**, 137-150 (1999).

Trautz, V., Seeing the light, *Chemistry & Industry*, **13**, 13 (2002).

Tsutsui, T. and Kashiwa, N., Gas-phase polymerization of propylene with a solid complex catalyst obtained from $Et(Ind)_2ZrCl_2$ and methylaluminoxane, *Polymer*, **32**, 2671-2673 (1991).

Unger, K. K., *Porous silica: its properties and use as support in column liquid chromatography*, Elsevier Scientific Publications Co., Amsterdam, p. 8-9 (1979).

van Looveren, L. K., Geysen, D. F., Vercruysse, K. A., Wouters, B. H., Grobet, P. J. and Jacobs, P. A., Methylalumoxane MCM-41 as support in the co-oligomerization of ethane and propene with $[\{C_2H_4(1\text{-indenyl})_2\}Zr(CH_3)_2]$, *Angewadte Chemie International Edition*, **37(4)**, 517-520 (1998).

Veera, U. P., Weickert, G. and Agarwal, U. S., Modeling monomer transport by convection during olefin polymerization, *AIChE Journal*, **48**, 1062-1070 (2002).

vela Estrada, J. M. and Hamielec, A. E., Modelling of ethylene polymerization with Cp_2ZrCl_2/MAO catalyst, *Polymer*, **35**, 808-818 (1994).

Webb, S. W., Weist, E. L., Chiovetta, M. G., Laurence, R. L. and Conner, W. C., Morphological influences in the gas-phase polymerization of ethylene by silica supported chromium oxide catalysts, *The Canadian Journal of Chemical Engineering*, **69**, 665-681 (1991).

Weickert, G., Meier, G. B., Pater, J. T. M. and Westerterp, K. R., The particle as microreactor: catalytic propylene polymerizations with supported metallocenes and Ziegler-Natta catalysts, *Chemical Engineering Science*, **54**, 3291-3296 (1999).

Weickert, G., Samson, J. J., Roos, P. and Westerterp, K. R., Investigation of olefin polymerization with Ziegler-Nata andmetallocenes, *DECHEMA Monographs*, **131**, 235-248 (1995).

Wester, T. S. and Ystenes, M., Kinetic studies of the injection of comonomers during polymerization of ethane and propene with $MgCl_2$-supported Ziegler-Natta catalysts, *Macromolecular Chemistry and Physics*, **198**, 1623-1648 (1997).

Whittaker, H. L. and Wills, G. B., A study of the surface-catalyzed polymerization of ethylene on chromium oxide-silica-alumina catalysts, *Journal of Applied Polymer Science*, **13**, 1921-1927 (1969).

Wild, L., Temperature rising Elution Fractionation, *Advances in Polymer Science*, **98**, 1-47, (1991).

Woo, S. I., Ko, Y. S. and Han, T. K., Polymerization of ethylene over metallocenes confined inside the supercage of a NaY zeolite, *Macromolecular Rapid Communications*, **16**, 489-494 (1995).

Wu, L., Ethylene polymerization over morphology-controlled Ziegler-Natta catalysts, Ph.D. Thesis, Department of Chemical and Materials Engineering, University of Alberta (1999).

Wu, L., Lynch, D. T. and Wanke, S. E., Kinetics of gas-phase ethylene polymerization with morphology-controlled $MgCl_2$-supported $TiCl_4$ catalyst, *Macromolecules*, **32**, 7990-7998 (1999).

Xie, T., McAuley, K. B., Hsu, J. C. C. and Bacon, D. W., Gas phase ethylene polymerization: Production processes, polymer properties, and reactor modeling, *Industrial and Engineering Chemistry Research*, *33*, 449-479 (1994).

Xu, J. and Feng, L., Application of temperature rising elution fractionation in polyolefins, *European Polymer Journal*, **36**, 867-878 (2000).

Xu, J.-T., Zhu, Y.-B., Fan, Z.-Q. and Feng, L.-X., Copolymerization of propylene with various higher α-olefins using silica-supported *rac*-$Me_2Si(Ind)_2ZrCl_2$, *Journal of Polymer Science: Part A: Polymer Chemistry*, **39**, 3294-3303 (2001b).

Xu, Z. G., Chakravarti, S. and Ray, W. H., Kinetic study of olefin polymerization with a supported metallocene catalyst. I. Ethylene/propylene copolymerization in gas phase, *Journal of Applied Polymer Science*, **80**, 81-114 (2001a).

Zakharov, V. A. and Yermakov, Y. I., Kinetic study of ethylene polymerization with chromium oxide catalysts by a radiotracer technique, *Journal of Polymer Science: Part A-1*, **9**, 3129-3146 (1971).

Zakharov, V. A., Bukatov, G. D. and Yermakov, Y. I., On the mechanism of olefin polymerization by Ziegler-Natta catalysts, *Advances in Polymer Science*, **51**, 61-97 (1983).

Zhang, M., Characterization of Commercial Linear Low Density Polyethylenes by TREF, SEC, DSC, and Cross-Fractionation, *M.Sc., Thesis, University of Alberta,* Edmonton, Canada, p 33-37, (1999).

Zhang, R., Li, W., Liang, X., Wu, G., Lü, Y., Zhan, L., Lu, C. and Ling, L., Effect of hydrophobic group in polymer matrix or porosity of organic and carbon aerogels from sol–gel polymerization of phenolic resole and methylolated melamine, *Microporous and Mesoporous Materials*, **62**, 17-27 (2003).

Zhou, J-M., Li, N-H., Bu, N-Y., Lynch, D. T. and Wanke, S. E., Gas-phase ethylene polymerization over polymer-supported metallocene catalysts, *Journal of Applied Polymer Science*, **90**, 1319-1330 (2003).

Zhu, H., Jin, G-X. and Hu, N., Polymer immobilized silane bridged metallocene catalysts for ethylene polymerization, *Journal of Organometallic Chemistry*, **655**, 167-171 (2002).

Zoellner, K. and Reichert, K-H., Gas-phase polymerization of butadiene –kinetics, particle size distribution, modeling, *Chemical Engineering Science*, **56**, 4099-4106 (2001).

Zöllner, K. and Reichert, K-H., Video microscopy for the examination of the heterogeneous gas-phase polymerization, *Chemical Engineering and Technology*, **25**, 707-710 (2002).

Zurek, E. and Ziegler, T., A theoretical study of the insertion barrier of MAO (methylaluminoxane)-activated, Cp_2ZrMe_2-catalyzed ethylene polymerization: further evidence for the structural assignment of active and dormant species, *Faraday Discussions*, **124**, 93-109 (2003).

Zurek, E. and Ziegler, T., Toward the identification of dormant and active species in MAO (methylaluminoxane)-activated, dimethylzirconocene-catalyzed olefin polymerization, *Organometallics*, **21**, 83-92 (2002).

Appendix A: Summary of Catalyst Preparation and Composition

Details regarding the preparation of catalysts are provided in Table A-1. The composition of the catalyst based on the amounts of reagents used (calculated), and the composition determined by the instrumental neutron activation analysis, INAA (measured) are listed in Table A-2. Only the measured catalyst compositions were used in the analyses of polymerization activities.

Table A-1. Detailed description of catalysts preparation conditions*

Catalyst	Date Catalyst Prepared	Support	Support Details		Preparation Details								Catalyst recov'd[5] g
			Mass[1] g	Pretreatment condition	Toluene[2] mL	MAO**		Shaking Time[3], h	$(n\text{-BuCp})_2\text{ZrCl}_2$ Addition			Shaking Time, h	
						mL	mmol		mg	mmol	Toluene[4] mL		
HH01[6]	4-Feb-01	PE971124	1.501	80 °C, 18 h	-	10	15.18	6.3	23.7	58.59	5.7	14	1.550
HH02	2-Apr-01	PE971204	2.000	86 °C, 16 h	-	15	22.77		31	76.63	5	5.5	3.100
HH03	7-May-01	PE990908	2.500	70 °C, 5 h	-	11.5	25.93	16	38	93.94	4.5	21	3.300
HH04[7]	18-May-01	PE001018	1.525	50 °C, 21 h	-	7.2	16.24	5	27	66.74	5	16	
HH05[8]	24-May-01	PE001018	1.310	78 °C, 16.5 h	-	9	20.30	7.25	22.2	54.88	5	4.3	2.400
HH06	4-Jun-01	PE9023	1.500	70 °C, 20 h	-	10.5	15.94	23	18.3	45.24	4	3.5	2.050
HH07[9]	17-Jun-01	Porapak-T	1.500	80 °C, 16 h	-	15	22.77	51	28	69.22	4	3.5	2.400
HH08	26-Jun-01	PE981124	2.000	85 °C, 18.7 h	-	26.5	40.22	24	46	113.71	5	3.3	3.015
HH09	10-Jul-01	PE971124	1.500	75 °C, 16.5 h	10	5	7.59	4.7	9.7	23.98	2	3.3	1.529
HH10[10]	16-Jul-01	PE971204	0.780	80 °C, 17 h	4	5.2	7.89	3.2	9.5	23.48	3	3.2	1.140
HH11	26-Jul-01	PE990212	1.500	70 °C, 16 h	4	10	15.18	4.2	18	44.50	3	4.4	2.015
HH12	29-Jul-01	PE991119	1.500	82 °C, 18 h	10	10	15.18	3.8	17.9	44.25	3	2.5	1.370
HH13	12-Aug-01	PE971124	2.000	85 °C, 18.7 h	10	26	39.46	3.5	50	123.60	7	2.7	2.790
HH14	30-Aug-01	PE971124	1.000	75 °C, 16 h	5	15	22.77	4.2	26	64.27	5	2.7	1.425
HH15	5-Sep-01	PE971124	2.000	87 °C, 18 h	10	27	40.98	3.4	52	128.54	7	2.3	2.453
HH16	3-Oct-01	HayeSep-T	1.505	85 °C, 18.3 h	5	10	15.18	3.3	22.5	55.62	5	2.3	1.755
HH17	9-Oct-01	HayeSep-A	1.500	80 °C, 16 h	5	10	15.18	3	19	46.97	8	2	1.737
HH18	22-Oct-01	HayeSep-S	1.502	75 °C, 17.5 h	5	10	15.18	6.5	20.5	50.68	6	2	1.976
HH19	25-Oct-01	HayeSep-R	1.507	65 °C, 16 h	5	11	16.70	4	19	46.97	7	2.2	1.998
HH20[11]	1-Nov-01	HayeSep-C	1.500	70 °C, 17 h	5	11.5	17.45	3.4	20	49.44	5	1	1.990
HH21	8-Nov-01	HayeSep-B	1.460	75 °C, 15.7 h	5	10	15.18	3.7	20.5	50.68	7	2	1.912

* Continued on the next page

Table A-1. Cont'd

Catalyst	Date Catalyst Prepared	Support	Support Details		Preparation Details								Catalyst recov'd^5 g
			Mass^1 g	Pretreatment condition	Toluene^2 mL	MAO*		Shaking Time^3, h	$(n\text{-BuCp})_2ZrCl_2$ Addition			Shaking Time, h	
						mL	mmol		mg	mmol	Toluene^4 mL		
HH22	11-Mar-02	HayeSep-Q	2.001	75 °C, 17 h	10	4.9	7.44	4.1	20	49.44	5	2	2.440
HH23[12]	26-Mar-02	MAO				15	22.77		25.4	62.79	4	4.5	0.570
HH24[13]	26-Mar-02	MAO				15	22.77		25.4	62.79	4	6.7	0.580
HH25	26-May-02	HayeSep-R	1.510	75 °C, 16 h	6	10	15.18	3	20.3	50.18	5	2.4	1.890
HH26	11-Jun-02	HayeSep-R	1.502	75 °C, 16.5 h	7	10.2	15.48	4.5	22	54.38	7	2.5	2.255
HH27	19-Jun-02	HayeSep-R	1.502	75 °C, 20 h	5	20	30.36	3	31.3	77.37	5	3.2	2.669
HH28[14]	27-Jun-02	HayeSep-R	1.500	82 °C, 20 h	6	11	16.70	3.5	19	46.97	6	2.3	2.455
HH29	4-May-03	Sty/Dvb 1%	1.501	90 °C, 20 h	10	10.2	15.48	4	18.7	46.23	5	2.5	2.160

1. Mass before pretreatment
2. Volume of toluene used for suspending the support
3. Contact time of support/cocatalyst or support/cocatalyst/metallocene suspension on a shaker at ~200 rpm at room temperature
4. Amount of toluene used to prepare the metallocene solution added to the support/cocatalyst suspension
5. Free flowing catalysts have better recovery (from the preparation flask) than caked ones
6. MAO treated support was dried before addition of metallocene solution; 0.12 mL TIBA was used in making toluene solution of the metallocene
7. The support/MAO suspension cooled in ice bath ~30min, excess liq. Evacuated before adding Zr soln; incomplete metallocene transferred ~6mg
8. After 7.25h shaking, suspension left standing 66h; syringe leakage observed during transfer of metalloceen solution
9. Pretreated support cooled in salted ice bath ~40min before MAO addition
10. 5 mL MAO added to support suspension; 0.2mL MAO + 3 mL toluene used to dissolve metallocene
11. Support pretreated at 68°C for ~ 15h then 78°C for further 2h
12. Accidental short time exposure occurred during drying with liquid still in flask; bright yellow solution unchanged ; solvent recovered = 17.5 mL
13. After 35min evacuation at room T, flask placed in 45°C bath for 5h; Solvent recovered = 18 mL
14. Support treated with excess (with respect to N & O functional groups) TMA and dried before cat. preparation with MAO and metallocene

** HH03, HH04, HH05, and 02TM were prepared using MMAO-4 (~12% isobutyl and ~88% methyl groups)

Table A-2. Composition of supported catalysts*

				Catalyst Compostion					
				Calculated			Measured*		
Catalyst Desig.	Support Mass, g	Total Mass of Reagents g	Amount Catalyst Recovered g	Al mass%	Zr mass%	Al/Zr Ratio	Al mass%	Zr mass%	Al/Zr Ratio
HH01	1.501	2.400	1.550	17.06	0.22	259	ND	ND	ND
HH02	2.000	3.344	3.100	18.37	0.21	297	13.1 ± 0.3	0.181 ± 0.003	245
HH03	2.500	4.173	3.300	16.77	0.21	276	12.3 ± 0.4	0.152 ± 0.005	273
HH04	1.525	2.576		17.01	0.24	243	15.8 ± 0.4	0.159 ± 0.004	336
HH05	1.310	2.612	2.400	20.97	0.19	370	17.3 ± 0.5	0.104 ± 0.002	563
HH06	1.500	2.437	2.050	17.64	0.17	352	11.7 ± 0.3	0.152 ± 0.003	260
HH07	1.500	2.841	2.400	21.63	0.22	329	16.5 ± 0.4	0.128 ± 0.003	435
HH08	2.000	4.365	3.015	24.86	0.24	354	16.4 ± 0.4	0.209 ± 0.008	265
HH09	1.500	1.947	1.529	10.52	0.11	316	6.69 ± 0.15	0.061 ± 0.011	373
HH10	0.780	1.245	1.140	17.11	0.17	336	11.4 ± 0.3	0.138 ± 0.003	278
HH11	1.500	2.393	2.015	17.11	0.17	341	9.38 ± 0.24	0.093 ± 0.003	342
HH12	1.500	2.393	1.370	17.11	0.17	343	7.73 ± 0.18	0.119 ± 0.003	220
HH13	2.000	4.325	2.790	24.62	0.26	319	15.2 ± 0.4	0.285 ± 0.007	181
HH14	1.000	2.339	1.425	26.27	0.25	354	14.9 ± 0.4	0.235 ± 0.004	215
HH15	2.000	4.415	2.453	25.05	0.27	319	11.6 ± 0.3	0.187 ± 0.006	209
HH16	1.505	2.403	1.755	17.05	0.21	273	11.1 ± 0.3	0.131 ± 0.003	163
HH17	1.500	2.394	1.737	17.11	0.18	323	11.4 ± 0.3	0.102 ± 0.003	286
HH18	1.502	2.397	1.976	17.08	0.19	300	10.1 ± 0.2	0.162 ± 0.003	376
HH19	1.507	2.489	1.998	18.10	0.17	355	11.2 ± 0.3	0.164 ± 0.004	209
HH20	1.500	2.526	1.990	18.64	0.18	353	11.8 ± 0.3	0.181 ± 0.004	230
HH21	1.460	2.356	1.912	17.39	0.20	300	8.38 ± 0.20	0.189 ± 0.003	220
HH22	2.001	2.450	2.440	8.19	0.18	150	3.69 ± 0.08	0.112 ± 0.003	150
HH23	-	1.338	0.570	45.91	0.43	363	39.5 ± 1.3	0.804 ± 0.018	111
HH24	-	1.338	0.580	45.91	0.43	363	42.2 ± 1.5	0.836 ± 0.016	166
HH25	1.510	2.405	1.890	17.03	0.19	302	11.7 ± 0.3	0.161 ± 0.003	171
HH26	1.502	2.417	2.255	17.29	0.21	285	11.4 ± 0.3	0.181 ± 0.004	246
HH27	1.502	3.283	2.669	24.95	0.21	392	16.7 ± 0.5	0.202 ± 0.004	212
HH28	1.500	2.482	2.455	18.15	0.17	355	15.6 ± 0.4	0.138 ± 0.003	279
HH29	1.501	2.412	2.160	17.32	0.17	335	7.06 ± 0.16	0.128 ± 0.002	382

* Only the measured composition of catalysts were used in data analysis/discussion of results

Appendix B: Summary of Polymerization Conditions and Polymer Properties

Details of all polymerization runs made in this work are listed in chronological order in Table B-1. Inactive catalysts and polymerization runs not discussed in the thesis are also included in Table B-1 for completeness. The polymerization activities, and the measured properties of the polyolefins produced in the runs listed in Table B-1 are summarized in Table B-2. The polymerization activity of each run is given in different units to facilitate comparison of activities.

Table B-1. Conditions for polymerization runs

Date	Run Number[1]	Cat. Am't mg	Scavenger			Evac.[2] mtorr	Comonomer		Total Pres. psi	Length of Run[3]		PE Yield g	Comments
			Type	Am't mL	Al mmol		Type	Am't mL		Total h	R_{max} h		
7-Feb-01	HH01001	109	TIBA	0.29	1.144	no	1-C_6H_{12}	2.73	203	3.45		17	No maxima observed in 3.45 h
10-Feb-01	HH01002	110	TIBA	0.30	1.183	no	1-C_6H_{12}	2.74	202	2.37		22.7	C2H4 from 1-L reactor line (upstream purifiers)
12-Feb-01	HH01003	108	TIBA	0.30	1.183	no	1-C_6H_{12}	3.1	205	2.00	0.11	7.5	C2H4 from 1-L reactor line (downstream purifiers); T2 controlled to mimic 1-L rxtor
15-Feb-01	HH01004	113	TEAL	0.18	1.276	no	1-C_6H_{12}	2.8	205	3.00	2.31	162.5	
18-Feb-01	HH01005	82	TEAL	0.20	1.458	no	1-C_6H_{12}	3.31	205	2.61		14.92	ΔP of ~110 psi across shaft observed
19-Feb-01	HH01006	106	TEAL	0.22	1.604	no	1-C_6H_{12}	2.95	203	3.00		39.5	Ethylene fed thru evacuation port; no max. Rp
7-Mar-01	HH01011	108	TIBA	0.40	1.578	no	1-C_6H_{12}	2.71		?		0	Cat. injected as suspension in .23ML TIBA+1.5mL n-C_6; Cat. stuck in Injector
9-Mar-01	HH01012	104	TIBA	0.35	1.38	no	1-C_6H_{12}	3.13	206	0.67		0	Cat. injected as suspension in .13mL TIBA+1.5mL mineral oil; No Polymn;
10-Mar-01	HH01013	117	TIBA	0.65	2.564	no	1-C_6H_{12}	2.89	203	3.88	2.56	26.93	Max Rp is local; 2 maxima observed
23-Mar-01	HH01014	92	TEAL	0.16	1.167	no	1-C_6H_{12}	3	203	3.57	2.87	53.2	All-steel impeller; rpm decrease in run 430 to 370; cat. injected stirrer on
24-Mar-01	HH01015	93	TEAL	0.14	1.021	no	1-C_6H_{12}	3.09	203	3.50	3.1	99.2	TEAL 2 droplets in cat. holder above top salt layer
25-Mar-01	HH01016	93	TIBA	0.33	1.302	no	1-C_6H_{12}	2.93	203	3.59	3.5	30	No max.; C_2/N_2 purifiers exchanged
30-Mar-01	HH01017	60	TIBA	0.70	2.761	no	None	none		7.00		46.3	Variable P slurry run
1-Apr-01	HH01018	80	TIBA	0.15	0.592	no	None	none	135	3.13		16.5	Slurry homopolmn; cat susp .15mL TIBA+2.2mL n-C_7; weighted average pressure
8-Apr-01	HH02020	101	TIBA	0.31	1.223	no	1-C_6H_{12}	3	201.6	1.83		0	No polymerization
6-May-01	HH02033	80	TIBA	0.05	trace	30	1-C_6H_{12}	3.07				0	TIBA injected before connecting cat holder; vented after 5 min
12-May-01	HH03036	100	TIBA	0.07	0.276	no	None	none	206.5	2.50		2.5	
13-May-01	HH03037	101	TIBA	0.10	trace	55	1-C_6H_{12}	3.01	201	1.25		?	
15-May-01	HH04038	62	TIBA	0.07	trace	42	1-C_6H_{12}	2.81		0.75		0	No polymerization observed
31-May-01	HH05039	100	TIBA	0.10	0.394	no	1-C_6H_{12}	3.17	203	1.50		5.42	
1-Jun-01	HH05040	106	TIBA	0.07			1-C_6H_{12}	3	203	2.50	1.79	19.2	Salt bed = 160g NaCl
4-Jun-01	HH05041	101	none	-	-	-	1-C_6H_{12}	2.96	200	2.50	1.15	16.7	No scavenger used
5-Jun-01	HH05042	104	none	-	-	no	None	none	206	1.00		0.8	160g NaCl bed, no scavenger
11-Jun-01	HH06043	102	none	-	-	-	1-C_6H_{12}	3.06	205	1.00	0.8	13.39	No scavenger used
12-Jun-01	HH06044	113	TIBA	0.07	trace	48	1-C_6H_{12}	3.03	204	1.00	0.23	37.93	
16-Jun-01	HH06045	102	TIBA	0.07	trace	48	1-C_6H_{12}	5.89	203	1.00	0.82	18.34	
17-Jun-01	HH06046	113	TIBA	0.07	trace	46	1-C_6H_{12}	5.96	201.6	1.00	0.66	29.12	
18-Jun-01	HH06047	112	TIBA	0.07	trace	50	None	none	200.6	1.00	0.03	23.03	
22-Jun-01	HH07048	106	TIBA	0.07	trace	46	1-C_6H_{12}	5.29	203	1.00	0.04(.56)	28.9	
25-Jun-01	HH07049	107	TIBA	0.09	trace	40	None	none	202	1.00	0.26	24.79	
26-Jun-01	HH07050	104	TIBA	0.07	trace	45	1-C_6H_{12}	3.26	202	1.00	0.28	70.46	

Table B-1. Cont'd

Date	Run Number[1]	Cat. Am't mg	Scavenger			Evac.[2] mtorr	Comonomer		Total Pres. psi	Length of Run[3]		PE Yield g	Comments
			Type	Am't mL	Al mmol		Type	Am't mL		Total h	R_{max} h		
9-Nov-02	HH07235	100.4	TIBA	0.15	trace	no	None		200.5	1.00		18	
10-Nov-02	HH07236	102	TIBA	0.15	trace	no	None		201	1.00		11.2	
11-Nov-02	HH07237	100.4	TIBA	0.15	trace	no	None		201.6	1.00		13.45	
14-Dec-02	HH07251	99.7	TIBA	0.15	trace	no	None		301	1.00		26	300 psi run
15-Dec-02	HH07252	100	TIBA	0.15	trace	no	None		401	1.00		18.6	400 psi run
16-Dec-02	HH07253	100	TIBA	0.15	trace	no	None		101	1.00		3.27	100 psi run
13-Apr-03	HH07282	100.5	TIBA	0.15	trace	vent	None		207	1.00		13.8	90°C run, temp effect
14-Apr-03	HH07283	103.4	TIBA	0.16	trace	vent	None		190	1.00		9.58	60°C run, temp effect
15-Apr-03	HH07284	101	TIBA	0.15	trace	vent	None		184	1.00		2.3	50°C run, temp effect
16-Apr-03	HH07285	102.8	TIBA	0.15	trace	vent	None		194	1.00		19.6	70°C run, temp effect
5-May-03	HH07293	107.5	TIBA	0.15	trace	vent	None		210	1.00		13	100°C run, temp effect
4-Jul-01	HH08051	90.1	TIBA	0.07	trace	45	1-C_6H_{12}	3.41	203	1.00	0.08	57.44	rpm decreased from 470 to 370 during run
5-Jul-01	HH08052	59.2	TIBA	0.07	trace	43	1-C_6H_{12}	3.5	203.4	1.00	0.08	64.6	
6-Jul-01	HH08053	32	TIBA	0.07	trace	60	1-C_6H_{12}	3.77	202.4	1.00	0.073	50.98	
7-Jul-01	HH08054	32	TIBA	0.06	trace	80	None	none	202.7	1.00	0.023	28.22	
11-Jul-01	HH08055	15.9	TIBA	0.07	trace	90	1-C_6H_{12}	3.52	202	1.00	0.33	27.12	
17-Jul-01	HH08058	14.3	TIBA	0.07	trace	56	None	none	201	1.00	0.02	6.73	
27-Jul-01	HH08062	25.7	TIBA	0.07			1-C_6H_{12}	3.38	200.6	1.03	0.65	66.8	
8-Aug-01	HH08068	25	TIBA	0.07	trace	60	1-C_6H_{12}	4.29	203.3	1.00	0.43	16.68	Metering valve to GC closed during evac.; impurities might have been introduec on opening
9-Aug-01	HH08069	25.5	TIBA	0.07	trace	60	1-C_6H_{12}	4.28	202.6	1.00	0.15	12.7	
10-Aug-01	HH08070	26.5	TIBA	0.08	trace	60	1-C_6H_{12}	4.25	200.1	1.00	0.40	17.3	T controller OFF; T (bath, hot) set at 82.2°C
11-Aug-01	HH08071	25.7	TIBA	0.07	trace	60	1-C_6H_{12}	3.5	202	1.00	0.06	11.9	
13-Aug-01	HH08073	52	TIBA	0.07	0.276	no	1-C_6H_{12}	4.29	199.9	1.00	0.38	76.2	
12-Jul-01	HH09056	103	TIBA	0.07	trace	65	1-C_6H_{12}	3.55	203	1.03	0.18	78.1	
16-Jul-01	HH09057	30.7	TIBA	0.07	trace	58	None	none	202	1.00	0.06	20.31	
12-Aug-01	HH09072	40.6	TIBA	0.07	trace	50	1-C_6H_{12}	4.31	204	1.00	0.25	10.82	
20-Dec-02	HH09254	50.1	TIBA	0.15	0.592	no	None	none	251	1.00		48.63	Effect of [TIBA] & contact order; N2 = 51 psi
21-Dec-02	HH09255	50.2	TIBA	0.15	trace	no	None	none	251.5	1.00		18.56	50 psi N2
23-Dec-02	HH09256	50	TIBA	0.15	0.592	no	None	none	251.3	1.00		17.4	3 min contact (cat + TIBA); 51 psi N2; Gbox regen Dec 21-22
26-Dec-02	HH09257	50	TIBA	0.15	trace	no	None	none	252	1.00		16.39	52 psi N2; 3 min contact
28-Dec-02	HH09258	49.8	TIBA	0.16	0.611	no	None	none	251	1.00		37.8	Repeat of HH09256
29-Dec-02	HH09259	49.9	TIBA	0.15	0.592	no	None	none	207	1.00		64.2	0 min contact no N2
30-Dec-02	HH09260	50	TIBA	0.15	trace	no	None	none	100	1.00		13.11	
1-Jan-03	HH09261	39.8	TIBA	0.15	trace	no	None	none	300.5	1.00		22	300 psi run
2-Jan-03	HH09262	30.7	TIBA	0.15	trace	no	None	none	400.7	1.00		25.8	400 psi run

Table B-1. Cont'd

Date	Run Number[1]	Cat. Am't mg	Scavenger			Evac.[2] mtorr	Comonomer		Total Pres. psi	Length of Run[3]		PE Yield g	Comments
			Type	Am't mL	Al mmol		Type	Am't mL		Total h	R_{max} h		
4-Jan-03	HH09263	40.5	TIBA	0.15	trace	no	None	none	200	1.00		28.2	
6-Jan-03	HH09264	49.9	TIBA	0.15	0.592	no	None	none	251	1.00		32.88	50 psi N_2; repeat of HH09256; TIBA inj'd at >100°C
1-Mar-03	HH09265	49.8	TNOA	0.26	0.59	no	None	none	205	1.00		13	
31-Mar-03	HH09276	51.5	TIBA	0.15	0.592	vent	None	none	184	1.00		13.1	50°C run, temp effect
1-Apr-03	HH09277	49.8	TIBA	0.15	0.592	vent	None	none	189	1.00		25.6	60°C run, temp effect
2-Apr-03	HH09278	45.7	TIBA	0.15	0.592	vent	None	none	194	1.00		20.96	70°C run, temp effect
3-Apr-03	HH09279	39	TIBA	0.15	0.592	vent	None	none	204	1.00		17.94	90°C run, temp effect
4-Apr-03	HH09280	36.5	TIBA	0.15	0.592	vent	None	none	194	1.00		17.84	70°C run, temp effect Repeat run
6-Apr-03	HH09281	42.7	TIBA	0.15	0.592	vent	None	none	194	1.00		20.8	70°C run, temp effect Repeat run
17-Apr-03	HH09286	50.4	TIBA	0.08	0.316	no	1-C_6H_{12}	3.13	203	1.00		3.33	90°C run, temp effect
20-Jul-01	HH10059	50	TIBA			82	1-C_6H_{12}	3.9	202.4	1.00	0.59	20.79	rpm = 550
22-Jul-01	HH10060	50.7	TIBA			76	None	none	202	1.00	0.38	1.19	
23-Jul-01	HH10061	52	TIBA	0.07	0.276	no	1-C_6H_{12}	4.94	201.8	1.50	0.69	31.97	
27-Nov-01	HH10118	50.5	TIBA	0.06	0.237	no	1-C_6H_{12}	4.25	203.7	1.00	0.81	18.2	
1-Dec-01	HH10119	61.6	TIBA	0.07	trace	54	1-C_6H_{12}	4.36	203.3	0.17	-	2.11	10min run
2-Dec-01	HH10120	60.4	TIBA	0.08	trace	60	1-C_6H_{12}	4.28	203.5	0.02	-	0.094	1 min run
3-Dec-01	HH10121	51.6	TEAL	0.03	0.219	no	1-C_6H_{12}	4.41	202.9	1.75	1.40	37.44	0.03mL TEAL+0.05mL n-C7 for complete injection
18-Mar-03	HH10271	82.5	TIBA	0.15	0.59	no			201	2.43		2.85	Catalyst prepolymerized by propylene
28-Jul-01	HH11063	60	TIBA	0.07	trace	80	1-C_6H_{12}	4	203	1.75	0.12	18.6	
29-Jul-01	HH11064	70	TIBA	0.07	trace	60	1-C_6H_{12}	7.1	204.4	1.00	0.70	27.8	
30-Jul-01	HH11065	70	TIBA	0.06	trace	74	1-C_6H_{12}	2.26	202.8	1.00	0.30	38.4	
22-Dec-01	HH11126	76.1	TIBA	0.08	trace	45	None	none	200.2	1.00	0.04	11.31	Normal evacuation only at 60°C; reactor heated 97°C/10 mtorr 1h before experiment
31-Jul-01	HH12066	66	TIBA	0.08	trace	65	1-C_6H_{12}	3.02	202.1	1.00	0.21	16.5	
5-Aug-01	HH12067	71	TIBA	0.11	trace	64	1-C_6H_{12}	4.33	200.1	1.00	0.24	30	Modified 3 compartment bath
23-Dec-01	HH12127	84.9	TIBA	0.08	trace	45	None	none	200	1.00	0.05	14.91	
14-Aug-01	HH13074	40.6	TIBA	0.07	trace	80	1-C_6H_{12}	4.31	203.5	1.00	0.15	39.4	2 siphon tubes: buffer to cold only
15-Aug-01	HH13075	40.8	TIBA	0.08	trace	80	1-C_6H_{12}	4.31	201.6	1.00	0.20	68.4	6 siphon tubes (4 to hot; 2 to cold)
16-Aug-01	HH13076	40.8	TIBA	0.08	trace	80	1-C_6H_{12}	4.31	200.9	1.00	0.16	18.83	2 siphon tubes (1 to hot; 1 to cold)
17-Aug-01	HH13077	40.7	TIBA	0.09	trace	78	1-C_6H_{12}	4.31	203.4	1.02	0.36	41.2	T controller ON; low rpm 300, high bed 160g
18-Aug-01	HH13078	41.3	TIBA	0.08	trace	80	1-C_6H_{12}	4.28	205.5	1.00	0.26	70.3	T controller OFF; high rpm 600
19-Aug-01	HH13079	41.9	TIBA	0.10	trace	80	1-C_6H_{12}	4.37	199.6	1.00	0.29	51.3	Anchor imp. Installed (Teflon); low rpm
20-Aug-01	HH13080	40.5	TIBA	0.09	trace	80	1-C_6H_{12}	4.34	203.3	1.00	0.47	15.7	160 g NaCl bed; anchor imp., low rpm
21-Aug-01	HH13081	40.8	TIBA	0.12	trace	80	1-C_6H_{12}	4.28	202.3	1.00	0.07	4.1	160 g NaCl bed; anchor imp.
29-Aug-01	HH13082	42.5	TIBA	0.07	trace	84	1-C_6H_{12}	4.36	202.6	1.00	0.20	7.28	Crackly noise and rpm change during run
1-Sep-01	HH14083	46.9	TIBA	0.10	trace	75	1-C_6H_{12}	4.36	202	1.00	0.14	12.8	
2-Sep-01	HH14084	47	TIBA	0.08	trace	53	1-C_6H_{12}	4.34	202	1.00	0.42	25.1	T controller OFF; turbine imp.

Table B-1. Cont'd

Date	Run Number[1]	Cat. Am't mg	Scavenger			Evac.[2] mtorr	Comonomer		Total Pres. psi	Length of Run[5]		PE Yield g	Comments
			Type	Am't mL	Al mmol		Type	Am't mL		Total h	R_{max} h		
6-Sep-01	HH14085	103	TIBA	0.08	trace	37	1-C_6H_{12}	4.31	203.8	1.00	0.19	49.7	
24-Dec-01	HH14128	60	TIBA	0.08	trace	45	None	none	200	1.08	0.03	15.26	
25-Dec-01	HH14129	60.3	TEAL	0.04	0.255	no	1-C_6H_{12}	4.25	199.4	1.00	0.63	57.6	TEAL + 0.075mL n-C_7 for complete transfer; 350&400 rpm used
14-Jan-02	HH14130	60.2	TIBA	0.05	0.20	no	None	none	204	1.00	0.43	23.14	
20-Jan-02	HH14131	60.6	TIBA	0.06	trace	38	1-C_6H_{12}	4.45	199.4	1.00		41.87	
29-Mar-02	HH14149	60.3	TIBA	0.05	0.20	no	1-C_6H_{12}	4.5	203.9	1.00		50.4	
5-Apr-02	HH14153	60.8	TIBA	0.05	0.20	no/90	None	none	199.9	1.00		17.7	TIBA/N_2 + Cat, 3 min, evac to 90 mtorr, C_2H_4
14-Apr-02	HH14156	61.2	TIBA	0.05	0.20	no	None	none	201	1.00		28.5	TIBA/N_2(50psi) + Cat. 50 sec, C_2H_4
15-Apr-02	HH14157	60	TIBA	0.09	0.35	no	None	none	201.1	1.00		35.8	TIBA/N_2(50psi) + Cat. 50 sec, C_2H_4
19-Apr-02	HH14158	61.4	TIBA	0.05	0.20	no	None	none	203	1.75		89.8	Repeat of HH14130 but with 50 pi N_2
20-Apr-02	HH14159	61.4	TIBA	0.05	0.20	no	None	none	204.5	0.75		17.9	
21-Apr-02	HH14160	61.4	TIBA	0.05	0.20	no	None	none	203.7	0.75		16.7	TIBA mistakenly injected under vacuum
29-Apr-02	HH14163	60.3	TIBA	0.06	0.24	no	None	none	204.8	0.75		15.22	
3-May-02	HH14164	61.8	TIBA	0.05	0.20	no	None	none	205.5	0.75		11.91	
4-May-02	HH14165	60.7	TIBA	0.05	0.20	no	None	none	201.6	1.00		81.2	TIBA + Cat./N_2 50psi 50 sec, C_2H_4
13-May-02	HH14171	61.7	TIBA	0.05	0.20	no	None	none	204.5	1.00		35.2	
9-Sep-01	HH15086	40.8	TIBA	0.08	trace	77	1-C_6H_{12}	4.26	203.3	1.00	0.18	70.3	
10-Sep-01	HH15087	41.7	TIBA	0.09	trace	74	1-C_6H_{12}	6.56	202.7	1.00	0.36	40.7	Old helical c. coil added in series; 1-C_6 inj'd under vac.
12-Sep-01	HH15088	42.5	TIBA	0.17	0.67	no	1-C_6H_{12}	2.1	196.5	1.00	0.29	60.72	1L Rxtor
13-Sep-01	HH15089	42.6	TIBA	0.08	trace	77	1-C_6H_{12}	4.32	203.8	1.00	0.22	56.4	
14-Sep-01	HH15090	42.7	TIBA	0.08	trace	76	1-C_6H_{12}	4.32	197.7	1.00	0.23	62.75	T controller OFF
18-Sep-01	HH15091	42.5	TIBA	0.07	trace	80	1-C_6H_{12}	4.34	186.8	1.00	0.22	59.5	Repeat of 89; P_{C2} down to 180 psi low cylinder pressure
21-Sep-01	HH15092	42.8	TIBA	0.08	trace	70	1-C_6H_{12}	4.38	200.6	1.00	0.28	52.3	New C_2H_4 cylinder; static mixer installed
23-Sep-01	HH15093	50	TIBA	0.08	trace	85	1-C_6H_{12}	4.28	203.7	1.00	0.23	65.93	
30-Sep-01	HH15094	57.8	TIBA	0.09	trace	77	1-C_6H_{12}	3.27	103.1	1.00	0.49	33.4	60°C run
4-Oct-01	HH15095	69.5	TIBA	0.07	0.28	no	None	none	203.5	1.00	0.62	38.42	
25-Nov-01	HH15117	59.7	TIBA	0.05	0.20	no	1-C_6H_{12}	4.28	205.1	1.00	0.36	71.4	
26-Jan-02	HH15134	100	TIBA	0.06	0.24	no	None	none	204.8	1.02		76.3	
27-Jan-02	HH15135	92	TIBA	0.19	0.75	no	None	none	205.1	1.50		188.2	After 16 min polym'n rpm increased by 100 to 550 to improve heat transfer
5-Feb-02	HH15138	62.6	TIBA	0.22	0.87	no	None	none	202.1	1.08		137.7	For Ibn Waleed; reaction stopped due to crackly impeller noise
9-Feb-02	HH15139	70.9	TIBA	0.20	0.79	no	None	none	206	0.42		0	With H_2 44.2psi at 93.6°C; no rxn in 25 min; leak detected in air side-arm
10-Feb-02	HH15140	65	TIBA	0.20	0.79	no	None	none	204.8	1.29		0	With H_2 12psi at 93°C; no reaction
17-Feb-02	HH15141	50	TIBA	0.20	0.79	no	None	none/H_2	205.5	1.42		43.5	With H_2 (10psi in 1/8" tube); after 12 min reactor was evacuated 5psi, C_2H_4 reinstated
18-Feb-02	HH15142	82.3	TIBA	0.19	0.75	no	None	none/H_2	204.6	2.00		76.8	With H_2 (4.8psi in 1/8" X 30" SS tube)

Table B-1. Cont'd

Date	Run Number[1]	Cat. Am't mg	Scavenger			Evac.[2] mtorr	Comonomer		Total Pres. psi	Length of Run[3]		PE Yield g	Comments
			Type	Am't mL	Al mmol		Type	Am't mL		Total h	R_{max} h		
23-Feb-02	HH15143	110.8	TIBA	0.20	0.79	no	None	none/H_2	206.5	2.00		160	With H_2 (10.2 psi in 1/8" X 30" SS tube) @ 70°C
25-Feb-02	HH15144	100.5	TIBA	0.19	0.75	no	None	none/H_2	202.1	3.50		111.2	With H_2 (0.1 psi in rxtor)
27-Apr-02	HH15161	60.5	TIBA	0.05	0.20	no	1-$C_{10}H_{20}$	7.0	203.4	1.00		27.7	Copolymerization with 1-decene (1-C_{10} inj'n problem, partial needle blockage)
28-Apr-02	HH15162	60.3	TIBA	0.05	0.20	no	1-$C_{10}H_{20}$	7.0	203.5	1.00		32.7	Copolymerization with 1-decene (TIBA inj'n problem, partial needle blockage)
12-Jul-02	HH15192	61.1	TIBA	0.07	0.28	no	C_3H_6	9.6	200	1.00		25.6	Propylene amount = 10 psi at 93.6°C
15-Jul-02	HH15193	63	TIBA	0.07	0.28	no	C_3H_6	31.9	200	1.00		110.6	Propylene amount =32.8 psi at 92.7°C
20-Mar-03	HH15273	61.2	TIBA	0.15	0.59	no	C_3-Homo			0.42		--	No prod. No cat in reactor; completely ground
5-Oct-01	HH16096	76.5	TIBA	0.07	trace	75	1-C_6H_{12}	4.21	197.7	1.00	0.23	41.45	
6-Oct-01	HH16097	80.4	TIBA	0.07	trace	70	None	none	201.1	1.00	0.36	19.56	
7-Oct-01	HH16098	109	TIBA	0.08	trace	70	1-C_6H_{12}	2.52	103.8	1.00	0.50	16.47	60°C run
10-Oct-01	HH16099	80.7	TIBA	0.07	trace	76	1-C_6H_{12}	4.33	201	1.00	0.40	43.05	Catalyst prepolymerized with 1-C_6, 5 min in 50 psi N_2; P_{total} = 251 psi
5-May-02	HH16166	84.5	TIBA	0.07	0.28	no	None	none	200	1.75		27.9	TIBA + Cat./N_2 60 sec, C_2H_4
6-May-02	HH16167	85.3	TIBA	0.07	0.28	no	None	none	200	1.25		26.5	TIBA + Cat./N_2 65 sec, C_2H_4
10-May-02	HH16168	84.5	TIBA	0.07	0.28	no	None	none	199	1.25		23.5	TIBA + C_2H_4 + N_2, Cat.
11-May-02	HH16169	85.7	TIBA	0.07	0.28	no	None	none	200	1.25		25.2	TIBA + C_2H_4 + N_2, Cat.
12-May-02	HH16170	84.6	TIBA	0.07	trace	57	None	none	199	1.25		27.8	TIBA (trace)+ (51/100 psi N_2/ C_2H_4) in rxtor, Cat
24-May-02	HH16172	86	TIBA	0.07	0.28	no	None	none	200	0.75		1.67	TIBA + Cat./N_2 60 sec, C_2H_4
27-May-02	HH16175	90.2	TIBA	0.07	0.28	no	1-C_6H_{12}	5.0	203.9	1.25		60.5	
28-May-02	HH16176	89	TIBA	0.07	0.28	no	None	none	202	0.40			TIBA + Cat./N_2 60 sec, C_2H_4; Very low Rp
19-Jul-02	HH16195	92	TIBA	0.07	0.28	no	None		201	1.00		3.9	Catalyst exposed to TIBA in N_2 (52psi) 1 min before C_2H_4; P_{total} = 252 psi
26-Jul-02	HH16199	87.9	TIBA	0.07	trace	70	None		202	1.00		7.4	Catalyst in N_2 environment for 1 min before ethylene
11-Oct-01	HH17100	80	TIBA	0.07	trace	57	1-C_6H_{12}	2.05	203	1.00	0.38	27.7	
12-Oct-01	HH17101	84	TIBA	0.08	trace	60	None	none	199.6	1.00	0.27	19.34	
14-Oct-01	HH17102	80	TIBA	0.07	trace	80	1-C_6H_{12}	4.29	204.4	1.00	0.35	27.84	
26-Oct-02	HH17227	80.3	TIBA	0.15	0.59	no	1-C_6H_{12}	4.5	202	2.50		63.3	
27-Oct-02	HH17228	82.4	MAO	0.40		no	1-C_6H_{12}	4.57	203.5	2.50		18.2	
28-Oct-02	HH17229	81.5	MAO	4.00		no	1-C_6H_{12}	4.52	204.5	2.50		?	Salt coated with product, cannot weigh
1-Nov-02	HH17230	82	TIBA	0.15	trace	no	1-C_6H_{12}	4.5	200	2.50		57.24	Trace + no = external TIBA removed by dilution
2-Nov-02	HH17231	81.2	TIBA	0.15	trace	no	1-C_6H_{12}	4.5	200.5	2.50		57.34	
3-Nov-02	HH17232	82.5	TIBA	0.15	trace	no	1-C_6H_{12}	4.51	201	2.50		46.74	
4-Nov-02	HH17233	81.8	TIBA	0.15	trace	no	1-C_6H_{12}	4.5	201	2.50		80.1	
8-Nov-02	HH17234	81.5	TIBA	0.15	trace	no	1-C_6H_{12}	4.51	200.5	2.50		76.4	
21-Oct-01	HH18103	76	TIBA	0.07	trace	60	1-C_6H_{12}	2.3	203.6	1.00	0.50	36.4	

Table B-1. Cont'd

Date	Run Number[1]	Cat. Am't mg	Scavenger Type	Scavenger Am't mL	Scavenger Al mmol.	Evac.[2] mtorr	Comonomer Type	Comonomer Am't mL	Total Pres. psi	Length of Run[3] Total h	Length of Run[3] R_{max} h	PE Yield g	Comments
22-Oct-01	HH18104	76.7	TIBA	0.07	trace	58	None	none	199.1	1.00	0.09	7.7	
23-Oct-01	HH18105	76.4	TIBA	0.08	trace	60	1-C_6H_{12}	4.62	204.8	1.00	0.46	65.3	
24-Oct-01	HH18106	77.2	TIBA	0.07	trace	76	1-C_6H_{12}	7.23	202	1.00	0.61	28.05	
12-Aug-02	HH18207	79	TIBA	0.07	0.28	no	1-C_6H_{12}	4.55	153	1.00		8.25	
16-Nov-02	HH18238	75.1	TIBA	0.15	trace	no	1-C_6H_{12}	12.06	200.5	1.00		42.6	
17-Nov-02	HH18239	74.5	TIBA	0.15	trace	no	1-C_6H_{12}	11.08	201	1.00		34.91	
18-Nov-02	HH18240	76.2	TIBA	0.15	trace	no	1-C_6H_{12}	4.6	200.5	1.00		47.34	
7-Dec-02	HH18247	80	TIBA	0.15	trace	no	None		401	1.00		4.3	Low homopolymerization activity even at high P
13-Dec-02	HH18250	77.5	TIBA	0.15	trace	no	1-C_6H_{12}	4.6	200.4	1.00		49.9	
21-Mar-03	HH18274	82	TIBA	0.15	0.59	no	C_3-homo			1.00			$C_3^=$ homopolymerization; little waxy product collected
18-Apr-03	HH18287	80.2	TIBA	0.15	trace	vent	1-C_6H_{12}	4.76	203	1.00		73.83	90°C run, temp effect
19-Apr-03	HH18288	81.5	TIBA	0.16	trace	vent	1-C_6H_{12}	4.77	194	1.00		23	70°C run, temp effect
20-Apr-03	HH18289	83.1	TIBA	0.15	trace	vent	1-C_6H_{12}	4.65	187	1.00		11.01	60°C run, temp effect
21-Apr-03	HH18290	74.5	TIBA	0.15	trace	vent	1-C_6H_{12}	4.65	210	1.00		23	100°C run, temp effect
22-Apr-03	HH18291	80.8	TIBA	0.15	trace	vent	1-C_6H_{12}	4.66	199	1.00		55	80°C run, temp effect
3-May-03	HH18292	77.4	TIBA	0.15	trace	vent	1-C_6H_{12}	4.83	214	1.00		30.6	100°C Repeat run, temp effect
28-Oct-01	HH19107	76.3	TIBA	0.08	trace	60	1-C_6H_{12}	2.3	203.8	1.00	0.53	37.9	
29-Oct-01	HH19108	76.9	TIBA	0.07	trace	57	1-C_6H_{12}	4.72	200.4	1.23	0.63	52.04	
30-Oct-01	HH19109	77.2	TIBA	0.09	trace	70	None	none	198.3	1.00	0.08	3.233	
20-Nov-01	HH19116	81	TIBA	0.08	trace	95	1-C_6H_{12}	4.25	250	0.37	0.12	2.7	New anchor impeller; failed injection at 200 psi
8-Dec-01	HH19122	78.7	TIBA	0.07	0.28	no	1-C_6H_{12}	4.32	204.8	1.78	1.33	31.9	
9-Dec-01	HH19123	80.2	TEAL	0.04	0.292	no	1-C_6H_{12}	4.25	200.7	3.50	1.87	40.28	TEAL + 0.06mL n-C_7 for complete transfer
10-Dec-01	HH19124	77.7	TIBA	0.03	0.12	no	1-C_6H_{12}	4.28	202.8	1.25	0.37	35.41	
11-Dec-01	HH19125	76.3	TNOA	0.10	0.218	no	1-C_6H_{12}	4.32	202.9	1.25	0.90	43.5	TNOA scavenger
21-Jan-02	HH19132	81	TIBA	0.07	0.28	no	1-C_6H_{12}	4.17	226	2.00		11.16	Extra dry Air ~1 mg injected during deactivation phase
22-Jan-02	HH19133	82	TIBA	0.07	0.26	no	1-C_6H_{12}	4.36	199.5	2.07		22.21	Extra dry Air ~0.5 mg injected during acceleration phase
29-Jan-02	HH19136	81.6	TIBA	0.06	0.24	no	1-C_6H_{12}	4.48	206.6	2.00		36.53	Extra dry air injection after 30 min polymn
4-Feb-02	HH19137	81.5	TIBA	0.06	0.24	no	1-C_6H_{12}	4.44	200.7	3.00		29.8	Extra dry air injection after 13 min polymn
12-Mar-02	HH19145	82.2	TIBA	0.06	0.24	no	1-C_6H_{12}	4.42	201.6	2.00		??	Extra dry air (40psi x 30"x1/8"OD tube) injection after ~12 min polymn
25-May-02	HH19173	76.8	TIBA	0.06	0.24	no	None	none	202	0.50		0	After 15min polymerization 1-C_6H_{12} added no reaction still after >17 min; P_{total}=253 psi
30-Mar-03	HH19275	85.2	TIBA	0.16	0.61	no	1-C_6H_{12}	4.57	204	1.25		37.8	Run for high TIBA effect on activity
5-Nov-01	HH20110	75.4	TIBA	0.08	trace	65	1-C_6H_{12}	5.26	202.6	1.00	0.73	23.48	
6-Nov-01	HH20111	77.4	TIBA	0.08	trace	65	1-C_6H_{12}	4.47	203.9	1.00	0.61	30.7	
12-Nov-01	HH20114	76.2	TIBA	0.08	trace	65	None	none	200.2	1.00	0.10	4.6	
26-May-02	HH20174	76.3	TIBA	0.07	trace	66	None	none	200	1.00			Very low activity; max C_2H_4 flow < 10 SCCM

Table B-1. Cont'd

Date	Run Number[1]	Cat. Am't mg	Scavenger			Evac.[2] mtorr	Comonomer		Total Pres. psi	Length of Run[3]		PE Yield g	Comments
			Type	Am't mL	Al mmol		Type	Am't mL		Total h	R_{max} h		
20-Jul-02	HH20196	76.4	TIBA	0.05	0.20	no	C_3H_6	6.93	204	2.00		27.65	Propylene amount = 7.2 psi at 93.7°C
21-Jul-02	HH20197	78.5	TIBA	0.05	0.20	no	None		204.6				No reaction observed
22-Jul-02	HH20198	77.5	TIBA	0.05	0.20	no	1-C_6H_{12}	4.6	204	2.00		63.2	
10-Mar-03	HH20268	139.4	TIBA	0.15	0.59	vent	None		202	0.25		1.723	Low yield run for EDX
11-Mar-03	HH20269	101.1	TIBA	0.15	0.59	vent	None		202	1.00		3.21	No seed bed used
17-Mar-03	HH20270	86	TIBA	0.15	0.59					1.05		0.47	Catalyst prepolymerized with C_3H_6; no P reduction during the batch operation
10-Nov-01	HH21112	85.2	TIBA	0.08	trace	60	1-C_6H_{12}	4.33	200.2	1.00	0.23	52.91	
11-Nov-01	HH21113	75.4	TIBA	0.08	trace	65	None	none	199.8	1.00	0.07	16	
19-Nov-01	HH21115	78.0	TIBA	0.07	trace	75	1-C_6H_{12}	2.38	200.4	1.00	0.16	45.02	
8-Sep-02	HH21208	78.0	TIBA	0.05	trace	75	1-C_6H_{12}	6.53	204	1.00		20.66	
9-Sep-02	HH21209	77.8	TIBA	0.07	trace	69	1-C_6H_{12}	6.31	200	2.00		14.63	
13-Sep-02	HH21210	77.8	TIBA	0.07	0.28	no	1-C_6H_{12}	4.48	204	1.00		95.78	
14-Sep-02	HH21211	46.8	TIBA	0.07	0.28	no	1-C_6H_{12}	4.58	204	1.00		9.5	
15-Sep-02	HH21212	48.6	TIBA	0.07	0.28	no	1-C_6H_{12}	4.57	203	1.00		6.31	
20-Sep-02	HH21213	46.9	TIBA	0.07	0.28	no	1-C_6H_{12}	4.58	204	1.00		10.03	
21-Sep-02	HH21214	48.2	TIBA	0.07	<0.28	no	1-C_6H_{12}	<4.59	203	1.12		3.6	Some reactor content escaped after scavenging, see lab book
22-Sep-02	HH21215	47.2	TIBA	0.07	0.28	no	1-C_6H_{12}	5.59	205	1.00		5.64	
23-Sep-02	HH21216	48.7	TIBA	0.08	0.30	no	1-C_6H_{12}	4.57	205	1.00		16.26	
28-Sep-02	HH21217	60.0	TIBA	0.15	0.57	no	1-C_6H_{12}	4.51	204	1.00		87.4	
29-Sep-02	HH21218	52.2	TIBA	0.15	0.59	no	1-C_6H_{12}	4.59	203.5	1.00		70	
30-Sep-02	HH21219	51.7	TIBA	0.15	0.59	no	1-C_6H_{12}	4.57	206	1.00		82.65	
1-Oct-02	HH21220	53.9	TIBA	0.17	0.65	no	1-C_6H_{12}	4.67	206.7	1.00		64.71	
2-Oct-02	HH21221	51.6	TIBA	0.15	trace	1200	1-C_6H_{12}	4.5	201	1.00		8.47	
6-Oct-02	HH21222	41.0	TIBA	0.15	0.59	no	1-C_6H_{12}	4.5	203.5	1.00		66.2	
7-Oct-02	HH21223	42.0	TIBA	0.15	0.59	no	1-C_6H_{12}	4.5	204	1.17		64.1	Pretreated NaCl seed bed (140-190°C) 30h; Reactor evacuated at 93°C, 23 mtorr
12-Oct-02	HH21224	40.2	TIBA	0.15	0.59	no	1-C_6H_{12}	4.58	204	1.33		57.45	As above + MAO pretreated cat holder salt
14-Oct-02	HH21225	41.2	TIBA	0.15	0.59	no	1-C_6H_{12}	4.74	203	1.33		64.96	MAO pretreated cat holder salt
15-Oct-02	HH21226	41.8	TIBA	0.15	0.59	no	1-C_6H_{12}	4.51	204	1.17		73.4	
13-Mar-02	HH22146	60.0	TIBA	0.10	0.39	no	None	none	203.5	2.00		3.864	
15-Mar-02	HH22147	82.5	TIBA	0.08	trace	60	1-C_6H_{12}	4.33	198.9	1.50		38.7	
18-Mar-02	HH22148	82.3	TIBA	0.09	trace	60	None	none	200.1	2.90		11.19	
28-Jul-02	HH22200	89.6	TIBA	0.07	trace	88	1-C_6H_{12}	4.6	205	1.00		6.25	
29-Jul-02	HH22201	86.7	TIBA	0.05	0.20	no	1-C_6H_{12}	4.72	201	1.25		15.88	
2-Aug-02	HH22202	87.5	TIBA	0.09	0.35	no	1-C_6H_{12}	4.88	203	1.25		15.8	
3-Aug-02	HH22203	88.7	TIBA	0.15	0.59	no	1-C_6H_{12}	4.85	202	1.25		81.4	
4-Aug-02	HH22204	86.5	TIBA	0.20	0.79	no	1-C_6H_{12}	4.92	203	1.50		55.8	Vacuum not as good as recent previous runs
5-Aug-02	HH22205	88.6	TIBA	0.20	0.79	no	1-C_6H_{12}	4.8	203.3	1.50		80.6	

Table B-1. Cont'd

Date	Run Number[1]	Cat. Am't mg	Scavenger			Evac.[2] mtorr	Comonomer		Total Pres. psi	Length of Run[3]		PE Yield g	Comments
			Type	Am't mL	Al mmol		Type	Am't mL		Total h	R_{max} h		
9-Aug-02	HH22206	86.2	TIBA	0.15	0.59	no	None		152	1.00		3.13	Used 150 psi due to low cylinder Pressure
2-Mar-03	HH22266	87	TNOA	0.27	0.59	no	1-C_6H_{12}	4.81	203	0.25		--	Zero injection; monomer leak into catalyst before injection. Solid plug
4-Mar-03	HH22267	85.3	TNOA	0.27	0.59	no	1-C_6H_{12}	4.81	203	1.22		9.7	
30-Mar-02	HH23150	10.3	TIBA	0.05	0.20	no	None	none	201.7	1.00		13.02	
31-Mar-02	HH23151	10.2	TIBA	0.05	0.20	no	1-C_6H_{12}	4.5	204.5	1.00		56.6	
1-Apr-02	HH23152	10.1	TIBA	0.06	trace	50	None	none	200.5	0.58		7.74	200 psi
23-Nov-02	HH23241	10	TIBA	0.15	trace	no	None	none	201	1.00		13.34	200 psi
24-Nov-02	HH23242	10.1	TIBA	0.15	trace	no	None	none	300	1.00		7.84	300 psi run
25-Nov-02	HH23243	10	TIBA	0.15	trace	no	None	none	102	1.00		1	100 psi run
29-Nov-02	HH23244	10	TIBA	0.15	trace	no	None	none	100.5	0.88		0.848	100 psi run
30-Nov-02	HH23245	10.1	TIBA	0.15	trace	no	None	none	401	1.00		51.8	400 psi run
6-Dec-02	HH23246	10.1	TIBA	0.15	trace	no	None	none	300.5	1.00		10.4	300 psi run
8-Dec-02	HH23248	15	TIBA	0.15	trace	no	None	none	401	1.00		32.3	2.4 psi H2 added initially
9-Dec-02	HH23249	25.1	TIBA	0.15	trace	no	None	none	401	1.00		84.3	20.1 psi H2 added initially; yield is integrated, low Mw lumped with NaCl
6-Apr-02	HH24154	10.1	TIBA	0.05	0.20	no	None	none	203.9	1.00		18.21	
7-Apr-02	HH24155	10	TIBA	0.05	0.20	no	1-C_6H_{12}	4.5	205.5	1.07		27.8	
8-Jun-02	HH25177	75	TIBA	0.06	trace	120	None	none	204.6	0.67		0.16	Very low Rp
9-Jun-02	HH25178	75.9	TIBA	0.07	trace	88	1-C_6H_{12}	4.54	204	1.00		6.42	
10-Jun-02	HH25179	100	TIBA	0.05	0.20	no	1-C_6H_{12}	5.25	201.3	1.08		11.55	No evacuation of any part (possible Q-connect leak); P_{total} = 219psi
28-Jun-02	HH25187	101.2	TIBA	0.05	0.20	no	1-C_6H_{12}	4.39	204	1.00		18.24	Similar HH25179, N2 removed after Q-connect to cat. holder leak fixed
15-Jun-02	HH26180	75.7	TIBA	0.07	trace	80	1-C_6H_{12}	4.84	204.8	1.00		4.03	He leak check done on June 12 '02
16-Jun-02	HH26181	75	TIBA	0.07	trace	80	None	none	204.6	1.17		0.8	
17-Jun-02	HH26182	100.3	TIBA	0.05	0.20	no	1-C_6H_{12}	4.85	199.8	1.50		27.2	
30-Jun-02	HH26188	105.3	TIBA	0.05	0.20	no	1-C_6H_{12}	4.41	203.4	1.17		18.1	
16-Jul-02	HH26194	101	TIBA	0.05	0.20	no	C_3H_6	33	200	2.00		95.3	Propylene amount =34.2 psi at 92.5oC
19-Mar-03	HH26272	82	TIBA	0.15	0.59	no				1.00		2.85	Propylene homopolymerization
21-Jun-02	HH27183	100.2	TIBA	0.06	0.24	no	1-C_6H_{12}	4.46	200	1.00		29.7	
22-Jun-02	HH27184	75.9	TIBA	0.07	trace	72	1-C_6H_{12}	4.29	205	1.00		5.83	
23-Jun-02	HH27185	101	TIBA	0.07	trace	72	1-C_6H_{12}	4.34	204	1.00		9.12	
24-Jun-02	HH27186	100	TIBA	0.07	trace	70	None	none	200.2	1.00		2.24	
1-Jul-02	HH27189	100.4	TIBA	0.05	0.20	no	1-C_6H_{12}	4.51	205	1.00		33.13	
5-Jul-02	HH28190	101	TIBA	0.05	0.20	no	1-C_6H_{12}	4.31	205	1.00		4.86	
6-Jul-02	HH28191	100.5	TIBA	0.07	trace	70	1-C_6H_{12}	4.32	204	1.00		4.98	
6-May-03	HH29294	63	TIBA	0.15	trace	vent	None		201	1.00		3.72	Gel type support: STY/DVB 1%
7-May-03	HH29295	62.4	TIBA	0.15	trace	vent	1-C_6H_{12}	2.01	201	1.03		9.1	

Table B-1. Cont'd

Date	Run Number[1]	Cat. Am't mg	Scavenger			Evac.[2] mtorr	Comonomer		Total Pres. psi	Length of Run[5]		PE Yield g	Comments
			Type	Am't mL	Al mmol		Type	Am't mL		Total h	R_{max} h		
8-May-03	HH29296	64.6	TIBA	0.15	trace	vent	1-C_6H_{12}	4.02	200	1.00		8.34	
12-May-03	HH29297	64	TIBA	0.15	trace	vent	1-C_6H_{12}	6.01	201	1.55		11.7	
11-Apr-01	HHTM022	107	TIBA	0.30	1.18	no							Catalyst 02TM
14-Apr-01	HHTM023	102	TIBA	0.30	1.18	no	none			1.00		6.8	Flow thru shaft port
15-Apr-01	HHTM024	103	TIBA	0.30	1.18	no	none			1.00		2.5	Needle blockage ~0.2 mL TIBA injected; shaft port; anchor impeller used
16-Apr-01	HHTM025	106	TIBA	0.22	0.87	no	none		205				TEAL purged 3x with 200psi N_2 before TIBA; product darkened by blade/reactor abrasion
22-Apr-01	HHTM026	106	TIBA	0.20	0.79	no	none			1.25		13.5	
23-Apr-01	HHTM027	107	TIBA	0.10	0.39	no	none			2.00		56.9	
28-Apr-01	HHTM028	103	TIBA	0.20	0.79	no	none		206	4.25		67.6	Polymerization at 310 rpm
29-Apr-01	HHTM029	104	TIBA	0.05	0.20	no	none			1.00		31.2	
30-Apr-01	HHTM030	103	TIBA	0.07	0.28	no	none			1.00		42.5	
1-May-01	HHTM031	103	none				none			1.00		35.7	
4-May-01	HHTM032	72	TIBA	0.06	trace	45	1-C_6H_{12}	2.8	205			65.9	
8-May-01	HHTM034	71	none				1-C_6H_{12}	3.1	206	1.00		66.8	
11-May-01	HHTM035	70	none				1-C_6H_{12}	3.18	206	1.00		43.6	
24-Feb-01	HHXX007	96	TEAL	0.15	1.094	no	1-C_6H_{12}	2.62	203	3.50	1.39	48.1	Cat. JM54;Injector septum valve closed overnight
25-Feb-01	HHXX008	96	TIBA	0.30	1.18	no	1-C_6H_{12}	2.64	203	1.25	1	24.8	Wall T as control variable
3-Mar-01	HHXX009	96	TIBA	0.39	1.54	no	1-C_6H_{12}	2.95	206	3.25		111	Cat. Injector: 1/4" tube with 2 Slok valves
4-Mar-01	HHXX010	98	TIBA	0.40	1.58	no	1-C_6H_{12}	2.62	210	1.50		40.5	Catalyst injection line at 200psi N_2,then ethylene upstream; no max Rp in ~1.5h
6-Apr-01	HHXX019	103	TIBA	0.51	2.01	no				5.37			
10-Apr-01	HHXX021	302	TIBA	0.52	2.05	no	none		205				

1. The first four characters identify the catalysts, e.g. Catalyst HH22 was used for Run HH22200.
2. Denotes whether reactor was evacuated (to stated vac. Level, mtorr) or not
3. Initially means all comonomer added at beginning of run; several means comonomer was added several times during run.
4. Reactor gas phase analyzed for 1-hexene/ethylene ratio by gas chromatography during run.
5. Rmax is the time taken to reach the maximum ethylene polymerization activity

Table B-2. Summary of measured polymer properties

Date	Run Number[1]	Prod'ty	Avgerage Activity			Bulk Density g/cm³	Molar mass		Poly-dispersity	Comments
		$\frac{\text{g PE}}{\text{g cat}}$	$\frac{\text{g PE}}{\text{g cat}\cdot\text{h}}$	$\frac{\text{g PE}}{\text{g cat}\cdot\text{bar}\,C_2H_4\cdot\text{h}}$	$\frac{\text{kg PE}}{\text{mol Zr}\cdot\text{h}}$		M_n, ×10⁻³	M_w, ×10⁻³		
7-Feb-01	HH01001	156.0	45.2	3.230	1852.0	0.268				
10-Feb-01	HH01002	206.4	87.2	6.261	3572.2	0.425				
12-Feb-01	HH01003	69.4	34.7	2.457	1422.5	0.325				
15-Feb-01	HH01004	1438.1	479.4	33.913	19637.5	0.276				
18-Feb-01	HH01005	182.0	69.7	4.932	2855.9	0.276				
19-Feb-01	HH01006	372.6	124.2	8.874	5088.6	0.279				
7-Mar-01	HH01011	0.0	0.0	0.000	0.0	-				
9-Mar-01	HH01012	0.0	0.0	0.000	0.0	-				
10-Mar-01	HH01013	230.2	59.3	4.238	2430.3	0.388				
23-Mar-01	HH01014	578.3	162.0	11.572	6635.7	0.426				
24-Mar-01	HH01015	1066.7	304.8	21.774	12485.1	0.482				
25-Mar-01	HH01016	322.6	89.8	6.417	3679.4	0.462				
30-Mar-01	HH01017	771.7	110.2		4516.1	0.168				Slurry run
1-Apr-01	HH01018	206.3	65.8	7.072	2696.6					
8-Apr-01	HH02020	0.0	0.0	0.000	0.0					
6-May-01	HH02033	0.0								
12-May-01	HH03036	25.0	10.0	0.702	599.7	0.404				
13-May-01	HH03037									
15-May-01	HH04038									
31-May-01	HH05039	54.2	36.1	2.582	3178.7	0.319				
1-Jun-01	HH05040	181.1	72.5	5.176	6373.8	0.376				
4-Jun-01	HH05041	165.3	66.1	4.796	5818.3	0.393				
5-Jun-01	HH05042	7.7	7.7	0.542	676.7	ND				
11-Jun-01	HH06043	131.3	131.3	9.287	7883.7	0.496				
12-Jun-01	HH06044	335.7	335.7	23.864	20158.2	0.421				
16-Jun-01	HH06045	179.8	179.8	12.846	10798.1	0.447				
17-Jun-01	HH06046	257.7	257.7	18.539	15476.0	0.434				
18-Jun-01	HH06047	205.6	205.6	14.867	12348.8	0.4				

Table B-2. Summary of measured polymer properties (Cont'd)

Date	Run Number[1]	Prod'ty	Avgerage Activity			Bulk Density g/cm^3	Molar mass		Poly-dispersity	Comments
		$\frac{\text{g PE}}{\text{g cat}}$	$\frac{\text{g PE}}{\text{g cat} \cdot \text{h}}$	$\frac{\text{g PE}}{\text{g cat} \cdot \text{bar} C_2H_4 \cdot \text{h}}$	$\frac{\text{kg PE}}{\text{mol Zr} \cdot \text{h}}$		M_n, ×10^{-3}	M_w, ×10^{-3}		
22-Jun-01	HH07048	272.6	272.6	19.479	19376.9	0.348	25.6	101.7	4.0	
25-Jun-01	HH07049	231.7	231.7	16.634	16465.9	0.281				
26-Jun-01	HH07050	677.5	677.5	48.643	48150.7	0.273	36.6	94.0	2.6	
9-Nov-02	HH07235	179.3	179.3	12.969	12741.8	0.282	52.0	135.8	2.6	Mn, Mw for cat holder plug same
10-Nov-02	HH07236	109.8	109.8	7.923	7803.9	0.287	49.9	131.0	2.6	
11-Nov-02	HH07237	134.0	134.0	9.637	9521.0	0.269	52.4	137.9	2.6	Homopolym 80°C
14-Dec-02	HH07251	260.8	260.8	12.565	18534.1	0.266	61.9	153.6	2.5	300 psi run
15-Dec-02	HH07252	186.0	186.0	6.727	13219.2	0.247	60.8	154.2	2.5	400 psi run
16-Dec-02	HH07253	32.7	32.7	4.696	2324.0	0.310	37.3	111.8	3.0	100 psi run
13-Apr-03	HH07282	137.3	137.3	9.621	9759.0	0.300	40.4	114.6	2.8	Homopolym 90°C
14-Apr-03	HH07283	92.6	92.6	7.072	6584.7	0.274	72.2	175.7	2.4	Homopolym 60°C; repeat diluted 81975, 210730, 2.57
15-Apr-03	HH07284	22.8	22.8	1.795	1618.5	0.270	69.5	178.9	2.6	Homopolym 50°C; repeat diluted 75390, 197105, 2.61
16-Apr-03	HH07285	190.7	190.7	14.254	13550.5	0.280	62.9	150.9	2.4	Homopolym 70°C
5-May-03	HH07293	120.9	120.9	8.352	8594.6	0.303	33.3	94.6	2.8	Homopolym 100°C
4-Jul-01	HH08051	637.5	637.5	45.547	27872.6	0.362	44.4	114.4	2.6	MM values for fiber & aggl. Lower
5-Jul-01	HH08052	1091.2	1091.2	77.808	47708.8	0.405	48.1	116.7	2.4	MM values for powder Lower
6-Jul-01	HH08053	1593.1	1593.1	114.158	69652.7	0.406	36.1	103.7	2.9	MM values for translucent particles lower
7-Jul-01	HH08054	881.9	881.9	63.098	38556.3	0.413	73.7	159.8	2.2	MM values for powder Lower
11-Jul-01	HH08055	1705.7	1705.7	122.464	74572.8	0.419	52.9	129.4	2.4	MM values for translucent particles lower
17-Jul-01	HH08058	470.6	470.6	33.959	20576.3	0.408	74.4	194.6	2.6	
27-Jul-01	HH08062	2599.2	2523.5	182.449	110330.1	0.412	49.4	103.6	2.1	MM values for powder slightly Lower
8-Aug-01	HH08068	667.2	667.2	47.598	29170.5	0.428	30.7	90.9	3.0	
9-Aug-01	HH08069	498.0	498.0	35.652	21774.7	0.438	40.2	114.6	2.9	~same Mn (prtcl & pwdr); Mw pwdr > prtcl
10-Aug-01	HH08070	652.8	652.8	47.317	28542.2	0.412	42.6	108.8	2.6	
11-Aug-01	HH08071	463.0	463.0	33.245	20244.3	0.384	45.3	131.7	2.9	values for granules lower
13-Aug-01	HH08073	1465.4	1465.4	106.317	64067.8	0.455	47.9	106.3	2.2	values for pwdr lower
12-Jul-01	HH09056	758.3	736.2	52.595	110870.3	0.428	43.7	96.3	2.2	For WP; for TP mn=27.63; Mw=151.70

Table B-2. Summary of measured polymer properties (Cont'd)

Date	Run Number[1]	Prod'ty	Avgerage Activity			Bulk Density g/cm^3	Molar mass		Poly-dispersity	Comments
		$\frac{g\ PE}{g\ cat}$	$\frac{g\ PE}{g\ cat \cdot h}$	$\frac{g\ PE}{g\ cat \cdot bar\ C_2H_4 \cdot h}$	$\frac{kg\ PE}{mol\ Zr \cdot h}$		$M_n, \times 10^{-3}$	$M_w, \times 10^{-3}$		
16-Jul-01	HH09057	661.6	661.6	47.499	99634.6	0.406	82.6	168.6	2.0	
12-Aug-01	HH09072	266.5	266.5	18.947	40136.5	0.393	49.6	123.9	2.5	For WP; for TP Mn=24684; Mw=89726
20-Dec-02	HH09254	970.7	970.7	56.087	146185.8	0.35	79.5	168.8	2.1	
21-Dec-02	HH09255	369.7	369.7	21.321	55681.8	0.44	73.0	150.3	2.1	
23-Dec-02	HH09256	348.0	348.0	20.084	52410.4	0.39	83.0	166.9	2.0	
26-Dec-02	HH09257	327.8	327.8	18.866	49368.2	0.39	88.6	178.4	2.0	
28-Dec-02	HH09258	759.0	759.0	43.859	114314.4	0.39	76.1	162.2	2.1	
29-Dec-02	HH09259	1286.6	1286.6	90.143	193764.0	0.38	76.5	164.0	2.1	
30-Dec-02	HH09260	262.2	262.2	38.028	39488.6	0.4	52.8	121.6	2.3	100psi; med sized particles; sml:57.78,133.15; big: 50.828, 110.669
1-Jan-03	HH09261	552.8	552.8	26.678	83248.8	0.41	82.4	170.1	2.1	300psi; med sized particles; sml:94.047,193.583; big:69.533, 149.862
2-Jan-03	HH09262	840.4	840.4	30.418	126566.8	0.43	88.3	176.8	2.0	400psi; med sized particles; sml:95.279,196.507; big: 75.818, 158.27
4-Jan-03	HH09263	696.3	696.3	50.493	104865.5	0.41	72.1	150.4	2.1	200psi; med sized particles; sml: 66.405, 145.018; big: 64.431, 135.254
6-Jan-03	HH09264	658.9	658.9	38.074	99236.1	0.38	79.2	170.1	2.1	
1-Mar-03	HH09265	261.0	261.0	18.468	39314.5	0.406				
31-Mar-03	HH09276	254.4	254.4	20.050	38309.2	0.345	103.2	216.5	2.1	Homopolym 50°C
1-Apr-03	HH09277	514.1	514.1	39.447	77419.3	0.377	93.8	196.4	2.1	Homopolym 60°C to repeat?
2-Apr-03	HH09278	458.6	458.6	34.288	69073.9	0.398	93.7	191.6	2.0	Homopolym 70°C
3-Apr-03	HH09279	460.0	460.0	32.703	69278.2	0.449	70.0	145.1	2.1	Homopolym 90°C
4-Apr-03	HH09280	488.8	488.8	36.540	73610.6	0.380	80.5	163.5	2.0	Homopolym 70°C
6-Apr-03	HH09281	487.1	487.1	36.417	73362.5	0.392	86.7	177.2	2.0	Homopolym 70°C repeat dilute 75981, 168633, 2.22
17-Apr-03	HH09286	66.1	66.1	4.720	9950.7	0.406	63.2	142.4	2.3	copolym 90°C; transparent particles 26.06k, 93.689k
20-Jul-01	HH10059	415.8	415.8	29.795	27483.6	0.341	35.1	92.2	2.6	Homopolym 50°C
22-Jul-01	HH10060	23.5	23.5	1.685	1551.4	0.313	76.2	201.9	2.7	If small low Mn,Mw peak included; Mn=32.028, pd=6.1
23-Jul-01	HH10061	614.8	409.9	29.457	27091.7	0.326	35.4	88.4	2.5	
27-Nov-01	HH10118	360.4	360.4	25.660	23821.5	0.368	39.7	106.4	2.7	

Table B-2. Summary of measured polymer properties (Cont'd)

Date	Run Number[1]	Prod'ty	Avgerage Activity			Bulk Density g/cm^3	Molar mass		Poly-dispersity	Comments
		$\frac{\text{g PE}}{\text{g cat}}$	$\frac{\text{g PE}}{\text{g cat}\cdot\text{h}}$	$\frac{\text{g PE}}{\text{g cat}\cdot\text{bar}\,C_2H_4\cdot\text{h}}$	$\frac{\text{kg PE}}{\text{mol Zr}\cdot\text{h}}$		M_n, $\times10^{-3}$	M_w, $\times10^{-3}$		
1-Dec-01	HH10119	34.3	205.5	14.662	13584.4	0.246	28.0	132.1	4.7	
2-Dec-01	HH10120	1.6	93.4	6.655	6172.1	ND				
3-Dec-01	HH10121	725.6	414.6	29.637	27405.4	0.281	34.6	90.3	2.6	
18-Mar-03	HH10271	34.5	14.2	1.026	939.7	0.326	52.2	152.6	2.9	
28-Jul-01	HH11063	310.0	177.1	12.656	17441.6	0.399				
29-Jul-01	HH11064	397.1	397.1	28.179	39102.9	0.352				
30-Jul-01	HH11065	548.6	548.6	39.231	54012.7	0.334				
22-Dec-01	HH11126	148.6	148.6	10.767	14633.2	0.29	57.5	155.5	2.7	
31-Jul-01	HH12066	250.0	250.0	17.941	19235.0	0.334	31.7	107.4	3.4	
5-Aug-01	HH12067	422.5	422.5	30.625	32509.9	0.385	26.9	93.5	3.5	
23-Dec-01	HH12127	175.6	175.6	12.735	13512.1	0.307	56.8	151.8	2.7	
14-Aug-01	HH13074	970.4	970.4	69.163	31019.4	0.451	41.5	107.2	2.6	Molar mass (particle ~ powder)
15-Aug-01	HH13075	1676.5	1676.5	120.607	53586.9	0.356	34.8	98.0	2.8	Powder: Mn 50681, Mw 115501, PD=2.3
16-Aug-01	HH13076	461.5	461.5	33.318	14752.1	0.448				
17-Aug-01	HH13077	1012.3	992.4	70.765	31722.4	0.424	35.8	88.8	2.5	
18-Aug-01	HH13078	1702.2	1702.2	120.132	54408.7	0.44				
19-Aug-01	HH13079	1224.3	1224.3	88.963	39135.1	0.427	40.5	101.4	2.5	
20-Aug-01	HH13080	387.7	387.7	27.655	12391.0	0.393				
21-Aug-01	HH13081	100.5	100.5	7.204	3212.1	0.407				
29-Aug-01	HH13082	171.3	171.3	12.262	5475.3	0.47				
1-Sep-01	HH14083	272.9	272.9	19.595	10587.1	0.441	36.3	96.9	2.7	Powder: lower Mn 11.894, Mw 81.720,PD=6.9
2-Sep-01	HH14084	534.0	534.0	38.343	20716.6	0.418				
6-Sep-01	HH14085	482.5	482.5	34.338	18718.1	0.404	36.7	91.6	2.5	
24-Dec-01	HH14128	254.3	235.5	17.077	9135.3	0.347	81.8	185.1	2.3	values for samples 70h in GC lower
25-Dec-01	HH14129	955.2	955.2	69.478	37055.0	0.394	37.8	90.7	2.4	
14-Jan-02	HH14130	384.4	384.4	27.328	14911.1	0.379	93.2	206.5	2.2	
20-Jan-02	HH14131	690.9	690.9	50.254	26802.3	0.394	37.0	87.7	2.4	
29-Mar-02	HH14149	835.8	835.8	59.451	32423.1	0.384	29.5	73.4	2.5	Mn, Mw for pwdr ~30% higher

Table B-2. Summary of measured polymer properties (Cont'd)

Date	Run Number[1]	Prod'ty $\frac{g\ PE}{g\ cat}$	Avgerage Activity $\frac{g\ PE}{g\ cat \cdot h}$	Avgerage Activity $\frac{g\ PE}{g\ cat \cdot bar\ C_2H_4 \cdot h}$	Avgerage Activity $\frac{kg\ PE}{mol\ Zr \cdot h}$	Bulk Density g/cm^3	Molar mass M_n, ×10^{-3}	Molar mass M_w, ×10^{-3}	Poly-dispersity	Comments
5-Apr-02	HH14153	291.1	291.1	21.121	11293.1	0.41	61.9	136.0	2.2	Mn, Mw for pwdr ~30% higher
14-Apr-02	HH14156	465.7	465.7	33.602	18064.9	0.44	73.6	160.7	2.2	
15-Apr-02	HH14157	596.7	596.7	43.031	23145.9	0.46	77.2	169.3	2.2	~30% diff. Between the 2 particles used in GC
19-Apr-02	HH14158	1462.5	835.7	59.709	32419.9	0.43	54.4	145.3	2.7	pwdr values ~40% higher; High RI baseline noise 3-4x
20-Apr-02	HH14159	291.5	388.7	27.567	15078.7	0.4	114.8	230.6	2.0	High RI baseline noise 3-4x; irregular fragments not inj'd -visible insolubles
21-Apr-02	HH14160	272.0	362.6	25.820	14067.9	0.38	98.7	202.4	2.1	irregular fragments not inj'd -visible insolubles
29-Apr-02	HH14163	252.4	336.5	23.833	13055.0	0.34	97.7	203.3	2.1	irregular fragments not inj'd -visible insolubles
3-May-02	HH14164	192.7	257.0	18.135	9967.9	0.35	101.4	217.8	2.1	irregular fragments not inj'd -visible insolubles
4-May-02	HH14165	1337.7	1337.7	96.237	51893.1	0.43	67.4	143.7	2.1	irregular fragments not inj'd -visible insolubles
13-May-02	HH14171	570.5	570.5	40.460	22130.9	0.45	96.7	203.4	2.1	
9-Sep-01	HH15086	1723.0	1723.0	122.920	83898.1	0.43	42.2	96.9	2.3	particles & powder almost same Mw
10-Sep-01	HH15087	976.0	976.0	69.835	47524.3	0.413	40.4	97.5	2.4	Agglom: Mn 20068, Mw 98347, PD=4.9
12-Sep-01	HH15088	1428.7	1428.7	105.450	69566.5	0.38	35.7	89.9	2.5	Powder: Mn 52097, =Mw 111110, PD=2.1
13-Sep-01	HH15089	1323.9	1323.9	94.217	64465.4	0.437	38.7	87.6	2.3	Powder: Mn 44085, Mw 120538, PD=2.7
14-Sep-01	HH15090	1469.6	1469.6	107.806	71555.5	0.455	36.0	86.7	2.4	Powder: Mn 42714, Mw 110159, PD=2.6
18-Sep-01	HH15091	1400.0	1400.0	108.697	68168.7	0.42	39.7	90.0	2.3	Powder: Mn 48459, Mw 111809, PD=2.3
21-Sep-01	HH15092	1222.0	1222.0	88.347	59499.7	0.392				
23-Sep-01	HH15093	1318.6	1318.6	93.883	64205.2	0.409				
30-Sep-01	HH15094	577.9	577.9	81.288	28136.9	0.428				
4-Oct-01	HH15095	552.8	552.8	39.398	26917.2	0.404	78.0	169.1	2.2	
25-Nov-01	HH15117	1196.0	1196.0	84.571	58234.6	0.36				
26-Jan-02	HH15134	763.0	750.5	53.148	36543.1	0.402	80.0	170.0	2.1	
27-Jan-02	HH15135	2046.0	1364.0	96.452	66415.1	0.4	68.0	160.0	2.4	
5-Feb-02	HH15138	2199.7	2036.7	146.162	99172.9	0.364	78.0	170.0	2.2	
9-Feb-02	HH15139		NA							
10-Feb-02	HH15140									
17-Feb-02	HH15141	870.0	614.1	43.342	29902.7	0.456	77.2	168.6	2.2	pwdr samples have insolubles, no GC
18-Feb-02	HH15142	933.2	466.6	33.074	22719.0	0.447	71.2	155.5	2.2	pwdr samples have insolubles, no GC

Table B-2. Summary of measured polymer properties (Cont'd)

Date	Run Number[1]	Prod'ty	Avgerage Activity			Bulk Density g/cm^3	Molar mass		Poly-dispersity	Comments
		$\frac{g\ PE}{g\ cat}$	$\frac{g\ PE}{g\ cat \cdot h}$	$\frac{g\ PE}{g\ cat \cdot bar\ C_2H_4 \cdot h}$	$\frac{kg\ PE}{mol\ Zr \cdot h}$		M_n, $\times10^{-3}$	M_w, $\times10^{-3}$		
23-Feb-02	HH15143	1444.0	722.0	50.710	35156.6	0.42	75.0	155.0	2.1	
25-Feb-02	HH15144	1106.5	316.1	22.687	15393.2	0.44	51.0	122.0	2.4	
27-Apr-02	HH15161	457.9	457.9	32.647	22293.7		28.6	92.1	3.2	1-decene copolymer; flaky parts 50% lower; PD=6.4
28-Apr-02	HH15162	542.3	542.3	38.648	26405.1		38.7	108.2	2.8	1-decene copolymer
12-Jul-02	HH15192	419.0	419.0	30.383	20401.2					
15-Jul-02	HH15193	1755.6	1755.6	127.306	85481.4					C_2/C_3 copolymer
20-Mar-03	HH15273									propylene homopolym: No cat. Recovd; no prod
5-Oct-01	HH16096	541.8	541.8	39.749	37700.4	0.26	35.3	94.4	2.7	
6-Oct-01	HH16097	243.3	243.3	17.546	16927.6	0.23	55.1	149.5	2.7	
7-Oct-01	HH16098	151.1	151.1	21.112	10513.6	0.25	23.6	97.5	4.1	
10-Oct-01	HH16099	533.5	533.5	38.492	37117.8	0.30	33.6	85.4	2.5	
5-May-02	HH16166	330.2	188.7	13.682	13127.8	0.31	73.0	179.9	2.5	
6-May-02	HH16167	310.7	248.5	18.023	17293.0	0.26	73.4	175.5	2.4	
10-May-02	HH16168	278.1	222.5	16.215	15480.5	0.29	77.3	180.0	2.3	
11-May-02	HH16169	294.0	235.2	17.059	16367.9	0.26	76.2	181.4	2.4	
12-May-02	HH16170	328.6	262.9	19.159	18291.4	0.18	55.0	144.9	2.6	
24-May-02	HH16172	19.4	25.9	1.878	1801.5	0.24	49.7	130.7	2.6	
27-May-02	HH16175	670.7	536.6	38.167	37335.5	0.26	35.7	90.4	2.5	
28-May-02	HH16176		v/low			ND				
19-Jul-02	HH16195	42.4	42.4	3.059	2949.6	0.19	55.7	146.9	2.6	2nd GPC: 51,251; 139,601; 2.7); same Mn,w for wht & trnsp particles
26-Jul-02	HH16199	84.2	84.2	6.044	5857.7	0.18	58.3	145.0	2.5	2nd GPC: 52,613; 148,804; 2.8); same Mn,w fot wht & trnsp particles
11-Oct-01	HH17100	346.3	346.3	24.738	30854.9	0.26				
12-Oct-01	HH17101	230.2	230.2	16.729	20516.9	0.24				
14-Oct-01	HH17102	348.0	348.0	24.692	31010.9	0.27				
26-Oct-02	HH17227	788.3	315.3	22.639	28098.5	0.313				
27-Oct-02	HH17228	220.9	88.3	6.297	7873.0	0.356				
28-Oct-02	HH17229	#VALU!	#VALUE!	#VALUE!	#VALU!	0.281				
1-Nov-02	HH17230	698.0	279.2	20.248	24881.7	0.362				

Table B-2. Summary of measured polymer properties (Cont'd)

Date	Run Number[1]	Prod'ty	Avgerage Activity			Bulk Density g/cm^3	Molar mass		Poly-dispersity	Comments
		$\frac{\text{g PE}}{\text{g cat}}$	$\frac{\text{g PE}}{\text{g cat} \cdot \text{h}}$	$\frac{\text{g PE}}{\text{g cat} \cdot \text{bar } C_2H_4 \cdot \text{h}}$	$\frac{\text{kg PE}}{\text{mol Zr} \cdot \text{h}}$		M_n, ×10^{-3}	M_w, ×10^{-3}		
2-Nov-02	HH17231	706.2	282.5	20.432	25170.8	0.360				
3-Nov-02	HH17232	566.5	226.6	16.352	20194.3	0.360				
4-Nov-02	HH17233	979.2	391.7	28.262	34903.9	0.340				
8-Nov-02	HH17234	937.4	375.0	27.124	33414.1	0.360				
21-Oct-01	HH18103	478.9	478.9	34.117	26920.9	0.384				almost all spherical particles
22-Oct-01	HH18104	100.4	100.4	7.313	5642.8	0.285	70.9	201.6	2.8	almost all spherical particles
23-Oct-01	HH18105	854.7	854.7	60.528	48042.0	0.408				almost all spherical particles
24-Oct-01	HH18106	363.3	363.3	26.087	20422.9	0.393				almost all spherical particles
12-Aug-02	HH18207	104.4	104.4	9.899	5869.9	0.480				almost all spherical particles
16-Nov-02	HH18238	567.2	567.2	41.032	31883.9	0.395	31.6	82.4	2.6	
17-Nov-02	HH18239	468.6	468.6	33.811	26338.7	0.410	31.0	85.9	2.8	
18-Nov-02	HH18240	621.3	621.3	44.939	34920.0	0.410	32.2	81.5	2.5	cf. #238+239 & 240 => min. effect of 1-C6 incororation on Mn,w
7-Dec-02	HH18247	53.8	53.8	1.944	3021.2	0.310	63.2	171.6	2.7	
13-Dec-02	HH18250	643.9	643.9	46.598	36191.0	0.410				
21-Mar-03	HH18274					NA				Only little waxy material recovered
18-Apr-03	HH18287	920.6	920.6	65.770	51744.0	0.416	36.5	82.1	2.2	Copoly 90°C; Transp prtcls: 22.030, 71.664
19-Apr-03	HH18288	282.2	282.2	21.098	15862.5	0.429	36.3	87.5	2.4	Copoly 70°C; Transp prtcls: 21.565, 88.580
20-Apr-03	HH18289	132.5	132.5	10.276	7447.1	0.440	35.9	94.1	2.6	Copoly 60°C; Transp prtcls: 21.548, 104.921
21-Apr-03	HH18290	308.7	308.7	21.322	17352.9	0.468	33.7	83.9	2.5	Copoly 100°C; Transp prtcls: 16.922, 76.785
22-Apr-03	HH18291	680.7	680.7	49.609	38260.7	0.399	34.5	79.5	2.3	Copoly 80°C; Transp prtcls: 20.911, 75.707
3-May-03	HH18292	395.3	395.3	26.794	22221.9	0.420	32.1	80.2	2.5	Copoly 100°C; Transp prtcls: 25.033, 87.110
28-Oct-01	HH19107	496.7	496.7	35.349	27639.2	0.392	35.0	86.3	2.5	
29-Oct-01	HH19108	676.7	548.7	39.711	30531.9	0.435	36.7	89.5	2.4	2nd GPC: 34,774; 86,981; 2.5)
30-Oct-01	HH19109	41.9	41.9	3.063	2330.2	_	87.1	244.9	2.8	
20-Nov-01	HH19116	33.3	90.1	5.226	5012.9	ND				
8-Dec-01	HH19122	405.3	228.4	16.172	12706.6	0.4	32.1	88.9	2.8	
9-Dec-01	HH19123	502.2	143.5	10.370	7984.7	0.43	36.1	90.4	2.5	
10-Dec-01	HH19124	455.7	364.6	26.073	20286.4	0.44	35.2	88.3	2.5	

Table B-2. Summary of measured polymer properties (Cont'd)

Date	Run Number[1]	Prod'ty	Avgerage Activity			Bulk Density g/cm^3	Molar mass		Poly-dispersity	Comments
		$\frac{g\ PE}{g\ cat}$	$\frac{g\ PE}{g\ cat \cdot h}$	$\frac{g\ PE}{g\ cat \cdot bar\ C_2H_4 \cdot h}$	$\frac{kg\ PE}{mol\ Zr \cdot h}$		M_n, $\times 10^{-3}$	M_w, $\times 10^{-3}$		
11-Dec-01	HH19125	570.1	456.1	32.602	25378.5	0.44	36.4	88.2	2.4	
21-Jan-02	HH19132	137.8	68.9	4.421	3833.2	0.421	40.8	107.7	2.6	
22-Jan-02	HH19133	270.9	131.1	9.528	7292.5	0.444	32.9	89.3	2.7	
29-Jan-02	HH19136	447.7	223.8	15.790	12454.9	0.414	30.4	81.1	2.7	
4-Feb-02	HH19137	365.6	121.9	8.808	6781.9	0.402	22.5	78.2	3.5	
12-Mar-02	HH19145									Have visible insolubles no GPC
25-May-02	HH19173	0.0	0.0	0.000	0.0	NA				
30-Mar-03	HH19275	443.7	354.9	25.234	19749.4	0.364				
5-Nov-01	HH20110	311.4	311.4	22.292	15677.3	0.353	35.1	102.3	2.9	
6-Nov-01	HH20111	396.6	396.6	28.213	19968.3	0.314	35.5	97.1	2.7	
12-Nov-01	HH20114	60.4	60.4	4.373	3039.1	0.257	86.2	236.1	2.7	GPCFeb4,'03; Mn=79.162, Mw=234.483, pdi=2.9
26-May-02	HH20174		v/low			ND				
20-Jul-02	HH20196	361.9	181.0	12.865	9109.9	0.36	46.4	115.3	2.5	C2/C3 copolymer
21-Jul-02	HH20197									
22-Jul-02	HH20198	815.5	407.7	28.988	20527.2	0.38	32.0	78.4	2.4	
10-Mar-03	HH20268	12.4	49.4	3.550	2489.0	0.42				
11-Mar-03	HH20269	31.8	31.8	2.280	1598.4	0.2	116.0	272.0	2.3	homopolym no seedbed
17-Mar-03	HH20270	5.5	5.2		262.0	0.37				
10-Nov-01	HH21112	621.0	621.0	44.988	29998.7	0.34	30.7	87.4	2.8	
11-Nov-01	HH21113	212.2	212.2	15.403	10250.7	0.32				
19-Nov-01	HH21115	577.2	577.2	41.771	27881.5	0.31	34.9	88.4	2.5	
8-Sep-02	HH21208	264.9	264.9	18.831	12795.0	0.444				
9-Sep-02	HH21209	188.0	94.0	6.818	4541.9	0.336				
13-Sep-02	HH21210	1231.1	1231.1	87.525	59470.3	0.413				
14-Sep-02	HH21211	203.0	203.0	14.432	9805.8	0.374				
15-Sep-02	HH21212	129.8	129.8	9.276	6271.9	0.371				
20-Sep-02	HH21213	213.9	213.9	15.204	10330.8	0.39				
21-Sep-02	HH21214	74.7	66.7	4.764	3221.4	0.35				

Table B-2. Summary of measured polymer properties (Cont'd)

Date	Run Number[1]	Prod'ty	Avgerage Activity			Bulk Density g/cm^3	Molar mass		Poly-dispersity	Comments
		$\frac{g\ PE}{g\ cat}$	$\frac{g\ PE}{g\ cat \cdot h}$	$\frac{g\ PE}{g\ cat \cdot bar C_2H_4 \cdot h}$	$\frac{kg\ PE}{mol\ Zr \cdot h}$		M_n, ×10^{-3}	M_w, ×10^{-3}		
22-Sep-02	HH21215	119.5	119.5	8.454	5772.2	0.33				
23-Sep-02	HH21216	333.9	333.9	23.621	16128.6	0.37				
28-Sep-02	HH21217	1456.7	1456.7	103.561	70366.3	0.33				
29-Sep-02	HH21218	1341.0	1341.0	95.572	64778.7	0.39				
30-Sep-02	HH21219	1598.6	1598.6	112.551	77224.9	0.38				
1-Oct-02	HH21220	1200.5	1200.5	84.234	57991.9	0.35				
2-Oct-02	HH21221	164.1	164.1	11.844	7929.4	0.38				
6-Oct-02	HH21222	1614.6	1614.6	115.074	77997.2	0.41				
7-Oct-02	HH21223	1526.2	1308.2	93.004	63193.0	0.4				
12-Oct-02	HH21224	1429.1	1072.1	76.220	51789.1	0.39				
14-Oct-02	HH21225	1576.7	1182.5	84.485	57123.7	0.41				
15-Oct-02	HH21226	1756.0	1505.1	107.007	72707.7	0.37				
13-Mar-02	HH22146	64.4	32.2	2.295	2621.5	0.436				almost all spherical particles
15-Mar-02	HH22147	469.1	312.7	22.803	25460.0	0.363	30.9	83.1	2.7	almost all spherical particles
18-Mar-02	HH22148	136.0	46.9	3.398	3817.0	0.294	61.1	152.1	2.5	almost all spherical particles
28-Jul-02	HH22200	69.8	69.8	4.935	5678.9	0.42	32.3	102.2	3.2	almost all spherical particles
29-Jul-02	HH22201	183.2	146.5	10.573	11929.3	0.39	34.6	94.5	2.7	almost all spherical particles
2-Aug-02	HH22202	180.6	144.5	10.321	11760.6	0.45	30.4	91.5	3.0	almost all spherical particles
3-Aug-02	HH22203	917.7	734.2	52.711	59769.9	0.36	34.4	81.7	2.4	almost all spherical particles
4-Aug-02	HH22204	645.1	430.1	30.725	35012.1	0.37	34.0	82.3	2.4	almost all spherical particles
5-Aug-02	HH22205	909.7	606.5	43.265	49374.4	0.37	34.3	80.3	2.3	almost all spherical particles
9-Aug-02	HH22206	36.3	36.3	3.465	2956.2	0.36	77.1	212.1	2.8	almost all spherical particles
2-Mar-03	HH22266	#VALU!	#VALUE!							No cat. Injected
4-Mar-03	HH22267	113.7	93.4	6.676	7607.2	0.45	33.9	98.1	2.9	
30-Mar-02	HH23150	1264.1	1264.1	90.894	14341.4	0.29	94.3	213.9	2.3	
31-Mar-02	HH23151	5549.0	5549.0	393.540	62955.5	0.38	35.1	88.7	2.5	
1-Apr-02	HH23152	766.3	1321.3	95.575	14990.3	0.27	79.5	196.3	2.5	
23-Nov-02	HH23241	1334.0	1334.0	96.255	15134.7	0.33	65.2	161.8	2.5	200 psi run

Table B-2. Summary of measured polymer properties (Cont'd)

Date	Run Number[1]	Prod'ty	Avgerage Activity			Bulk Density g/cm³	Molar mass		Poly-dispersity	Comments
		$\frac{g\ PE}{g\ cat}$	$\frac{g\ PE}{g\ cat \cdot h}$	$\frac{g\ PE}{g\ cat \cdot bar C_2H_4 \cdot h}$	$\frac{kg\ PE}{mol\ Zr \cdot h}$		M_n, ×10⁻³	M_w, ×10⁻³		
24-Nov-02	HH23242	776.2	776.2	37.527	8806.7	0.31	60.6	162.7	2.7	300 psi run
25-Nov-02	HH23243	100.0	100.0	14.219	1134.5	0.33	37.8	110.1	2.9	100 psi run; yield =1.0g/10mg
29-Nov-02	HH23244	84.8	96.0	13.854	1089.2	0.3	35.8	124.1	3.5	100 psi run; yield = 0.85g/10mg
30-Nov-02	HH23245	5128.7	5128.7	185.494	58187.0	0.28	79.0	184.2	2.3	400 psi run: values for powder; hollow shell is 79.01 & 177.93 k
6-Dec-02	HH23246	1029.7	1029.7	49.697	11682.3	0.31	61.4	164.1	2.7	300 psi run; repeat of HH23242
8-Dec-02	HH23248	2153.3	2153.3	77.881	24430.3	0.35	4.0	15.6	3.9	Ptotal=400 psi; Phydrgen=2.4 psi; avg. of 8 inj.
9-Dec-02	HH23249	3358.6	3358.6	121.472	38104.1	0.41	1.3	9.5	7.3	Ptotal=400 psi; Phydrgen=20 psi; for granule = 1.118 & 11.05 k
6-Apr-02	HH24154	1803.0	1803.0	128.244	19669.7	0.29	82.1	195.3	2.4	
7-Apr-02	HH24155	2780.0	2606.2	183.932	28432.3	0.41	27.1	92.3	3.4	
8-Jun-02	HH25177	2.1	3.2	0.226	180.5	ND				
9-Jun-02	HH25178	84.6	84.6	6.014	4795.2	0.44	31.3	114.2	3.7	
10-Jun-02	HH25179	115.5	106.6	7.682	6044.3	0.45	25.4	104.2	4.1	
28-Jun-02	HH25187	180.2	180.2	12.814	10217.8	0.44	33.9	98.3	2.9	
15-Jun-02	HH26180	53.2	53.2	3.770	2685.9	0.48	13.6	90.5	6.7	
16-Jun-02	HH26181	10.7	9.1	0.648	461.1	0.35	51.5	201.5	3.9	
17-Jun-02	HH26182	271.2	180.8	13.123	9121.2	0.45	30.5	90.2	3.0	
30-Jun-02	HH26188	171.9	147.3	10.503	7431.2	0.45	31.5	99.4	3.2	
16-Jul-02	HH26194	943.6	471.8	34.212	23802.3					
19-Mar-03	HH26272	34.8	34.8		1753.5	0.308	32.9	135.7	4.1	propylene homopolymer
21-Jun-02	HH27183	296.4	296.4	21.494	13370.8	0.38	31.4	94.9	3.0	
22-Jun-02	HH27184	76.8	76.8	5.434	3464.9	0.43	29.7	93.5	3.1	Mw for white particles; for translucent: 78.341/8.435=9.3
23-Jun-02	HH27185	90.3	90.3	6.420	4073.3	0.43	29.0	102.8	3.5	Translucent particles: Q = 81.081/8.081=10.0
24-Jun-02	HH27186	22.4	22.4	1.623	1010.5	0.31	53.5	150.6	2.8	
1-Jul-02	HH27189	330.0	330.0	23.345	14885.3	0.37	35.9	91.6	2.6	Mw for white particles; for translucent: 93.471/20.972=4.5
5-Jul-02	HH28190	48.1	48.1	3.404	3180.8	0.46	11.0	84.1	7.6	
6-Jul-02	HH28191	49.6	49.6	3.523	3275.6	0.43	10.1	79.8	7.9	
6-May-03	HH29294	59.0	59.0	4.261	4198.5	0.39				

Table B-2. Summary of measured polymer properties (Cont'd)

Date	Run Number[1]	Prod'ty	Avgerage Activity			Bulk Density g/cm^3	Molar mass		Poly-dispersity	Comments
		$\frac{g\ PE}{g\ cat}$	$\frac{g\ PE}{g\ cat \cdot h}$	$\frac{g\ PE}{g\ cat \cdot bar\ C_2H_4 \cdot h}$	$\frac{kg\ PE}{mol\ Zr \cdot h}$		M_n, $\times 10^{-3}$	M_w, $\times 10^{-3}$		
7-May-03	HH29295	145.8	141.6	10.216	10067.2	0.36				
8-May-03	HH29296	129.1	129.1	9.362	9179.5	0.42				
12-May-03	HH29297	182.8	117.9	8.510	8386.1	0.42				
11-Apr-01	HHTM022				0.0					
14-Apr-01	HHTM023	66.7	66.7		2372.9					
15-Apr-01	HHTM024	24.3	24.3		863.9					
16-Apr-01	HHTM025				0.0					
22-Apr-01	HHTM026	127.4	101.9		3626.5					
23-Apr-01	HHTM027	531.8	265.9		9463.9		74.1	169.4	2.3	
28-Apr-01	HHTM028	656.3	154.4	10.872	5496.6		64.8	159.4	2.5	
29-Apr-01	HHTM029	300.0	300.0		10678.1		77.3	181.9	2.4	
30-Apr-01	HHTM030	412.6	412.6		14686.7		72.3	186.1	2.6	
1-May-01	HHTM031	346.6	346.6		12336.8		63.1	180.9	2.9	
4-May-01	HHTM032	915.3			0.0		73.0	175.7	2.4	
8-May-01	HHTM034	940.8	940.8	66.239	33488.2					
11-May-01	HHTM035	622.9	622.9	43.852	22169.8					
24-Feb-01	HHXX007	501.0	143.2	10.228						
25-Feb-01	HHXX008	258.3	206.7	14.765						
3-Mar-01	HHXX009	1156.3	355.8	25.048						
4-Mar-01	HHXX010	413.3	275.5	19.028						
6-Apr-01	HHXX019									
10-Apr-01	HHXX021									
12-May-03										

1. See footnote 1 in Table B-1